Computational Screening of Energy Materials

Pandey, Mohnish; Jacobsen, Karsten Wedel; Thygesen, Kristian Sommer

Publication date:
2015

Computational Screening of Energy Materials

PhD Thesis

Mohnish Pandey

DTU Physics
Department of Physics

CAMd
Center for Atomic-scale Materials Design

Computational Screening of Energy Materials
PhD Thesis
July 2015

Mohnish Pandey
mohpa@fysik.dtu.dk

Supervisors:
Karsten Wedel Jacobsen
Kristian Sommer Thygesen

Center for Atomic-scale Materials Design
Department of Physics
Technical University of Denmark

Preface

This thesis is submitted for the candidacy of PhD degree in Physics from the Technical University of Denmark. The work contained in the thesis was carried out at the Center for Atomic-scale Materials Design (CAMd), Department of Physics in the period from August 2012 to July 2015 under the supervision of Prof. Karsten W. Jacobsen and Prof. Kristian S. Thygesen.

I cannot thank enough my supervisors Karsten and Kristian for their continuous support in my projects. Every bit of discussion I had with them improved my understanding of the subject matter. Their immense zeal in the projects and their unparalleled guidance always kept me motivated and helped me to get over the bottlenecks I faced during my research.

Also, I would like to thank Aleksandra, Ivano, Filip, Niels and Thomas for all the suggestions and discussions regarding different projects. Big thanks to Chris, Kirsten, Kristian, Martin, Niels and Simon Lamowski for generously agreeing to proofread the thesis and for the good times at CAMd. A deep gratitude to Jens Jørgen and Marcin for helping in the code developments and troubleshootings and Ole for taking such a good care of Niflheim for its seamless functioning. A huge thanks to Marianne for making my move to Denmark easy by taking care of all the rigmarole and other administrative matters.

Among friends my special thanks to Kristian for his continuous support and invitations for Indian festival dinners to make me feel home. I would also like to thank my other colleagues at CAMd - Korina, Manuel, Morten, Per, Simone and Ulrik for all the fun times.

Last but not least my heartfelt thanks to my family members for their continuous support and my girlfriend Shrutija for not letting me feel the long-distance relationship really as long-distance and supporting me in all the ways she could.

Mohnish Pandey
Kongens Lyngby, July 2015

Abstract

The current energy consumption of the worlds population relies heavily on fossil fuels. Unfortunately, the consumption of fossil fuels not only results in the emission of greenhouse gases which have deleterious effect on the envrionment but also the fossil fuel reserve is limited. Therefore, it is the need of the hour to search for environmentally benign renewable energy resources. The biggest source of the renewable energy is our sun and the immense energy it provides can be used to power the whole planet. However, an efficient way to harvest the solar energy to meet all the energy demand has not been realized yet.

A promising way to utilize the solar energy is the photon assisted water splitting. The process involves the absorption of sunlight with a semiconducting material (or a photoabsorber) and the generated electron-hole pair can be used to produce hydrogen by splitting the water. However, a single material cannot accomplish the whole process of the hydrogen evolution. In order do so, a material should be able to absorb the sunlight and generate the electron-hole pairs and evolve hydrogen at the cathode and oxygen at anode using the generated electron and hole respectively.

This thesis using first-principle calculations explores materials for the light absorption with the bandgap, band edge positions and the stability in aqueous conditions as descriptors. This strategy results in a handful of materials which can act as good photoabsorbers for the water splitting reaction. Additionally, strategies to tune the bandgap for different applications is also explored. To carry out the cathode reaction, two-dimensional metal dichalcogenides and oxides are explored with a suggestion of few potential candidates for the hydrogen evolution reaction.

The thermodynamics of all the above process requires an accurate description of the energies with the first-principle calculations. Therefore, along this line the accuracy and predictability of the Meta-Generalized Gradient Approximation functional with Bayesian error estimation is also assessed.

Resumé

Jordens befolkning er i dag fuldstændig afhængig af fossile brændstoffer for at producere den nødvendige energi. Denne afhængighed er meget ufordelagtig, idet lageret af tilgængelige fossile brændstoffer er stærkt begrænset samtidigt med, at afbrændingen af fossile brændstoffer producerer klimaskadelige drivhusgasser. Det er derfor nødvendigt, at finde miljøsikre vedvarende energikilder. Den største tilgængelige vedvarende energikilde er solen, hvis energiudladning er stor nok til at dække hele vores planets energiforbrug. Dog mangler vi stadigvæk en måde hvorpå solenergien kan høstes effektivt.

En lovende metode til at opfange solenergi er foton-assisteret vandspaltning. Denne metode indbefatter et halvleder-materiale, der absorberer en foton hvilket genererer et elektron-hul par, som kan bruges til at producere brint via vandspaltning. Det er dog umuligt for et enkelt materiale, at stå for hele den foton-assisterede vandspaltnings proces. For at muliggøre processen er det nødvendigt både at have et foton-absorberende materiale, der absorberer sollyset og genererer elektron-hul parret, et anodemateriale, der faciliterer iltudvindingsdelen af vandspaltning ved hjælp af det genererede hul, samt et katodemateriale, som anvender den genererede elektron til at udvikle brint.

I denne afhandling anvendes første princip beregninger til at finde foton-absorberende materialer, hvor materialernes båndgab, placering af båndkanten samt materialernes stabilitet i vand bruges som deskriptorer. Ved brug af denne strategi identificeres en håndfuld foton-absorberende materialer, som værende velegnede til brug i foton-assisteret vandspaltning. Derudover undersøges flere muligheder for at optimere et materiales båndgab til brug i forskellige sammenhænge. En række todimensionale metaldichalkogener og metaloxider undersøges til brug som katodematerialer, og flere potentielt brugbare kandidater præsenteres.

Det er nødvendigt at bruge metoder, der giver akkurate første princip energier, for korrekt at beskrive termodynamikken i alle de ovenfor nævnte processer. Derfor undersøges præcisionen af funktionalet med Meta-Generaliseret Gradient Approksimation baseret Bayesiansk fejl-estimation.

List of papers

- Heats of Formation of Folids with Error Estimation: The mBEEF Functional with and without Fitted Reference Energies M. Pandey and K. W. Jacobsen, *Physical Review B 91 (23), 235201 (2015)*

- Two-Dimensional Metal Dichalcogenides and Oxides for Hydrogen Evolution: A Computational Screening Approach M. Pandey, A. Vojvodic, K. S. Thygesen and K. W. Jacobsen, *The Journal of Physical Chemistry Letters 6 (9), 1577-1585 (2015)*

- New Light-Harvesting Materials Using Accurate and Efficient Bandgap Calculations I. E. Castelli, F. Hüser, M. Pandey, H. Li, K. S. Thygesen, B. Seger, A. Jain, K. A. Persson, G. Ceder and K. W. Jacobsen, *Advanced Energy Materials 5 (2) (2015)*

- Band-gap Engineering of Functional Perovskites Through Quantum Confinement and Tunneling I. E. Castelli, M. Pandey, K. S. Thygesen and K. W. Jacobsen, *Physical Review B 91 (16), 165309 (2015)*

Contents

Chapter 1

Introduction

Chemical fuels are the most widely used energy resource due to their high energy density and ease of availability. Additionally, storing chemical fuels and transferring them from one place to another is easier e.g. through pipelines. Therefore, all the above factors made society heavily dependent on them for its energy consumption which is increasing every year. Eventually, the increasing consumption of fossil fuels is leading to increased greenhouse gas emissions. For example, the global CO_2 emission in 2001 was approximately 24.07 gigaton/year (Gt/yr) which is projected to increase to 40.3 Gt/yr by 2050 and 48.8 Gt/yr by the end of 2100 [1]. An increase in CO_2 emission by almost two times in the next three decades will pose a serious threat to the environment. Additionally, the availability of the fossil fuels will also become scarce at some point. Therefore, it is the need of the hour to search for environmentally benign and abundant renewable energy resources.

Renewable energy sources e.g. wind energy, hydro-electricity, solar thermal conversion, solar electricity, solar fuels etc. may serve as viable alternatives to the fossil fuels [2]. Among all renewable energy resources, the biggest source of the renewable energy is our sun and the immense energy it provides can be used to power the whole planet. However, we are very far from realizing the dream of being completely dependent on the sun for our energy requirements. The challenge lies in utilizing the solar energy in an efficient and economical way [1, 2]. However, concerted and continuous efforts by theoreticians and experimentalists are being put in order to overcome these challenges. Figure 1.1 shows a model of the workflow for the materials design with mutual feedback of the experimentalists and theoreticians.

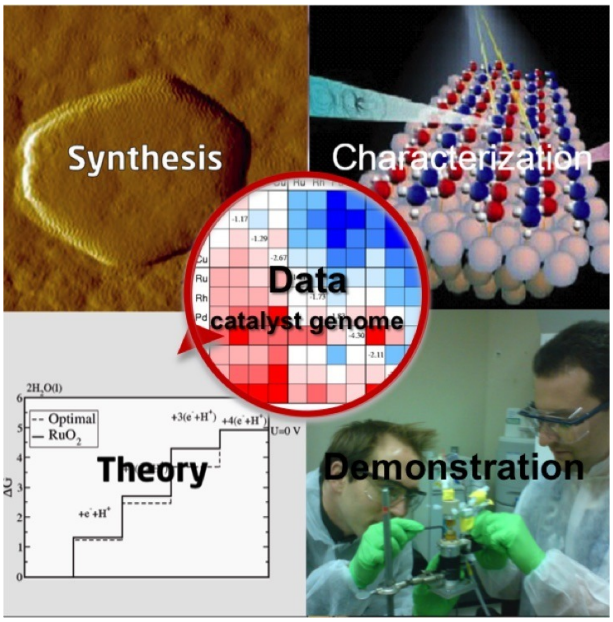

Figure 1.1: Concerted effort of experimentalists and theoreticians. The mutual feedback from each other leads to an efficient materials design and understanding of a given physical/chemical process. Image courtesy: SUNCAT (http://suncat.stanford.edu).

Among many possible ways to utilize solar energy one of the most promising ways is to harvest the solar energy for the photon assisted water splitting. The process proceeds via absorption of sunlight with a semiconducting material and the generated electron-hole pairs can be used to produce hydrogen by splitting the water [3]. Unfortunately, the process is not as simple as it sounds and the main challenge lies in finding a material which can accomplish the whole process of hydrogen evolution efficiently. In order to do so, a material should be able to absorb the sunlight to generate electron-hole pairs and evolve hydrogen at cathode and oxygen at anode using the generated electron and hole respectively. All these criteria are hard to meet by a single material. An additional constraint is also imposed by the abundance and toxicity of different elements going in the workflow of materials design [4]. Because of all the complications involved, even after decades of explorations for a suitable material for photoelectrochemical watersplitting, the best material has not been

found. Additionally, due to limited resources and time a large materials space makes it intractable to find a material experimentally which can carry out the above process. On the other hand, the quantum mechanical calculations on large number of materials can be done with relatively less resources and time. Therefore, inputs are required from the quantum mechanical calculations to accelerate the process of materials design.

This thesis, using first-principle calculations, explores materials for the light absorption using the bandgap, band edge positions and the stability in aqueous conditions as descriptors. This strategy results in handful of materials which can act as good photoabsorbers for the water splitting reaction. Additionally, strategies to tune the bandgap for different applications is also explored. To carry out the cathode reaction, two-dimensional metal dichalcogenides and oxides are explored with suggestion of few potential candidates for the hydrogen evolution reaction.

The thermodynamics of all the above processes requires an accurate description of the energies with first-principle calculations. Therefore, along this line the accuracy and predictability of the Meta-Generalized Gradient Approximation functional with Bayesian error estimation is also assessed.

Chapter 2

Theory

In this chapter a brief description of the electronic structure method is presented. An introduction to the Density Functional Theory (DFT) and the approximations used for the calculations of the energies and the bandgaps is discussed. A condensed overview of the practicalities of the electronic structure calculations is also presented.

2.1 Schrödinger Equation

A complete quantum mechanical description of a system requires the knowledge of an abstract object called the wavefunction. In principle, the wavefunction can be obtained by solving the time dependent Schrödinger equation which can be written as [5]:

$$i\hbar\frac{\partial|\Psi\rangle}{\partial t} = H|\Psi\rangle, \tag{2.1}$$

where $|\Psi\rangle$ and H are the wavefunction and the Hamiltonian of the system respectively. The Hamiltonian holds the information of the total energy of the system that is conserved for a time independent potential. Hence, the stationary state solution to the Schrödinger equation will be a product of the time dependent phase and a time independent part which is nothing but the eigenfunction of the Hamiltonian. Therefore, calculating the stationary state of the Hamiltonian is central to the time independent description of a system.

Since our interest lies in understanding the physical and chemical properties of materials which are governed by the electrons in time independent potential

in most of the cases, it is relevant to consider the time independent Schrödinger equation. The time independent Schrödinger equation in the position basis can be written as [6]:

$$H\Psi(\mathbf{r},\,\mathbf{R}) = E(\mathbf{r},\,\mathbf{R})\Psi(\mathbf{r},\,\mathbf{R}), \tag{2.2}$$

where $E(\mathbf{r},\,\mathbf{R})$ is the eigenvalue of the Hamiltonian of the system and $\mathbf{r}$ and $\mathbf{R}$ represent the electronic and nuclear coordinates. In an expanded form the Hamiltonian can be written as:

$$\begin{aligned} H = &-\sum_{I=1}^{N}\frac{\hbar^2}{2M_I}\nabla_I^2 - \sum_{i=1}^{n}\frac{\hbar^2}{2m_i}\nabla_i^2 + \frac{e^2}{2}\sum_{I=1}^{N}\sum_{J\neq I}^{N}\frac{Z_I Z_J}{|\mathbf{R}_I - \mathbf{R}_J|} \\ &+\frac{e^2}{2}\sum_{i=1}^{n}\sum_{j\neq i}^{n}\frac{1}{\mathbf{r}_i - \mathbf{r}_j} - e^2\sum_{I=1}^{N}\sum_{i=1}^{n}\frac{Z_I}{|\mathbf{R}_I - \mathbf{r}_i|}, \end{aligned} \tag{2.3}$$

where first and second term on the right hand side represent the kinetic energy of the nuclei and electrons respectively, third term corresponds to the nuclear-nuclear Coulomb interaction, fourth term represents the electron-electron Coulomb interaction and the last term is Coulomb interaction between the electrons and nuclei.

Unfortunately, the eigenvalues and eigenfunctions of the full Hamiltonian with coupled electronic and nuclear degrees of freedom can only be obtained for very few simple systems. Therefore, approximations are needed to make the electronic structure problem tractable.

2.1.1 Adiabatic and Born-Oppenheimer approximation

One of the commonly used approximation to decouple the nuclear and electronic degrees of freedom is the adiabatic approximation. It is based on the fact that the ratio of of the mass of the electrons and nuclei is very small, therefore, the electrons instantaneously adjust their wavefunctions if there is a dynamical evolution of the nuclear wavefunctions. In other words, due to the sluggish dynamics of the nuclear wavefunction the electrons are always in a stationary state of the Hamiltonian with the instantaneous nuclear potential. The wavefunction of the system within the adiabatic approximation can be written as [6]:

$$\Psi(\mathbf{R},\mathbf{r},t) = \Theta_n(\mathbf{R},t)\Phi_n(\mathbf{R},\mathbf{r}), \tag{2.4}$$

where n denotes the n^{th} adiabatic state of the electrons, $\Theta_n(\mathbf{R},t)$ represents the nuclear wavefunction and $\Phi_n(\mathbf{R},\mathbf{r})$ denotes the electronic wavefunction.

In the above ansatz, the dependence of electronic wavefunction on the nuclear coordinates gives a correction for the electronic eigenvalues of the order m/M(which comes from applying the kinetic energy operator of the nuclei on the electronic wavefunctions). The small correction of the order m/M when included results to the adiabatic approximation and when neglected gives the so called Born-Oppenheimer approximation. The Born-Oppenheimer approximation results in an electronic Schrödinger equation Hamiltonian which can be written as [6]:

$$\hat{h}_e = -\sum_{i=1}^{n} \frac{\hbar^2}{2m_i}\nabla_i^2 + \frac{e^2}{2}\sum_{i=1}^{n}\sum_{j\neq i}^{n} \frac{1}{\mathbf{r}_i - \mathbf{r}_j} - e^2 \sum_{I=1}^{N}\sum_{i=1}^{n} \frac{Z_I}{|\mathbf{R}_I - \mathbf{r}_i|}.$$

The above approximation simplifies the electronic problem significantly but not sufficiently to make it tractable for complex systems. The complexity mainly arises from the electron-electron interaction term in the electronic Hamiltonian. Density functional theory (DFT) which is discussed in the next section provides an elegant way to solve the electronic structure problem of complex electronic systems.

2.2 Density Functional Theory: An Introduction

The density functional theory came into being from the two theorems by Hohenberg and Kohn which are [7]:
Theorem 1: The electronic density uniquely determines the external potential up to a trivial additive constant.
Theorem 2: The ground state energy of an electron system is a universal functional of the ground state electronic density.

Above theorems make it possible to map an interacting system to a non-interacting electron system with the same electronic density leading to so called Kohn-Sham equations. The non-interacting electron system is much easier to solve since the wavefunction of the system factorizes. The mapping significantly simplifies the electronic structure problem since the electronic density which is dependendent only on three coordinates becomes the central object as opposed to the wavefunction in the Schrödinger equation which has 3N degrees of freedom. The potential which enters the independent particle Hamiltonian can be derived from the total energy of the system if one knows how the energy depends on the electronic density. Kohn-Sham equation for independent

particles can be written as:

$$\left\{-\frac{1}{2}\nabla^2 + v_{ext}(\mathbf{r}) + \int d^3r \frac{n(\mathbf{r})}{|\mathbf{r}-\mathbf{r}'|} + v_{xc}[n](\mathbf{r})\right\}\phi_i(\mathbf{r}) = \epsilon_i\phi_i(\mathbf{r}). \tag{2.5}$$

The first term denotes the kinetic energy operator, second term is the external potential which typically comes from nuclei, third term is the Hartree potential and $v_{xc}[n](\mathbf{r})$ represents the exchange-correlation potential which arises from the antisymmetric and many body nature of the wavefunction. The exchage-correlation potential $v_{xc}[n](\mathbf{r})$ entering the Kohn-Sham equation can be written as:

$$v_{xc}[n](\mathbf{r}) = \frac{\delta E_{xc}}{\delta n(\mathbf{r})}. \tag{2.6}$$

Up to this point no approximations in the Kohn-Sham system has been made, therefore, the formalism in principle is exact. But our ignorance about the exact form of E_{xc} demands approximations to calculate the ground state properties of the system hence deviating us from exactness. Fortunately, the approximations for the exchange-correlation energy make the quantum mechanical treatement of complex materials tractable with a reasonable accuracy. Few of the well know approximations are the local density approximation (LDA) [8], the generalized gradient approximation (GGA) [9], and hybrid functionals e.g. HSE06 [10, 11]. A brief overview of the different approximations is given in the following subsection.

2.2.1 Local (Spin) Density Approximation (L(S)DA) and Generalized Gradient Approximation (GGA)

The local density approximation is the first approximation employed in the density functional theory. It is built using the free electron gas as a model system, and is therefore expected to perform well for systems with reasonably homogeneous charge density. Since its inception it has been widely used and has produced remarkable results. The exchange energy density under the framework of the LDA can be written as:

$$\epsilon_X(n(\mathbf{r}))^{LDA} = -\frac{3}{4}\left(\frac{3}{\pi}\right)^{1/3} n(\mathbf{r})^{1/3}. \tag{2.7}$$

The correlation part has been derived from quantum Monte Carlo calculations and can be found in Ref. [6]. Despite being quite succesful LDA occasionally performs badly especially for the systems having very inhomogeneous charge

density. One might conclude that this behavior arises due to the local nature of the functional. Therefore, a natural way to improve over LDA is to include the gradients of density in the energy functional. The generalized gradient approximation provides such a framework to improve over the LDA functional by an inclusion of the density gradients. The most commonly used functional under the GGA framework is known as PBE functional named after its developers [9]. In the PBE functional the exchange energy density of the LDA is augmented by an enhancement factor which depends on the density and its gradient. The PBE exchange energy can be expressed as:

$$E_X^{GGA} = \int d^3r \epsilon_X(n(\mathbf{r}))^{LDA} F_X(s), \tag{2.8}$$

where $F_X(s)$ denotes the exchange enhancement factor with $s = |\nabla n(\mathbf{r})]/2k_F n(\mathbf{r})$. One of the crucial property that the enhancement factor should have is that in the limit of very small s it should behave in a way that the PBE exchange energy approaches the exchange energy with the LSDA. Keeping this in mind the following expression for $F_X(s)$ has been proposed:

$$F_X(s) = 1 + \kappa - \frac{\kappa}{1 + \mu s^2/\kappa}. \tag{2.9}$$

The inclusion of the exchange enhancement factor in the exchange energy showed significant improvement over the LDA functionals for the systems with significantly varying charge density. Since then the PBE functional has been one of the most widely used functional in electronic structure problems.

2.3 Calculation of Bandgaps with DFT

Despite being quite successful in the prediction of ground state properties of real materials, Kohn-Sham DFT (KS-DFT) has some drawabacks [12]. One of the most commonly known problem with KS-DFT is the systematic underestimation of bandgaps [13]. Over the years, numerous studies have been performed in order to have an understanding of the bandgap problem and at the same time finding its solution. A very thorough study to understand the different sources of the errors in the bandgap prediction has been done in the Ref. [13]. For example, depending on the convexity (concavity) of the functional between the integer particle number, localization (delocalization) leads to too high (low) bandgap predictions for the periodic systems. Therefore, it would be desirable to include an additional localization effect in the concave

functionals (like LDA) whereas employing a delocalization effect in the convex functionals would improve the bandgap predictions.

As explained in Ref. [13] the energy in LDA like functional behave linearly between integer points in periodic systems. Therefore one would expect it to give correct bandgaps. But, the linear behavior has wrong slopes due to which it systematically underestimates the bandgap. To account for the incorrect slopes the correction in the derivative discontinuity can be applied leading to improved prediction of the bandgap. One such functional is the GLLB-SC functional which includes an explicit calculation of the derivative discontinuity. The details of the functional can be found in Ref. [14, 15].

The other method to improve over the LDA/GGA functionals is to incorporate a fraction of Hartree-Fock exchange (or exact exchange) which has a convex behavior. Thus, the Hartree-Fock exchange when added in an appropriate fraction in the LDA exchange gives a reasonable behavior between the integer points of the particle number. Generally, the LDA/GGA functionals having a fraction of exact exchange are called hybrid functionals. Most commonly used hybrid functionals in condensed matter systems are PBE0 and HSE03/HSE06 [10, 11, 16, 17]. A brief introduction to the HSE functional will be provided here since its implementation in GPAW was carried out as a part of this thesis.

2.3.1 A Brief Introduction to the Hybrid Functionals

The PBE0 or HSE functionals have 25 % of exact exchange (at least that is how it started) mixed with 75 % of GGA exchange. The exchange correlation energy in the PBE0 functional can be written as:

$$E_{xc}^{PBE0} = 0.25E_x^{HF} + 0.75E_x^{PBE} + E_c^{PBE}. \tag{2.10}$$

The $(1\ /|r - r'|)$ dependence of HF exchange gives rise to a singularity at r = r'(or q = q' in reciprocal space). Therefore, it is essential to get rid of the singularity to prevent divergence. Additionally, a very high density of k-points is required to resolve the interaction near the singularity.

The singularity problem has been remedied in the HSE functionals by having an additional term which prevents the exchange term from diverging. The HSE functional has many commonalities with the PBE0 functionals. However, in the HSE functional the exchange is screened by a screening parameter as opposed to the PBE0 functional which has a bare (or unscreened) exact exchange. The exchange interaction in the HSE is divided into a short range

and a long range part using the error function and can be written as:

$$\frac{1}{r} = \frac{erfc(\omega r)}{r} + \frac{erf(\omega r)}{r}. \tag{2.11}$$

The above expression shows how the splitting of the exchange interaction is achieved. The first term on the right hand side denotes the short range (SR) exact exchange whereas the second terms denotes the long range (LR) exchange interaction. The strength of the screening is decided by the value of the parameter ω. The final expression for the exchange energy after the splitting can be written as:

$$\begin{aligned} E_x^{HSE} &= 0.25E_x^{HF,SR}(\omega) + 0.25E_x^{HF,LR}(\omega) + 0.75E_x^{PBE,SR}(\omega) \\ &\quad + E_x^{PBE,LR}(\omega) - 0.25E_x^{PBE,LR}(\omega). \end{aligned} \tag{2.12}$$

It turns out that for a range of ω values pertinent for real physical systems, the $E_x^{HF,LR}(\omega)$ term cancels the $-E_x^{PBE,LR}(\omega)$ term. Thus the reduced equation for exchange-correlation energy is:

$$E_{xc}^{HSE} = 0.25E_x^{HF,SR}(\omega) + 0.75E_x^{PBE,SR}(\omega) + E_x^{PBE,LR}(\omega) + E_c^{PBE}. \tag{2.13}$$

From the above equation we can see that the exchange energy has two parts, one is screened HF exchange and the other is screened GGA exchange. The expression for screened exact exchange in the plane-wave basis can be written as [18]:

$$\begin{aligned} V_{\mathbf{k}}(\mathbf{G},\mathbf{G'}) &= \langle \mathbf{k} + \mathbf{G}|\hat{V}_x|\mathbf{k} + \mathbf{G'}\rangle \\ &= -\frac{4\pi e^2}{\Omega}\sum_{m\mathbf{q}} 2w_{\mathbf{q}} f_{\mathbf{q}m} \\ &\times \sum_{\mathbf{G''}} \frac{C^*_{\mathbf{q}m}(\mathbf{G' - G''})C_{\mathbf{q}m}(\mathbf{G - G''})}{|\mathbf{k - q} + \mathbf{G''}|^2} \\ &\times (1 - e^{|\mathbf{k - q} + \mathbf{G''}|^2/4\omega^2}). \end{aligned} \tag{2.14}$$

In the above equation we can see that the exchange term does not have a singularity at $|\mathbf{k - q} + \mathbf{G''}| = 0$. In the HSE06 functional the optimized value of the parameter ω is 0.11 a_0^{-1} (where a_0 is the Bohr radius). The current implementation of HSE in GPAW is non self-consistent in which the GGA and HF exchange interactions are calculated with PBE calculated ground state density and wavefunctions.

2.4 Implementation of DFT in the GPAW (Grid-based Projector Augmented Wave) code

The first step in a practical implementation of DFT is choosing a basis for the expansion of the wavefunctions. There are wide variety of bases and one is preferred over the other depending on the kind of the calculations. In the current version GPAW has plane wave, grid and linear combination of atomic orbitals (LCAO) as basis sets [19, 20]. In principle, one can solve the all electron problem without making any approximation for the core electrons, but that is not usually the case. Since for most of the applications the valence electrons govern the behavior of materials, its desirable to make approximations for the core electrons in order to make the calculations computationally less demanding. Many codes use pseudopotential in which the core electrons act as mere spectators and provide an effective potential to the valence electrons [21]. One of the drawbacks of the pseudopotential method is that one completely looses the information of the core electrons which might be required in few cases. In order to circumvent this issue with the pseudopotentials, Blöchl proposed the projector augmented wave (PAW) method [22].

2.4.1 A Brief Introduction to the PAW Method

The oscillatory behavior of the wavefunctions in the core regions requires large number of basis functions for the expansion, therefore, making the calculations computationally demanding. In the Blöchl formalism a linear transformation is applied to an auxilliary smooth wavefunction in order to obtain the full all electron Kohn-Sham (KS) wavefunction. The operation can be written as [23]:

$$|\psi_n\rangle = \mathcal{T}|\tilde{\psi}_n\rangle, \tag{2.15}$$

where $|\psi_n\rangle$ and $|\tilde{\psi}_n\rangle$ are the true and auxilliary wavefunctions respectively. One of the properties required by the transformation operator is that it should not affect the wavefunction outside a given cutoff radius. The above requirement is due the similar nature of the true wavefunction and the auxilliary wavefunction outside the cutoff radius. Therefore $\mathcal{T}$ can be written as:

$$\mathcal{T} = I + \sum_a \mathcal{T}^a, \tag{2.16}$$

a denotes the atom index and with the expression above the $\mathcal{T}^a$ does not have any effect outside the cutoff radius. The true wavefunction inside the augmentation sphere can be expanded in terms of the partial waves and the partial

waves can be be obtained by the application of the transformation operator on the auxilliary smooth partial waves. The above steps along with the completeness of the smooth partial waves give the expression of the transformation operator which then can be used to get the full KS wavefunction. Thus, by the this approach one always have the access to the full wavefunction.

Chapter 3

Heats of Formation of the Solids

3.1 Introduction

In the last chapter a brief description about the density functional theory (DFT) was provided with a short introduction to the different functionals and their accuracy. In this chapter, one of the application of DFT is looked at i.e. the calculation of heats of formation of the solid compounds with different functionals particularly focussing on the accuracy of their predictions.

The accuracy of the energetics of a thermodynamic process obtained with the different functionals depends on the fortuituous cancellation of errors. However, if the nature of species on the different side of a reaction differs significantly then the cancellation of errors may not be complete thus leading to an inaccurate energetics. For example, one of the most basic reaction is the formation of the solids from the elements in their reference state. In this case the chemical environment of the solid formed is very different from the chemical environment of the elemental phases. In cases like these the cancellation of errors may not be complete thus ending up giving inaccurate results [24]. The same reason renders standard LDA/GGA to give the heat of formation of the solids deviating from experiments by $\sim$0.25 eV per atom [25]. Therefore, large errors in the prediction of the heats of formation may not be appropriate in situations like large scale screening of materials where thermodynamic stability is one of the main criterion for the existence of the compounds [26, 27]. Hence, in order to get greater accuracy higher level methods are required. On

the other hand, most of the higher level methods are computationally quite expensive and cannot be used for large scale computations.

Recently a method has been proposed by Stevanovic *et al.* which uses the experimental heats of formation and DFT total energies to fit the elemental reference energies in order get better prediction for the standard heats of formation [28, 25]. In the work by Stevanovic *et al.* DFT+U [29] has been used with non-zero U for the transition metals. However, in our work we find that the other functionals like PBE [9], RPBE [30] and TPSS [31, 32, 33, 34, 35] give similar prediction as PBE+U after fitting the reference energies. Surprisingly TPSS being a meta-GGA does not improve the prediction and has similar error as the standard GGA functionals. But, the recently developed Bayesian error estimation meta-GGA functional known as mBEEF improves the predictions significantly. Additionally, it provides the uncertainties in the formation energies as well thus giving the information of the trust radius of the results. The details of the mBEEF functional can be found in the Ref. [36].

3.2 Calculation of the heats of formation without the fitting

The heat of formation of a solid calculated with DFT can be written as:

$$\Delta H^{DFT}(A_{p1}B_{p2}..) = E(A_{p1}B_{p2}..) - \Sigma p_i \mu_i^0, \tag{3.1}$$

where $E(A_{p1}B_{p2}..)$ indicates the total energy of $A_{p1}B_{p2}..$ calculated with DFT and the μ_i^0 denotes the chemical potentials of the elements under standard conditions calculated with DFT. The entropic and zero point corrections have been ignored in the expression above.

For the current work, a set of 257 compounds has been selected to compare different functionals for the calculation of heats of formation. Compounds have been selected to ensure that the space of relevant elements is spanned. Figure 3.1 (a), (c), (e), (g) and (i) show the calculated heats of formation versus the experimental values for the different functionals. The figure indicates that the RPBE functional deviates the most from the experimental values, which is also expected since the functional parameters have been fitted to give accurate adsorption energies which makes it a bit worse for the prediction of the bulk properties. Additionally, PBE, PBE+U and TPSS give similar predictions thus TPSS despite being meta-GGA does not perform better than the functionals at the GGA level. Therefore, before any fitting of the experimental values, mBEEF outperforms other functionals in the predictions with

significantly lower mean absolute error (MAE) and standard deviation (σ). It can also be seen that the experimental values are within the uncertainties predicted by the mBEEF ensemble.

3.3 Calculation of the heats of formation with the fitting

As mentioned before, the different chemical environment of the multinary compounds and the reference phases leads to an incomplete error cancellation in calculating the energy differences i.e. the heats of formation. This behavior was manifested in the predictions in the previous section which was based on the DFT reference energies of the elemental phases. Fitted elemental reference phase energy (FERE) method [25] solves this problem to some extent by adding corrections to the DFT reference energies. The value of the corrections is calculated by minimizing the root mean square (RMS) error of the predicted and the experimental values. The FERE heats of formation can be expressed as:

$$\begin{aligned}\Delta H^{FERE}(A_{p1}B_{p2}..) = E(A_{p1}B_{p2}..) \\ -\Sigma p_i(\mu_i^0 + \delta\mu_i^0),\end{aligned} \tag{3.2}$$

The only difference between the equation above and the equation (3.1) is the term $\delta\mu_i^0$ which denotes the correction to reference energy of the elemental phase.

As mentioned before, a dataset of 257 compounds has been chosen for experimental heats of formation, [25, 37] on the other hand, the number of elements relevant for this work is limited to 62. Therefore, the calculation of the corrections involves solving an overdetermined set of equations which can be done by minimizing the RMS error $\sqrt{\sum_i(\Delta H^i_{Expt.} - \Delta H^i_{DFT})^2}$. Few points have to be kept in mind while fitting the reference energies, for example, a reasonable size of the dateset should be taken to avoid over- or under-fitting and the quality of the fit should be validated on a test dataset which has compounds not used in the fitting procedure.

The calculated heats of formation with the FERE procedure applied to the different functionals is shown in the Figure 3.1 (b), (d), (f), (h) and (j). As can be seen from the figure, different functionals clearly improve the predictions when augmented with the FERE procedure. After the fitting procedure is applied all the functionals give similar predictions with almost same MAE and σ. It is worth noticing that the mBEEF predictions before the fitting

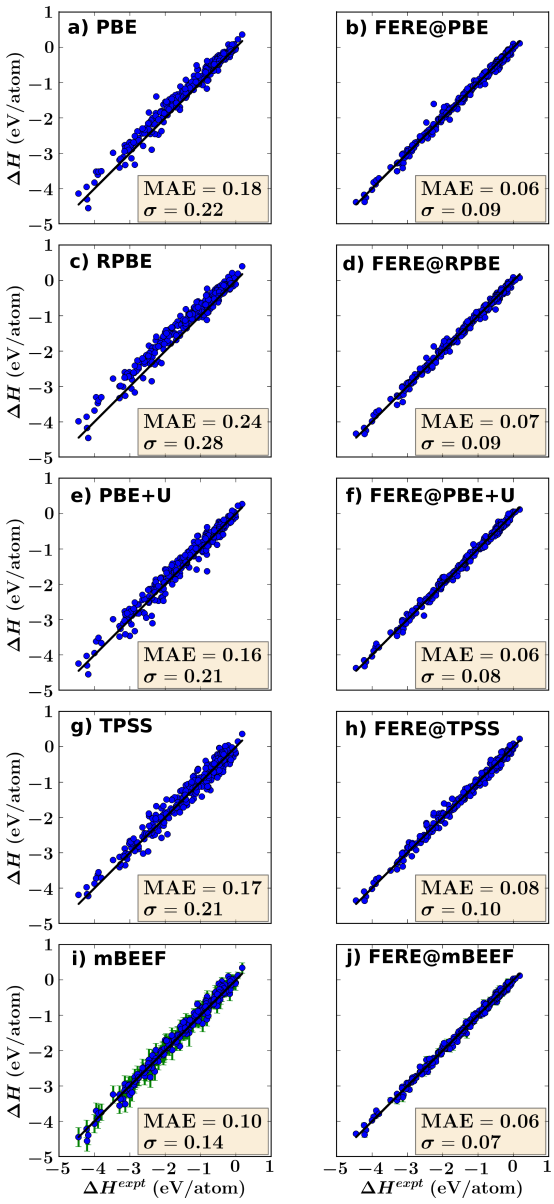

Figure 3.1: (a), (c), (e), (g) and (i) show the calculated heats of formation with different functionals. The mean absolute error (MAE) and the standard deviation (σ) of the the difference of the calculated heats of formation and the experimental values is also shown in the plots. The black line shows the experimental heat of formation. The figure has been taken from the Paper-1.

is not too off from the predictions of the other functionals after the fitting. A possible reason for the better predictions of the mBEEF functional is the fitting of the parameters of the functional to different experimental dataset [36]. Additionally, the reduced uncertainties in the Figure 3.1 (j) results from fitting the ensemble as well to the experimental heats of formation. The individual heats of formation with the mBEEF functional with and without the fitting is shown in the Table 1 of the Paper-1.

3.4 Outliers in the different predictions

The statistical quantity σ indicates that there must be some predictions which deviate from the actual value (in the present case, the experimental values) by more than of the order of σ [38] and these predictions are called outliers. A commonly used measure to call a prediction as an outlier is the value of 2σ which puts 95 % confidence in the results lying within the width of 2σ. Based on this criterion, outliers selected for different functionals without and with the FERE are shown in the Table 3.1. and 3.2

Table 3.1 shows that the PBE and RPBE have common outliers to some extent whereas the PBE+U, TPSS and the mBEEF functional have none or very few common outliers. The feature in the Table 3.1 worth noticing is that in a few cases all the functionals except mBEEF deviate from the experiments significantly, for example, in the PBE, RPBE, PBE+U and TPSS, deviation is as high as 0.85, 0.66, 0.82 and 0.57 eV respectively whereas the maximum deviation in the mBEEF prediction is 0.41 eV. Therefore, even without the FERE the mBEEF predictions do not significantly deviate from the experimental values.

Table 3.2 shows the predictions after the fitting procedure has been applied. As expected the magnitude of the deviation from the experimental heats of formation decreases after employing the fitting. On the other hand, it can also be seen from the table that the nature of the outliers significantly changes after the fitting has been applied which is expected in a fitting model since the datapoints contributing to large errors get penalized more. Additionally, the common feature of a large variation in the nature of the outliers before and after the fitting rules out the possibility of the experimental errors to some extent and rather puts more weight to the limitations of the functionals.

Table 3.1: Outliers in the calculations without using the FERE scheme. The compounds exhibiting deviations of the calculated heats of formation from the experimental values by more than 2σ have been identified as outliers. The values of σ for the different functionals are shown in Fig. 3.1. δH denotes the difference between calculated and experimental heats of formation. Table has been taken from the Paper-1.

PBE	δH_{PBE}	RPBE	δH_{RPBE}	PBE+U	δH_{PBE+U}	TPSS	δH_{TPSS}	mBEEF	δH_{mBEEF}
Al_2O_3	0.48	Al_2O_3	0.69	Al_2O_3	0.48	AlP	0.45	AuF_3	-0.30
BaS	-0.52	FeF_2	0.61	BaS	-0.52	BaI_2	-0.48	CaF_2	-0.35
BaO	-0.47	FeO	0.60	BaO	-0.47	$BiBr_3$	-0.51	CdF_2	-0.34
FeF_2	0.61	GaN	0.57	CrS	-0.82	CaS	0.48	Cu_2Se	0.31
FeO	0.49	HfO_2	0.65	CrF_3	-0.47	FeF_2	0.57	FeSe	0.35
GaS	0.45	NiF_2	0.66	Cr_2O_3	-0.75	GaP	0.43	GaN	0.33
LaN	0.46	-	-	GaN	0.42	Ga_2S_3	0.44	Ga_2S_3	0.37
MnS	0.60	-	-	Ga_2S_3	0.44	NiF_2	0.57	GaS	0.41
NiF_2	0.85	-	-	GaS	0.45	$PbBr_2$	-0.45	GeSe	0.37
-	-	-	-	Ge_4O_8	0.42	$SrBr_2$	-0.49	Ge_4O_8	0.29
-	-	-	-	MnS	-0.48	SrI_2	-0.55	NbF_5	-0.38
-	-	-	-	Mn_3O_4	-0.42	ZnS	0.43	OsO_4	-0.30
-	-	-	-	V_2O_3	-0.42	ZrS_2	0.47	PbF_2	-0.31
-	-	-	-	-	-	-	-	SnO_2	0.28
-	-	-	-	-	-	-	-	TiN	-0.30

Table 3.2: Outliers in the calculations using the FERE scheme. The compounds exhibiting deviations of the calculated heats of formation from the experimental values by more than 2σ have been identified as outliers. The values of σ for the different functionals are shown in Fig. 3.1. δH denotes the difference between calculated and experimental heats of formation. Table has been taken from the Paper-1.

PBE	δH^{FERE}_{PBE}	RPBE	δH^{FERE}_{RPBE}	PBE+U	δH^{FERE}_{PBE+U}	TPSS	δH^{FERE}_{TPSS}	mBEEF	δH^{FERE}_{mBEEF}
CuF_2	0.22	CuF_2	0.23	CoS	0.20	$BaCl_2$	0.24	CaF_2	-0.18
FeF_2	0.33	FeF_2	0.27	Co_3O_4	-0.23	CaS	0.21	CdF_2	-0.18
FeSe	-0.19	MnO_2	-0.21	CrO_2	0.17	CsF	-0.23	Co_3O_4	-0.19
MnO_2	-0.25	NbF_5	-0.32	Fe_2O_3	-0.17	FeF_2	0.29	Fe_2O_3	-0.17
NbF_5	-0.29	Ni_3S_2	-0.18	GaF_3	0.16	KCl	0.32	FeF_2	0.19
Ni_3S_2	-0.21	NiF_2	0.38	GeO_2	0.20	NbF_5	-0.26	GaP	-0.16
NiF_2	0.65	PbF_2	-0.18	MgF_2	0.19	NiF_2	0.37	KF	-0.17
RuO_4	-0.19	RuO_4	-0.33	NbF_5	-0.23	RbI	0.25	Li_3Sb	0.18
TaF_5	-0.22	TaF_5	-0.24	SnO_2	0.17	SrS	0.25	MgO	-0.15
ZrSi	-0.24	ZrSi	-0.26	TaF_5	-0.18	SrI_2	-0.24	MgF_2	0.17
ZrS_2	0.26	ZrS_2	0.24	TiN	-0.19	TlI	0.26	MnO_2	-0.16
-	-	-	-	VN	0.26	ZrSi	-0.24	NbF_5	-0.20
-	-	-	-	V_2O_3	-0.36	ZrS_2	0.35	TiN	-0.17
-	-	-	-	ZnF_2	0.19	-	-	ZnF_2	0.18
-	-	-	-	ZrS_2	0.16	-	-	ZrS_2	0.16

3.5 True versus predicted error in the mBEEF functional

As previously shown in the Figure 3.1 in most of the cases the experimental values lie within the predicted uncertainties by the mBEEF functional with slight overestimation (large errorbars) of the predicted errors. However, the size of uncertainties decreased significantly with the FERE. Therefore, in order to understand the distribution of error before and after the fitting a histogram of the true error (ΔH_{mBEEF} - $\Delta H_{Expt.}$ and ΔH^{FERE}_{mBEEF} - $\Delta H_{Expt.}$) divided by the predicted error (σ_{BEE} and σ^{FERE}_{BEE}) is plotted in the Figure 3.2. The histogram is a running average calculated as [38]:

$$P(\frac{1}{2}[x_i + x_{i+J}]) \approx \frac{J}{N(x_{i+J} - x_i)}, \tag{3.3}$$

with x_i as the statistical quantity plotted in the histogram and an intermediate value 20 for the parameter J has been chosen.

If the predicted error matches exactly the true error then one would expect that the distribution would be a Gaussian of unit width (shown in green in the figure). However, in the Figure 3.2 this is not the case. As also noticed before, the tendency of the mBEEF to overestimate the errors in manifested in the large peak around zero in (a) which renders the mBEEF to have most of the experimental values lie within the uncertainties.

However, with the FERE the distribution flattens out and becomes closer to the unit Gaussian implying that the real and the predicted error are close. The tail in the histogram indicates those cases where the predicted error is smaller than the actual error. This is a fairly common feature of the ensemble approach [39].

3.6 Cross validation

As pointed out before, the fitting model should be such that the data is neither overfitted nor underfitted. Therefore, it is of utmost importance that the quality of the fit is tested on a dataset (also called as test set) which is not included in the fitting dataset (also called as training set). A good quality fit should provide a reasonable prediction on a new dataset. A point worth noticing in the current fitting scheme is that only binary compounds have been used in fitting dataset, therefore good predictions are expected for the new binary compounds. Additionally, reasonable predictions can be expected

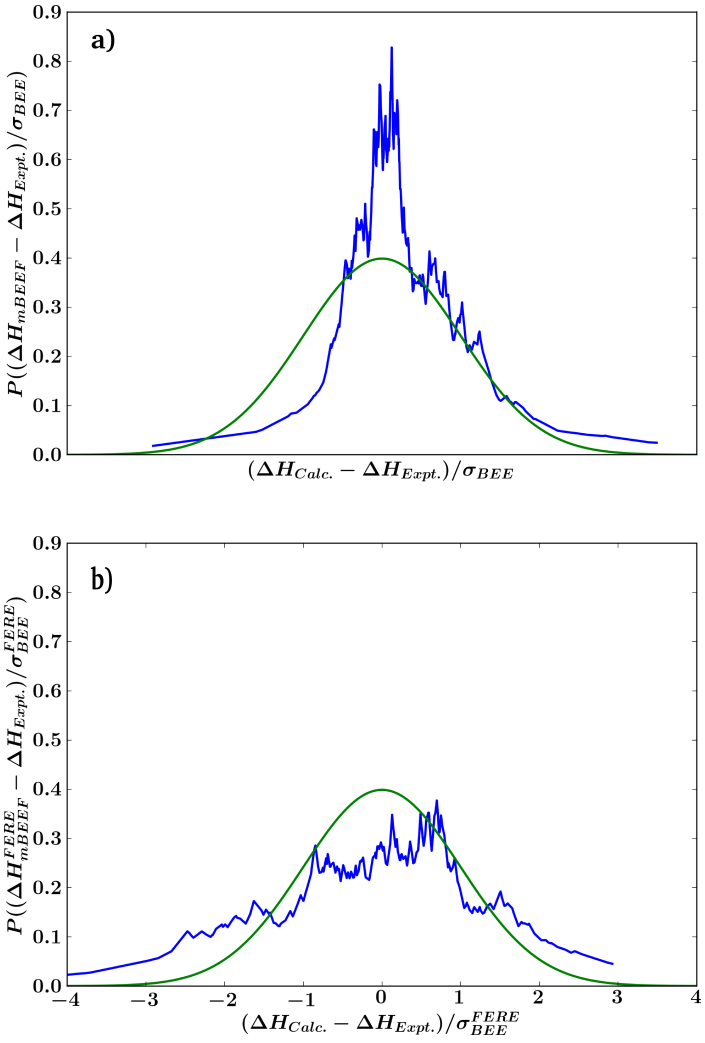

Figure 3.2: (a) shows the histogram of the true error divided by the predicted error before the fitting (b) shows the histogram of the true error divided by the predicted error after the fitting. The figure has been taken from the Paper-1.

for ternary/tertiary compounds only if their chemical environment does not differ significantly from the compounds used in the fitting procedure. Hence, a test set containing a mix of binary and ternary compounds has been selected for the validation of the fitting.

Table 3.3 and 3.4 show the heats of formation of the test set without and with the fitting respectively. The clear decrease in the MAE and σ shows the absence of overfitting. As expected in any regression scheme, the improvement with the fitted model is not as much as the improvement seen in the training dataset.

In the test set also, the mBEEF predictions without the fitting has the same quality as the other functionals with the fitting and the improvement with the fitting is only moderate in the case of the mBEEF. Therefore, a reasonable prediction with the mBEEF can be obtained even without using the fitting with only negligibly increased computational cost as compared to other GGAs.

3.7 Conclusion

The rapidly growing area of the computational screening of the energy materials requiring reasonable predictions of the stability has led forward this work. The synergetic use of the DFT total energies and the experimental heats of formation provides a framework to improve the predictions. Originally, the scheme was developed for the PBE+U functionals but in this work similar improvements has been seen for the other functionals like PBE, RPBE, TPSS and mBEEF as well.

We see that the recently developed mBEEF functional which has been optimized using variety of experimental dataset gives better predictions as compared to the other functionals. Additionally, the mBEEF functional also provides reasonable estimate of the uncertainties in the predictions, the feature which other functionals used in this work lack. However, the uncertainties estimated by the mBEEF ensemble is in general overestimated which can further be reduced by using the FERE scheme along with the reduction of the true error as well.

Despite giving improved results FERE scheme has some drawbacks as well. The corrections are primarily based on nature of the bonding environment in the training set, therefore, it may not significantly improve the predictions for the systems differing from the systems used in the training set, for example, in metal alloys which have significantly different chemical environment than the semiconductors used in the training set. Therefore, higher level functionals

Table 3.3: Heats of formation of test dataset with different functionals without the fitting. All the energies are in eV/atom. Table has been taken from the Paper-1.

Compound	$\Delta H_{Expt.}$	ΔH_{PBE}	ΔH_{RPBE}	ΔH_{PBE+U}	ΔH_{TPSS}	ΔH_{mBEEF}
$AgNO_3$	-0.26	-0.40	-0.31	-0.53	-0.47	-0.60 ± 0.22
$AlPO_4$	-2.99	-2.71	-2.58	-2.71	-2.86	-2.97 ± 0.19
$BeSO_4$	-2.16	-1.99	-1.83	-1.99	-2.09	-2.19 ± 0.16
BiOCl	-1.27	-1.26	-1.11	-1.26	-1.62	-1.26 ± 0.16
$CdSO_4$	-1.61	-1.42	-1.27	-1.42	-1.53	-1.59 ± 0.17
$CuCl_2$	-0.76	-0.51	-0.32	-0.70	-0.80	-0.74 ± 0.21
$TiBr_3$	-1.42	-1.24	-1.23	-1.52	-1.71	-1.37 ± 0.08
$NaClO_4$	-0.66	-0.54	-0.41	-0.54	-0.67	-0.63 ± 0.15
$CaSO_4$	-2.48	-2.24	-2.06	-2.24	-2.37	-2.40 ± 0.17
Cs_2S	-1.24	-1.01	-0.92	-1.01	-1.47	-1.16 ± 0.18
$CuWO_4$	-1.91	-1.59	-1.41	-1.76	-1.72	-1.68 ± 0.21
PbF_4	-1.95	-2.13	-2.05	-2.13	-2.26	-2.32 ± 0.23
$MgSO_4$	-2.22	-1.97	-1.79	-1.97	-2.09	-2.16 ± 0.16
SrSe	-2.00	-2.04	-1.98	-2.04	-2.76	-2.29 ± 0.16
$NiSO_4$	-1.51	-1.11	-0.96	-1.35	-1.23	-1.42 ± 0.23
$FeWO_4$	-1.99	-1.73	-1.58	-2.01	-1.87	-1.84 ± 0.21
GeP	-0.11	+0.04	+0.09	+0.04	-0.19	+0.14 ± 0.08
VOCl	-2.10	-1.79	-1.68	-2.45	-2.07	-2.11 ± 0.24
$LiBO_2$	-2.67	-2.42	-2.30	-2.42	-2.57	-2.58 ± 0.17
$NaBrO_3$	-0.69	-0.52	-0.41	-0.52	-0.71	-0.60 ± 0.13
$CoSO_4$	-1.53	-1.09	-0.95	-1.43	-1.24	-1.40 ± 0.23
$PbSeO_4$	-1.05	-0.94	-0.81	-0.94	-1.13	-1.04 ± 0.16
Mn_2SiO_4	-2.56	-1.83	-1.77	-2.58	-2.01	-2.29 ± 0.23
$ZnSO_4$	-1.70	-1.37	-1.20	-1.37	-1.47	-1.53 ± 0.16
MAE		0.24	0.35	0.16	0.20	0.12
σ		0.28	0.39	0.19	0.26	0.16

are required to improve the description at the electronic structure level and thereby making the FERE scheme unnecessary and the mBEEF functional seems to be promising in that direction.

Table 3.4: Heats of formation of test dataset with different functionals with the fitting. All the energies are in eV/atom. Table has been taken from the Paper-1.

Compound	$\Delta H_{Expt.}$	ΔH^{FERE}_{PBE}	ΔH^{FERE}_{RPBE}	ΔH^{FERE}_{PBE+U}	ΔH^{FERE}_{TPSS}	ΔH^{FERE}_{mBEEF}
$AgNO_3$	-0.26	-0.58	-0.67	-0.68	-0.45	-0.63 ± 0.16
$AlPO_4$	-2.99	-2.95	-2.97	-2.94	-3.02	-3.03 ± 0.07
$BeSO_4$	-2.16	-2.22	-2.23	-2.21	-2.19	-2.25 ± 0.11
BiOCl	-1.27	-1.25	-1.20	-1.23	-1.32	-1.23 ± 0.09
$CdSO_4$	-1.61	-1.61	-1.62	-1.60	-1.60	-1.63 ± 0.12
$CuCl_2$	-0.76	-0.75	-0.60	-0.84	-0.79	-0.81 ± 0.07
$TiBr_3$	-1.42	-1.38	-1.39	-1.61	-1.38	-1.43 ± 0.05
$NaClO_4$	-0.66	-0.76	-0.77	-0.73	-0.68	-0.65 ± 0.16
$CaSO_4$	-2.48	-2.41	-2.41	-2.41	-2.46	-2.43 ± 0.12
Cs_2S	-1.24	-1.27	-1.24	-1.33	-1.97	-1.23 ± 0.06
$CuWO_4$	-1.91	-1.62	-1.60	-1.75	-1.65	-1.71 ± 0.07
PbF_4	-1.95	-2.19	-2.19	-2.11	-2.24	-2.13 ± 0.08
$MgSO_4$	-2.22	-2.22	-2.21	-2.21	-2.20	-2.24 ± 0.10
SrSe	-2.00	-2.25	-2.26	-2.29	-2.66	-2.29 ± 0.05
$NiSO_4$	-1.51	-1.35	-1.36	-1.54	-1.33	-1.50 ± 0.11
$FeWO_4$	-1.99	-1.81	-1.81	-1.94	-1.86	-1.89 ± 0.06
GeP	-0.11	-0.01	+0.03	-0.05	-0.28	-0.02 ± 0.07
VOCl	-2.10	-1.97	-1.98	-2.41	-2.05	-2.12 ± 0.07
$LiBO_2$	-2.67	-2.61	-2.61	-2.58	-2.64	-2.61 ± 0.05
$NaBrO_3$	-0.69	-0.74	-0.76	-0.72	-0.69	-0.66 ± 0.11
$CoSO_4$	-1.53	-1.30	-1.34	-1.56	-1.31	-1.43 ± 0.11
$PbSeO_4$	-1.05	-1.07	-1.09	-1.06	-1.07	-1.08 ± 0.09
Mn_2SiO_4	-2.56	-2.17	-2.19	-2.38	-2.10	-2.25 ± 0.08
$ZnSO_4$	-1.70	-1.61	-1.61	-1.61	-1.60	-1.62 ± 0.11
MAE		0.12	0.13	0.11	0.15	0.09
σ		0.16	0.17	0.15	0.25	0.14

Chapter 4

Hydrogen Evolution from Two-Dimensional Materials

4.1 Introduction

Storage of energy in the form of chemical bonds is one of the most used and efficient way of storing the energy. Transferring energy from one place to other in form of chemical bonds is easier as compared to the other means such as electricity. On the other hand, the deteriorating environmental conditions due to the excess burning of the petroleum fuels needs our attention to look for the alternative forms of chemical energy not having deleterious effect on the environment. One such fuel is hydrogen which can be used in the fuel cells thus involving no emission of greenhouse gas whatsoever [40, 41]. However, a cheap and efficient way of producing hydrogen has not been realized yet [42, 43, 44]. One of the bottleneck to reduce the cost of hydrogen production is the use of expensive catalysts like Platinum a cheaper and efficient alternative of which has not been found yet. Recent theoretical and experimental investigations of the bulk Ni_2P for hydrogen evolution reaction (HER) show promising results and hopefully in the future will serve as a viable alternative to Platinum for the HER [45, 46, 47].

Additionally, over the last few years, two-dimensional (2D) MoS_2 has been explored for its activity towards the HER with some promising results [48, 49, 50, 51, 52]. The initial effort of the MoS_2 research was focussed on the edges of the 2H structure of the MoS_2 nanoparticle having metallic character as opposed to the semiconducting states on the basal plane [53, 54]. Unfor-

tunately, relatively limited number of active sites on the edges gives very low exchange current density for the HER. However, recent experiments on the other polymorph of the MoS_2 and WS_2 known as 1T structure demonstrated the activity of the basal plane for the HER thus giving access to relatively larger number of active sites [49, 48, 50]. Additionally, the difference in energy of the 1T and 2H phase MoS_2 or WS_2 decreases as the dimensionality of the system is reduced from three (bulk) to two (monolayer) thus making it feasible to synthesize the HER active metastable phase in the 2D form [55]. The different activity of the 2H and 1T phase broadens the materials space for HER which is the basis of this work. In this work, the basal planes of 100 different metal dichalcogenides and oxides have been explored in both the 2H and 1T structure for the HER. Primarily, criterion of stability of the material with respect to the standard reference phases and other competing phases and the free energy of the hydrogen adsorption on the basal plane has been used as descriptors for the screening of materials for the HER.

4.2 Details of the atomic structure

The 2H and 1T structures differ by the arrangement of the chalcogen/oxygen atom around the metal atoms. The 2H structure has prismatic arrangement of the chalcogen/oxygen atoms around the metal atom whereas in the 1T structure they are octahedrally arranged. The 2H and 1T structures are shown in the Figure 4.1 (a) and (f) respectively. The black square represents the unit cell of the structures. Other structures shown in the 2H and 1T class are the distorted derivatives of the 2H and 1T structures. The distorted structures have been broadly classified based on their symmetry group which have been identified using certain cutoff for the rotations/translations to account for the residual forces in the structures. In order to identify the the distorted structures, atoms are slightly displaced from their symmetric position in a bigger unit cell in order to break the symmetry of the structure and then the relaxation is performed.

The above procedure captures all the distortions if any in the 2×2 unit cell. There might be other distortions in the larger unit cell but those cases have not been considered here. Fortunately, the charge density wave (CDW) structures in compounds like TiS_2 [56, 57] distorted structure of MoS_2, WS_2 etc. [58, 59], exhibiting quantum spin Hall effect (QSH) and the distortions in ReS_2 [60] are captured by the above procedure thus supporting our results. However, the choice of 0.01 eV/atom for the threshold of energy to differentiate between the symmetrical and the distorted structure categorize TiS_2 as symmetrical

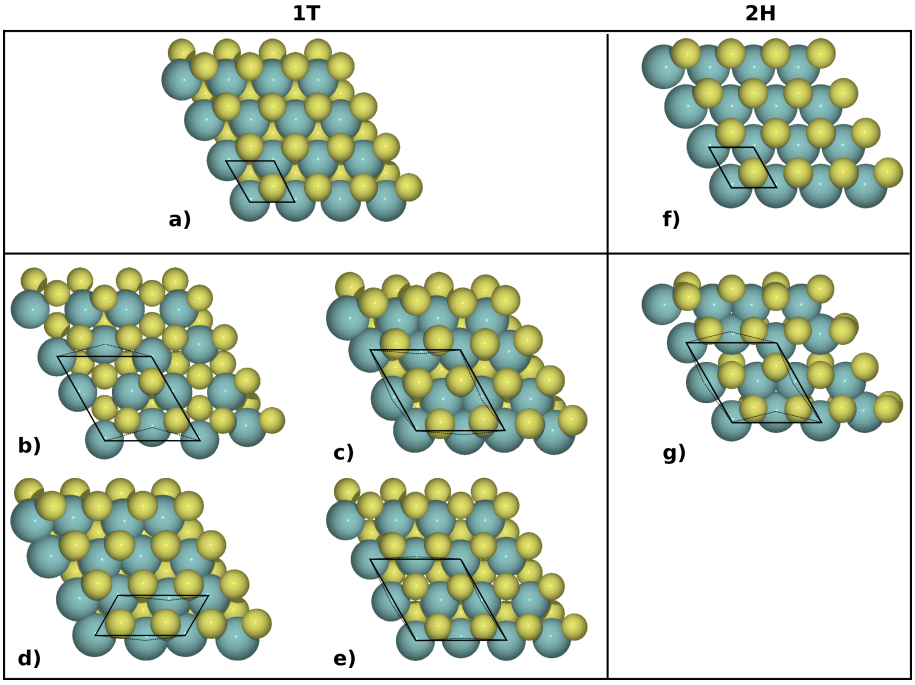

Figure 4.1: (a), (f) show the 1T undistorted 1T and 2H structures respectively. Yellow spheres represent the chalcogen atoms and the cyan spheres represent the metal atoms. (b) - (e) show the distortions in the 1T structure. The unit cell of the distorted structure is shown with black solid lines and the distortion of the atoms from their ideal symmetric position is shown with black dotted lines. (g) represents the distorted 2H structure with a similar description as above. The figure has been taken from the Paper-2.

structure. But, it turns out that the CDW structure of the TiS_2 and the symmetrical structure are very close in energy having the difference of the order of 0.005 eV/atom and surprisingly these differences are captured with the above procedure. On the other hand, the adsorption energy of the hydrogen is similar on the symmetrical and the distorted structure in the case of CDW structures, therefore, they have been categorized as symmetrical for consistency due to the threshold of 0.01 eV/atom. Table 4.1 summarizes the results for the distorted structures which are classified based on the space group (based on Herman-Maugin notation) of the distorted structure and the size of the reduced unit cell capturing the distortion. Symmetry analysis for the classification has been performed using the tool given in Ref. [61]. The cutoff of of 0.05 Å on the rotations/translations has been used in order to allow for inaccuracies or residual forces.

Table 4.1: Classification of different compounds exhibiting distortions based on the space group (based on Herman-Maugin notation) of the distorted structure and the size of the reduced unit cell capturing the distortions.

Class	MX_2	Group	Unit cell	Class	MX_2	Group	Unit cell
2H	CoS_2	P1	2×2	2H	$CoSe_2$	P1	2×2
2H	IrS_2	P1	2×2	2H	OsS_2	P1	2×2
2H	$OsSe_2$	P1	2×2	2H	PdS_2	P1	2×2
2H	$PdSe_2$	P1	2×2	2H	$PdTe_2$	P1	2×2
2H	ReO_2	P1	2×2	2H	ReS_2	P1	2×2
2H	$ReSe_2$	P1	2×2	2H	RhS_2	P1	2×2
2H	$RhSe_2$	P1	2×2	2H	$RhTe_2$	P1	2×2
2H	RuO_2	P1	2×2	2H	RuS_2	P1	2×2
2H	$RuSe_2$	P1	2×2	2H	ScS_2	P1	2×2
2H	$ScSe_2$	P1	2×2				
1T	CoS_2	P1	2×2	1T	CrS_2	P1	2×2
1T	$CrSe_2$	P1	2×2	1T	FeS_2	P1	2×2
1T	IrS_2	P1	2×2	1T	$IrSe_2$	P1	2×2
1T	ReO_2	P1	2×2	1T	$ReTe_2$	P1	2×2
1T	RhS_2	P1	2×2	1T	RuS_2	P1	2×2
1T	$RuTe_2$	P1	2×2	1T	MoO_2	P1	2×1
1T	MoS_2	P1	2×1	1T	$MoSe_2$	P1	2×1
1T	$MoTe_2$	P1	2×1	1T	OsS_2	P1	2×1
1T	$OsSe_2$	P1	2×1	1T	$OsTe_2$	P1	2×1
1T	WS_2	P1	2×1	1T	WSe_2	P1	2×1
1T	WTe_2	P1	2×1	1T	ReS_2	$P\bar{1}$	2×2
1T	$ReSe_2$	$P\bar{1}$	2×2	1T	$RuSe_2$	$P\bar{1}$	2×2
1T	TaO_2	$P\bar{1}$	2×2	1T	$CoSe_2$	P3m1	2×2
1T	$IrTe_2$	P3m1	2×2	1T	NbO_2	P3m1	2×2
1T	OsO_2	P3m1	2×2	1T	$RhSe_2$	P3m1	2×2
1T	RuO_2	P3m1	2×2	1T	WO_2	P3m1	2×2

4.3 Stability with respect to the standard states

In the last chapter, the standard heat of formation of the compounds was discussed. It has to be negative for a compound if the compound has to be stable with respect to the standard states of the constituent elements. Therefore, as a first step the calculation of the heat of formation of the compounds has been performed for all the 2D materials explored here. The heatmap in the Figure 4.2 shows the heats of formation of the compounds in the 2H and 1T structure and the difference in energy of the two structures. The figure shows that a significant fraction of the compounds have positive heats of formation thus unstable [62]. Figure 4.2 (c) shows the difference in energies of the 2H and 1T structure. The figure clearly shows that in most of the cases the 2H and 1T structures are energetically very close. One of the important implication of the two structures having similar energy is that the HER active phase can be synthesized and stabilized under normal condition with suitable synthetic routes and the same fact has been realized in the case of MoS_2 and WS_2 [50, 48]. However, an ideal situation would be that the HER active phase is the most stable phase. But, if that is not the case then a small degree of metastability would make it feasible to synthesize the HER active phase. As a side note, since the standard heat of formation by definition is the stability with respect to standard states, the stability with respect to other competing phases might also be important, however, stability with respect to the other phases has only been considered for the compounds meeting the criteria for the HER activity.

However, Figure 4.2 only shows the heats of formation of the perfectly symmetrical 2H and 1T structures. But, as discussed in the last section the possible distortions have also been explored for all the compounds hence it is crucial to assess the energy difference of the perfectly symmetrical and the distorted phase of the compounds. Figure 4.3 shows the relative energy of the distorted phase with respect to the symmetric phase. The white squares corresponds to the compounds manifesting massive distortions leading to the structures not belonging to either of the 2H or 1T class, therefore, they are ignored. As can be seen from the figure, a large fraction of compounds do not show any distortions.

4.4 Adsorption of hydrogen on the basal planes

One of the widely accepted mechanism for the HER is the Volmer-Heyrovsky mechanism which is a two step process; the first step is the adsorption of H on the active site and the second step is the bond formation between the two

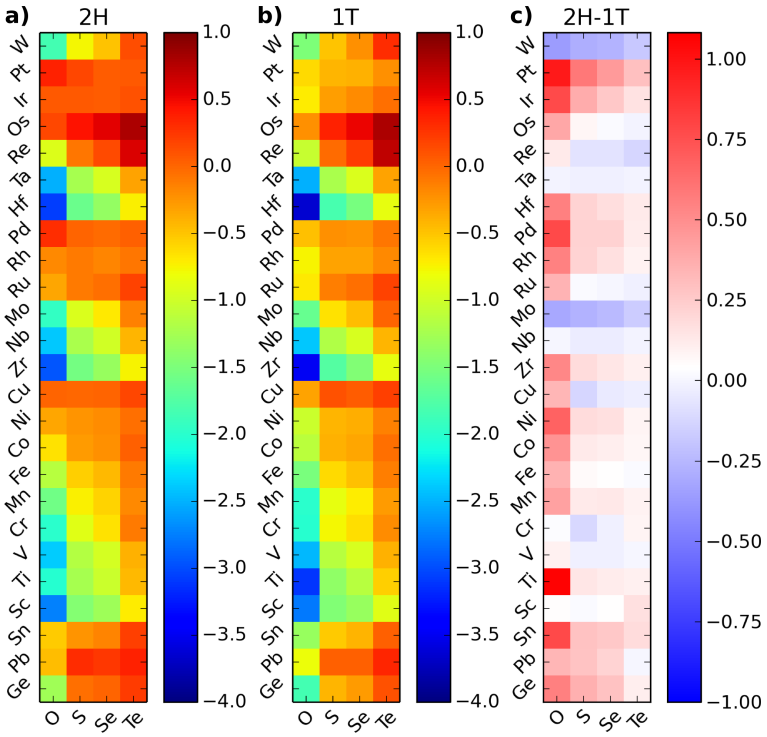

Figure 4.2: (a), (b) show the standard heats of formation of the compounds in the 2H and 1T structure respectively. (c) shows the difference of the heats of the compounds in the 2H and 1T structure. All the energies are in eV/atom. The figure has been taken from the Paper-2.

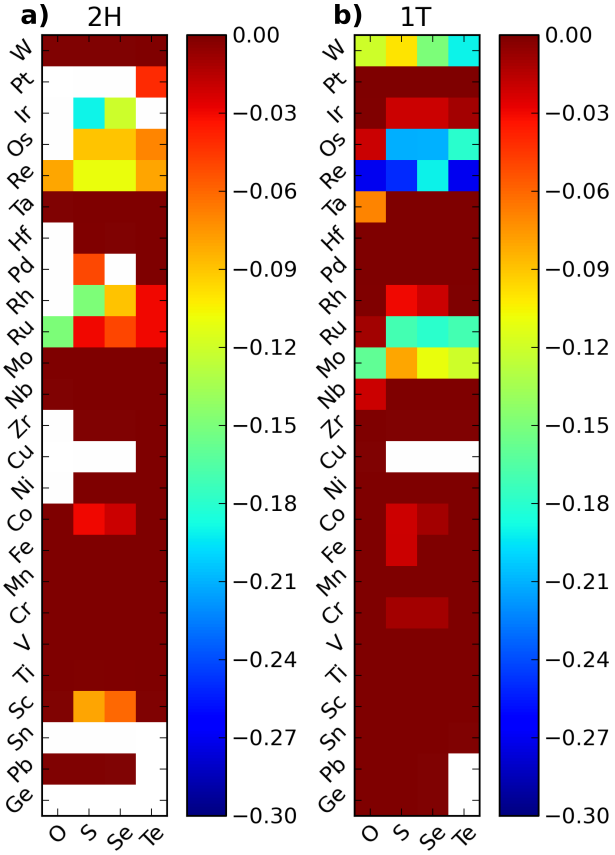

Figure 4.3: (a) and (b) show the energy of the distorted structures (eV/atom) with respect to the perfectly symmetrical 2H and 1T structures, respectively. The white squares denote massive reconstructions upon relaxation thus leading to structures not belonging to the 2H and 1T class of structures. All the energies are in eV/atom. The figure has been taken from the Paper-2.

adsorbed hydrogen to evolve the gaseous hydrogen [63, 64]. Schematically, the energetics of the process is shown in the Figure 4.4.

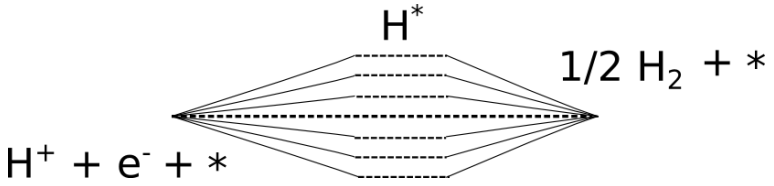

Figure 4.4: Schematic of the Volmer-Heyrovsky route for the HER.

The product and the reactant are at the same level of energy in the Figure 4.4 due to the assumption that the process is at equlibrium under standard conditions thus have zero free energy. Active site in the figure is denoted by the *. It can be seen from the figure that the intermediate H* may lie higher or lower in energy than the product and the reactant. If the intermediate lies higher in energy than the reactant then the first step will be uphill and if it lies lower in the energy than the reactant then the second process will be uphill. Therefore, based on the thermodynamic argument if the process has a zero barrier, then the free energy for the adsorption of hydrogen has to be zero [48, 65, 42]. Although the free energy for the hydrogen adsorption provides a descriptor for the HER activity, it does not provide any information about the kinetic barrier for the process but we do not explore the kinetic pathways in this work.

In order to assess the reactivity of the basal plane the hydrogen adsorption energy has been calculated for different active sites on the surface. We find that the hydrogen prefers to adsorb on chalcogen/oxygen atoms in tilted positions in most of the cases and does not prefers to adsorb on the metal site. In a perfectly symmetric structure all the chalcogen atoms are equivalent thus considering just one of them suffices. However, in the distorted structures, the broken symmetry leads to inequivalent chalcogen sites, therefore, all the inequivalent sites have been explored for the hydrogen adsorption and the site with the lowest adsorption energy has been chosen for further analysis. The coverage of 0.25 monolayer (ML) has been chosen initially and the higher coverage (0.5 ML) is only considered for those structures which bind hydrogen too strongly ($\Delta H_H^{ads} \geq -0.8$) for 0.25 ML. However, it has been found that at higher coverages the structures massively distort leading to the structures not belonging to either of the 2H or 1T class, therefore, higher coverages have not been considered any further.

The compounds have been grouped based on the nature of the metal atom 'M' in MX_2 i.e. the compounds have been put in the same group if the metal atoms belong to the same group in the periodic table; based on this categorization the plots for hydrogen adsorption energies are shown in the Figure 4.5.

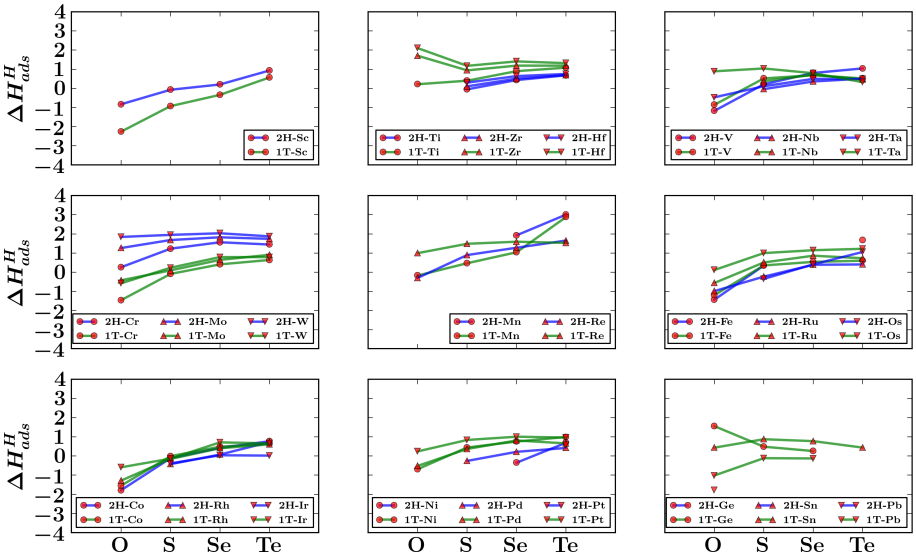

Figure 4.5: Hydrogen adsorption energies of the individual groups. The compounds have been grouped based on the nature of the metal atom 'M' in MX_2 i.e. the compounds have been put in the same group if the metal atoms belong to the same group in the periodic table. The missing data points represent massive reconstruction upon the hydrogen adsorption thus omitted from the plot. All the energies are in eV. The figure has been taken from the Paper-2.

The plot clearly shows that adsorption energies on the 2H and 1T structures do not follow any systematic trend in most of the cases, therefore, a simple systematic analysis cannot be performed to rationalize the different activities of the different structures. However, the group containing Cr, Mo and W (group-6) shows an opposite trend as the group containing Ti, Zr and Hf (group-4). In the group-6 the 1T structure binds hydrogen strongly whereas in the group-4 the 2H structure has higher binding energy. Therefore, only the group-4 and group-6 have been selected to understand the origin of different

reactivity in different structures.

Since the strength of the bonding depends on how the adsorbate states hybridize with the adsorbent states, the position of the center of the p level of the chalcogen atoms might give a clue about the strength of the bonding [65, 66]. The center of the p band with respect to the Fermi level can be calculated as

$$\epsilon_p = \frac{\int_{-\infty}^{\infty} \rho(\epsilon)\epsilon d\epsilon}{\int_{-\infty}^{\infty} \rho(\epsilon) d\epsilon} \tag{4.1}$$

The results for the sulphides and selenides of Mo, W, Ti and Zr in both the 2H and 1T structures are summarized in the Table 4.2. The table indicates that in the case of Mo and W, the 1T structure has higher binding energy (ΔH^H_{ads}) for the hydrogen whereas in the case of Ti and Zr hydrogen binds strongly in the 2H structure. It can also be seen that the compounds which have higher binding energy have the center of the p-level closer to the Fermi level. For example, in the case of group-6, the center of the p-level in the 2H structure lies deeper with respect to the Fermi level as compared to the 1T structure whereas in the group-4 the trend is opposite. Thus, it can be concluded that the position of the p band center is somewhat correlated to the binding energy.

Table 4.2: Heat of adsorption of hydrogen ΔH^H_{ads} and the center of the p-band ϵ_p for sulphides and selenides of Mo, W (group-6) and Ti, Zr (group-4) in the 2H and 1T structures.

2H	ϵ_p	ΔH^H_{ads}	1T	ϵ_p	ΔH^H_{ads}
MoS_2	-2.00	1.68 ± 0.07	MoS_2	-1.23	0.10 ± 0.13
$MoSe_2$	-1.74	1.82 ± 0.13	$MoSe_2$	-1.46	0.64 ± 0.11
WS_2	-2.32	1.95 ± 0.08	WS_2	-1.37	0.23 ± 0.14
WSe_2	-2.03	2.03 ± 0.14	WSe_2	-1.29	0.78 ± 0.15
TiS_2	-1.02	-0.05 ± 0.13	TiS_2	-1.45	0.40 ± 0.09
$TiSe_2$	-0.89	0.44 ± 0.12	$TiSe_2$	-1.38	0.90 ± 0.10
ZrS_2	-0.96	0.11 ± 0.10	ZrS_2	-1.42	0.94 ± 0.07
$ZrSe_2$	-0.80	0.51 ± 0.10	$ZrSe_2$	-1.34	1.19 ± 0.09

However, as shown in the Figure 4.6 there is hardly any trend when the difference of the adsorption energies is plotted against the difference of the center of the p level for large number of compounds. The absence of any trend can be attributed to the large variation in the nature of the metal atoms which makes it harder to generalize the analysis above for all the groups.

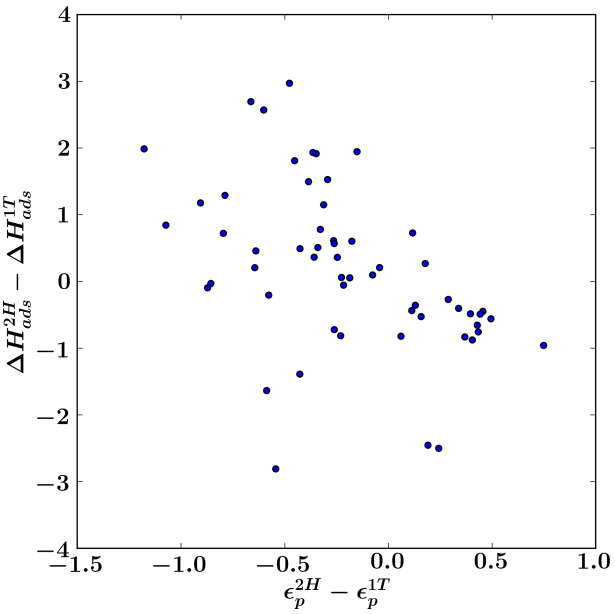

Figure 4.6: The difference in the adsorption energy of the 2H and 1T phase versus the difference of the center of the p bands of the corresponding phases.

4.5 Candidates for the HER

In the previous section the hydrogen adsorption energy was discussed which in the present context is nothing but the difference of energies of the reactant and the product side calculated with DFT. As discussed before, the descriptor for the HER is the free energy of the reaction which has to be close to zero. Therefore, additional terms are required in enthalpy which will give the estimate of the free energy. The additional terms come from the entropic contributions and zero point corrections. The entropy of the the adsorbed state is approximated to zero due to negligible number of the microstates in the adsorbed state as compared to hydrogen in the gas phase. The zero point energy contribution comes from the vibrations of the atoms analogous to the ground state of the quantum mechanical harmonic oscillator.

A very crude approximation has been made while adding the corrections corresponding to the zero point and entropic contributions. The correction for

the same has been calculated for the 1T-MoS_2 and then the same correction has been used for the all the other materials. This is not a perfectly valid assumption, however, a tolerance of 0.5 eV for the free energy to account for the errors introduced due to different approximations at different levels will likely capture the variability in the zero point and entropic corrections. In the case of 1T-MoS_2 as mentioned before the entropic corrections for the adsorbed state has been ignored [54]. The calculated zero point corrections for the adsorbed hydrogen comes out as 0.39 eV. The zero point energy of the hydrogen in the gas phase has been taken from the Ref. [67] and is found to be 0.27 eV and entropy of the gaseous hydrogen has been takes as 0.40 as mentioned in the Ref. [68]. By taking the difference of the corrections in the gas phase and the adsorbed state ΔZPE comes out as 0.12 eV and -TΔS comes out as 0.40 eV, therefore, ΔZPE -TΔS comes out to be 0.26 eV (per hydrogen atom). Therefore, the correction of 0.26 eV is added to the adsorption energies for all the compounds to have an estimate of the free energy.

As mentioned before, the optimum value of the free energy for the HER is 0.0 eV, however, an energy window of 0.5 eV is taken to account for different effects like strain, coverage and solvation [48, 69]. Additionally, the estimate of the uncertainties is obtained in the calculation with the BEEF-vdW using the ensemble in Ref. [70]. Having the uncertainties along with the energy window of 0.5 eV helps to calculate the probability for a material to have the free energy of the hydrogen adsorption to lie within 0.5 eV around zero. The calculated probability helps to rank the material in order of their suitability for the HER [71]. The probabilities are calculated as:

$$P(|\Delta G| \leq 0.5) = \frac{1}{\sqrt{2\pi\sigma^2}} \int_{-0.5-\bar{E}}^{0.5+\bar{E}} \exp\left(-\frac{E^2}{2\sigma^2}\right) dE. \tag{4.2}$$

Using the above equation, the ranking of the material meeting the criteria of having the free energy for the HER (including the uncertainties) to lie in the range (-0.5, 0.5) eV is shown in the Figure 4.7. The number of compounds fulfilling these criterion in the 2H structure in the plot is 23 whereas in the 1T structure there are 30 compounds meeting the required criterion.

The plot clearly shows that there are very few compounds which are present in both the 2H and 1T structure indicating that the chemical properties might differ significantly in different structures of the same compound. Additionally, the occurence of the compounds like MoS_2 and WS_2 in the 1T structure which have already been found experimentally as possible HER materials gives credibility to our approach [50, 48].

Up to this point the stability of the compounds have been considered only

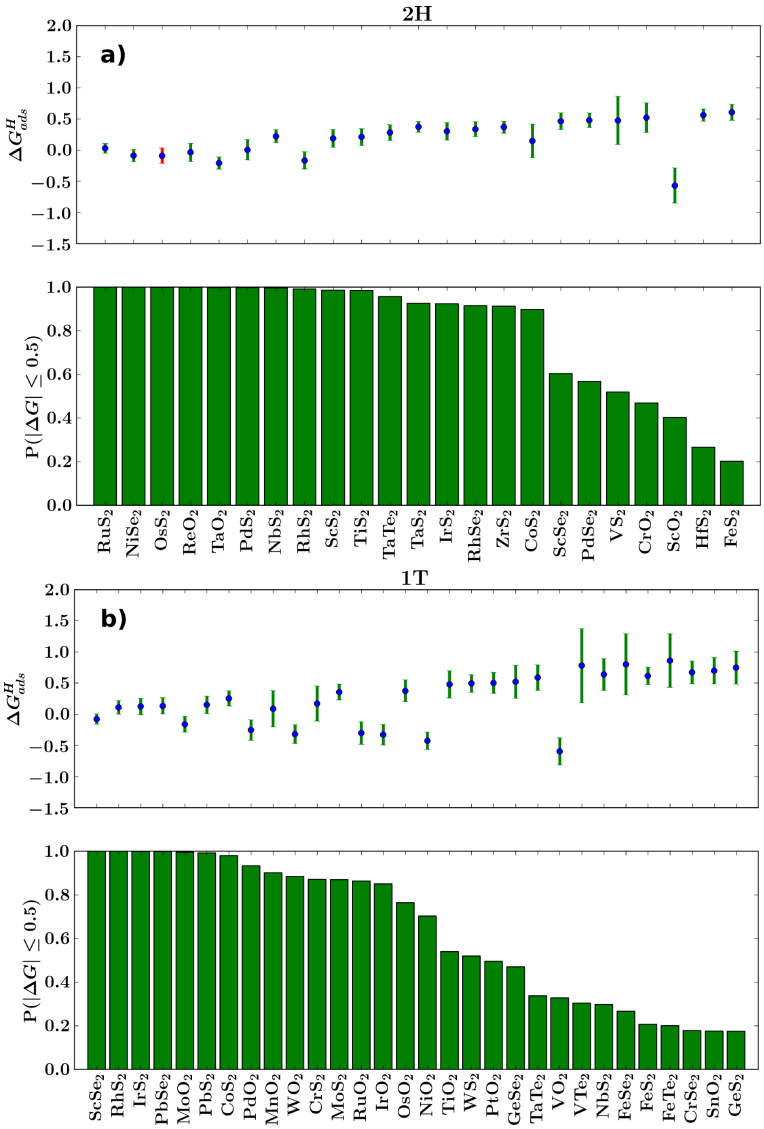

Figure 4.7: (a) Calculated free energy for the hydrogen adsorption (ΔG^H_{ads}) along with the uncertainties and the probabilities (P($|\Delta G| \leq 0.5$)) that the compounds have for the free energy to lie in the range (-0.5, 0.5) eV in the 2H structure. Red error bar indicate instability of the compound with respect to the standard state. (b) Similar plot as (a) for the 1T structure.

with respect to the standard states of the elements whereas there might be other potentially competing phases hampering the growth of the 2D materials for the HER. Therefore, it is crucial to have a deeper look on the stability of materials potentially suitable for the HER. If the metastability of the candidate material comes out to be too large as compared to the competing phase then its unlikely that the candidate material can be synthesized and stabilized under normal conditions. Therefore, the stability check for the candidate material has been performed with respect to the other competing phases with same stochiometry. Additionally, in the present work we do not explore the stability of the compounds in aqueous medium because in some recent works a good control over the stability of the compounds in water has been achieved by the use of stabilizing agents [72]. All the competing bulk structures are taken from the The Open Quantum Materials Database (OQMD) [73] and then the energy of candidate material is compared to the energy of the convex hull in order to have an estimate of the degree of metastability. The data is shown in the Table 4.3 and 4.4.

ΔH in the tables denotes standard heats of formation calculated with the FERE method and ΔH_{hull} denotes the convex hull [73]. The symbol * in superscript denotes the cases where the convex hull has been calculated as the linear combination of the energies of two compounds because no compounds were present with 1:2 stoichiometry in the database. δH_{hull} denotes the energy of the monolayer with respect to the convex hull. ΔH_{Expt} is the experimental heat of formation of the compound (if available) lying on the convex hull. The initial list of the candidates for the HER is also compared to the predicted 2D materials by Lebègue *et. al* [74]. In order to have an estimate of the metastability of the 2H structure with respect to the 1T structure or vice-versa the difference of the two is also shown as $\Delta H_{2H/1T}$ ($\Delta H_{1T/2H}$). Finally, the previously discussed probability $P(|\Delta G| \leq 0.5)$ is also listed in the table. All the energies mentioned in the table are in eV/atom.

Few important points worth noticing in the table are:

- In all the cases the 2H and 1T structure do not differ by more than ∼0.4 eV which is similar to the degree of metastability in MoS_2 and WS_2 in the 2H and 1T structure and both the compounds can be synthesized in the stable 2H phase and metastable 1T phase under normal conditions. Similar degree of metastability in other compounds suggest that if they can be synthesized in one structure then it is likely that they can be synthesized in the other structure as well.

- Few of the HER materials like PdS_2, $PdTe_2$ proposed in this work have also been predicted by Lebègue *et. al* [74] to exist in the monolayer form.

The fact that they lie above the hull by only ∼0.4 eV led us to made a choice of the threshold energy of 0.4 eV for the stability (or the feasibility of existence) of the monolayer with the respect to the hull. The choice of the threshold energy helps to narrow down the candidates even more, for example compounds like OsS_2, ReO_2, $OsSe_2$, ScO_2, RuO_2 in the 2H class of candidates and OsO_2 in the 1T class of candidates lying above the hull by more than 0.4 eV can be safely discarded. The names of the discarded compounds are italicized in Table 4.3 and 4.4.

- On comparing the list of the candidates with the list of the predicted 2D materials by Lebègue *et. al* [74], the compounds common in both the lists are selected. Given the fact that the heurestic approach of Lebègue *et. al* which is based on the feasibility of cleaving a bulk structure along a certain direction due to the weak interlayer interaction gives a clue that the compounds common in both the list are potentially synthesizable, therefore, potential candidates for the HER. The potential candidates are marked in bold in the Table 4.3 and 4.4.

In conclusion, this work systematically explores the materials space in the two-dimensional 2H and 1T structure for the hydrogen evolution reaction using the free energy of hydrogen adsorption as a computational descriptor. The requirement of the activity on the basal plane ensures the presence of large number of active sites as compared to previously explored 2H structure of the MoS_2 which only has the activity on the edges. A fairly large window chosen for value of the descriptor provides a flexibility to tune the adsorption energy of the hydrogen by different means, for example, strain, environment, doping etc. Additionally, the robust stability analysis of the candidates found suitable for the HER provides a list of candidates which do not have very high degree of metastability with respect to the bulk compounds thus potentially synthesizable. The adopted approach also predicts already known MoS_2 and WS_2 in 1T structure as candidates for HER thus supporting our approach. Finally, the most probable list of candidates is proposed based on work by Lebègue *et. al*. The calculations therefore invite for further investigation of some of the best candidates suggested here like PdS_2, NbS_2, TiS_2, TaS_2, ZrS_2, $PdSe_2$, HfS_2 in the 2H structure and CrS_2, $TaTe_2$, VTe_2, NbS_2, $CrSe_2$ in the 1T structure in addition to MoS_2 and WS_2 which are already known.

Table 4.3: Relevant energies for analysis of the stabilities of the obtained HER candidates in the 2H-derived structures. ΔH denotes the calculated standard heat of formation. ΔH_{hull} denotes the heat of formation of the most stable compound (i.e. at the convex hull) in the OQMD database[73]. The symbol * in superscript corresponds to the situation where no bulk structure with the compound composition lies on the convex hull according to the database. In that case ΔH_{hull} is calculated as a linear combination of several structures. δH_{hull} denotes the difference between the two previous columns, i.e. it shows how much the 2D compound lies above or below the convex hull. ΔH_{Expt} indicates the experimental standard heats of formation as listed in the OQMD database. Lebègue *et. al.* [74] have analyzed the possibilities for forming 2D compounds based on the layered character of the bulk structures and their result is also listed in the Table. $\Delta H_{2H/1T}$ is the difference between the energies in the two (possibly distorted) 2H and 1T structures. Finally $P(|\Delta G| \leq 0.5$ is the probability that the free energy of hydrogen adsorption lies within 0.5 eV from zero

2H-MX_2	ΔH	ΔH_{hull}	δH_{hull}	$\Delta H_{Expt.}$	Ref. [74]	$\Delta H_{2H/1T}$	$P(\lvert\Delta G\rvert \leq 0.5$
RuS_2	-0.31	-0.70	0.39	-0.71	No	-0.01	1.00
$NiSe_2$	-0.21	-0.34	0.13	-0.38	No	0.17	1.00
OsS_2	0.34	-0.60	0.94	NA	No	-0.01	1.00
ReO_2	-0.91	-1.42	0.51	-1.52	No	0.05	1.00
TaO_2	-2.58	-3.00	0.42	NA	No	-0.07	1.00
PdS_2	0.01	-0.31	0.32	-0.28	Yes	0.17	1.00
NbS_2	-1.21	-1.20	-0.01	NA	Yes	-0.04	1.00
RhS_2	-0.11	-0.48	0.37	NA	No	0.07	0.99
ScS_2	-1.46	-1.46	0.00	NA	No	-0.06	0.99
TiS_2	-1.23	-1.37	0.14	-1.41	Yes	0.15	0.98
$TaTe_2$	-0.32	-0.45	0.13	NA	Yes	0.00	0.96
TaS_2	-1.24	-1.22	-0.02	-1.22	Yes	-0.02	0.93
IrS_2	-0.11	-0.48	0.37	-0.46	No	0.22	0.92
$RhSe_2$	-0.17	-0.45	0.28	NA	No	0.07	0.92
ZrS_2	-1.55	-1.73	0.18	-1.99	Yes	0.19	0.91
CoS_2	-0.33	-0.48	0.15	-0.51	No	0.01	0.90
$ScSe_2$	-1.30	-1.25*	-0.05	NA	No	-0.01	0.60
$PdSe_2$	-0.02	-0.33	0.31	NA	Yes	0.22	0.57
VS_2	-1.16	-1.14	-0.02	NA	No	-0.02	0.52
CrO_2	-1.99	-2.15	0.16	-2.01	No	0.03	0.47
ScO_2	-2.74	-3.17*	0.43	NA	No	0.05	0.40
HfS_2	-1.62	-1.80	0.18	NA	Yes	0.22	0.26
FeS_2	-0.54	-0.73	0.19	-0.59	No	0.05	0.06

Table 4.4: Similar table as Table 4.3 for the 1T candidates. NA in the seventh column indicates that due to massive reconstructions the compound is discarded from the 2H class. All the energies are in eV/atom.

1T-MX_2	ΔH	ΔH_{hull}	δH_{hull}	$\Delta H_{Expt.}$	Ref. [74]	$\Delta H_{1T/2H}$	P($\lvert\Delta G\rvert \leq 0.5$
$ScSe_2$	-1.34	-1.25*	-0.09	NA	No	0.01	1.00
RhS_2	-0.32	-0.48	0.16	NA	No	-0.07	1.00
IrS_2	-0.30	-0.48	0.18	-0.46	No	-0.22	1.00
$PbSe_2$	0.04	-0.31*	0.35	NA	No	-0.22	1.00
MoO_2	-1.79	-1.95	0.16	-2.04	No	0.31	1.00
PbS_2	0.03	-0.32*	0.35	NA	No	-0.28	0.99
CoS_2	-0.34	-0.48	0.14	-0.51	No	-0.01	0.98
PdO_2	-0.48	-0.41	-0.07	NA	No	NA	0.93
MnO_2	-2.00	-1.98	-0.02	-1.80	No	-0.43	0.90
WO_2	-1.61	-1.89	0.28	NA	No	0.24	0.88
CrS_2	-0.77	-0.71	-0.06	NA	Yes	0.12	0.87
MoS_2	-0.66	-0.93	0.27	-0.95	Yes	0.28	0.87
RuO_2	-0.71	-0.94	0.23	-1.05	No	-0.20	0.86
IrO_2	-0.70	-0.94	0.24	-0.86	No	NA	0.85
OsO_2	-0.23	-1.10	0.87	-1.02	No	NA	0.76
NiO_2	-1.01	-0.79*	-0.22	NA	No	NA	0.70
TiO_2	-3.10	-3.29	0.19	-3.26	No	-1.11	0.54
WS_2	-0.59	-0.78	0.19	-0.90	Yes	0.18	0.52
PtO_2	-0.61	-0.62	0.01	NA	No	NA	0.50
$GeSe_2$	-0.27	-0.34	0.07	-0.39	No	NA	0.47
$TaTe_2$	-0.32	-0.45	0.13	NA	Yes	0.00	0.34
VO_2	-2.47	-2.63	0.16	-2.48	No	-0.10	0.32
VTe_2	-0.40	-0.45	0.05	NA	Yes	0.00	0.30
NbS_2	-1.18	-1.20	0.02	NA	Yes	0.04	0.30
$FeSe_2$	-0.48	-0.56	0.08	NA	No	-0.05	0.26
FeS_2	-0.61	-0.73	0.12	-0.59	No	-0.06	0.21
$FeTe_2$	-0.11	-0.20	0.09	-0.25	No	-0.02	0.20
$CrSe_2$	-0.63	-0.46	0.17	NA	Yes	0.02	0.18
SnO_2	-1.33	-2.10	0.77	-1.99	No	NA	0.18
GeS_2	-0.42	-0.55	0.13	-0.42	No	NA	0.17

Chapter 5

Materials for Light Absorption

5.1 Introduction

In the last chapter the need to find alternative energy resources has been discussed. It was primarily based on the catalytic aspect of the hydrogen production. This chapter is mainly focussed on the absorption of sunlight with semiconducting materials and the absorbed light can be used to produce hydrogen by splitting the water. Harvesting the sunlight is crucial because solar energy is the most promising alternative resource which can meet the growing energy requirement on top of being environmentally benign as compared to the fossil fuels. Some of the routes to harness the solar energy are solar cells, thermoelectrics, photoelectrochemical inter-conversion of chemicals etc [75, 76, 77, 78, 79, 80, 81, 82, 83]. Photo-electrochemical routes to produce chemicals have an added advantage of producing chemicals not just to be used as fuels but also for other purposes [84].

One of the simplest photoelectrochemical reactions is the splitting of water into oxygen and hydrogen. The advent of TiO_2 as a material to split the water into hydrogen and oxygen revolutionized the research in the area of photoelectrochemical energy conversion [83]. But the wide bandgap of TiO_2 limits its performance only to the ultraviolet (UV) region of solar spectrum. Despite continuous effort for more than three decades no abundant and efficient binary compound has been found to accomplish the task of visible light driven water splitting. The limited search space of binary compounds shifted the focus

to the compounds having more than two elements, especially ternary oxides which are quite stable under aqueous condition and irradiation [85, 86, 87]. One of the biggest advantages of the ternary/quaternary compounds is that there exist lots of possibilities of tuning the bandstructure by choosing different combination of elements. A few of the widely studied ternary compounds are oxide perovskites, vanadates, tantalates etc. [26, 88, 85, 86, 87, 89]. Therefore, in order to find multicomponent compounds for efficient light absorption, in this study a large number of compounds in the Materials Project Database [90, 91] have been explored. Additionally, the possibility of tuning the bandgap by layering of different semiconducting perovskites has also been explored using $BaSnO_3$ and $BaTaO_2N$ as model systems.

5.2 Mechanism of photoelectrochemical water splitting

The splitting of water using the sunlight is based on the fact that the absorption of sunlight generates electron-hole pairs in the semiconductor. The generated electron-hole pair if have the right energy splits the water to the oxygen and hydrogen. The overall water splitting reaction can be written as [3]:

$$2H_2O \rightarrow 2H_2 + O_2. \tag{5.1}$$

The oxidation and reduction reactions separately are

$$2H_2O + 4h^+ \rightarrow O_2 + 4H^+, \tag{5.2}$$

$$2H^+ + 2e^- \rightarrow H_2. \tag{5.3}$$

By definition of the normal hydrogen electrode (NHE) the free energy of the equation 5.3 is zero. The equation 5.2 however is uphill with a thermodynamic barrier of 1.23 eV [3]. If we ignore the overpotentials involved in the reaction for a moment then the maximum chemical potential of generated electron (equivalently the conduction band minimum (CBM)) should be zero with respect to the NHE whereas the minimum chemical potential of the generated hole (equivalently the valence band maximum (VBM)) should be greater than 1.23 V. However, due to various overpotentials involved the energy required by the electrons and holes to carry out the reaction is higher than the thermodynamic voltages mentioned above. A schematic of the photon induced water splitting reaction described above is shown in the Figure 5.1.

As mentioned above the voltage of 1.23 V does not account for any overpotentials or non-equilibrium phenomena. The minimum overpotential associated with the oxygen evolution reaction (OER) is ∼0.4 V and with the hydrogen evolution reaction (HER) is 0.1 V [88]. Additionally, the irradiation condition disrupts the equlibrium population of the electrons i.e separate quasi-Fermi levels have to be introduced for the conduction and valence band for the electron population. This lowers the effective driving force for the redox reactions. Typically, the correction due the effect of quasi-Fermi level is taken as ∼0.3 eV [88]. If all the above mentioned effects are added, it turns out that the semiconductor should have the bandgap of at least 2 eV. In the following sections the results and discussions about the screening of materials for the photoelectrochemical water splitting is based on the above mentioned details.

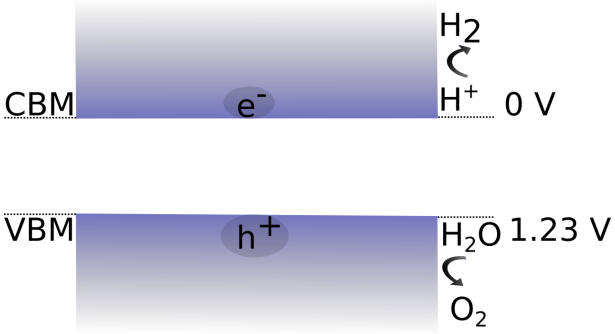

Figure 5.1: Schematic of the photon induced water splitting reaction.

5.3 Different methods for the bandgap calculation

As mentioned before, the screening has been performed for the materials available in the Materials Project Database. The Materials Project Database contains the subset of compounds present in the experimental database called as The Inorganic Crystallographic Structures Database (ICSD).[92] The ICSD contains the compounds which have been synthesized experimentally, therefore, one can expect that the screened materials from the ICSD will be synthesizable under certain experimental conditions. However, the ICSD does

not have information about the stability of the materials in aqueous conditions which is also explored in this work for the stability of the photocatalysts under *in-situ* conditions.

In chapter 1 a few different methods to calculate the bandgap of the semiconductors were discussed along with their pros and cons. It has also been pointed out that the calculation of the bandgap in a screening study should be reasonably accurate and at the same time efficient. The previously discussed GLLB-SC functional meets both the criteria in most of the cases. Therefore, in the present study the bandgap of ∼2400 compounds has been calculated with the GLLB-SC functional. Additionally, to test the validity of the calculated bandgap with the GLLB-SC functional the previously discussed hybrid functional HSE06 and the many body perturbation theory in different flavors like G_0W_0, GW_0 and GW have also been used for a few selected materials. The comparison is shown in the Figure 5.2. The plot is divided into the high and low bandgap materials. The figure shows that HSE06 tends to underestimate the bandgap a bit with respect to GLLB-SC. On the other hand, GW which is an eigenvalue self-consistent flavor of the GW approximation dovetails very well with the GLLB-SC bandgaps in the low bandgap region. Additionally, GLLB-SC has a mean absolute error (MAE) of 0.38 eV with respect to GW thus closer to the GW predictions as compared to HSE06 and G_0W_0 which have the MAE of 0.46 and 0.51 eV respectively. GW_0, being closest to the GW prediction with a MAE of only 0.29 eV, is highly computationally expensive as compared to GLLB-SC. Therefore, GLLB-SC being reasonably accurate and an order of magnitude computationally cheaper than the GW approximation serves the purpose of bandgap prediction in a screening study. Table 5.1 summarizes the above mentioned mean absolute (signed) error in the bandgap of the compounds lying in the low region calculated with different methods with respect to the other methods.

Table 5.1: Mean absolute (signed) error in eV for the materials in the small bandgap region in Figure 5.2 using LDA, GLLB-SC, HSE06, G_0W_0 and GW_0 and GW

xc_{ref}	LDA	GLLB-SC	HSE06	G_0W_0	GW_0	GW
xc						
LDA	-	1.64 (-1.64)	1.21 (-1.21)	1.08 (-1.08)	1.30 (-1.30)	1.59 (-1.59)
GLLB-SC	1.64 (1.64)	-	0.61 (0.43)	0.59 (0.56)	0.52 (0.34)	0.38 (0.05)
HSE06	1.21 (1.21)	0.61 (-0.43)	-	0.25 (0.13)	0.29 (-0.09)	0.46 (-0.38)
G_0W_0	1.08 (1.08)	0.59 (-0.56)	0.25 (-0.13)	-	0.22 (-0.22)	0.51 (-0.51)
GW_0	1.30 (1.30)	0.52 (-0.32)	0.29 (0.09)	0.22 (0.22)	-	0.29 (-0.29)
GW	1.59 (1.59)	0.38 (-0.05)	0.46 (0.38)	0.51 (0.51)	0.29 (0.29)	-

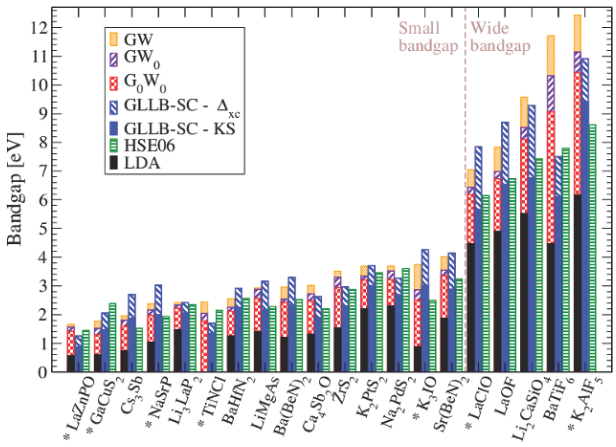

Figure 5.2: Bandgaps of few selected materials calculated with different methods versus the GLLB-SC calculated bandgaps. The figure is taken from the Paper-3.

5.4 Candidates for photoelectrochemical water splitting

A few crucial properties a material should have for an efficient absorption of light for photoelectrochemical water splitting are:

- Bandgap in the range of visible spectrum because the solar spectrum is dominated by the visible light.
- Proper band edge positions in order to straddle the redox levels of water in order to have the generated electron and hole at the right chemical potential to carry out the reaction.
- Stability of the compound in water because the reaction takes place in an aqueous medium.

Apart from the above mentioned properties, good electron-hole mobility, low recombination rates etc. are also required for greater efficiency. However, modeling of transport processes, recombination, defect centers etc. is much more complicated therefore not considered here for an initial stage of the screening.

In order to capture light in the visible range, the bandgap should lie between ∼1.5-3.0 eV. Therefore the calculated bandgap with GLLB-SC should lie in this range for efficient absorption of the solar light by the material. The position of the band edges in general depend on the surface termination,[93] therefore, in order to calculate the band edges slab calculations have to be performed. However, the position of the band edges can also be calculated with the empirical formula [94]:

$$E_{\mathrm{VBM,CBM}} = (\chi_A^x \chi_B^y \chi_C^z)^{1/(x+y+z)} \pm E_{\mathrm{gap}}/2 + E_0, \tag{5.4}$$

$E_{\mathrm{VBM,CBM}}$ is the position of the valence and conduction band edge respectively of the compound $A_xB_yC_z$, χ's are the electronegativity, E_{gap} is the bandgap and E_0=-4.5 V is the potential of the NHE with respect to the vacuum level and the '+', '-' signs correspond to the VBM and CBM respectively. The above empirical formula provides band edges which dovetail with the slab method and experiments in most of the cases [94] with few exceptions.[95] Finally, the stability in aqueous conditions can be calculated by the Pourbaix diagram.[96, 97] However, having a very tight threshold of the energy ΔE for the stability may result in stability diagrams which do not' agree with experiments.[96] The reason behind this disagreement is that the stability is not only the result of thermodynamics but the kinetics as well. On the other hand, the Pourbaix diagrams do not contain any information about the kinetics therefore a larger energy threshold has to be employed in order to account for the phases which are kinetically protected. The sensitivity towards the threshold can be seen in the Figure 5.3 which is the histogram of the GLLB-SC calculated bandgap of all the 2400 materials considered in this work. The figure clearly shows that when a very tight threshold of 0 eV is chosen the for stability, most of the compounds turn out to be unstable in water even though many of them have been observed to be stable in experimental conditions. However, when a threshold of 1 eV is chosen, a reasonable number of compounds are stable in aqueous conditions. Therefore, a threshold of 1 eV is used to check for the stability of the compounds having suitable absorption properties for the photoelectrochemical water splitting.

The final criteria used for the screening can be summarized as:

- $1.7 \leq E_{\mathrm{gap}} \leq 3.0$ eV (to account the errors in the GLLB-SC calculated bandgap and overpotentials).

- VBM $\geq$ 1.6 V and CBM $\leq$ -0.1 V with respect to the NHE (to account for the overpotentials).

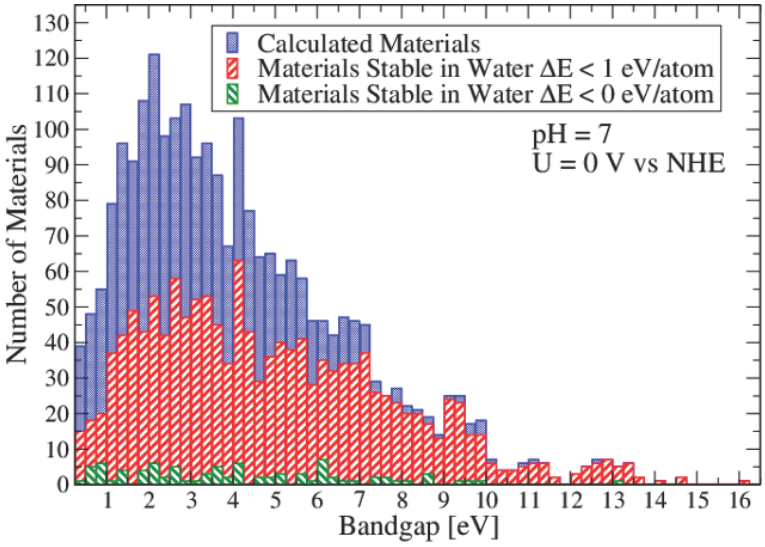

Figure 5.3: Histogram of the GLLB-SC calculated bandgap of all 2400 materials. Different color denote the stable compounds for different threshold of energy chosen for the stability in aqueous condition with pH = 7 and U = 0 V with respect to the NHE. The figure is taken from the Paper-3.

- $\Delta E \leq 1$ eV (to account for the metastability and kinetic stabilization) at pH = 7 and -0.4 $\leq$ V $\leq$ 2.2 V which is the typical operating voltage of the device.

The materials meeting all the above criteria are selected from the pool of 2400 are selected from the pool of ∼2400 and shown in the Figure 5.4. In the figure ΔE denotes the degree of stability of the material, the position of the direct and indirect band edge positions are shown in red and black respectively. It is suprising that out of ∼2400 materials only a handful of materials follow all the specified criteria. However, in recent experiments [72] a good control over the stability of semiconductors in water has ben achieved by using protective polymeric layers. Therefore, the size of the materials space might be expanded by relaxing the criteria of the stability in aqueous medium. The compounds written in green and underlined in the Figure 5.4 have been realized previously for different photoelectrochemical applications, [98, 99, 100, 101, 102, 103, 104, 105] and are therefore expected to serve as viable candidates for photoelectrochemical water splitting.

5.5 Bandgap engineering of functional perovskites

The previous section dealt with a specific application of solar light absorption i.e photoelectrochemical water splitting. However, the other applications like photovoltaics, transparent conducting oxides etc. require different size of the bandgap.[75, 76] We also saw that different factors limit the suitability of a material for a given application e.g stability in water, toxicity, cost etc. Therefore, a systematic strategy is required to tune the bandgap of an already existing material which meets the requirement of toxicity, stability etc.

In this section the possibility of tuning the bandgap by the layering of two perovskites, namely $BaSnO_3$ and $BaTaO_2N$ is explored. The bandgap tuning especially in perovskites has also been explored in previous works in systems like SrVO3, SrTiO3 etc.[106, 107, 108, 109, 110, 111] The choice of $BaSnO_3$ and $BaTaO_2N$ as a model system here stems from the fact that both the compounds have been explored recently as light absorbers for the photoelectrochemical water splitting applications and have similar lattice constants thus the layered system will not be subjected to a high stress. The protypical structure of the layered compound is shown in the Figure 5.5. The α ($BaSnO_3$) and β ($BaTaO_2N$) are stacked along the z-direction while x and y direction have the periodicity of the cubic perovskite structure and the tuning of the bandgap is explored by varying the number of layers of α (n_α) and the number of layers of β (n_β).

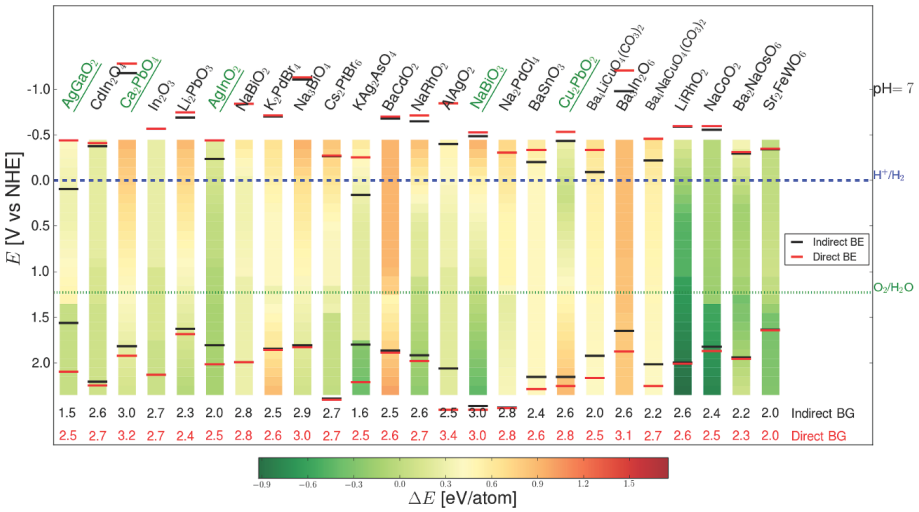

Figure 5.4: Materials fulfilling the criteria of the bandgap, band edge positions and stability in water in neutral pH condition and in the voltage range of -0.4 to 2.2 V. ΔE denotes the degree of stability of the material. The position of the direct and indirect band edge positions are shown in red and black respectively. The figure is taken from the Paper-3.

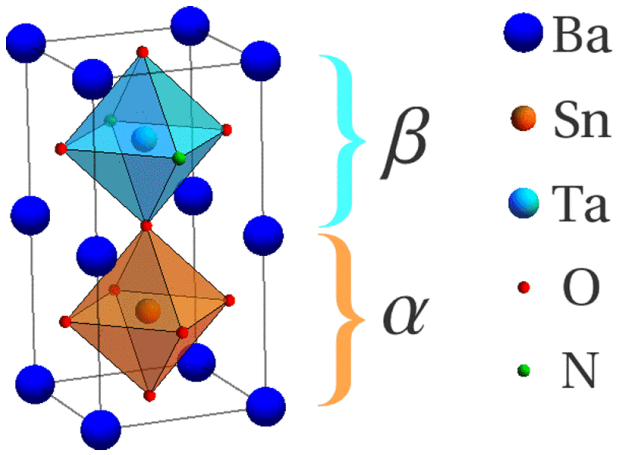

Figure 5.5: The structure formed with the layering of $BaSnO_3$ and $BaTaO_2N$. α represents $BaSnO_3$ and β represents $BaTaO_2N$. Stacking is done along the z-direction while x and y direction has the periodicity of the cubic perovskite structure. The figure is taken from the Paper-4.

The calculation of the bandgap has been performed with the GLLB-SC functional and the obtained bandgaps for $BaSnO_3$ and $BaTaO_2N$ are 3.33 and 1.84 eV which are in good agreement with the measured experimental bandgap of 3.1 and 1.9 eV for $BaSnO_3$ and $BaTaO_2N$ respectively.[112, 113] For comparison, the HSE06 calculated values of the bandgaps are 2.89 and 1.71 eV which is slightly lower than the GLLB-SC calculated bandgaps as expected.

The calculated bandgap of heterostructure for different n_α and n_β is shown in the Figure 5.6. The figure shows that the highest bandgap of 2.26 eV is obtained for the $\alpha\beta$ stacking and the lowest value of 1.26 eV for $\alpha_6\beta_6$ sequence. The variation of the bandgap by 1 eV for different stacking sequences implies a high degree of tunability of the bandgap by stacking different layers. The wide variation in the bandgap can be understood in terms of the quantum confinement and quantum tunneling effect. The sketch in the Figure 5.7 shows how the local position of the conduction band edge moves downwards upon increasing the number of α and β layers resulting to decreased confinement.

In order to understand the shift of the local conduction band edge on changing the number of layers the location and nature of the CBM and VBM

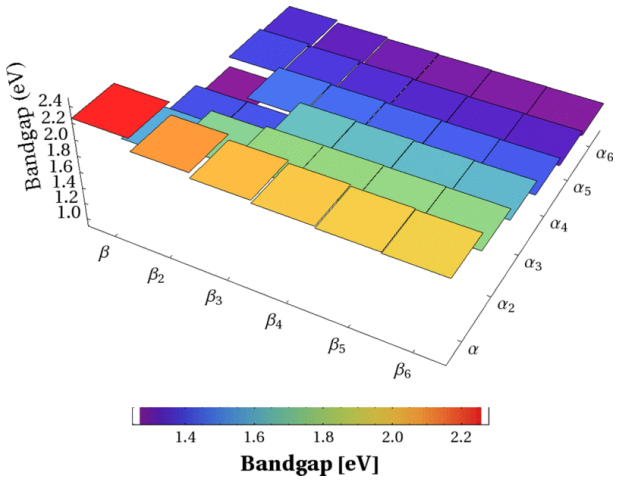

Figure 5.6: The bandgap of the heterostructure as a function of n_α and n_β. Each rectangle in the plot represents a compound with the stacking sequence $\alpha_n\beta_m$. The figure is taken from the Paper-4.

states are analyzed. In Figure 5.8 the wavefunctions of the VBM and CBM states are plotted for $\alpha\beta$ and $\alpha_2\beta$. The figure shows that the VBM mainly consists of the N_{2p} orbitals in both $\alpha\beta$ and $\alpha_2\beta$ and is located in the β region of the heterostructure. Additionally, calculations also suggest that the along with the character the position of the VBM state also does not change relative to low-lying level for the different structures, therefore, it can be safely assumed that it is only the nature and position of the conduction band which is responsible for the bandgap variation in $\alpha\beta_n$. It can also be seen that in $\alpha\beta$ the CBM states are located in the TaON plane and mainly consists of the Ta d orbitals. Therefore, in order to see if the same trend is followed in $\alpha\beta_n$ as the number of β layers is increased the weights of the CBM state is analyzed. The Figure 5.9 shows the planar average (xy plane) of the weights of the CBM state in the real space. The area of the circle represents the magnitude of the weight for the different planes stacked along the z-direction. The boxes represent the unit cell and the dotted lines the interface between the α and β layers. As expected the CBM state is mainly comprised of the Ta d orbitals and located on the TaON plane. The figure also shows that as the number of β layers is increased the CBM states become less confined therefore resulting

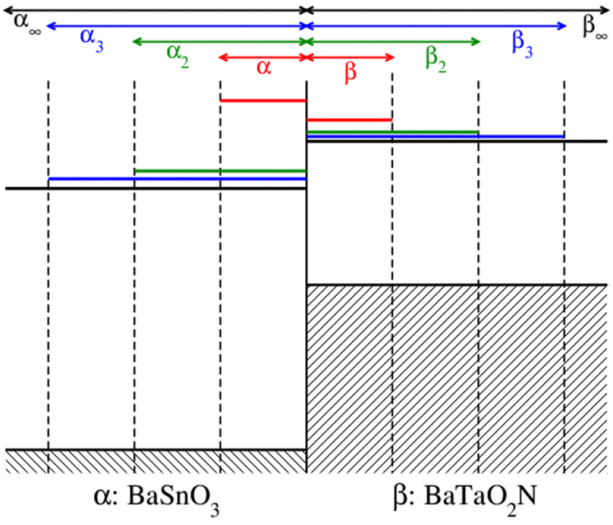

Figure 5.7: Sketch of the electronic level positions at an interface between α and β for different number of layers. The decreased number of layers resulting to increased confinement moves the local position of the conduction band edge upwards. The figure is taken from the Paper-4.

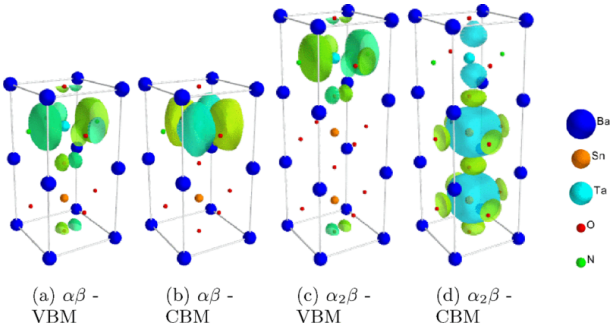

Figure 5.8: Wavefunctions of the VBM and CBM states for selected hetereostructures. The figure is taken from the Paper-4.

to the downshift of the state eventually leading to decrease in the bandgap.

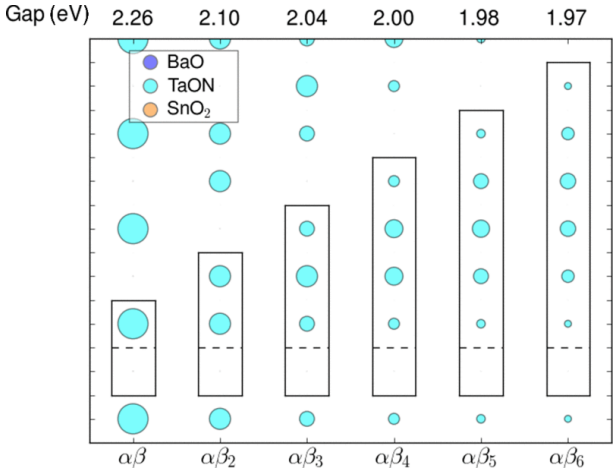

Figure 5.9: Planar average of the weights of the CBM state in the real space and the area of the circle represents the magnitude of the average. The unit cell is sketched as rectangles and the dotted lines show the interface between the α and β layers. As expected the CBM state is mainly composed of the Ta d orbitals. The bandgaps for different structures is also shown on the top. The figure is taken from the Paper-4.

Until now, the behavior of the heterostructure has only been analyzed with only one α layer. However, the scenario significantly changes when the number of α layers is increased as shown in the Figure 5.10. The figure shows the similar plot as in Figure 5.9 with the only difference that it has two α layers as opposed to the Figure 5.9 which has one. As can be seen from the figure that the CBM is now located mainly in the α part of the heterostructure and primarily consists of the Sn s states. A small weight in the β part of the structure represents the tunneling effect. However, as expected the tunneling effect decreases as the number of β layers is increased and almost diminishes in going from $\alpha_2\beta_2$ to $\alpha_2\beta_3$. Additionally, the weights look similar in all the structures. Therefore, the weights being similar and the diminishing of the tunneling effect results to almost no bandgap change as the number of β layers ≥ 3.

In the last two kind of heterostructures it is found that keeping the number of α layers to one has only confinement effect on increasing the number of β

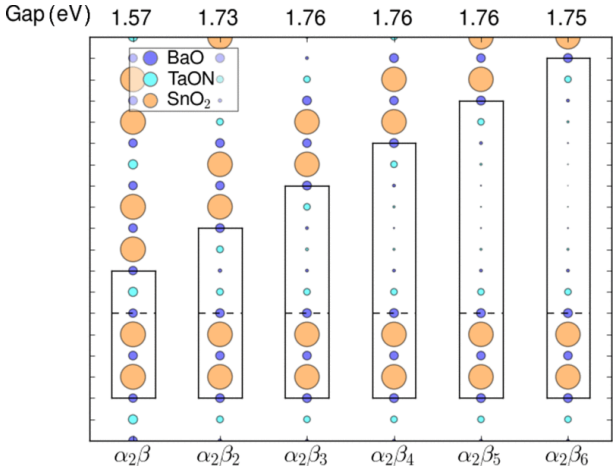

Figure 5.10: Similar plot as in 5.9 with the only difference that it has two α layers as opposed to the Figure 5.9 which has one. The CBM states now mainly comprise of the Sn s states. The very small weight in the β region indicates tunneling effect which almost diminished as the number of layers of β is increased beyond 2. The figure is taken from the Paper-4.

layers and for two α layers it is mainly the tunneling effect responsible for the bandgap variation. Therefore, it can be expected that if the number of α layers is increased while keeping the number of β layers constant the variation of the bandgap would be an interplay between the confinement and the tunneling effect. In order to see this effect the Figure 5.11 shows similar plot as Figure 5.9 & 5.10 with the difference that the number of β layers is fixed to one while the number of α layers is increased. The behavior for $\alpha\beta$ and $\alpha_2\beta$ is already shown in the Figure 5.9 & 5.10. In going from $\alpha_2\beta$ to $\alpha_6\beta$ the tunneling as well as confinement decreses. However, the decreased tunneling has the opposite effect as the decreased confinement i.e as the tunneling decreases the bandgap increases as in Figure 5.10 whereas the decreasing confinement decreases the bandgap as in Figure 5.9. These two competing effects results to a minima in the bandgap for the for a particular number of α layers. The Figure 5.11 shows that up to 4 α layers the confinement effect dominates thus leading to the bandgap reduction in moving from $\alpha_2\beta$ to $\alpha_4\beta$, however, in going from $\alpha_4\beta$ to $\alpha_5\beta$ the diminishing tunneling dominates over the decreased confinement thus result in an increase in the bandgap. The above analysis for different

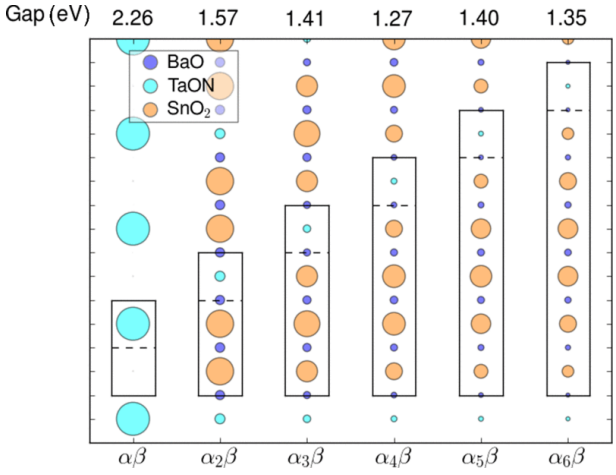

Figure 5.11: Similar plot as in 5.9 with the difference that the number of β layer is fixed to one and the number of α layer is varied. As the number of α layer is increased beyond $\alpha_2\beta$ the tunneling and confinement effect compete with each other result in decreasing of the bandgap up to $\alpha_4\beta$ and then the increase of the bandgap. The figure is taken from the Paper-4.

heterostructures shows how different effects can be tuned to tailor the bandgap and the variation can be understood with simple physical arguments. Since the analysis is quite general, therefore, it can be applied to other heterostructures as well.

5.6 Conclusion

In this chapter a pool of ∼2400 materials is explored which can absorb solar light for photoelectrochemical water splitting. The criteria imposed for the bandgap, band edge positions and the stability in aqueous solution in neutral pH for a certain potential range gives a handful of candidates which can serve as good photoabsorber for the water splitting reaction. The careful comparison of the bandgap with different methods involving hybrid functionals and many body perturbation theory methods assures credibility to the method that is used for the bandgap calculation of a large number of materials. A literature survey for the materials in the list of candidates found which can act as good photoabsorbers suggests Ca_2PbO_4, Cu_2PbO_2 $AgGaO_2$, $AgIn_2$ and $NaBiO_3$ as potential candidates.

Additionally, a strategy to engineer the bandgap is also explored via layering of different lattice matched structures. For the model systems explored i.e $BaSnO_3$ and $BaTaO_2N$ the calculations suggest that the variations in the bandgap of the structure can be understood with the simple arguments of confinement and tunneling effects. This strategy can be applied to other lattice matched systems for bandgap engineering.

Chapter 6

Trends in Stability and Bandgaps of Binary Compounds in Different Crystal Structures

6.1 Introduction

One of the simplest class of compounds are binary compounds which only have two constituent elements and different crystal structures e.g wurtzite, zinblende, rocksalt, NiAs and rutile. Often times, same compound exists in different crystal structures under different conditions and different structures may have significantly different properties. For example, the anatase phase of TiO_2 is found to be photo-catalytically active [83] where as the rutile phase is not [114] even though both the structures are energetically very close with rutile phase being slightly more stable than anatase phase [115]. Additionally, rocksalt structure of ZnO which is significantly lower in stability as compared to the native wurtzite structure has been stabilized in MgO matrix [116, 117]. Thus, above studies suggest that compounds with different degree of metastability can be synthesized and stabilized at normal conditions which motivated us to explore different crystal structures of the same compound. In the current work we explore four different crystal structures of the binary compounds in AB stoichiometry where A and B are chosen from a set of 44 and 16 elements

respectively. In the set A, metals which may lead to magnetic compounds have been ignored due to large degree of uncertainty in their bandgap calculations whereas set B contains non-metals. First principle calculations were carried out to determine the stability and bandgap of all the compounds. We systematically arrange the compounds in tabular form using Pettifor maps which involves the ordering of elements based on the their chemical scale factor [118]. We also explore alloys of 32 binary compounds having the band gap in the range of 1.0-3.5 eV inspired by recent experiments on solid solutions for photo-electrochemical water splitting applications [119, 3]. Clustering analysis [120] of the alloy compounds divides 32 compounds into different groups with compound belonging to the same group behaving similarly for bandgaps upon alloying, thus giving the freedom too choose one compound over the other from the same class if required.

6.2 Results and Discussions

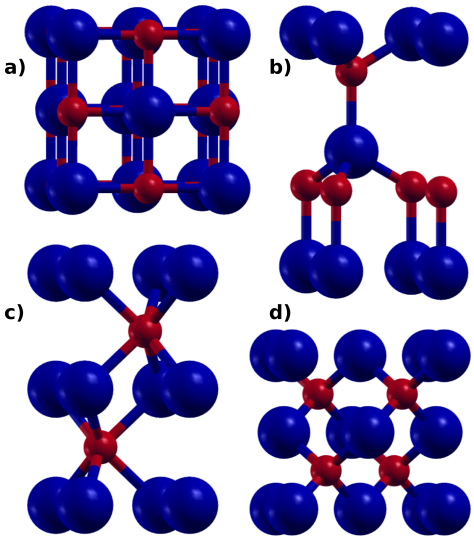

Figure 6.1: Crystal structures explored in the current work. (a) Rocksalt structure (Space Group - $Fm\bar{3}m$) (b) Wurtzite structure (Space Group - $P6_3mc$) (c) NiAs structure (Space Group - $P6_3/mmc$) (d) Zincblende structure (Space Group - $F\bar{4}3m$)

Table 6.1: Grouping of compounds in Figure 6.3 based on the range of geometric mean of chemical scale factor χ

Group	Range($\sqrt{\chi_A \chi_B}$)
1	0.00 - 1.45
2	1.45 - 1.75
3	1.75 - 1.95
4	1.95 - 2.10
5	2.10 - 2.30
6	2.30 - 3.10

Table 6.2: Standard enthalpy ΔH of formation of binary compounds in wurtzite structure having the bandgap in the range of 1.0 - 3.5 eV chosen to form ternary wurtzite structures for bandgap engineering of binary compounds. ΔH^{OQMD} shows the enthalpy of formation of the with same stoichiometry in the minimum energy structure and ΔH^{hull} represents the enthalpy above the convex hull calculated from OQMD database. [73] All the energies are mentioned in eV/atom.

Compound	ΔH	ΔH^{OQMD}	ΔH^{hull}	Compound	ΔH	ΔH^{OQMD}	ΔH^{hull}
GaN	-0.72	-0.59	-0.13	ZnO	-1.77	-1.68	-0.09
ScN	-2.05	-2.04	-0.01	GeO	-1.03	-1.94	0.45
AgF	-0.94	-1.21	0.27	SnO	-1.18	-1.58	0.40
PbO	-0.97	-1.36	0.39	AgI	-0.32	-0.38	0.06
LaN	-1.50	-1.44	-0.06	YN	-1.97	-1.81	-0.16
InP	-0.33	-0.37	0.04	GaP	-0.59	-0.55	-0.04
AlAs	-0.62	-0.49	-0.14	AlP	-0.86	-0.76	-0.10
AgCl	-0.56	-0.67	0.11	AgBr	-0.46	-0.55	0.09
CdTe	-0.37	-0.47	-0.10	AlSb	-0.32	-0.17	-0.15
CdSe	-0.69	-0.64	-0.05	ZnTe	-0.56	-0.47	-0.09
ZnSe	-0.90	-0.72	-0.18	CdS	-0.75	-0.81	0.06
GeS	-0.42	-0.42	0.00	AlI	-0.27	-0.05	0.27
AlBr	-0.58	-0.31	0.34	GeSe	-0.33	-0.22	-0.11
SnS	-0.48	-0.66	0.18	SnSe	-0.44	-0.48	0.04
PbS	-0.41	-0.71	0.30	PbSe	-0.38	-0.57	0.19
GeTe	-0.05	-0.09	0.04	PbTe	-0.05	-0.41	0.36

Figure 6.2 shows the ball and stick model of the crystal structures explored in the present work. Binary compounds crystallizing in NiAs and wurtzite structures have four atoms in the unit cell with the coordination number of six and four respectively, whereas the primitive unit cell of the rocksalt and zincblende structures contains two atoms with a coordination number of six and four respectively. In the light of recent experiments on the synthesis of compounds violating chemical/octet rules under extreme conditions we do not impose any chemical rules to narrow down the search space in our calculations

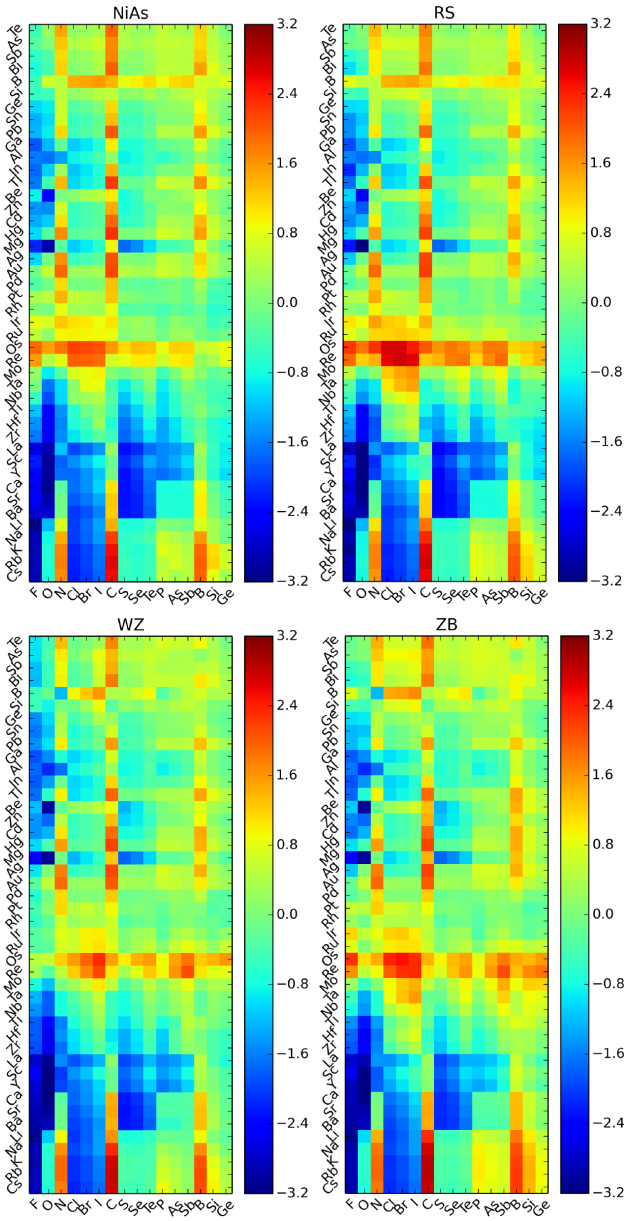

Figure 6.2: Heatmap of standard enthalpy of formation of compounds in different crystal structures. Each square in the heat map represents a compounds with constituent elements represented by ordinate and abscissa of that square.

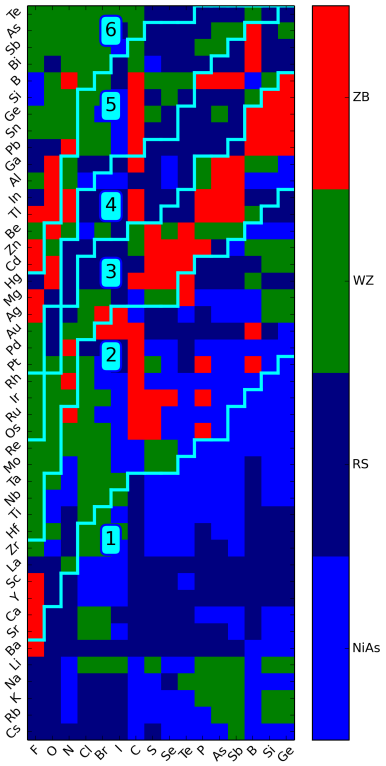

Figure 6.3: Representation of regions where particular structure has lowest standard enthalpy of formation as compared to other crystal structures. The compounds are represented in the same way as in Figure 6.2. Based on geometric mean of the chemical scale factor χ [118] the plot is divided into six different regions where the value of geometric mean increases on moving from '1' to '6'.

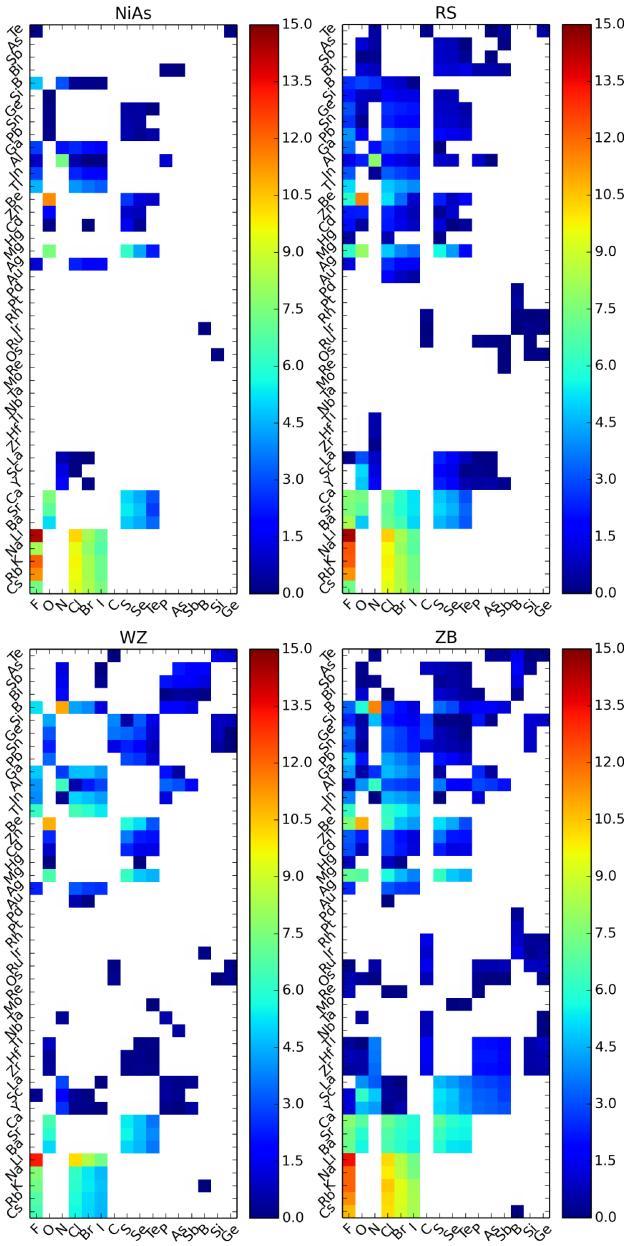

Figure 6.4: Band gap of compounds in different crystal structures. The white region in the plots shows the metallic compound i.e. with zero bandgap

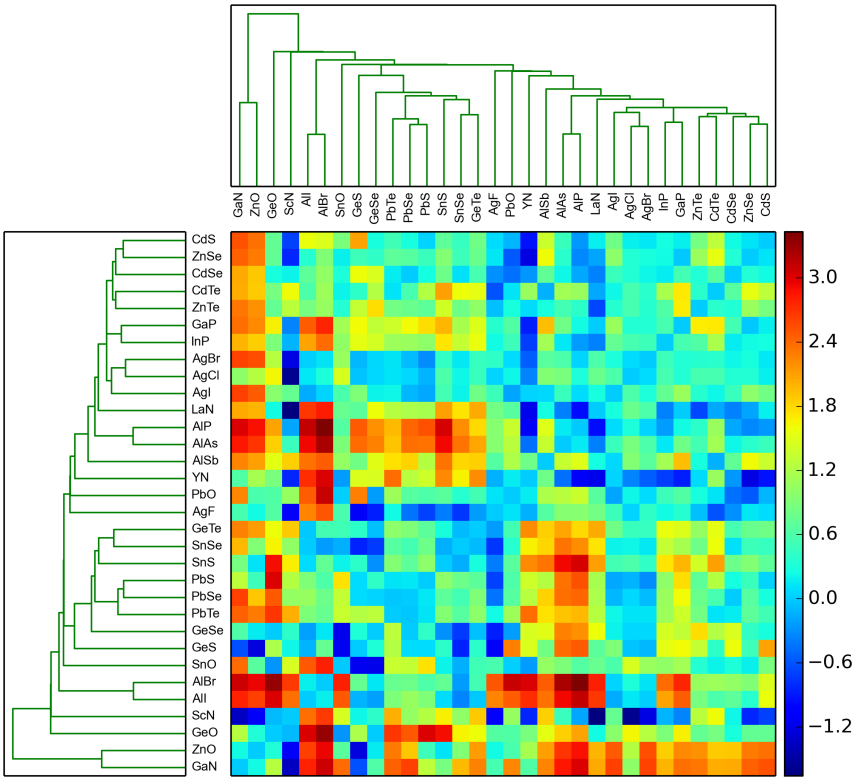

Figure 6.5: Dendrogram based on difference of average bandgap of the constituent compounds in the alloy and calculated bandgap of the alloy. The constituent compounds have been selected from the pool of compounds with wurtzite structure and having the bandgap in the range of 1.0-3.5 eV.

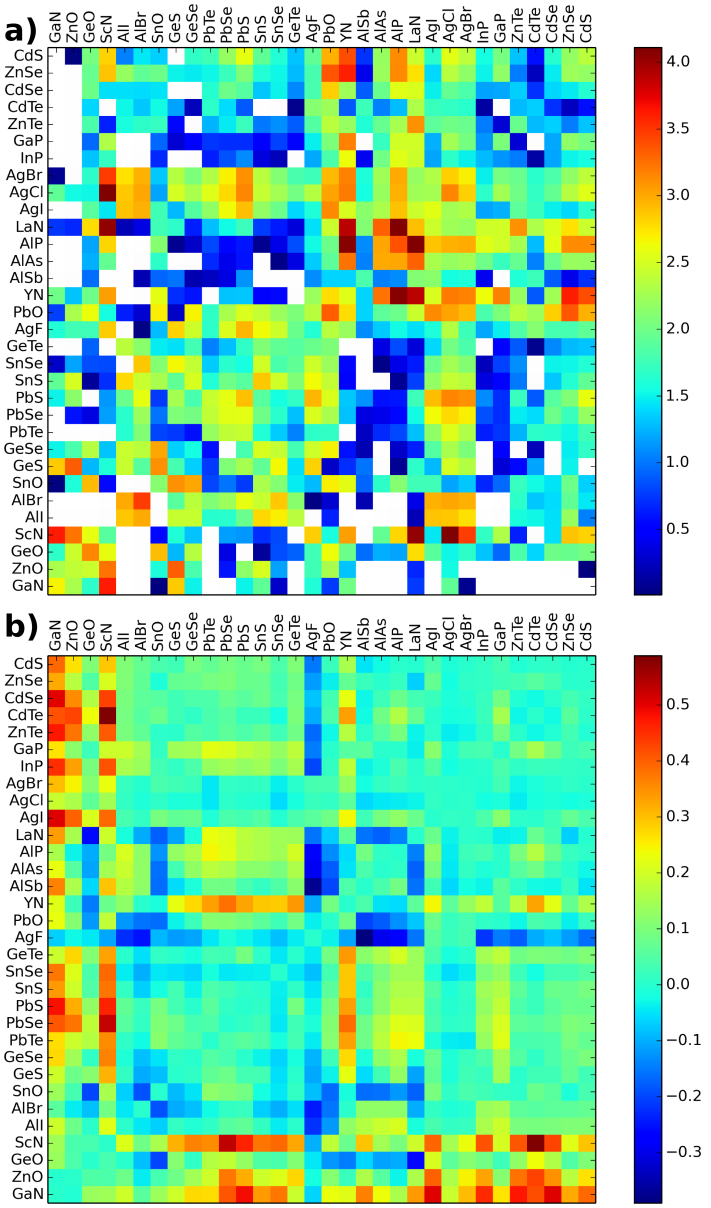

Figure 6.6: (a) Calculated bandgap of the alloys. The constituent compounds have wurtzite structures with the bandgap lying in the range of 1.0-3.5 eV. White spaces show alloys with zero bandgap. (b) Shows enthalpy of mixing of the alloy compounds with respect to constituent compounds.

[121]. In our work we calculate the stability of compounds with respect to the standard reference states only. Since our interest lies in comparing the trends in thermodynamic and electronic properties of the compounds in different crystal structures with 1:1 stoichimetry, we do not consider the compounds with the stoichiometry different from 1:1. In the calculations we ignore few metals leading to magnetic structures since a reliable approach to calculate the bandgap of magnetic semiconductors with the GLLB-SC functional has not been developed yet.

Figure 6.2 shows the heatmaps of the standard heat of formation of all the compounds in which the elements are arranged as per the chemical scale χ proposed by Pettifor [118]. As can be seen from the figure that the heat of formation in all four crystal structures follow the similar pattern which indicates that if the compound is stable with respect to the standard states in one crystal structure it will be stable in the other crystal structure as well. But negative formation energy does not guarantees that the structure can be stabilized in that phase which is inhibited by the existence of other competing phases in the ambient environment. But the control over the ambient condition for the growth can be achieved by for example temperature, pressure, surfactants and doping [122, 123, 124]. Pressure as one of the control mechanism in the growth process gives a tool to stabilize structure with different volumes. For example, if the most stable structure has a lower volume (e.g. rocksalt or NiAs) then applying tensile stress may favor the higher volume phase (e.g. wurtzite or zincblende) whereas a lower volume phase will be favored under compressive stress if the most stable structure has a higher volume. The above process can be realized in experiments [116, 125] with the growth on a substrate with different lattice mismatch thus providing a way to apply the compressive and tensile stress. Thus, above strategies to manipulate crystal structures suggest that the compounds can possibily be synthesized and stabilized in different crystal structures with different volumes. Therefore, in the current work we choose crystal structures spanning a wide range of volumes with the zincblende and wurzite having higher volumes due to low coordination number as opposed to the rocksalt and NiAs structures which have larger coordination number thus lower volumes.

In addition to the standard heat of formation as shown in Figure 6.2 one might also be interested in region where a particular crystal structure has the lowest enthalpy of formation as compared to other crystal structures. Figure 6.3 shows the minimum energy crystal structure for different compounds. As can be inferred from the figure, there are very few isolated regions for a given crystal structure. Hence, compounds when arranged in Pettifor maps form clusters having the same most stable crystal structure. Therefore, we

group the compounds in Figure 6.3 in six different groups based on the geometric mean of the chemical scale factor χ [118]. The range of geometric mean of groups is shown in Table 6.1.

The grouping in Figure 6.3 shows an apparent correlation between the crystal structure and the geometic mean of the chemical scale factor of the compounds. For very small values of geometric mean (Group 1) the compound prefers to have the low volume structure i.e. rocksalt or NiAs whereas at larger values(Group 6) the compound prefer to have more open structure i.e. wurtzite or zincblende. Few green parts in the Group 1 for compounds like LiF, LiCl is the artifact of the calculation since these compounds are known to have the rocksalt structure. On the other hand,the difference in energies of the wurtzite and rocksalt structure of these compounds as per our calculations is of the order of 0.05 eV which is small and can be safely ignored. The region of extreme values of the geometric mean in Figure 6.3 i.e. Group 1 and 6 are the region of extreme ionicity of the compounds with very small values indicating large ionicity (more closed structures) whereas very large values showing greater covalent character (more open structures) [118]. On the other hand, the region of moderate ionicity i.e. Group 2-5 is not dominated by one crystal structure. Group 2 has large fraction of WZ and NiAs structures, Group 3 ZB structure, Group 4 RS structure and Group 5 WZ and RS structures.

In Figure 6.4 we show the bandgap of all the compounds. The white regions in the heatmap show the zero bandgap materials by which we can see that out of 704 materials in each group very few turn out be semiconducting with the smallest number of semiconductors in the NiAs structure and the largest number in the ZB structure. The plot also shows that despite having the similar heat of formation, the wurtzite and zincblende have quite dissimilar trend in bandgaps(especially indirect gap) which is a well known phenomenon [126]. Hence, in cases where the WZ and ZB have significantly different bandgaps, stabilizing the structure with the required bandgap can be achieved efficiently due to the similar heats of formation.

In addition to modifying the structures to tune the bandgap, bandgap engineering can also be achieved by making solid solutions of different semiconductors. The same has been realized in the experiments in recent works carried out in Domen's group [119, 3] in which the mixture of GaN and ZnO has the bandgap of $\sim$2.5 eV as opposed to the bandgap of $\sim$3.4 eV of the constituent compounds GaN and ZnO. Thus, these experimental results suggest that the alloying can be used as a method for the bandgap tailoring. Hence, guided by the above experiments we also explore the alloys of binary compounds in the wurtzite structures having the bandgap in the range of 1.0 - 3.5 eV. The stability of the alloy with respect to the constituent compounds

mixed in an equimolar ratio is described by the enthalpy of mixing as

$$\Delta H_{mix}^{ABCD} = E_{tot}^{ABCD} - E_{tot}^{AB} - E_{tot}^{CD} \tag{6.1}$$

where E_{tot}^{i} is the total energy of the compound 'i'. Table 6.2 shows the heat of formation of the compounds in the wurtzite structure having the bandgap in the range of 1.0-3.5 eV, ΔH is the heat of formation calculated in the present work, ΔH^{OQMD} is the heat of formation as given in the OQMD (The Open Quantum Materials Database) database [73] for the structure which has the minimum energy at 1:1 stochiometry and ΔH^{hull} is the relative energy of the compound in the current work with respect to the convex hull as given in the OQMD database. Since the enthalpies in OQMD database are based on DFT reference energies whereas we use corrected reference energies as proposed by Stevanovic *et al.* [25], therefore the difference 0.15 eV/atom or less in ours and OQMD calculations will lie within in the error bar due to the different methods used for the calculation of the reference energies. Compounds like AlI, AlBr which are significantly above the convex hull and have no structure which is stable at 1:1 stochiometry and also expected to be unstable based on the valence rule can be ruled out as they may not be possibly synthesized under normal/moderate conditions. On the other hand, compounds like GeO, AgF and PbO have different structures other than the wurtzite which are stable and lie below the convex hull. Even though energy of the wurtzite structure of these compounds lies above the convex hull by $\sim$0.35 eV/atom (Table 6.1), its likely that they can be stabilized in the wurtzite form since they exist in structures which are stable at the same stoichiometry. So, their synthesis/stabilization might be possible under moderate conditions.

In order to study the trends we made a crude approximation of the solid solution with a unit cell of four atoms due large computational time required for a larger unit cell. Based on the previous works, we believe the that the approximations made will not change the results drastically [127].

The similarity between the compounds forming the mixture in terms of the deviation of the bandgap of the mixture from the average of the bandgaps of constituent compounds has been assessed by the so-called dendrogram plot. Dendrogram is a tree diagram used in the generating hierarchical structures among the elements representing the data [120]. In Figure 6.5, we show the dendrogram plot with euclidean metric of the difference of the average bandgap of the constituent compounds and the calculated bandgap of the alloy. The clustering in a dendrogram is based on the distance measure (d_{AB}) of two

components given as

$$d_{AB} = \sum_{CD} \left(\frac{E^{gap}_{AB} + E^{gap}_{CD}}{2} - E^{gap}_{ABCD} \right)^2 \tag{6.2}$$

In the equation above AB corresponds to the compound for which the distance measure has to be calculated and the summation index CD corresponds to other compounds in the set of binary compounds which are combined with AB to form alloys. Based on the distance measure the compounds with cutoff distance measures will be clustered together. The clustering of compounds like ZnO and GaN, CdS and CdSe, ZnTe and CdTe, for which the thermodynamic/light absorption properties of the solid solutions have already been explored experimentally complements our study [119, 128, 129]. As one would expect on the chemical grounds, clustering naturally leads to the grouping of the chalcogenides of the Group 12 elements, chalcogenides of Group 14 elements, silver halides and the compounds of the trivalent ions with the Group 15 elements. As can be seen from the values close to zero along the block diagonal in the dendrogram plot that in most of the cases when the mixtures are formed from compounds in the same group, the resultant bandgaps differ only by ∼0.5 eV from the average of the bandgaps. On the other hand, mixing of the compounds from different groups leads to a significant reduction of the bandgap with respect to the average of the bandgaps in most of the cases as shown with the red blocks. The detailed description of the above trend would require electronic structure analysis of every mixture which is beyond the scope of the current work.

Figure 6.6(a) and (b) show the bandgap and enthalpy of mixing ΔH_{mix} of the mixture as given by equation (6.1). Since, The positive correlation between the bandgap and the stability [130] renders some of the mixtures metallic due to the large positive heat of mixing. As one would anticipate that the mixing of compounds with very different lattice constants will be energetically unfavorable, the red regions in Figure 6.6(b) manifest the expected trend. For example, ZnO, GaN, ScN have similar volumes, so their mixture with the tellurides, selenides or compounds of lead which have much larger volumes result to significantly positive heat of mixing which in turn leads to zero bandgap of those mixtures. Thus, exploring mixtures of compounds with similar lattice constant will have a higher probability of giving compounds with a finite bandgap.

Combiningly, Figure 6.5 and 6.6 show that the bandgap of most of the stable mixtures along the block diagonal 1 (bottom left to top right) have bandgap of ∼2.5 eV except the block containing the chalcogenides of zinc and

cadmium which has lower bandgap due to low bandgaps of the constituent compounds. On the other hand, stable compounds along the block diagonal 2 (top left to bottom right) are low bandgap mixtures with the bandgap ∼1.5 eV. Thus, the dichotomy in the bandgaps allows us to look in a definite region of the materials space for the required range of bandgaps suitable for the application in hand.

6.3 Conclusion

In the current work we have carried out a systematic analysis of the compounds in different crystal structures spanning a wide range of volumes and having the AB stoichiometry. The correlation between the crystal structure and the chemical scale factor χ gives a rationale to understand the effect of electronegativity on the crystal structure of the compounds. In addition to the binary compounds, detailed analysis of their alloys gives a rationale for the bandgap engineering via solid solutions of the semiconductors. The analysis carried out in the current work for the binary semiconductors can also be generalized to the systems containing more than two elements thus providing an elegant route to tailor the bandgap as required by the application in hand like photo-electrochemical water splitting, solar cells.

Chapter 7

Final Remarks

In the previous chapters, challenges involved in the process of materials design have been looked at. The challenges are not only faced by experimentalists but by theoreticians as well. The bottlenecks in experiments come from the limited resources and time whereas the computational scientists having access to powerful computers are limited by the accuracy of the computational methods and approximations made to mimic the experiments. But, these limitations in no way stop us to move forward. Experimental tools are becoming increasingly advanced whereas day to day developments in theory and algorithms are making computations more and more reliable.

In this work, an attempt to solve some of the materials design problem with computations and some strategies to face future challenges for the same are looked at. The assessment of recently developed mBEEF functional for the prediction of the heats of formation is an example for theoretical developments whereas the screening of materials for light absorption and hydrogen evolution reaction is an attempt to solve materials design problem regarding energy. Finally, exploring one of the many methods for the bandgap engineering shows how we can expand the materials space by using the already existing materials for different applications.

In all the above problems, we got help from the available experimental data whether it was heats of formation, activity for hydrogen evolution or the photoelectrochemical water splitting. This implies that no matter how fast, cheap and efficient computer simulations become, at the end of the day the calculated numbers have to agree with experiments. As Feynman once said: "It doesn't matter how beautiful your theory is, it doesn't matter how smart you are. If it doesn't agree with experiment, it's wrong." Therefore,

the experiments and theory have to go hand in hand to solve materials design problem in a reliable and efficient way.

One of recent examples of the synergistic effort of the experiments and theory is machine learning. People are trying to solve materials design problems using machine learning. However, the reliability of machine learning for different fields is different. For example, machine learning in astronomy is reasonably reliable because the experimental data is provided only by a very few telescopes which are very well tested. On the other hand, machine learning in materials design suffers with a lot of ambiguity, for example, variations in pseudopotentials, different electronic structure codes, plethora of unreliable experimental data etc. Therefore, I personally feel that the dream of solving materials design problem with machine learning is very far from realizable in the near future and we still have to resort to more fundamental science than blindly using computers.

Bibliography

[1] N. S. Lewis and D. G. Nocera. PNAS, 103:15729–15735, 2006.

[2] N. Armaroli and V. Balzani. Angew. Chem. Int. Ed., 46:52–66, 2007.

[3] K. Maeda and K. Domen. Chem. Mater., 22:612–623, 2010.

[4] P. C. K. Vesborg and T. F. Jaramillo. RSC Adv., 2:7933–7947, 2012.

[5] E. Schrödinger. Annalen der Physik, 384:361–376, 1926.

[6] J. Kohanoff. Electronic Structure Calculations for Solids and Molecules. Cambridge University Press, 2006. Cambridge Books Online.

[7] P. Hohenberg and W. Kohn. Phys. Rev., 136:B864, 1964.

[8] W. Kohn and L. J. Sham. Phys. Rev., 140:A1133, 1965.

[9] J. P. Perdew, K. Burke, and M. Ernzerhof. Phys. Rev. Lett., 77:3865, 1996.

[10] J. Heyd, G. E. Scuseria, and M. Ernzerhof. J. Chem. Phys., 118:8207, 2003.

[11] A. V. Krukau, O. A. Vydrov, A. F. Izmaylov, and G. E. Scuseria. J. Chem. Phys., 125:224106, 2006.

[12] A. J. Cohen, P. Mori-Sánchez, and W. Yang. Science, 321(5890):792–794, 2008.

[13] P. Mori-Sánchez, A. J. Cohen, and W. Yang. Phys. Rev. Lett., 100(14):146401, 2008.

[14] O. Gritsenko, R. van Leeuwen, E. van Lenthe, and E. J. Baerends. Phys. Rev. A, 51:1944, 1995.

[15] M. Kuisma, J. Ojanen, J. Enkovaara, and T. T. Rantala. Phys. Rev. B, 82:115106, 2010.

[16] J. P. Perdew, M. Ernzerhof, and K. Burke. J. Chem. Phys., 105:9982, 1996.

[17] C. Adamo and V. Barone. J. Chem. Phys., 110:6158, 1999.

[18] J. Paer, M. Marsman, K. Hummer, G. Kresse, and I. C. Gerber. J. Chem. Phys., 124:154709, 2006.

[19] J. Enkovaara, C. Rostgaard, J. J. Mortensen, J. Chen, M. Dułak, L. Ferrighi, J. Gavnholt, C. Glinsvad, V. Haikola, H. A. Hansen, H. H. Kristoffersen, M. Kuisma, A. H. Larsen, L. Lehtovaara, M. Ljungberg, O. Lopez-Acevedo, P. G. Moses, J. Ojanen, T. Olsen, V. Petzold, N. A. Romero, J. Stausholm-Møller, M. Strange, G. A. Tritsaris, M. Vanin, M. Walter, B. Hammer, H. Häkkinen, G. K. H. Madsen, R. M. Nieminen, J. K. Nørskov, M. Puska, T. T. Rantala, J. Schiøtz, K. S. Thygesen, and K. W. Jacobsen. Journal of Physics: Condensed Matter, 22(25):253202, 2010.

[20] J. J. Mortensen, L. B. Hansen, and K. W. Jacobsen. Phys. Rev. B, 71:035109, 2005.

[21] D. Vanderbilt. Phys. Rev. B, 41:7892–7895, 1990.

[22] P. E. Blöchl. Phys. Rev. B, 50:17953–17979, 1994.

[23] C. Rostgaard. *arXiv preprint arXiv:0910.1921v2*, 2009.

[24] M. Fuchs, J. L. F. Da Silva, C. Stampfl, J. Neugebauer, and M. Scheffler. Phys. Rev. B, 65:245212, 2002.

[25] V. Stevanović, S. Lany, X. Zhang, and A. Zunger. Phys. Rev. B, 85:115104, 2012.

[26] I. E. Castelli, T. Olsen, S. Datta, D. D. Landis, S. Dahl, K. S. Thygesen, and K. W. Jacobsen. Energy Environ. Sci., 5:5814–5819, 2012.

[27] X. Zhang, V. Stevanović, M. d'Avezac, S. Lany, and A. Zunger. Phys. Rev. B, 86:014109, 2012.

[28] S. Lany. Phys. Rev. B, 78:245207, 2008.

[29] S. L. Dudarev, G. A. Botton, S. Y. Savrasov, C. J. Humphreys, and A. P. Sutton. Phys. Rev. B, 57:1505, 1998.

[30] B. Hammer, L. B. Hansen, and J. K. Nørskov. Phys. Rev. B, 59:7413, 1999.

[31] J. M. Tao, J. P. Perdew, V. N. Staroverov, and G. E. Scuseria. Phys. Rev. Lett., 91(14):146401, 2003.

[32] R. Peverati and D. G. Truhlar. Phil. Trans. R. Soc. A, 372:2011, 2014.

[33] L. A. Constantin, E. Fabiano, and F. Della Sala. . Chem. Theory Comput., 9(5):2256–2263, 2013.

[34] J. Sun, J. P. Perdew, and A. Ruzsinszky. Proceedings of the National Academy of Sciences, 112(3):685–689, 2015.

[35] F. Della Sala, E. Fabiano, and L. A. Constantin. Phys. Rev. B, 91:035126, 2015.

[36] J. Wellendorff, K. T. Lundgaard, K. W. Jacobsen, and T. Bligaard. J. Chem. Phys., 140:144107, 2014.

[37] Standard thermodynamic properties of chemical substances, 2000. `http://www.update.uu.se/~jolkkonen/pdf/CRC_TD.pdf`.

[38] W. H. Press, B. P. Flannery, S. A. Teukolsky, and W. T. Vetterling. Numerical Recipes in C. Cambridge University Press, 1988.

[39] K. S. Brown S. L. Frederiksen, K. W. Jacobsen and J. P. Sethna. Phys. Rev. Lett., 93(16):165501, 2004.

[40] M. S. Dressselhaus and I. L. Thomas. Nature, 414:332–337, 2001.

[41] G. W. Crabtree, M. S. Dresselhaus, and M. V. Buchanan. Phys. Today, 57:39–44, 2004.

[42] J. Greeley, T. F. Jaramillo, J. L. Bonde, I. Chorkendorff, and J. K. Nørskov. Nat. Mater., 5:909–913, 2006.

[43] Y. Okamoto, S. Ida, J. Hyodo, H. Hagiwara, and T. J. Ishihara. J. Am. Chem. Soc., 133:18034–18037, 2011.

[44] S. Cobo, J. Heidkamp, P.-A. Jacques, J. Fize, V. Fourmond, L-Guetaz, B. Jousselme, V. Ivanova, H. Dau, S. Palacin, M. Fontecave, and V. Artero. Nat. Mater., 11:802–807, 2012.

[45] P. Liu and J. A. Rodriguez. J. Am. Chem. Soc., 127:14871–14878, 2005.

[46] E. J. Popczun, J. R. McKone, C. G. Read, A. J. Biacchi, A. M. Wiltrout, N. S. Lewis, and R. E. Schaak. J. Am. Chem. Soc., 135:9267–9270, 2013.

[47] L. Feng J. Rossmeisl M. H. Hansen, L. A. Stern and X. Hu. Phys. Chem. Chem. Phys., 17:10823–10829, 2015.

[48] D. Voiry, H. Yamaguchi, J. Li, R. Silva, D. C. B. Alves, T. Fujita, M. Chen, T. Asefa, V. B. Shenoy, G. Eda, and M. Chhowalla . Nat. Mater., 12:850–855, 2013.

[49] M. A. Lukowski, A. S. Daniel, F. Meng, A. Forticaux, L. Li, and S. Jin. J. Am. Chem. Soc., 135:10274–10277, 2013.

[50] D. Voiry, M. Salehi, R. Silva, T. Fujita, M. Chen, T. Asefa, V. B. Shenoy, G. Eda, and M. Chhowalla. Nano Letters, 13:6222–6227, 2013.

[51] H. Wang, Z. Lu, D. Kong, J. Sun, T. M. Hymel, and Y. Cui. ACS Nano, 8:4940–4947, 2014.

[52] T. F. Jaramillo, K. P. Jørgensen, J. Bonde, J. H. Nielsen, S. Horch, and I. Chorkendorff. Science, 317:100–102, 2007.

[53] M. V. Bollinger, K. W. Jacobsen, and J. K. Nørskov. Phys. Rev. B, 67:085410, 2003.

[54] B. Hinnemann, P. G. Moses, J. Bonde, K. P. Jørgensen, J. H. Nielsen, S. Horsch, I. Chorkendorff, and J. K. Nørskov. J. Am. Chem. Soc., 127:5308–5309, 2005.

[55] A. N. Enyashin, L. Yadgarov, L. Houben, I. Popov, M. Weidenbach, R. Tenne, M. Bar-Sadan, and G. Seifert. J. Phys. Chem. C, 115:24586–24591, 2011.

[56] K. Rossnage. J. Phys.: Condens. Matter, 23:213001, 2011.

[57] K. Dolui and S. Sanvito. *arXiv preprint arXiv:1310.1866*, 2013.

[58] L. Fu X. Qian, J. Liu and J. Li. Science, 346:1344–1347, 2014.

[59] M. Kan, J. Y. Wang, X. W. Li, S. H. Zhang, Y. W. Li, Y. Kawazoe, Q. Sun, and P. Jena. J. Phys. Chem. C, 118:1515–1522, 2014.

[60] S. Tongay, H. Sahin, C. Ko, A. Luce, W. Fan, K. Liu, J. Zhou, Y.-S. Huang, C.-H. Ho, J. Yan, D. F. Ogletree, S. Aloni, J. Ji, S. Li, J. Li, F. M. Peeters, and J. Wu. Nat. Commun., 5:3252, 2014.

[61] H. T. Stokes and D. M. Hatch. J. Appl. Cryst., 38:237–238, 2005.

[62] C. Ataca, H. Şahin, and S. Ciraci. J. Phys. Chem. C, 116:8983–8999, 2012.

[63] S. Trasatti. J. Electroanal. Chem., 39:163, 1972.

[64] J. O'M. Bockris, A. K. N. Reddy, and M. Gamboa-Aldeco. Modern Electrochemistry 2A 2nd ed. Kluwer Academic/Plenum Publishers: New York, 1998.

[65] C. Tsai, F. A.-Pedersen, and J. K. Nørskov. Nano Letters, 14:1381–1387, 2014.

[66] C. Tsai, J. K. Nørskov K. Chan, and F. A.-Pedersen. J. Phys. Chem. Lett., 5:3884–3889, 2014.

[67] K. K. Irikura. J. Phys. Chem. Ref. Data, 36:389, 2007.

[68]

[69] L. C. Seitz, Z. Chen, A. J. Forman, B. A. Pinaud, J. D. Benck, and T. F. Jaramillo. ChemSusChem, 7:1372, 2014.

[70] J. Wellendorff, K. T. Lundgaard, A. Møgelhøj, V. Petzold, D. D. Landis, J. K. Nørskov, T. Bligaard, and K. W. Jacobsen. Phys. Rev. B, 85:235149, 2012.

[71] A. J. Medford, J. Wellendorff, A. Vojvodic, F. Studt, F. A.-Pedersen, K. W. Jacobsen, T. Bligaard, and J. K. Nørkov. Science, 345:197, 2014.

[72] S. Mubeen, J. Lee, N. Singh, M. Moskovitsb, and E. W. McFarland. Energy Environ. Sci., 6:1633, 2013.

[73] J. E. Saal, S. Kirklin, M. Aykol, B. Meredig, and C. Wolverton. JOM, 65:1501–1509, 2013.

[74] S. Lebègue, T. Björkman, M. Klintenberg, R. M. Nieminen, and O. Eriksson. Phys. Rev. X, 3:031002, 2013.

[75] L. Vayssierres. On Solar Hydrogen and Nanotechnology. John Wiley and Sons (Asia) Pvt. Ltd, 2009.

[76] G.A. Chamberlain. Solar Cells, 8(1):47 – 83, 1983.

[77] M. Grätzel. J. Photochemistry and Photobiology C: Photochemistry Reviews, 4(2):145 – 153, 2003.

[78] M. Ni, M. K.H. Leung, D. Y.C. Leung, and K. Sumathy. Renewable and Sustainable Energy Reviews, 11(3):401 – 425, 2007.

[79] A. Kudo and Y. Miseki. Chem. Soc. Rev., 38:253–278, 2009.

[80] K. Sayama Z. Zou, J. Ye and H. Arakawa. Nature, 414:625–627, 2001.

[81] L. Schmidt-Mende, A. Fechtenkötter, K. Müllen, E. Moons, R. H. Friend, and J. D. MacKenzie. Science, 293(5532):1119–1122, 2001.

[82] A. Hagfeldt and M. Grätzel. Accounts of Chemical Research, 33(5):269–277, 2000.

[83] A. Fujishima and K. Honda. Nature, 238:37–38, 1972.

[84] B. Kumar, M. Llorente, J. Froehlich, T. Dang, A. Sathrum, and C. P. Kubiak. Annual Review of Physical Chemistry, 63(1):541–569, 2012.

[85] C. S. Enache, D. Lloyd, M. R. Damen, J. Schoonman, and R. van de Krol. The Journal of Physical Chemistry C, 113(44):19351–19360, 2009.

[86] Y. Liang, T. Tsubota, L. P. A. Mooij, and R. van de Krol. The Journal of Physical Chemistry C, 115(35):17594–17598, 2011.

[87] F. F. Abdi and R. van de Krol. The Journal of Physical Chemistry C, 116(17):9398–9404, 2012.

[88] K. S. Thygesen S. Dahl I. Chorkendorff T. F. Jaramillo I. E. Castelli, D. D. Landis and K. W. Jacobsen. Energy Environ. Sci., 5:9034–9043, 2012.

[89] M. Oshikiri, M. Boero, J. Ye, Z. Zou, and G. Kido. J. Chem. Phys., 117(15):7313–7318, 2002.

[90] G. Hautier W. Chen W. D. Richards S. Dacek S. Cholia D. Gunter D. Skinner G. Ceder A. Jain, S. P. Ong and K. A. Persson. APL Materials, 1:011002, 2013.

[91] M. Pandey H. Li K. S. Thygesen B. Seger A. Jain K. A. Persson G. Ceder K. W. Jacobsen I. E. Castelli, F. Hüser. Adv. Energy Mater., 5:1400915, 2015.

[92] A. Belsky, M. Hellenbrandt, V. L. Karen, and P. Luksch. Acta Cryst., B58:364–369, 2002.

[93] D. S. Ginley W. Tumas V. Stevanovic, S. Lany and A. Zunger. Phys. Chem. Chem. Phys., 16:3706, 2014.

[94] M. A. Butler and D. S. Ginley. J. Electrochem. Soc., 125:228–232, 1978.

[95] Filip A. Rasmussen and Kristian S. Thygesen. J. Phys. Chem. C, 119(23):13169–13183, 2015.

[96] K. S. Thygesen I. E. Castelli and K. W. Jacobsen. Top. Catal., 57(1–4):265–272, 2014.

[97] P. Lazic K. A. Persson, B. Waldwick and G. Ceder. Phys. Rev. B, 85:235438, 2012.

[98] A. E. Lavat R. P. Diez, E. J. Baran and M. C. Grasselli. J. Phys. Chem. Solids, 56:135, 1995.

[99] K. Rubesova and D. Sykorova. J. Sol-Gel Sci. Technol., 49:228, 2009.

[100] C. L. Teske H. Szillat. Z. Anorg. Allge. Chem., 620:1307, 1994.

[101] R. Nagarajan H. Yanagi, J. Tate and A. W. Sleight. Solid State Commun., 122:295, 2002.

[102] H. Irie Y. Maruyama and K. Hashimoto. J. Phys. Chem. B, 110:23274, 2006.

[103] D. Chen Z. G. Zou S. X. Ouyang, N. Kikugawa and J. H. Ye. J. Phys. Chem. C, 113:1560, 2009.

[104] M. Katagiri T. Kako, Z. G. Zou and J. H. Ye. Chem. Mater., 19:198, 2007.

[105] Q. Z. Liu Y. F. Zhu J. J. Liu, S. F. Chen and J. F. Zhang. Chem. Phys. Lett., 572:101, 2013.

[106] H. Kumigashira S. Okamoto S. Aizaki A. Fujimori K. Yoshimatsu, T. Okabe and M. Oshima. Phys. Rev. Lett., 104:147601, 2010.

[107] M. Kobayashi K. Horiba T. Yoshida A. Fujimori M. Oshima K. Yoshimatsu, E. Sakai and H. Kumigashira. Phys. Rev. B, 88:115308, 2013.

[108] H. Kumigashira T. Yoshida A. Fujimori K. Yoshimatsu, K. Horiba and M. Oshima. Science, 333:319, 2011.

[109] S. Kumar S. J. May J. A. Borchers B. B. Maranwille J. Zarestky S. G. E. te Velthuis J. van den Brink T. S. Santos, B. J. Kirby and A. Bhattacharya. Phys. Rev. Lett., 107:167202, 2011.

[110] C. R. Freeze C. A. Jackson, J. Y. Zhang and S. Stemmer. Nat. Commun., 5:1, 2014.

[111] B. Ehrlich C. Grote and R. F. Berger. Phys. Rev. B, 90:205202, 2014.

[112] H. W. Eng H. Mizoguchi and P. M. Woodward. Inorg. Chem., 43:1667, 2004.

[113] H. Hara J. N. Kondo D. Yamasita, T. Takata and K. Domen. Solid State Ionics, 172:591, 2004.

[114] T. Luttrell, S. Halpegamage, J. Tao, A. Kramer, S. Sutter, and M. Batzill. Scientific Reports, 4:4043, 2014.

[115] M. Lazzeri, A. Vittadini, and A. Selloni. Phys. Rev. B, 63:155409, 2001.

[116] S. W. H. Eijt, J. de Roode, H. Schut, B. J. Kooi, and J. Th. M. De Hosson. App. Phys. Lett., 91:201906, 2007.

[117] A. N. Baranov, O. O. Kurakevych, V. A. Tafeenko, P. S. Sokolov, G. N. Panin, and V. L. Solozhenko. Jour. App. Phys., 107:073519, 2010.

[118] D. G. Pettifor. Jour. Phys. C:Solid State Phys., 19:285–313, 1986.

[119] K. Maeda, T. Takata, M. Hara, N. Saito, Y. Inoue, H. Kobayashi, and K. Domen. Jour. Am. Chem. Soc., 127:8286–8287, 2005.

[120] I. E. Castelli and K. W. Jacobsen. Modelling Simul. Mater. Sci. Eng., 22:055007, 2014.

[121] W. Zhang, A. R. Oganov, A. F. Goncharov, Q. Zhu, S. E. Boulfelfel, A. O. Lyakhov, E. Stavrou, M. Somayazulu, V. B. Prakapenka, and Z. Konopkova. Science, 342:1502–1505, 2013.

[122] M. Pandey and R. G. S. Pala. Jour. Chem. Phys., 136:044703, 2012.

[123] M. Pandey and R. G. S. Pala. Jour. Phys. Chem. C, 117:7643–7647, 2013.

[124] P. Gangwar, M. Pandey S. Sivakumar, R. G. S. Pala, and G. Parthasarathy. Cryst. Growth Des., 13:2344–2349, 2013.

[125] H. L. Meyerheim, C. Tusche, A. Ernst, S. Ostanin, I. V. Maznichenko, K. Mohseni, N. Jedrecy, J. Zegenhagen, J. Roy, I. Mertig, and J. Kirschner. Phys. Rev. Lett., 102:156102, 2009.

[126] C-Y. Yeh, S.-H. Wei, and A. Zunger. Phys. Rev. B, 50(8):2715(R), 1994.

[127] J. N. Hart and N. L. Allan. Adv. Mater., 25:2989–2993, 2013.

[128] V.R. Sidorko and L.V. Goncharuk. J. Alloys Compd., 228:13–15, 1995.

[129] M. A. Hossain, J. R. Jennings, N. Mathews, and Q. Wang. Phys. Chem. Chem. Phys., 14:7154–7161, 2012.

[130] J. Portier, H. S. Hilal, I. Saadeddin, S. J. Hwang, M. A. Subramanian, and G. Campet. Prog. Solid State Ch., 32:207–217, 2004.

Papers

Paper I

Heats of formation of solids with error estimation: The mBEEF functional with and without fitted reference energies
M. Pandey and K. W. Jacobsen Physical Review B 91 (23), 235201 (2015)

Heats of formation of solids with error estimation: The mBEEF functional with and without fitted reference energies

Mohnish Pandey and Karsten W. Jacobsen*

Center for Atomic-scale Materials Design, Department of Physics, Technical University of Denmark, DK-2800 Kongens Lyngby, Denmark

(Received 30 January 2015; revised manuscript received 12 May 2015; published 3 June 2015)

The need for prediction of accurate electronic binding energies has led to the development of different schemes for combining density functional calculations, typically at the level of the generalized gradient approximation (GGA), with experimental information. We analyze one such scheme by Stevanović *et al.* [Phys. Rev. B **85**, 115104 (2012)] for predictions of compound enthalpies of formation using fitted elemental-phase reference energies. We show that different versions of GGA with or without +U and a meta-GGA (TPSS) lead to comparable accuracy after fitting the reference energies. Our results also show that the recently developed mBEEF, a Bayesian error estimation functional, gives comparable accuracy with the other functionals even without the fitting. The mBEEF functional furthermore supplies an ensemble estimate of the prediction errors in reasonable agreement with the actual errors. We also show that using the fitting scheme on the mBEEF ensemble leads to improved accuracy including realistic error estimation.

DOI: 10.1103/PhysRevB.91.235201 PACS number(s): 71.15.Mb, 31.15.eg, 71.15.Nc

I. INTRODUCTION

In the past two decades, Kohn-Sham density functional theory (KS-DFT) based electronic structure calculations [1,2] have greatly enhanced our understanding of the properties of materials. The drastic reduction in the number of degrees of freedom in the electronic structure problem within the KS-DFT framework makes it an efficient tool for quantum mechanical description of materials. The key ingredient in the KS-DFT is an energy functional which depends on the ground-state electronic density and the accuracy of calculations depends on the quality of the approximations applied to the functional. Efficient and realistic description of materials requires calculations which are not too computationally expensive and reasonably accurate. In the generalized gradient approximation framework (GGA) the PBE functional [3] has been widely used and has a reasonable trade-off between accuracy and efficiency. Despite being remarkably successful in the past, it has its limitations as well. For example, the heats of formation predicted by the PBE functional deviate from experiments by ∼0.25 eV/atom [4] which makes it difficult to predict the stabilities of compounds in many cases. It severely plagues the process of searching for new materials for different applications where stability of the compounds is one of the main criteria [5–7].

Recently, Stevanović *et al.* proposed a scheme known as fitted elemental reference phase energies (FERE) to improve the prediction of the heats of formation of semiconductors [4,8]. Their scheme is based on the idea of using the reference phase energies as parameters and calculating these parameters by minimizing the root mean square (rms) error between the calculated and experimental heats of formation. The scheme uses a mixture of the PBE and PBE with Hubbard-U correction (PBE+U) for the calculation of the heats of formation. The proposed scheme shows clear improvement when comparing with the experimental heats of formation of solids. In the present work, we carry out similar analysis with a class of GGA functionals, namely, the PBE without Hubbard-U corrections, PBE with U corrections, and RPBE [9]. We furthermore exploit the possibilities at the meta-GGA level by including the TPSS functional [10–14] as a representative together with a recently developed meta-GGA functional mBEEF [15], a Bayesian error estimation functional. One of the advantages of the mBEEF functional over the other functionals is that it supplies an error estimate which tells how reliable a particular calculated energy difference is. The details of the mBEEF functional and its comparison to other GGAs and meta-GGA functionals in terms of exchange enhancement factors can be found in Ref. [15]. Calculating the heats of formation on a test set of 24 compounds which have not been used in the the data set for fitting, we show that the mBEEF functional without any fitting is nearly as accurate as the fitted GGA functionals and the fitted TPSS functional and includes a realistic error prediction with a small overestimation. Applying the FERE scheme to the mBEEF ensemble leads to an improved prediction quality and a corresponding reduction of the predicted error bars. Quantitatively, the rms errors in the training data set with the PBE, RPBE, PBE+U, TPSS, and mBEEF functionals reduce from 0.22, 0.28, 0.21, 0.21, and 0.14 eV per atom to 0.09, 0.09, 0.08, 0.10, and 0.07 eV per atom.

II. COMPUTATIONAL METHODOLOGY

All the calculations in the current work use the GPAW code [16] with the projector augmented wave (PAW) [17] description of the atoms. We consider the PBE [3], RPBE [9], PBE+U [18], TPSS [10], and mBEEF [15] exchange-correlation functionals. For the PBE+U calculations, as suggested by Stevanović *et al.*, we use the value of $U = 3.0$ eV for all the transition elements except Ag and Cu for which we use a U value of 5.0 eV. In the calculations involving magnetism, the spin configurations have been taken from the lowest energy structure reported in the experiments. For example, the Fe reference state which has the bcc structure has been treated ferromagnetically whereas the iron oxide has been treated

*kwj@fysik.dtu.dk

antiferromagnetically as reported in the experiments. We use a real-space description of the wave functions with a grid spacing of 0.18 Å. A Fermi temperature of 0.05 eV for the solid phases is used to enhance convergence. Brillouin zone sampling is done with a k-point mesh of $33a_x^{-1} \times 33a_y^{-1} \times 33a_z^{-1}$ with the Monkhorst-Pack [19] sampling scheme. Forces are minimized down to 0.05 eV/Å for all the relaxations. Uncertainties in the heats of formations with the mBEEF functionals are explicitly calculated using the ensemble of functionals proposed in Ref. [20]. All the experimental heats of formation have been taken from Refs. [4,21].

III. RESULTS AND DISCUSSIONS

A. Heats of formation with the DFT

The standard heat of formation of a solid calculated with DFT is

$$\Delta H^{\mathrm{DFT}}(A_{p1}B_{p2}\dots) = E(A_{p1}B_{p2}\dots) - \Sigma p_i \mu_i^0, \quad (1)$$

where $E(A_{p1}B_{p2}\dots)$ indicates the total energy of $A_{p1}B_{p2}\dots$ calculated with DFT and the μ_i^0 denotes the chemical potentials of the elements under standard conditions calculated with DFT. The entropic and zero-point energy corrections have been ignored in the above expression. The calculation of the heats of formation using the above expression with the PBE, RPBE, TPSS, and PBE+U functionals provide a single number as the best estimate of the heat of formation. In comparison, the mBEEF functional provides both a best estimate but also via the ensemble of functionals an estimation of the error bar on the calculated heat of formation. The functionals in the mBEEF ensemble differ from each other by the values of the parameters defining the functional [15].

The calculated heats of formation versus the experimental heats of formation (eV/per atom) of a set of 257 binary compounds with the PBE, RPBE, PBE+U, TPSS, and mBEEF functionals are shown in Fig. 1, panels (a), (c), (e), (g), and (i). The set of compounds we use has about 80% overlap with the set of 252 compounds used by Stevanović *et al.* [4] and the full list of compounds is given in Table I along with the heats of formation calculated with the mBEEF and the mBEEF with fitting of reference energies. The difference between our data set and the one of Stevanović *et al.* gives rise to somewhat different results in detail but the trends remain the same. In the figure MAE and σ denote the mean absolute error and standard deviation with respect to the experimental heats of formation. The observed trend in Figs. 1(a) and 1(c) is a similar behavior for the PBE and RPBE functionals with underbinding in most of the cases with a very few overbinding cases. This behavior in the GGA functionals arises due to the overbinding of the reference phases and the underbinding in the multinary compounds leading to an incomplete cancellation of the errors [22]. In Fig. 1(e) the direction of the deviation in the PBE+U heats of formation is not very systematic, i.e., underbinding in some cases and overbinding in others. This behavior has also been observed in Ref. [23]. The predictions do not significantly improve with the TPSS functional as shown in Fig. 1(g). The MAE and rms in the TPSS predictions turn out to be similar to the GGA functionals. An important factor in the calculated errors is the dissimilar nature of the reactants and the products. Reactions in which both sides have similar compounds are

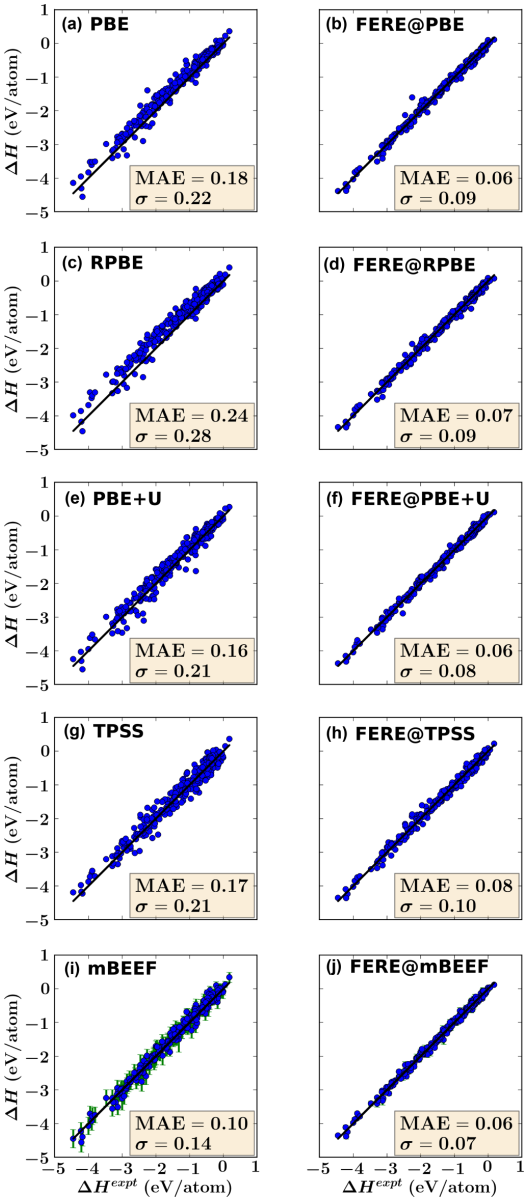

FIG. 1. (Color online) (a), (c), (e), (g), and (i) show the heats of formation calculated with the PBE, RPBE, PBE+U, TPSS, and mBEEF functionals, respectively, versus the experimental heats of formation. (b), (d), (f), (h), and (j) show the heats of formation calculated with PBE, RPBE, PBE+U, TPSS, and mBEEF functionals, respectively, versus the experimental heats of formation after correcting the reference phase energies using the experimental heats of formation as the training set. MAE and σ in (a)–(j) indicate the mean absolute error and standard deviation of the calculated heats of formation with respect to the experimental heats of formation.

TABLE I. The heats of formation of the solids used in the training set calculated with the mBEEF ($\Delta H_{\mathrm{mBEEF}}$) and mBEEF with the FERE ($\Delta H^{\mathrm{FERE}}_{\mathrm{mBEEF}}$). The experimental values (ΔH_{Expt}) are also given for comparison. All the energies are in eV/atom.

Compound	ΔH_{Expt}	$\Delta H_{\mathrm{mBEEF}}$	$\Delta H^{\mathrm{FERE}}_{\mathrm{mBEEF}}$	Compound	ΔH_{Expt}	$\Delta H_{\mathrm{mBEEF}}$	$\Delta H^{\mathrm{FERE}}_{\mathrm{mBEEF}}$
Ag_2Se	-0.15	0.02 ± 0.12	-0.07 ± 0.09	AgCl	-0.66	-0.56 ± 0.24	-0.58 ± 0.09
AgI	-0.32	-0.32 ± 0.13	-0.39 ± 0.08	Ag_2O	-0.11	-0.07 ± 0.20	-0.14 ± 0.03
Ag_2O_2	-0.06	-0.07 ± 0.19	-0.13 ± 0.04	$AlCl_3$	-1.82	-1.74 ± 0.19	-1.80 ± 0.05
AlF_3	-3.90	-3.93 ± 0.27	-3.85 ± 0.06	Al_2O_3	-3.47	-3.24 ± 0.24	-3.41 ± 0.07
AlN	-1.65	-1.55 ± 0.23	-1.72 ± 0.04	AlAs	-0.61	-0.66 ± 0.14	-0.64 ± 0.05
AlP	-0.85	-0.76 ± 0.15	-0.87 ± 0.06	Al_2Se_3	-1.18	-0.93 ± 0.12	-1.13 ± 0.04
AsI_3	-0.15	-0.18 ± 0.03	-0.12 ± 0.04	AuBr	-0.07	-0.11 ± 0.11	-0.06 ± 0.03
AuCl	-0.18	-0.27 ± 0.17	-0.12 ± 0.04	AuI	-0.00	-0.08 ± 0.11	0.03 ± 0.04
Au_2O_3	-0.01	-0.11 ± 0.19	-0.02 ± 0.05	$AuCl_3$	-0.17	-0.39 ± 0.20	-0.29 ± 0.05
AuF_3	-0.94	-1.24 ± 0.23	-1.01 ± 0.09	BN	-1.32	-1.38 ± 0.14	-1.34 ± 0.04
B_2O_3	-2.64	-2.60 ± 0.16	-2.61 ± 0.05	BaF_2	-4.17	-4.40 ± 0.28	-4.25 ± 0.04
BaO_2	-2.19	-2.19 ± 0.23	-2.22 ± 0.05	BaS	-2.38	-2.39 ± 0.17	-2.44 ± 0.04
$BaCl_2$	-2.95	-2.96 ± 0.23	-2.94 ± 0.04	BaO	-2.86	-2.75 ± 0.22	-2.77 ± 0.04
$BaBr_2$	-2.62	-2.48 ± 0.13	-2.59 ± 0.03	BaI_2	-2.10	-2.02 ± 0.11	-2.07 ± 0.04
BeO	-3.14	-2.95 ± 0.23	-3.03 ± 0.05	BeS	-1.21	-1.18 ± 0.16	-1.28 ± 0.04
BeI_2	-0.67	-0.64 ± 0.06	-0.72 ± 0.06	$BiBr_3$	-0.72	-0.71 ± 0.08	-0.81 ± 0.05
Bi_2O_3	-1.19	-1.17 ± 0.15	-1.16 ± 0.07	Bi_2S_3	-0.30	-0.29 ± 0.09	-0.31 ± 0.07
CaF_2	-4.21	-4.56 ± 0.29	-4.39 ± 0.07	CaI_2	-1.84	-1.82 ± 0.10	-1.84 ± 0.05
CaO	-3.29	-3.25 ± 0.25	-3.23 ± 0.04	CaS	-2.45	-2.43 ± 0.19	-2.43 ± 0.04
$CaBr_2$	-2.36	-2.26 ± 0.10	-2.34 ± 0.03	$CaCl_2$	-2.75	-2.78 ± 0.22	-2.72 ± 0.05
CaC_2	-0.21	-0.13 ± 0.12	-0.21 ± 0.04	CdS	-0.78	-0.77 ± 0.13	-0.80 ± 0.05
CdF_2	-2.42	-2.76 ± 0.29	-2.60 ± 0.08	CdO	-1.34	-1.20 ± 0.20	-1.20 ± 0.10
CdSe	-0.75	-0.71 ± 0.10	-0.74 ± 0.05	CdTe	-0.48	-0.61 ± 0.10	-0.51 ± 0.04
CdI_2	-0.70	-0.63 ± 0.07	-0.66 ± 0.05	CoS	-0.43	-0.28 ± 0.17	-0.31 ± 0.08
CoSe	-0.32	-0.27 ± 0.19	-0.31 ± 0.03	Co_3O_4	-1.32	-1.50 ± 0.38	-1.51 ± 0.14
Co_3S_4	-0.53	-0.45 ± 0.16	-0.49 ± 0.07	CrS	-0.81	-0.83 ± 0.16	-0.77 ± 0.12
CrF_3	-3.00	-3.26 ± 0.34	-3.04 ± 0.09	CrO_2	-2.07	-2.06 ± 0.28	-2.02 ± 0.06
Cr_2O_3	-2.36	-2.52 ± 0.33	-2.46 ± 0.07	CrF_4	-2.58	-2.72 ± 0.25	-2.50 ± 0.11
CsBr	-2.10	-1.99 ± 0.10	-2.10 ± 0.03	CsCl	-2.30	-2.25 ± 0.18	-2.27 ± 0.01
CsF	-2.87	-2.98 ± 0.22	-2.90 ± 0.04	Cu_3N	0.18	0.34 ± 0.14	0.12 ± 0.03
CuO	-0.82	-0.58 ± 0.21	-0.76 ± 0.04	Cu_2O	-0.58	-0.36 ± 0.20	-0.58 ± 0.05
CuF_2	-1.88	-1.85 ± 0.29	-1.80 ± 0.13	Cu_2Sb	-0.04	0.02 ± 0.05	-0.07 ± 0.04
CuI	-0.35	-0.15 ± 0.10	-0.33 ± 0.04	Cu_2Se	-0.21	0.10 ± 0.10	-0.13 ± 0.03
Cu_3P	-0.17	0.01 ± 0.05	-0.18 ± 0.09	CuS	-0.28	-0.17 ± 0.16	-0.37 ± 0.05
Fe_2O_3	-1.71	-1.69 ± 0.26	-1.89 ± 0.11	FeS	-0.52	-0.35 ± 0.12	-0.61 ± 0.04
FeF_2	-2.46	-2.27 ± 0.31	-2.27 ± 0.10	FeO	-1.41	-1.15 ± 0.19	-1.39 ± 0.08
FeSe	-0.39	-0.04 ± 0.11	-0.30 ± 0.13	GaN	-0.81	-0.48 ± 0.17	-0.72 ± 0.06
GaP	-0.47	-0.44 ± 0.08	-0.63 ± 0.05	GaAs	-0.39	-0.42 ± 0.08	-0.47 ± 0.02
GaSb	-0.22	-0.20 ± 0.06	-0.29 ± 0.03	$GaCl_3$	-1.36	-1.25 ± 0.20	-1.34 ± 0.09
GaF_3	-3.01	-2.96 ± 0.24	-2.92 ± 0.03	Ga_2O_3	-2.26	-1.99 ± 0.19	-2.21 ± 0.03
Ga_2S_3	-1.07	-0.70 ± 0.11	-0.95 ± 0.04	Ga_2Se_3	-0.85	-0.59 ± 0.08	-0.85 ± 0.03
GaSe	-0.83	-0.61 ± 0.06	-0.91 ± 0.03	GaS	-1.09	-0.68 ± 0.08	-0.98 ± 0.04
GeTe	-0.10	-0.04 ± 0.06	-0.17 ± 0.04	GeS	-0.39	-0.20 ± 0.08	-0.46 ± 0.03
Ge_3O_6	-1.90	-1.78 ± 0.16	-1.95 ± 0.07	GeSe	-0.48	-0.11 ± 0.07	-0.38 ± 0.04
Ge_4O_8	-2.00	-1.71 ± 0.15	-1.88 ± 0.08	HfN	-1.91	-1.74 ± 0.14	-1.94 ± 0.06
$HfCl_4$	-2.05	-2.07 ± 0.22	-2.11 ± 0.06	HfO_2	-3.95	-3.71 ± 0.23	-3.88 ± 0.05
HfF_4	-4.00	-4.07 ± 0.26	-3.98 ± 0.04	HgSe	-0.24	-0.26 ± 0.11	-0.31 ± 0.02
HgTe	-0.22	-0.32 ± 0.13	-0.23 ± 0.02	HgS	-0.30	-0.21 ± 0.13	-0.26 ± 0.03
HgO	-0.47	-0.36 ± 0.14	-0.38 ± 0.05	HgI_2	-0.36	-0.37 ± 0.07	-0.41 ± 0.02
$HgCl_2$	-0.77	-0.82 ± 0.21	-0.79 ± 0.07	InN	-0.10	0.00 ± 0.15	-0.12 ± 0.03
InP	-0.46	-0.34 ± 0.08	-0.41 ± 0.04	InTe	-0.50	-0.32 ± 0.04	-0.37 ± 0.06
InAs	-0.31	-0.39 ± 0.08	-0.31 ± 0.03	InS	-0.70	-0.61 ± 0.13	-0.78 ± 0.02
InSb	-0.16	-0.27 ± 0.07	-0.24 ± 0.03	IrO_2	-0.95	-0.79 ± 0.18	-0.92 ± 0.03
$IrCl_3$	-0.64	-0.59 ± 0.17	-0.64 ± 0.03	IrS_2	-0.48	-0.36 ± 0.14	-0.52 ± 0.03
K_2O	-1.25	-1.22 ± 0.21	-1.28 ± 0.05	K_2S	-1.31	-1.24 ± 0.16	-1.31 ± 0.04
K_2Se	-1.36	-1.24 ± 0.14	-1.31 ± 0.05	KF	-2.94	-3.19 ± 0.24	-3.11 ± 0.06
KCl	-2.26	-2.25 ± 0.17	-2.26 ± 0.02	K_2O_2	-1.28	-1.23 ± 0.22	-1.28 ± 0.06

TABLE I. (*Continued.*)

Compound	ΔH_{Expt}	$\Delta H_{\mathrm{mBEEF}}$	$\Delta H_{\mathrm{mBEEF}}^{\mathrm{FERE}}$	Compound	ΔH_{Expt}	$\Delta H_{\mathrm{mBEEF}}$	$\Delta H_{\mathrm{mBEEF}}^{\mathrm{FERE}}$
K_3As	-0.48	-0.40 ± 0.11	-0.35 ± 0.06	K_2S_2	-1.12	-1.11 ± 0.14	-1.18 ± 0.03
LaS	-2.36	-2.14 ± 0.16	-2.40 ± 0.07	LaN	-1.57	-1.32 ± 0.18	-1.53 ± 0.07
LaI_3	-1.73	-1.61 ± 0.09	-1.76 ± 0.03	$LaCl_3$	-2.78	-2.67 ± 0.23	-2.75 ± 0.06
Li_2O	-2.07	-2.00 ± 0.26	-2.07 ± 0.10	Li_2S	-1.52	-1.51 ± 0.15	-1.59 ± 0.03
Li_2Se	-1.45	-1.37 ± 0.11	-1.46 ± 0.04	Li_3N	-0.43	-0.45 ± 0.24	-0.50 ± 0.10
Li_3Sb	-0.83	-0.67 ± 0.07	-0.65 ± 0.09	LiF	-3.19	-3.37 ± 0.23	-3.30 ± 0.07
Li_3Bi	-0.60	-0.57 ± 0.05	-0.61 ± 0.09	LiCl	-2.12	-2.03 ± 0.17	-2.05 ± 0.11
Li_2O_2	-1.64	-1.58 ± 0.21	-1.64 ± 0.06	MgTe	-1.08	-1.05 ± 0.09	-1.06 ± 0.04
MgS	-1.79	-1.60 ± 0.15	-1.74 ± 0.06	MgSe	-1.52	-1.41 ± 0.12	-1.56 ± 0.05
MgO	-3.11	-3.14 ± 0.20	-3.26 ± 0.06	Mg_3Bi_2	-0.32	-0.23 ± 0.07	-0.32 ± 0.05
MgF_2	-3.88	-3.79 ± 0.25	-3.71 ± 0.05	MnS	-1.11	-1.08 ± 0.23	-1.03 ± 0.06
MnO_2	-1.80	-1.99 ± 0.28	-1.96 ± 0.09	Mn_3O_4	-2.05	-2.13 ± 0.28	-2.07 ± 0.01
Mn_2O_3	-1.99	-1.99 ± 0.27	-1.94 ± 0.02	MoS_2	-0.81	-0.83 ± 0.08	-0.86 ± 0.03
MoO_2	-2.03	-1.95 ± 0.18	-1.96 ± 0.04	MoO_3	-1.93	-1.93 ± 0.18	-1.95 ± 0.05
NaF	-2.97	-3.04 ± 0.21	-2.93 ± 0.05	Na_2O	-1.43	-1.49 ± 0.18	-1.51 ± 0.10
Na_2S	-1.26	-1.24 ± 0.12	-1.28 ± 0.03	Na_2Se	-1.18	-1.19 ± 0.12	-1.23 ± 0.04
Na_2C_2	0.06	0.12 ± 0.09	0.04 ± 0.03	NaCl	-2.13	-2.09 ± 0.17	-2.07 ± 0.06
Na_2S_2	-1.03	-0.97 ± 0.12	-1.02 ± 0.04	Na_2Se_2	-0.97	-0.95 ± 0.13	-1.00 ± 0.06
Na_3Bi	-0.46	-0.40 ± 0.07	-0.39 ± 0.06	Na_2O_2	-1.32	-1.26 ± 0.18	-1.29 ± 0.08
NbN	-1.22	-1.15 ± 0.13	-1.13 ± 0.04	NbO	-2.10	-2.06 ± 0.14	-2.07 ± 0.03
Nb_2O_5	-2.81	-2.85 ± 0.21	-2.87 ± 0.04	NbF_5	-3.13	-3.52 ± 0.23	-3.33 ± 0.13
NbO_2	-2.75	-2.76 ± 0.23	-2.77 ± 0.05	$NbCl_5$	-1.38	-1.46 ± 0.22	-1.42 ± 0.05
NiS	-0.43	-0.17 ± 0.12	-0.35 ± 0.04	NiSb	-0.34	-0.36 ± 0.07	-0.33 ± 0.06
NiTe	-0.28	-0.23 ± 0.06	-0.28 ± 0.03	NiSe	-0.31	-0.14 ± 0.09	-0.32 ± 0.03
Ni_3S_2	-0.42	-0.28 ± 0.13	-0.48 ± 0.03	OsO_4	-0.82	-1.12 ± 0.19	-0.83 ± 0.01
PI_3	-0.16	-0.05 ± 0.06	-0.06 ± 0.05	PCl_3	-0.83	-0.83 ± 0.21	-0.76 ± 0.09
PBr_5	-0.47	-0.31 ± 0.04	-0.42 ± 0.05	PCl_5	-0.77	-0.74 ± 0.19	-0.68 ± 0.06
PbO	-1.13	-1.08 ± 0.16	-1.08 ± 0.04	PbS	-0.52	-0.52 ± 0.14	-0.53 ± 0.06
PbF_2	-2.29	-2.60 ± 0.25	-2.43 ± 0.04	PbO_2	-0.96	-0.87 ± 0.18	-0.88 ± 0.05
$PbCl_2$	-1.24	-1.29 ± 0.19	-1.24 ± 0.06	$PbBr_2$	-0.96	-0.88 ± 0.09	-0.97 ± 0.03
PdO	-0.44	-0.56 ± 0.27	-0.52 ± 0.09	Pd_4S	-0.14	-0.14 ± 0.09	-0.07 ± 0.09
PdS	-0.39	-0.41 ± 0.19	-0.40 ± 0.07	PdS_2	-0.28	-0.31 ± 0.14	-0.33 ± 0.05
PtS	-0.42	-0.43 ± 0.18	-0.51 ± 0.03	PtS_2	-0.38	-0.36 ± 0.12	-0.44 ± 0.06
Pt_2O_2	-0.37	-0.19 ± 0.22	-0.24 ± 0.06	PtO_2	-0.57	-0.53 ± 0.20	-0.58 ± 0.04
RbF	-2.89	-2.95 ± 0.22	-2.87 ± 0.04	RbI	-1.73	-1.71 ± 0.09	-1.77 ± 0.05
Rb_2O	-1.17	-1.04 ± 0.21	-1.10 ± 0.05	Rb_2S	-1.25	-1.16 ± 0.15	-1.23 ± 0.04
Rb_2O_2	-1.22	-1.28 ± 0.20	-1.33 ± 0.05	RbCl	-2.26	-2.23 ± 0.17	-2.24 ± 0.02
ReO_3	-1.58	-1.63 ± 0.17	-1.69 ± 0.06	ReO_2	-1.54	-1.40 ± 0.17	-1.46 ± 0.05
RhO_2	-0.85	-0.87 ± 0.23	-0.87 ± 0.04	$RhCl_3$	-0.77	-0.87 ± 0.21	-0.81 ± 0.03
Rh_2S_3	-0.54	-0.53 ± 0.18	-0.55 ± 0.04	Rh_2O_3	-0.84	-0.80 ± 0.28	-0.79 ± 0.05
RuO_2	-1.05	-1.11 ± 0.22	-0.99 ± 0.06	$RuBr_3$	-0.36	-0.34 ± 0.08	-0.35 ± 0.04
$RuCl_3$	-0.53	-0.74 ± 0.20	-0.60 ± 0.04	RuO_4	-0.50	-0.58 ± 0.19	-0.53 ± 0.19
SbF_3	-2.37	-2.49 ± 0.23	-2.24 ± 0.07	Sb_2O_5	-1.44	-1.50 ± 0.19	-1.43 ± 0.06
ScAs	-1.39	-1.53 ± 0.06	-1.45 ± 0.03	ScF_3	-4.22	-4.22 ± 0.25	-4.11 ± 0.06
$ScCl_3$	-2.40	-2.37 ± 0.21	-2.39 ± 0.05	SiC	-0.34	-0.25 ± 0.09	-0.32 ± 0.07
SiO_2	-3.13	-3.06 ± 0.17	-3.09 ± 0.06	SiS_2	-0.88	-0.78 ± 0.06	-0.83 ± 0.06
$SiSe_2$	-0.61	-0.50 ± 0.06	-0.55 ± 0.06	Si_3N_4	-1.10	-1.17 ± 0.14	-1.15 ± 0.09
SnO	-1.48	-1.20 ± 0.14	-1.42 ± 0.04	SnS_2	-0.53	-0.37 ± 0.09	-0.56 ± 0.03
$SnSe_2$	-0.43	-0.28 ± 0.06	-0.48 ± 0.03	SnO_2	-1.97	-1.73 ± 0.21	-1.89 ± 0.05
SnS	-0.57	-0.34 ± 0.11	-0.58 ± 0.03	SnSe	-0.47	-0.27 ± 0.10	-0.52 ± 0.04
SrO_2	-2.19	-2.32 ± 0.23	-2.31 ± 0.06	SrO	-3.07	-3.08 ± 0.24	-3.05 ± 0.04
SrS	-2.45	-2.44 ± 0.19	-2.44 ± 0.04	$SrCl_2$	-2.86	-2.88 ± 0.23	-2.81 ± 0.05
$SrBr_2$	-2.48	-2.38 ± 0.11	-2.45 ± 0.03	SrI_2	-1.93	-1.92 ± 0.10	-1.93 ± 0.02
TaN	-1.30	-1.14 ± 0.13	-1.25 ± 0.05	$TaSi_2$	-0.47	-0.36 ± 0.17	-0.43 ± 0.07
Ta_2O_5	-3.03	-2.99 ± 0.23	-3.09 ± 0.06	TaF_5	-3.29	-3.56 ± 0.23	-3.41 ± 0.10
$TaCl_5$	-1.48	-1.51 ± 0.21	-1.51 ± 0.06	TiS	-1.41	-1.44 ± 0.10	-1.37 ± 0.06
TiS_2	-1.41	-1.41 ± 0.12	-1.38 ± 0.04	TiN	-1.58	-1.88 ± 0.12	-1.75 ± 0.03
Ti_2O_3	-3.15	-3.14 ± 0.19	-3.07 ± 0.03	TiAs	-0.78	-1.02 ± 0.05	-0.69 ± 0.03

TABLE I. (*Continued.*)

Compound	ΔH_{Expt}	ΔH_{mBEEF}	$\Delta H^{\text{FERE}}_{\text{mBEEF}}$	Compound	ΔH_{Expt}	ΔH_{mBEEF}	$\Delta H^{\text{FERE}}_{\text{mBEEF}}$
TiO_2	-3.26	-3.37 ± 0.21	-3.32 ± 0.05	TlI	-0.64	-0.70 ± 0.10	-0.67 ± 0.04
TlBr	-0.90	-0.95 ± 0.11	-0.97 ± 0.05	TlCl	-1.06	-1.16 ± 0.20	-1.08 ± 0.07
Tl_2O	-0.62	-0.68 ± 0.15	-0.61 ± 0.08	TlF	-1.68	-1.80 ± 0.21	-1.62 ± 0.03
Tl_2S	-0.34	-0.37 ± 0.12	-0.32 ± 0.05	VN	-1.13	-0.99 ± 0.13	-1.00 ± 0.08
V_2O_3	-2.53	-2.58 ± 0.29	-2.62 ± 0.11	V_2O_5	-2.29	-2.31 ± 0.20	-2.35 ± 0.06
VO_2	-2.47	-2.48 ± 0.23	-2.52 ± 0.04	WBr_6	-0.52	-0.41 ± 0.07	-0.51 ± 0.03
WO_3	-2.04	-2.08 ± 0.19	-2.05 ± 0.02	YAs	-1.68	-1.75 ± 0.08	-1.68 ± 0.02
YCl_3	-2.59	-2.63 ± 0.22	-2.67 ± 0.05	YF_3	-4.45	-4.45 ± 0.27	-4.36 ± 0.04
ZnO	-1.81	-1.57 ± 0.21	-1.75 ± 0.04	ZnSe	-0.85	-0.76 ± 0.12	-0.97 ± 0.02
ZnTe	-0.61	-0.56 ± 0.08	-0.64 ± 0.01	ZnS	-1.07	-0.89 ± 0.14	-1.10 ± 0.03
$ZnCl_2$	-1.43	-1.36 ± 0.19	-1.44 ± 0.05	ZnF_2	-2.64	-2.50 ± 0.25	-2.46 ± 0.05
ZrO_2	-3.80	-3.75 ± 0.23	-3.79 ± 0.05	$ZrCl_4$	-2.03	-2.11 ± 0.22	-2.08 ± 0.03
ZrSi	-0.80	-0.93 ± 0.11	-0.94 ± 0.05	ZrN	-1.89	-1.84 ± 0.13	-1.85 ± 0.06
ZrS_2	-1.96	-1.73 ± 0.14	-1.79 ± 0.06				

shown to give smaller errors when compared to experiments [22]. Figure 1(i) shows the calculated heats of formation with the mBEEF functional with calculated error bars indicated with green bars. The calculated values are significantly closer to the experimental values compared to the values obtained from the PBE, RPBE, PBE+U, and TPSS functionals. As can be seen from the figure the experimental values are within the error bars predicted by the mBEEF functional.

The mBEEF functional thus seems to be more accurate than both the GGA functionals and the TPSS which is also a meta-GGA functional. However, it should also be noted that in the construction of the mBEEF functional considerable optimization to experimental databases was performed. In the following we investigate how the scheme suggested by Stevanović *et al.* [4] helps in improving the predictions for the different functionals.

B. Heats of formation with the FERE

In the previous section we noticed that the limited predictability of the TPSS and the GGA functionals mainly arises from the different nature of the bonding in the multinary phases and the reference phases. The FERE scheme [4] circumvents this problem by adding corrections to the reference phase energies. The heats of formation calculated with the FERE can be written as

$$\Delta H^{\text{FERE}}(A_{p1}B_{p2}\dots) = E(A_{p1}B_{p2}\dots) - \Sigma p_i\left(\mu_i^0 + \delta\mu_i^0\right), \quad (2)$$

where the $\delta\mu_i^0$'s are the corrections added to the reference phase energies to improve the heats of formation. The values of the $\delta\mu_i^0$'s can be calculated by a linear regression fit by minimizing the root mean square (rms) error between the calculated (ΔH^{DFT}) and the experimental (ΔH^{Expt}) heats of formation. The size of the training set has to be sufficiently large to avoid any overfitting and the quality of the fit must be validated on a test set. The linear regression requires that the number of parameters in the linear model which need to be fitted to the observations be smaller than the number of data points; i.e., the system of the equations has to be overdetermined. We calculate 62 parameters which correspond to the corrections to the reference phase energies of 62 elements by using a training set of 257 compounds with the experimental heats of formation available. The parameters can be calculated using singular value decomposition (SVD) [24] by minimizing the rms error $|\Delta H_{\text{Expt}} - \Delta H_{\text{DFT}}|^2$. The calculated reference energies are tabulated in the Supplemental Material [25].

Figure 1, panels (b), (d), (f), (h), and (j), shows the heats of formation calculated after adding the corrections to the reference phase energies. The comparison with panels (a), (c), (e), (g), and (i) of the figure clearly shows that the MAE and σ are significantly reduced after applying the corrections to the reference phase energies. Interestingly, all the GGA functionals give similar heats of formation after employing the corrections even though they differ before applying the corrections. The TPSS functional does not perform any better than the GGA functionals after applying the corrections.

As noted the performance of mBEEF before fitting is somewhat better than the GGAs and the TPSS functional and in fact, as we shall see later, it is comparable to the fitted GGAs and the TPSS on a test set. However, for comparison we also apply the FERE fitting procedure to the mBEEF functional and this does naturally lead to an improvement on the training set. As mentioned before, we furthermore employ the fitting procedure on all the functionals in the mBEEF ensemble anticipating a reduction of the error and the fluctuations within the ensemble. This is indeed the case. In Fig. 1(j) we can see that the uncertainties are significantly reduced as compared to Fig. 1(i). The reduction in the size of the uncertainties is in agreement with the fact that the fitted mBEEF predictions are more accurate.

C. Analysis of outliers

The appearance of outliers with and without the fitting for the PBE, RPBE, and PBE+U functionals may occur for two reasons: (1) error in the experimental data, and (2) some systems are poorly described with the given functional. The compounds having the deviation of the calculated heat of formation (δH) from the experimental value by twice of the standard deviation (2σ) are shown in Table II. The table clearly shows that all the functionals except for PBE and RPBE

TABLE II. Outliers in the calculations without using the FERE scheme. The compounds exhibiting deviations of the calculated heats of formation from the experimental values by more than 2σ have been identified as outliers. The values of σ for the different functionals are shown in Fig. 1. δH denotes the difference between calculated and experimental heats of formation.

PBE	δH_{PBE}	RPBE	δH_{RPBE}	PBE+U	$\delta H_{\mathrm{PBE+U}}$	TPSS	δH_{TPSS}	mBEEF	$\delta H_{\mathrm{mBEEF}}$
Al_2O_3	0.48	Al_2O_3	0.69	Al_2O_3	0.48	AlP	0.45	AuF_3	−0.30
BaS	−0.52	FeF_2	0.61	BaS	−0.52	BaI_2	−0.48	CaF_2	−0.35
BaO	−0.47	FeO	0.60	BaO	−0.47	$BiBr_3$	−0.51	CdF_2	−0.34
FeF_2	0.61	GaN	0.57	CrS	−0.82	CaS	0.48	Cu_2Se	0.31
FeO	0.49	HfO_2	0.65	CrF_3	−0.47	FeF_2	0.57	FeSe	0.35
GaS	0.451	NiF_2	0.66	Cr_2O_3	−0.75	GaP	0.43	GaN	0.33
LaN	0.46			GaN	0.42	Ga_2S_3	0.44	Ga_2S_3	0.37
MnS	0.60			Ga_2S_3	0.44	NiF_2	0.57	GaS	0.41
NiF_2	0.85			GaS	0.45	$PbBr_2$	−0.45	GeSe	0.37
				Ge_4O_8	0.42	$SrBr_2$	−0.49	Ge_4O_8	0.29
				MnS	−0.48	SrI_2	−0.55	NbF_5	−0.38
				Mn_3O_4	−0.42	ZnS	0.43	OsO_4	−0.30
				V_2O_3	−0.42	ZrS_2	0.47	PbF_2	−0.31
								SnO_2	0.28
								TiN	−0.30

have none or very few common outliers. For example, the predictions for barium-containing compounds is a little worse only in the PBE, PBE+U, and the TPSS whereas the outliers containing chromium are present in the PBE+U functional only. On the other hand, even if the gallium is present in all the functionals it is not the same compound which is an outlier.

Additionally, the outliers present in the mBEEF calculations do not deviate from the experimental value by more than 0.41 eV per atom whereas the outliers present in the GGA functionals and the TPSS have deviations as high as 0.85 and 0.57 eV per atom, respectively. The deviations shown for the mBEEF functional are relative to a common rms error $\sigma = 0.14$ eV and not based on the ensemble estimated errors. The large variation in outliers with functional seems to indicate that the appearance of outliers is as might be expected not due to experimental errors but rather due to limitations of the different functionals.

Table III shows the outliers after the fitting has been applied. We see that the outliers are to a large extent different from the ones before the fitting and again they also vary considerably for the different functionals. This means that we cannot identify particular issues with specific systems. The PBE and RPBE functionals continue to have significant overlap of outliers after the fitting.

D. Statistical analysis of the mBEEF predictions

The error bars predicted by the mBEEF ensemble are in reasonable agreement with the actual errors as can be seen from Fig. 1(i). In order to study the quality of the error bar prediction in more detail we show in Fig. 2(a) a histogram of the actual error, i.e., the deviation between the mBEEF prediction and the experimental value ($\Delta H_{\mathrm{mBEEF}} - \Delta H_{\mathrm{Expt}}$) divided by the predicted error bar (σ_{BEE}). The histogram is a

TABLE III. Outliers in the calculations using the FERE scheme. The compounds exhibiting deviations of the calculated heats of formation from the experimental values by more than 2σ have been identified as outliers. The values of σ for the different functionals are shown in Fig. 1. δH denotes the difference between calculated and experimental heats of formation.

PBE	$\delta H_{\mathrm{PBE}}^{\mathrm{FERE}}$	RPBE	$\delta H_{\mathrm{RPBE}}^{\mathrm{FERE}}$	PBE+U	$\delta H_{\mathrm{PBE+U}}^{\mathrm{FERE}}$	TPSS	$\delta H_{\mathrm{TPSS}}^{\mathrm{FERE}}$	mBEEF	$\delta H_{\mathrm{mBEEF}}^{\mathrm{FERE}}$
CuF_2	0.22	CuF_2	0.23	CoS	0.20	$BaCl_2$	0.24	CaF_2	−0.18
FeF_2	0.33	FeF_2	0.27	Co_3O_4	−0.23	CaS	0.21	CdF_2	−0.18
FeSe	−0.19	MnO_2	−0.21	CrO_2	0.17	CsF	−0.23	Co_3O_4	−0.19
MnO_2	−0.25	NbF_5	−0.32	Fe_2O_3	−0.17	FeF_2	0.29	Fe_2O_3	−0.17
NbF_5	−0.29	Ni_3S_2	−0.18	GaF_3	0.16	KCl	0.32	FeF_2	0.19
Ni_3S_2	−0.21	NiF_2	0.38	GeO_2	0.20	NbF_5	−0.26	GaP	−0.16
NiF_2	0.65	PbF_2	−0.18	MgF_2	0.19	NiF_2	0.37	KF	−0.17
RuO_4	−0.19	RuO_4	−0.33	NbF_5	−0.23	RbI	0.25	Li_3Sb	0.18
TaF_5	−0.22	TaF_5	−0.24	SnO_2	0.17	SrS	0.25	MgO	−0.15
ZrSi	−0.24	ZrSi	−0.26	TaF_5	−0.18	SrI_2	−0.24	MgF_2	0.17
ZrS_2	0.26	ZrS_2	0.24	TiN	−0.19	TlI	0.26	MnO_2	−0.16
				VN	0.26	ZrSi	−0.24	NbF_5	−0.20
				V_2O_3	−0.36	ZrS_2	0.35	TiN	−0.17
				ZnF_2	0.19			ZnF_2	0.18
				ZrS_2	0.16			ZrS_2	0.16

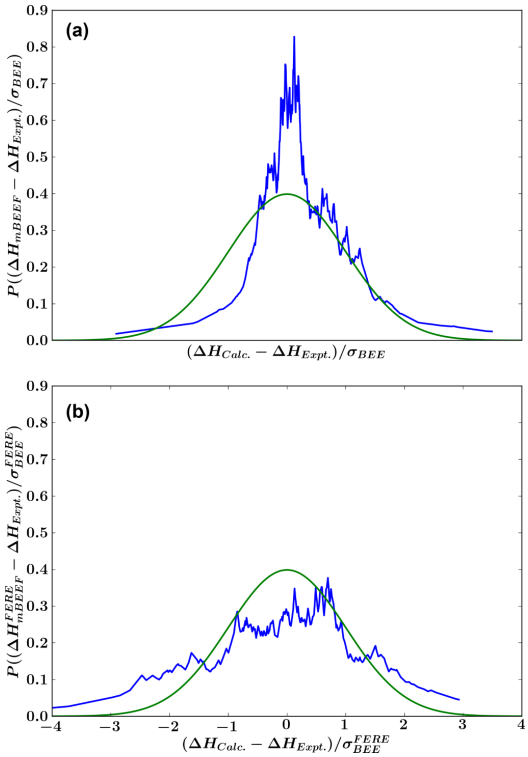

FIG. 2. (Color online) (a) Shows the probability distribution of the calculated error ($\Delta H_{\mathrm{mBEEF}} - \Delta H_{\mathrm{Expt}}$) in the heat of formation divided by the estimated error (σ_{BEE}) from the ensemble of functionals. (b) Shows the probability distribution of the calculated error ($\Delta H^{\mathrm{FERE}}_{\mathrm{mBEEF}} - \Delta H_{\mathrm{Expt}}$) in the heat of formation divided by the estimated error ($\sigma^{\mathrm{FERE}}_{\mathrm{BEE}}$) from the ensemble of functionals after correcting the reference phase energies. The ensemble energies have also been recalculated employing the fitting eventually giving the new error estimates $\sigma^{\mathrm{FERE}}_{\mathrm{BEE}}$. The green plots in (a) and (b) show the Gaussian distributions with zero mean and unit standard deviation.

running average calculated as [24]

$$P\left(\frac{1}{2}[x_i + x_{i+J}]\right) \approx \frac{J}{N(x_{i+J} - x_i)}, \tag{3}$$

with x_i being the ratio between actual error and predicted error, and the parameter $J = 20$. For a perfect statistical error prediction one could expect that the distribution would be Gaussian with a width of 1, which is also shown in the figure for comparison. The large peak in the histogram around zero shows that there is some tendency for the error prediction to be on the large side, but the overall agreement is quite good.

If the FERE fitting procedure is applied to the mBEEF ensemble the ratios of real to predicted errors result in the histogram shown in Fig. 2(b). Both the real ($\Delta H^{\mathrm{FERE}}_{\mathrm{mBEEF}} - \Delta H_{\mathrm{Expt}}$) and the predicted errors ($\sigma^{\mathrm{FERE}}_{\mathrm{BEE}}$) are now smaller but the relative distribution remains fairly close to a Gaussian of unit width. However, now a tail in the histogram appears indicating that for some systems the predicted error can be 3 or 4 times smaller than the actual error. This is a fairly common feature of the ensemble approach [26].

E. Cross validation

In any regression process it is necessary to validate the quality of the regression over a set of test data which is not the part of the training data set. Overfitting, i.e., more parameters in the model than required to model the data, will lead to poor prediction of the test data set. One of the most important features that a fitting scheme should possess is the predictability on a completely new data set. One might expect good predictions on a data set which is similar in nature to the training data set. For example, in our case, we expect a good predictability for the binary compounds since we use only binary compounds in the training data set. The fitting procedure provides corrections for the reference energies of the elements which are independent of the chemical environments of the atoms. Therefore, we can expect that if the environments change considerably, which can for example be the case for ternary or quarternary compounds, the improvement will be less pronounced.

Hence, in the test we not only include the binary compounds but the ternary compounds as well. We compose a set of 24 binary and ternary compounds where the experimental heats of formation are available and which are not present in the training data. We summarize the results in Table IV. As for the training set the MAE and σ in general show a significant decrease with the fitted reference energies indicating that we do not overfit. However, the improvement is somewhat less than for the training set which is also what could be expected. Also for the test set we see that the three functionals PBE, RPBE, and PBE+U reach the same level of accuray after fitting although PBE+U is considerably better before fitting. The performance of the TPSS functional does not seem to be any better than any of the GGA functionals. In fact the rms error for TPSS is only slightly reduced after fitting, while the MAE is reduced more. This behavior can be traced to a single system (Cs_2S), which is clearly poorly corrected by the fitting scheme. We have not been able to identify why this is the case. It can be noted that Cs was not included in the database considered by Stevanović *et al.* [4].

The most interesting feature is that the mBEEF functional already before fitting is of the same quality as the other functionals after fitting. Furthermore, the improvement of the mBEEF results using the fitting is only moderate. This means that moving to mBEEF the fitting procedure can be completely avoided at only a moderate cost in computational time (less than a factor to 2) compared to the GGAs.

In compounds such as SrSe and Mn_2SiO_4 the predictions with mBEEF remain the same after the fitting procedure; however, the estimated error is significantly reduced leading to large real error relative to the predicted uncertainty. It should be noted that it is an inherent limitation in the ensemble error estimation that fluctuations in the predictions can only result from fluctuations within the defined model space (i.e., meta-GGA in this case). If errors appear which cannot be described by such fluctuations an underestimation of the error may result.

TABLE IV. Heats of formation of the solid compounds calculated with the different functionals with and without employing the fitting procedure. The set below was not used in the training set for fitting the reference phase energies. All the energies are in eV/atom.

Compound	ΔH_{Expt}	ΔH_{PBE}	ΔH_{RPBE}	$\Delta H_{\mathrm{PBE+U}}$	ΔH_{TPSS}	$\Delta H_{\mathrm{mBEEF}}$	$\Delta H_{\mathrm{PBE}}^{\mathrm{FERE}}$	$\Delta H_{\mathrm{RPBE}}^{\mathrm{FERE}}$	$\Delta H_{\mathrm{PBE+U}}^{\mathrm{FERE}}$	$\Delta H_{\mathrm{TPSS}}^{\mathrm{FERE}}$	$\Delta H_{\mathrm{mBEEF}}^{\mathrm{FERE}}$
$AgNO_3$	−0.26	−0.40	−0.31	−0.53	−0.47	-0.60 ± 0.22	−0.58	−0.67	−0.68	−0.45	-0.63 ± 0.16
$AlPO_4$	−2.99	−2.71	−2.58	−2.71	−2.86	-2.97 ± 0.19	−2.95	−2.97	−2.94	−3.02	-3.03 ± 0.07
$BeSO_4$	−2.16	−1.99	−1.83	−1.99	−2.09	-2.19 ± 0.16	−2.22	−2.23	−2.21	−2.19	-2.25 ± 0.11
BiOCl	−1.27	−1.26	−1.11	−1.26	−1.62	-1.26 ± 0.16	−1.25	−1.20	−1.23	−1.32	-1.23 ± 0.09
$CdSO_4$	−1.61	−1.42	−1.27	−1.42	−1.53	-1.59 ± 0.17	−1.61	−1.62	−1.60	−1.60	-1.63 ± 0.12
$CuCl_2$	−0.76	−0.51	−0.32	−0.70	−0.80	-0.74 ± 0.21	−0.75	−0.60	−0.84	−0.79	-0.81 ± 0.07
$TiBr_3$	−1.42	−1.24	−1.23	−1.52	−1.71	-1.37 ± 0.08	−1.38	−1.39	−1.61	−1.38	-1.43 ± 0.05
$NaClO_4$	−0.66	−0.54	−0.41	−0.54	−0.67	-0.63 ± 0.15	−0.76	−0.77	−0.73	−0.68	-0.65 ± 0.16
$CaSO_4$	−2.48	−2.24	−2.06	−2.24	−2.37	-2.40 ± 0.17	−2.41	−2.41	−2.41	−2.46	-2.43 ± 0.12
Cs_2S	−1.24	−1.01	−0.92	−1.01	−1.47	-1.16 ± 0.18	−1.27	−1.24	−1.33	−1.97	-1.23 ± 0.06
$CuWO_4$	−1.91	−1.59	−1.41	−1.76	−1.72	-1.68 ± 0.21	−1.62	−1.60	−1.75	−1.65	-1.71 ± 0.07
PbF_4	−1.95	−2.13	−2.05	−2.13	−2.26	-2.32 ± 0.23	−2.19	−2.19	−2.11	−2.24	-2.13 ± 0.08
$MgSO_4$	−2.22	−1.97	−1.79	−1.97	−2.09	-2.16 ± 0.16	−2.22	−2.21	−2.21	−2.20	-2.24 ± 0.10
SrSe	−2.00	−2.04	−1.98	−2.04	−2.76	-2.29 ± 0.16	−2.25	−2.26	−2.29	−2.66	-2.29 ± 0.05
$NiSO_4$	−1.51	−1.11	−0.96	−1.35	−1.23	-1.42 ± 0.23	−1.35	−1.36	−1.54	−1.33	-1.50 ± 0.11
$FeWO_4$	−1.99	−1.73	−1.58	−2.01	−1.87	-1.84 ± 0.21	−1.81	−1.81	−1.94	−1.86	-1.89 ± 0.06
GeP	−0.11	+0.04	+0.09	+0.04	−0.19	$+0.14 \pm 0.08$	−0.01	+0.03	−0.05	−0.28	-0.02 ± 0.07
VOCl	−2.10	−1.79	−1.68	−2.45	−2.07	-2.11 ± 0.24	−1.97	−1.98	−2.41	−2.05	-2.12 ± 0.07
$LiBO_2$	−2.67	−2.42	−2.30	−2.42	−2.57	-2.58 ± 0.17	−2.61	−2.61	−2.58	−2.64	-2.61 ± 0.05
$NaBrO_3$	−0.69	−0.52	−0.41	−0.52	−0.71	-0.60 ± 0.13	−0.74	−0.76	−0.72	−0.69	-0.66 ± 0.11
$CoSO_4$	−1.53	−1.09	−0.95	−1.43	−1.24	-1.40 ± 0.23	−1.30	−1.34	−1.56	−1.31	-1.43 ± 0.11
$PbSeO_4$	−1.05	−0.94	−0.81	−0.94	−1.13	-1.04 ± 0.16	−1.07	−1.09	−1.06	−1.07	-1.08 ± 0.09
Mn_2SiO_4	−2.56	−1.83	−1.77	−2.58	−2.01	-2.29 ± 0.23	−2.17	−2.19	−2.38	−2.10	-2.25 ± 0.08
$ZnSO_4$	−1.70	−1.37	−1.20	−1.37	−1.47	-1.53 ± 0.16	−1.61	−1.61	−1.61	−1.60	-1.62 ± 0.11
MAE		0.24	0.35	0.16	0.20	0.12	0.12	0.13	0.11	0.15	0.09
σ		0.28	0.39	0.19	0.26	0.16	0.16	0.17	0.15	0.25	0.14

IV. CONCLUSION

The need for accurate predictions of material stabilities has led to the development of schemes combining DFT total energy calculations with experimental information. We have analyzed one such scheme for calculation of heats of formation which fit the reference energies for elemental systems. The scheme was developed with the PBE+U functional, but we show that comparable predictive power is obtained using other GGAs such as PBE or RPBE or the meta-GGA TPSS. We have furthermore seen that the mBEEF functional, which is a meta-GGA and which has been extensively optimized to a variety of experimental data, leads to much improved estimation of heats of formation even without applying the fitting procedure. The mBEEF functional furthermore includes realistic ensemble estimates of the calculated formation energies. Applying the fitting scheme to mBEEF leads to a further reduction of the error and narrows the ensemble error estimation accordingly.

The FERE scheme clearly has its limitations. The correction of only the binding energies of the reference systems makes most sense if the character of the bonding differs significantly between the material at hand and the reference systems. This is for example the case for a metal oxide, in which the bonding may be quite different from the one in an oxygen molecule and in the pure metal. However, oxygen can enter in many different ways in different materials and only improving on the molecular energy cannot be a solution to improved heats of formation in the long run. Moving to more accurate functionals is therefore a must, and the current work shows that applying a meta-GGA such as mBEEF already provides a significant improvement in the prediction of solid heats of formation.

ACKNOWLEDGMENTS

The authors acknowledge CASE (Catalysis for Sustainable Energy) initiative. CASE is funded by the Danish Ministry of Science, Technology and Innovation.

[1] P. Hohenberg and W. Kohn, Phys. Rev. **136**, B864 (1964).
[2] W. Kohn and L. J. Sham, Phys. Rev. **140**, A1133 (1965).
[3] J. P. Perdew, K. Burke, and M. Ernzerhof, Phys. Rev. Lett. **77**, 3865 (1996).
[4] V. Stevanovic, S. Lany, X. Zhang, and A. Zunger, Phys. Rev. B **85**, 115104 (2012).
[5] I. E. Castelli, T. Olsen, S. Datta, D. D. Landis, S. Dahl, K. S. Thygesen, and K. W. Jacobsen, Energy Environ. Sci. **5**, 5814 (2012).
[6] A. Jain, G. Hautier, C. J. Moore, S. P. Ong, C. C. Fischer, T. Mueller, K. A. Persson, and G. Ceder, Comput. Mater. Sci. **50**, 2295 (2011).

[7] X. Zhang, V. Stevanović, M. d'Avezac, S. Lany, and A. Zunger, Phys. Rev. B **86**, 014109 (2012).
[8] S. Lany, Phys. Rev. B **78**, 245207 (2008).
[9] B. Hammer, L. B. Hansen, and J. K. Nørskov, Phys. Rev. B **59**, 7413 (1999).
[10] J. M. Tao, J. P. Perdew, V. N. Staroverov, and G. E. Scuseria, Phys. Rev. Lett. **91**, 146401 (2003).
[11] R. Peverati and D. G. Truhlar, Philos. Trans. R. Soc. A **372**, 2011 (2014).
[12] L. A. Constantin, E. Fabiano, and F. Della Sala, Chem. Theory Comput. **9**, 2256 (2013).
[13] J. Sun, J. P. Perdew, and A. Ruzsinszky, Proc. Natl. Acad. Sci. USA **112**, 685 (2015).
[14] F. Della Sala, E. Fabiano, and L. A. Constantin, Phys. Rev. B **91**, 035126 (2015).
[15] J. Wellendorff, K. T. Lundgaard, K. W. Jacobsen, and T. Bligaard, J. Chem. Phys. **140**, 144107 (2014).
[16] J. Enkovaara, C. Rostgaard, J. J. Mortensen, J. Chen, M. Dułak, L. Ferrighi, J. Gavnholt, C. Glinsvad, V. Haikola, H. A. Hansen, H. H. Kristoffersen, M. Kuisma, A. H. Larsen, L. Lehtovaara, M. Ljungberg, O. Lopez-Acevedo, P. G. Moses, J. Ojanen, T. Olsen, V. Petzold, N. A. Romero, J. Stausholm-Møller, M. Strange, G. A. Tritsaris, M. Vanin, M. Walter, B. Hammer, H. Häkkinen, G. K. H. Madsen, R. M. Nieminen, J. K. Nørskov, M. Puska, T. T. Rantala, J. Schiøtz, K. S. Thygesen, and K. W. Jacobsen, J. Phys.: Condens. Matter **22**, 253202 (2010).
[17] G. Kresse and D. Joubert, Phys. Rev. B **59**, 1758 (1999).
[18] S. L. Dudarev, G. A. Botton, S. Y. Savrasov, C. J. Humphreys, and A. P. Sutton, Phys. Rev. B **57**, 1505 (1998).
[19] H. J. Monkhorst and J. D. Pack, Phys. Rev. B **13**, 5188 (1976).
[20] J. Wellendorff, K. T. Lundgaard, A. Møgelhøj, V. Petzold, D. D. Landis, J. K. Nørskov, T. Bligaard, and K. W. Jacobsen, Phys. Rev. B **85**, 235149 (2012).
[21] Standard thermodynamic properties of chemical substances, http://www.update.uu.se/~jolkkonen/pdf/CRC_TD.pdf.
[22] M. Fuchs, J. L. F. Da Silva, C. Stampfl, J. Neugebauer, and M. Scheffler, Phys. Rev. B **65**, 245212 (2002).
[23] G. Hautier, S. P. Ong, A. Jain, C. J. Moore, and G. Ceder, Phys. Rev. B **85**, 155208 (2012).
[24] W. H. Press, B. P. Flannery, S. A. Teukolsky, and W. T. Vetterling, *Numerical Recipes in C* (Cambridge University Press, Cambridge, 1988).
[25] See Supplemental Material at http://link.aps.org/supplemental/10.1103/PhysRevB.91.235201 for the reference energies calculated with different functionals with and without the fitting.
[26] S. L. Frederiksen, K. W. Jacobsen, K. S. Brown, and J. P. Sethna, Phys. Rev. Lett. **93**, 165501 (2004).

Supplementary Information: Heats of formation of solids with error estimation: the mBEEF functional with and without fitted reference energies.

Mohnish Pandey[1] and Karsten W. Jacobsen,[1]

[1] *Center for Atomic-scale Materials Design, Department of Physics, Technical University of Denmark, DK - 2800 Kongens Lyngby, Denmark*

(Dated: April 14, 2015)

TABLE I: Energies (in eV/atom) of the reference states of elements before and after the fitting

Element	μ_{PBE}	μ_{PBE}^{FERE}	μ_{RPBE}	μ_{RPBE}^{FERE}	μ_{PBE+U}	μ_{PBE+U}^{FERE}	μ_{TPSS}	μ_{TPSS}^{FERE}	μ_{mBEEF}	μ_{mBEEF}^{FERE}
Li	-1.904	-1.68	-1.796	-1.521	-1.904	-1.685	-2.481	-2.391	-4.62	-4.536
Be	-3.699	-3.413	-3.412	-3.056	-3.699	-3.406	-4.668	-4.24	-7.528	-7.406
B	-6.691	-6.612	-6.296	-6.244	-6.691	-6.682	-7.84	-7.646	-11.726	-11.773
Na	-1.322	-1.116	-1.201	-0.974	-1.322	-1.112	-4.701	-4.492	-15.925	-15.915
Mg	-1.614	-1.152	-1.422	-0.902	-1.614	-1.154	-5.343	-4.949	-18.121	-17.919
Al	-3.745	-3.058	-3.489	-2.714	-3.745	-3.103	-7.765	-7.049	-22.134	-21.773
Si	-5.393	-5.351	-5.094	-5.052	-5.393	-5.299	-9.543	-9.68	-25.89	-25.908
K	-1.232	-0.977	-1.133	-0.818	-1.232	-0.975	-7.092	-6.937	-32.652	-32.589
Ca	-1.663	-1.702	-1.473	-1.397	-1.663	-1.65	-8.06	-7.708	-35.485	-35.57
Zn	-1.201	-0.805	-0.818	-0.405	-1.201	-0.798	-8.592	-8.056	-61.628	-61.3
Ga	-2.899	-2.324	-2.544	-1.954	-2.899	-2.382	-10.126	-9.52	-66.906	-66.399
Ge	-4.499	-4.206	-4.161	-3.833	-4.499	-4.229	-11.448	-11.441	-72.126	-71.683
As	-4.648	-5.026	-4.278	-4.731	-4.648	-4.945	-11.764	-12.12	-75.744	-76.153
Rb	-0.926	-0.646	-0.814	-0.469	-0.926	-0.618	-8.185	-7.772	-87.101	-87.036
Sr	-1.677	-1.309	-1.488	-1.003	-1.677	-1.277	-8.095	-8.374	-91.307	-91.402
Cd	-0.958	-0.858	-0.563	-0.479	-0.958	-0.853	-6.97	-6.766	-130.798	-130.821
In	-2.793	-2.42	-2.426	-2.043	-2.793	-2.511	-8.594	-8.168	-137.051	-136.79
Sn	-4.149	-3.924	-3.815	-3.519	-4.149	-3.953	-9.468	-9.515	-142.951	-142.552
Sb	-4.463	-4.799	-4.093	-4.46	-4.463	-4.66	-9.599	-10.057	-147.587	-147.917
Te	-3.188	-3.314	-2.834	-3.016	-3.188	-3.268	-8.042	-8.177	-150.633	-150.804
Cs	-0.813	-0.504	-0.699	-0.333	-0.813	-0.437	-4.551	-3.886	-161.584	-161.519
Ba	-0.208	-1.365	0.024	-1.049	-0.208	-1.312	-4.588	-4.762	-166.612	-166.602
Hg	-0.917	-0.902	-0.543	-0.505	-0.917	-0.909	12.263	12.372	-308.363	-308.362
Tl	-2.569	-2.72	-2.17	-2.399	-2.569	-2.69	11.337	11.435	-316.931	-317.061
Pb	-3.875	-4.086	-3.49	-3.678	-3.875	-4.037	11.282	10.815	-325.376	-325.429
Bi	-4.717	-5.16	-4.334	-4.786	-4.717	-5.154	11.223	10.45	-333.537	-333.615
Sc	-4.667	-4.183	-4.366	-3.763	-3.29	-2.878	-11.312	-11.112	-40.093	-39.857
Ti	-6.701	-6.818	-6.296	-6.27	-4.303	-4.529	-13.529	-13.779	-44.225	-44.465
Y	-4.696	-4.104	-4.384	-3.668	-3.289	-2.844	-12.161	-11.813	-97.841	-97.554
Zr	-7.409	-7.269	-7.007	-6.778	-4.934	-4.981	-14.826	-14.851	-104.147	-104.108
Nb	-10.387	-10.523	-9.867	-9.918	-6.985	-7.41	-17.614	-17.889	-110.943	-110.977
Mo	-11.265	-11.707	-10.693	-11.062	-7.716	-8.104	-18.546	-18.813	-115.777	-115.834
Ru	-9.498	-10.24	-8.839	-9.597	-6.297	-7.733	-16.396	-16.939	-121.956	-122.391

Continued on next page

Element	μ_{PBE}	μ_{PBE}^{FERE}	μ_{RPBE}	μ_{RPBE}^{FERE}	μ_{PBE+U}	μ_{PBE+U}^{FERE}	μ_{TPSS}	μ_{TPSS}^{FERE}	μ_{mBEEF}	μ_{mBEEF}^{FERE}
Rh	-7.321	-7.309	-6.677	-6.506	-4.927	-5.661	-14.047	-13.963	-123.897	-123.991
Pd	-3.924	-4.008	-3.295	-3.329	-3.061	-3.411	-10.189	-10.504	-124.77	-124.889
Ag	-3.0	-2.887	-2.478	-2.396	-2.708	-2.781	-9.091	-9.053	-128.335	-128.251
La	-4.631	-3.922	-4.265	-3.488	-3.024	-2.722	-8.023	-7.424	-173.66	-173.225
Hf	-7.515	-7.06	-7.109	-6.481	-5.042	-4.645	-0.351	-0.011	-260.384	-259.967
Ta	-9.891	-9.938	-9.399	-9.355	-6.598	-6.798	-2.094	-2.232	-269.497	-269.265
Re	-11.673	-12.234	-11.081	-11.474	-7.951	-8.59	-2.586	-2.987	-284.828	-284.711
Os	-11.221	-13.821	-10.593	-13.804	-7.776	-10.239	-1.414	-3.323	-291.189	-292.814
Ir	-9.401	-9.509	-8.77	-8.704	-6.671	-7.443	0.959	1.13	-296.091	-295.784
Pt	-6.487	-6.575	-5.834	-5.854	-5.086	-5.641	4.667	4.937	-299.885	-299.82
Au	-3.251	-3.608	-2.665	-3.115	-2.951	-3.324	8.892	8.668	-303.481	-303.752
C	-9.224	-9.041	-8.808	-8.669	-9.224	-9.069	-10.548	-10.54	-15.405	-15.242
N	-8.482	-8.396	-8.301	-7.956	-8.482	-8.257	-10.078	-10.218	-15.89	-15.906
O	-5.296	-5.071	-5.164	-4.716	-5.296	-5.097	-7.237	-7.227	-14.146	-14.106
F	-1.982	-1.85	-1.879	-1.656	-1.982	-1.964	-4.51	-4.409	-12.572	-12.793
P	-5.362	-5.547	-5.054	-5.272	-5.362	-5.45	-10.024	-9.84	-27.769	-27.902
S	-4.058	-3.904	-3.841	-3.621	-4.058	-3.859	-9.091	-8.903	-28.577	-28.491
Cl	-1.73	-1.531	-1.635	-1.371	-1.73	-1.581	-6.86	-6.999	-28.461	-28.506
Se	-3.476	-3.419	-3.236	-3.145	-3.476	-3.373	-10.962	-10.879	-78.331	-78.242
Br	-1.604	-1.373	-1.395	-1.189	-1.604	-1.413	-8.654	-9.018	-80.263	-80.1
I	-1.483	-1.382	-1.26	-1.199	-1.483	-1.422	-5.923	-6.25	-153.497	-153.435
V	-8.538	-8.414	-8.048	-7.84	-5.245	-5.705	-15.485	-15.407	-48.275	-48.239
Cr	-9.447	-9.001	-8.887	-8.428	-5.931	-7.736	-16.616	-16.204	-51.629	-51.838
Mn	-9.811	-9.101	-9.271	-8.738	-7.11	-8.23	-17.157	-16.631	-54.674	-54.865
Fe	-9.077	-8.501	-8.596	-8.011	-7.039	-7.314	-16.46	-15.848	-56.897	-56.463
Co	-8.376	-8.188	-7.876	-7.533	-6.122	-6.337	-15.79	-15.601	-58.893	-58.915
Ni	-7.278	-6.915	-6.757	-6.363	-5.539	-5.416	-14.815	-14.428	-60.806	-60.529
Cu	-3.81	-3.506	-3.307	-2.99	-3.373	-3.243	-11.163	-10.928	-60.624	-60.321
W	-11.589	-12.593	-11.051	-12.076	-8.108	-9.06	-3.176	-3.858	-278.013	-278.279

Paper II

Two-Dimensional Metal Dichalcogenides and Oxides for Hydrogen Evolution: A Computational Screening Approach

M. Pandey, A. Vojvodic, K. S. Thygesen and K. W. Jacobsen The Journal of Physical Chemistry Letters 6 (9), 1577-1585 (2015)

THE JOURNAL OF PHYSICAL CHEMISTRY Letters

Letter

pubs.acs.org/JPCL

Two-Dimensional Metal Dichalcogenides and Oxides for Hydrogen Evolution: A Computational Screening Approach

Mohnish Pandey,[†] Aleksandra Vojvodic,[‡] Kristian S. Thygesen,[†,§] and Karsten W. Jacobsen*[,†]

[†]Center for Atomic-Scale Materials Design, Department of Physics, Technical University of Denmark, DK-2800 Kongens Lyngby, Denmark

[‡]SUNCAT Center for Interface Science and Catalysis, SLAC National Accelerator Laboratory, 2575 Sand Hill Road, Menlo Park, California 94025, United States

[§]Center for Nanostructured Graphene (CNG), Department of Physics, Technical University of Denmark, DK-2800 Kongens Lyngby, Denmark

Supporting Information

ABSTRACT: We explore the possibilities of hydrogen evolution by basal planes of 2D metal dichalcogenides and oxides in the 2H and 1T class of structures using the hydrogen binding energy as a computational activity descriptor. For some groups of systems like the Ti, Zr, and Hf dichalcogenides the hydrogen bonding to the 2H structure is stronger than that to the 1T structure, while for the Cr, Mo, and W dichalcogenides the behavior is opposite. This is rationalized by investigating shifts in the chalcogenide p levels comparing the two structures. We find that usually for a given material only at most one of the two phases will be active for the hydrogen evolution reaction; however, in most cases the two phases are very close in formation energy, opening up the possibility for stabilizing the active phase. The study points to many new possible 2D HER materials beyond the few that are already known.

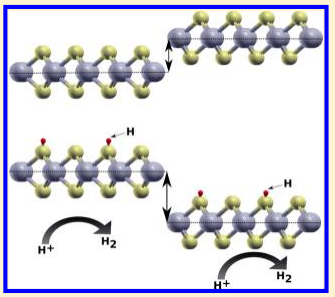

Hydrogen holds a crucial place in many chemical syntheses and in energy production;[1,2] however, an economical process for hydrogen production has not been fully realized yet. One of the main challenges lies in finding a cheap catalyst that can evolve hydrogen efficiently. Platinum, which is known to be one of the best catalysts for hydrogen evolution, is prohibitively expensive, thus precluding it to be used on large scales. Several other metals, metal surface alloys and metal oxides, have been studied for the same reaction, but unfortunately most of these are not both efficient and cheap at the same time.[3−5] Only recently a few and interesting candidates have been identified for hydrogen evolution reaction (HER), for example, Ni_2P.[6,7]

Recent promising experiments on 2D metal sulfides have opened up a new class of materials that could contain promising candidates for HER.[8−12] The 2D nature of these materials gives additional flexibility of nanostructuring and manipulating the structures, which is otherwise challenging in the 3D bulk form. For example, MoS_2 exists in both 2H and 1T phases in monolayer form, whereas the 1T phase is thermodynamically unfavorable in the bulk.[13] Despite the fact that the 2H-MoS_2 is one of the most studied 2D sulfides for HER, it has active sites on the edges only,[14,15] and the limited activity is ascribed to the inability of the 2H-MoS_2 basal plane to adsorb hydrogen.[10] The above limitation has been overcome by contemporary experiments on 1T-MoS_2 and WS_2, in which the entire sheet has been found to be catalytically active for HER.[8−10] The unusual difference between the 2H and 1T phases thus expands the material space to more structures that might be relevant for the given application.

In the present work, we explore the HER activity of the basal planes of 100 dichalcogenides and oxides (MX_2) in both the 2H and 1T class of structures using the free energy of hydrogen adsorption as a descriptor for the activity of the material.[3,16] Rather than assuming the existence of perfectly symmetrical 2H and 1T structures, we carefully look for deviations of the atomic structure from the perfectly symmetric 2H and 1T phases and choose the structure with minimum energy. (We continue using the terminology 2H and 1T for distorted structures as well to avoid cluttering of notations.) We choose 'M' from a set of 25 elements (shown in the ordinate of Figure 2) and 'X' from a set of 4 (shown in the abscissa of Figure 2) elements (chalcogens and oxygen). We find a significant difference in the hydrogen adsorption energy of the 2H and 1T phases of a given compound; on the other hand, the 2H and 1T phases show similar thermodynamic stability, thus making it possible to stabilize the structure showing activity toward HER despite the fact that it is not the most stable structure. To find a correlation between the adsorption energies and the nature of metal atoms, we group the compounds based on the position of the metal atoms in the periodic table. For the groups showing apparent

Received: February 17, 2015
Accepted: April 10, 2015
Published: April 10, 2015

DOI: 10.1021/acs.jpclett.5b00353
J. Phys. Chem. Lett. 2015, 6, 1577−1585

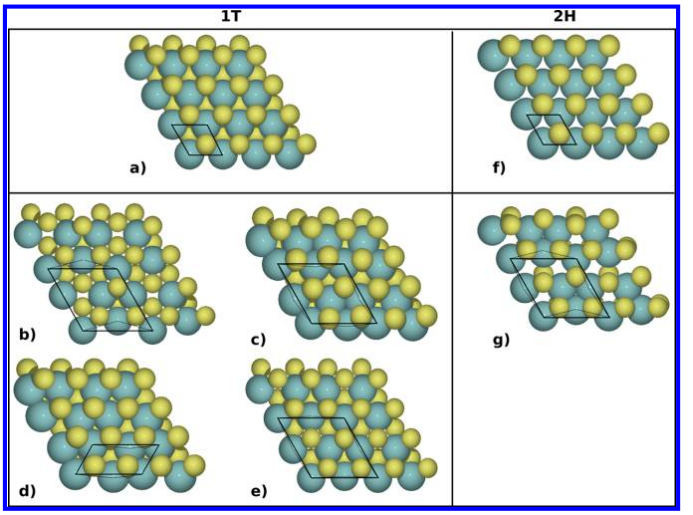

Figure 1. (a) Top view of a 1T monolayer ($P\bar{3}2/m1$ space group). (b) Monolayer with distortions belonging to the 1T class and $P1$ spacegroup with unit cell size 2 × 2. (c) Monolayer with distortions belonging to the 1T class and $P\bar{1}$ spacegroup with unit cell size 2 × 2. (d) Monolayer with distortions belonging to the 1T class and $P1$ spacegroup with unit cell size 2 × 1. (e) Monolayer with distortions belonging to the 1T class and $P3m1$ spacegroup with unit cell size 2 × 2. (f) Top-view of a 2H monolayer ($P\bar{6}m2$ space group). (g) Monolayer with distortions belonging to the 2H class and $P1$ spacegroup with unicell size 2 × 2. Unit cells have been drawn (black solid lines) to show the size of the unit cell, and a few selected bonds (black broken lines) between metal atoms have been shown to highlight the difference between different structures.

difference of the 2H and 1T phases for hydrogen adsorption, we show that the relative position of the p level of 'X' with respect to the Fermi level plays a decisive role for hydrogen adsorption. On the basis of the descriptor employed to screen the materials for HER, we point to many new possible 2D HER materials beyond the few that are already known.

In the present work, we use GPAW,[17] an electronic structure code based on the projector-augmented wave (PAW)[18] formalism. The PBE[19] functional is used for the calculation of lattice constants, and the calculated lattice constants have been used throughout the work. Structures showing distortions have been reoptimized, and the recalculated lattice constants are used. We calculate the heat of formation using the fitted elemental reference phase energies (FERE) scheme employed over the PBE calculated energies, as proposed by Stevanovic et al.[20] A grid spacing of 0.18 Å is used to expand the wave functions in real space, and a Fermi−Dirac smearing of 0.05 eV is employed to accelerate the convergence. The Brillouin zone for the smallest unit cell (1 × 1) is sampled using a Monkhorst−Pack[21] scheme with a k-point mesh of 18 × 18 × 1, and for 2 × 2 unit cells, we use a 9 × 9 × 1 k-point grid. All optimizations are carried out using a Quasi-Newton algorithm, and the forces are converged down to 0.05 eV/Å for all relaxations. Spin-polarized calculations are performed for the calculation of lattice constants as well as for the adsorption energies. Adsorption energies are calculated using the BEEF-vdW functional.[22] Uncertainties in adsorption energies are explicitly calculated using the ensemble of functionals proposed in ref 22. The calculated uncertainties are used to estimate the probability that a given material will have the free-energy descriptor for HER lying within a given range. The calculated probabilities help to rank the different materials based on their suitability[23] for HER. We add several corrections to the calculated total energy differences to estimate the adsorption free energy. The zero point energy corrections to the energies of all systems are to a first order approximation taken to be the same as the ones calculated for the 1T-MoS_2 monolayer structure. We get the zero-point correction of the adsorbed hydrogen as 0.39 eV at the standard state. We ignore the entropic corrections for the adsorbed state while calculating the total correction as in ref 15. The zero-point energy of the H_2 molecule has been taken from the ref 24 and is found to be 0.54 eV. The entropic correction of 0.40 eV from the gas-phase H_2 is taken from ref 25. By taking the difference of the corrections in the gas phase and the adsorbed state, ΔZPE comes out as 0.12 eV and $-T\Delta S$ comes out as 0.20 eV; therefore, $\Delta ZPE - T\Delta S$ comes out to be 0.32 eV.

The current work focuses on the 2H and 1T structures and their distorted derivatives of 2D metal dichalcogenides and oxides some of which have been realized in recent experiments.[10−12] The structural difference between the 1T and 2H phases originates from the difference in coordination environment around the metal atom. The 2H phase of MX_2 has a trigonal prismatic structure with 'M' at the center of the prism and 'X' at the vertices, where the 1T phase has an octahedral coordinated structure with 'M' at the center of the octahedron and 'X' at the vertices. Figure 1a,f shows the top view of the 2H and 1T structure, respectively. Figure 1b−e,g represents distorted derivatives of the 2H and 1T structures, which will be discussed later. The significant difference in atomic structure of the two phases might lead to differences in their thermodynamic and electronic properties. The difference in thermodynamic properties will directly influence the relative stability of the two phases, whereas different electronic properties will have an effect on the chemical reactivity. To detect the distortions, if any, in the 2H and 1T structures, we follow the steps: (1) Adsorb the hydrogen in the 2 × 2 unit cell to break the symmetry of the structure and allow the structure

DOI: 10.1021/acs.jpclett.5b00353
J. Phys. Chem. Lett. 2015, 6, 1577−1585

to relax. (2) Remove the hydrogen from the structure obtained from step 1 and relax the structure. (3) If the structure obtained after step 2 is the same as the perfectly symmetric structure, then there are no distortions present or else the structure is distorted. (4) Cases may exist in which step 2 leads to local minima in new structures; therefore, one has to compare the energy obtained after step 2 and the energy of the perfectly symmetric structure and choose the one with lower energy.

Following the steps previously outlined, the distortions present under HER conditions can most likely be obtained. Similar distortions in MoS_2 have been explored by Kan et al.,[26] but we see a wider range of distortions. Therefore, instead of using their terminology, we categorize the distortions in a more general way based on the space group and the size of the unit cell.

Figure 2a,b shows the calculated standard heats of formation of the 2D MX_2 compounds in the 2H and 1T phases. In

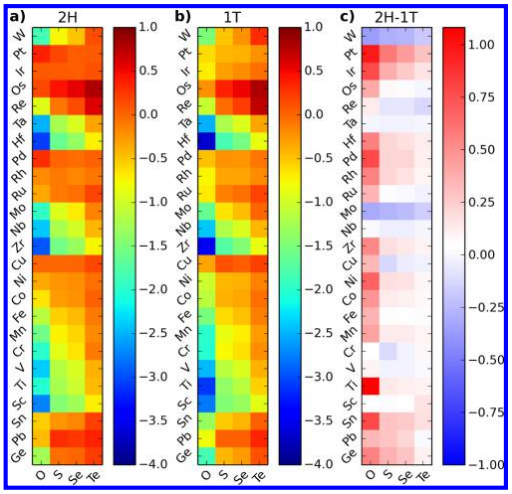

Figure 2. (a,b) Heatmap of standard heat of formation (in eV/atom) of compounds in undistorted 2H and 1T structures, respectively. (c) Difference in enthalpies between the 2H and 1T structures (in eV/atom) of different compounds. Each compound is represented by a square, and the constituent elements are represented by the corresponding ordinate and abscissa of the square. The difference in energies is in eV/atom.

calculating the standard heat of formation, we neglect any zero-point or entropic correction. As can be seen from the Figure the region of stable compounds is very similar in the two structures. With very few exceptions, the compound that is stable (unstable) in one structure exhibits stability (instability) in the other structure as well. Figure 2c shows the difference in enthalpies of the different compounds by which we can estimate the extent to which the two phases differ thermodynamically. The obtained trend in the relative stability of the 2H and 1T phases agrees well with the calculations of Ataca et al.[27] We see that for most of the compounds the energy difference between the 2H and the 1T phase is smaller than ~0.4 eV/atom. Recent experiments on MoS_2[10] and WS_2[8] show that the distorted 1T phase despite being energetically higher than the 2H phase by ~0.3 eV/atom can be stabilized. These experiments thus suggest that the metastable phase of a 2D MX_2 compound with a positive heat of formation as high as ~0.3 eV/atom relative to the stable phase can be synthesized and stabilized under normal conditions using suitable synthetic routes.[28] Thus, the generally small energy differences shown in Figure 2c indicate that the atomic structure of 2D MX_2 can be tuned, if required, for the application in hand. Therefore, we explore both the 2H and 1T class of structures of MX_2 to find suitable materials for HER.

Figure 3a,b shows the energy of distorted structures with respect to perfectly symmetric 2H and 1T structures,

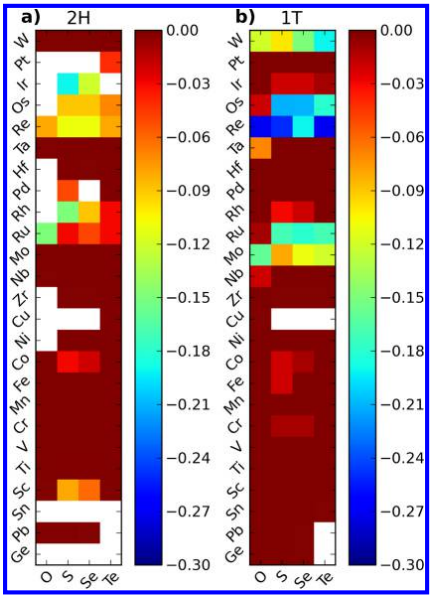

Figure 3. (a,b) Energy of the distorted structures (eV/atom) with respect to the perfectly symmetrical 2H and 1T structures, respectively. The white squares denote massive reconstruction upon relaxation, thus leading to structures not belonging to the 2H and 1T class of structures.

respectively. The white squares denote massive reconstruction upon relaxation, thus leading to structures neither belonging to the 2H or 1T class of structures. We do not investigate these systems any further. Upon analyzing the nature of reconstructions in the more moderately distorted structures, it turns out that the distortions occurring in the 1T structure can be categorized in four different symmetry groups, whereas the distortions in the 2H structure can be captured by only one group. Starting with the structures with slightly displaced atoms from their ideal positions in the perfect 2H and 1T structures, that is, without symmetries in a 2×2 unit cell, upon relaxation, some compounds in 1T structure gain symmetry in such a way that all of the symmetry operations can be captured in a 2×1 unit cell, thus leading to reduction in the size of unit cell. This is not the case for any of the 2H structures. Therefore, we categorize the distorted structures based on the space groups and the unit cell size using the tool described in ref 29. Table 1 shows the categorization of the distortions based on the space group and the size of the reduced unit cell. The forces cannot be brought down to exactly zero during the optimization

DOI: 10.1021/acs.jpclett.5b00353
J. Phys. Chem. Lett. 2015, 6, 1577−1585

Table 1. Categorization of Different Compounds Based on the Deviation of Their Structures from Perfect 2H or 1T Structures and the Size of the Unit Cell[a]

class	MX_2	group	unit cell	class	MX_2	group	unit cell
2H	CoS_2	$P1$	2 × 2	2H	$CoSe_2$	$P1$	2 × 2
2H	IrS_2	$P1$	2 × 2	2H	OsS_2	$P1$	2 × 2
2H	$OsSe_2$	$P1$	2 × 2	2H	PdS_2	$P1$	2 × 2
2H	$PdSe_2$	$P1$	2 × 2	2H	$PdTe_2$	$P1$	2 × 2
2H	ReO_2	$P1$	2 × 2	2H	ReS_2	$P1$	2 × 2
2H	$ReSe_2$	$P1$	2 × 2	2H	RhS_2	$P1$	2 × 2
2H	$RhSe_2$	$P1$	2 × 2	2H	$RhTe_2$	$P1$	2 × 2
2H	RuO_2	$P1$	2 × 2	2H	RuS_2	$P1$	2 × 2
2H	$RuSe_2$	$P1$	2 × 2	2H	ScS_2	$P1$	2 × 2
2H	$ScSe_2$	$P1$	2 × 2				
1T	CoS_2	$P1$	2 × 2	1T	CrS_2	$P1$	2 × 2
1T	$CrSe_2$	$P1$	2 × 2	1T	FeS_2	$P1$	2 × 2
1T	IrS_2	$P1$	2 × 2	1T	$IrSe_2$	$P1$	2 × 2
1T	ReO_2	$P1$	2 × 2	1T	$ReTe_2$	$P1$	2 × 2
1T	RhS_2	$P1$	2 × 2	1T	RuS_2	$P1$	2 × 2
1T	$RuTe_2$	$P1$	2 × 2	1T	MoO_2	$P1$	2 × 1
1T	MoS_2	$P1$	2 × 1	1T	$MoSe_2$	$P1$	2 × 1
1T	$MoTe_2$	$P1$	2 × 1	1T	OsS_2	$P1$	2 × 1
1T	$OsSe_2$	$P1$	2 × 1	1T	$OsTe_2$	$P1$	2 × 1
1T	WS_2	$P1$	2 × 1	1T	WSe_2	$P1$	2 × 1
1T	WTe_2	$P1$	2 × 1	1T	ReS_2	$P\bar{1}$	2 × 2
1T	$ReSe_2$	$P\bar{1}$	2 × 2	1T	$RuSe_2$	$P\bar{1}$	2 × 2
1T	TaO_2	$P\bar{1}$	2 × 2	1T	$CoSe_2$	$P3m1$	2 × 2
1T	$IrTe_2$	$P3m1$	2 × 2	1T	NbO_2	$P3m1$	2 × 2
1T	OsO_2	$P3m1$	2 × 2	1T	$RhSe_2$	$P3m1$	2 × 2
1T	RuO_2	$P3m1$	2 × 2	1T	WO_2	$P3m1$	2 × 2

[a]The class represents the type of undistorted structure to which the compound belongs, the group represents the space group of the distorted structure as per Herman−Maugin notation, and the unit cell represents the size of the reduced unit cell with respect to the 1 × 1 unit cell of the perfect 2H or 1T structures.

process; therefore, to overcome inaccuracies in the forces, we employ a cutoff of 0.05 Å on the rotations/translations to identify the symmetry operations. For six structures where the difference in energy of the distorted structure and the perfectly symmetrical structure is <0.01 eV per atom, we categorize them into the symmetrical structure for the previously mentioned reason. We find that for all of the distorted structures in the 2H class, the type of distortion is similar to the one shown in Figure 1g. Therefore, we categorize them in the same class as those that have the unit cell size of 2 × 2 and the space group $P1$. Figure 1b−e shows the four different types of distortions observed in the 1T structure. There are subtle differences in all of these four groups. Panel b does not have any symmetry and thus belongs to the $P1$ group, panel c shows the distortions similar to panel b but has an inversion symmetry and thus belongs to $P\bar{1}$ as also observed by Tongay et al. for ReS_2.[30] The distortions in panel d are such that the structure forms stripes with periodicity of one unit cell, resulting in a unit cell size of 2 × 1. Panel e has the least distortion and inherits most of the symmetry operations from the symmetric 1T structure and belongs to the $P3m1$ space group.

Additionally, as previously mentioned, discarding distorted phases that differ in energy from the perfectly symmetric structures by <0.01 eV per atom might result in missing some of the charge density wave (CDW) phases, for example, in TiS_2.[31,32] In the case of TiS_2 we found that for a 12 atom unit cell (2 × 2 unit cell) the distorted and the perfectly symmetric structure differ by only ∼0.04 eV (∼0.004 eV per atom). It turns out that due to similar energy differences the CDW phases of other compounds, for example, TaS_2, are all discarded due to the previously mentioned reason. Discarding the CDW phases does not affect our results for the HER, which is dependent only on the energy differences, which are very small in the previously mentioned cases.

In previous works the strength of hydrogen binding on a catalyst surface has been used as a descriptor for the ability to

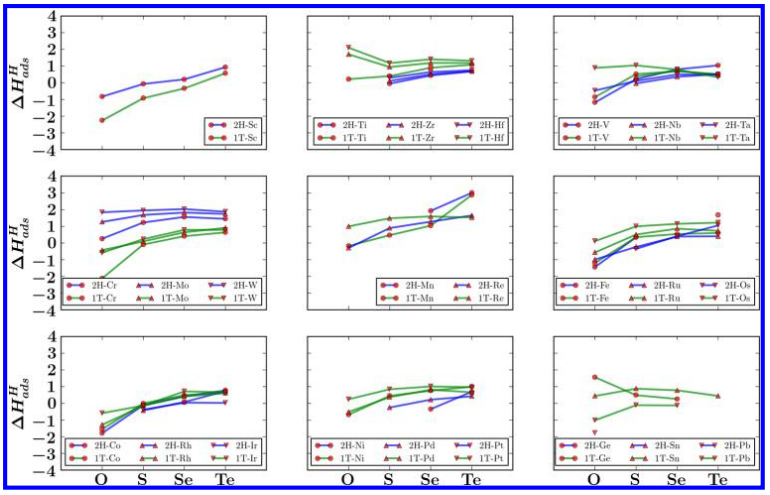

Figure 4. Adsorption energies of the individual groups of compounds. The grouping of the compounds is based on the position of the metal atom of MX_2 in the periodic table. The missing data points in the plots show the instability of those compounds toward hydrogen adsorption; that is, in these cases hydrogen pulls out the 'X' atom from the monolayer and moves far from the surface. All energies shown in the ordinates are in electronvolts.

DOI: 10.1021/acs.jpclett.5b00353
J. Phys. Chem. Lett. 2015, 6, 1577−1585

evolve hydrogen, and it has been found that the optimum value of the free energy of hydrogen adsorption (ΔG_H) on the surface of the material should be close to zero.[3,8,16] The free energy of hydrogen adsorption comes out as a descriptor based on the Volmer–Heyrovsky route for the HER. The steps involved in the Volmer–Heyrovsky process can be written as[33,34]

$$H^+ + e^- + * \rightarrow H^* \quad (1)$$

$$2H^* \rightarrow H_2 + 2^* \quad (2)$$

where * denotes the active site. At zero potential the free-energy difference between $H^+ + e^-$ and H_2 is (by definition) zero, and the intermediate state of adsorbed hydrogen provides an effective barrier for the process, which should be as close to zero as possible. Therefore, to determine the reactivity of the basal plane, we first calculate the hydrogen adsorption energy on different sites. The adsorption energy is calculated relative to the hydrogen molecule and the most stable clean substrate within the given class (1T or 2H). In all of the 1T and 2H classes of the MX_2 structures, we find that the most favorable hydrogen adsorption site on the basal plane is on top of the chalcogen/oxygen atoms. For distorted structures, depending on the symmetry, H will bind differently to the different chalcogen/oxygen atoms. For further analysis we select the adsorption site with the strongest binding. We start with one-fourth (0.25 ML) of a monolayer of coverage (one hydrogen per four chalcogen/metal atom) and select only the compounds binding hydrogen too strongly ($\Delta H_H^{ads} \geq -0.8$) for higher coverages. Calculations for higher H adsorption coverages reveal massive reconstructions, and the final structures do not belong to any of the structure in the 2H and 1T class; therefore, we choose not to explore the cases of higher coverage any further and focus only on one-fourth of a monolayer of coverage in the current work. To establish the trends in the strength of hydrogen binding, we use the heat of adsorption (total energy differences) and incorporate zero-point energies and entropic effects only in the stage of evaluating the suitability of materials for HER.

Figure 4 shows the calculated heats of hydrogen adsorption (ΔH_{ads}^H) on the 2H and 1T basal planes with 0.25 ML coverage of hydrogen. Upon hydrogen adsorption, not all of the surfaces are stable; therefore, we discard the compounds (missing data points) in the plots that are unstable toward hydrogen adsorption, that is, in these cases hydrogen pulls out the 'X' atom from the monolayer and moves far from the surface or the structure massively reconstructs and transforms to a structure not belonging to the 2H or 1T class. As can be seen, the heat of adsorption varies widely by several electronvolts. An overall trend is that the bonding strength is increased as the electronegativity of the chalcogenide is increased. There is clearly no simple relation between the hydrogen bonding to the 2H and 1T structures. Depending on the metal and chalcogenide in question the bonding to the 1T class may be stronger or weaker than the bonding to the 2H class.

To shed some light on the chemistry behind the different adsorption energies, we shall focus on only two of the metal groups that stand out in Figure 4. For the metals Ti, Zr, and Hf the bonding to the 2H structure is clearly stronger than that for the 1T, while for the metals Cr, Mo, and W we have an opposite trend. To understand these opposite behaviors we analyze the density of states (DOS) projected onto the 'X' p orbital in MX_2.[16] Figure 5a–d shows the DOS of pristine

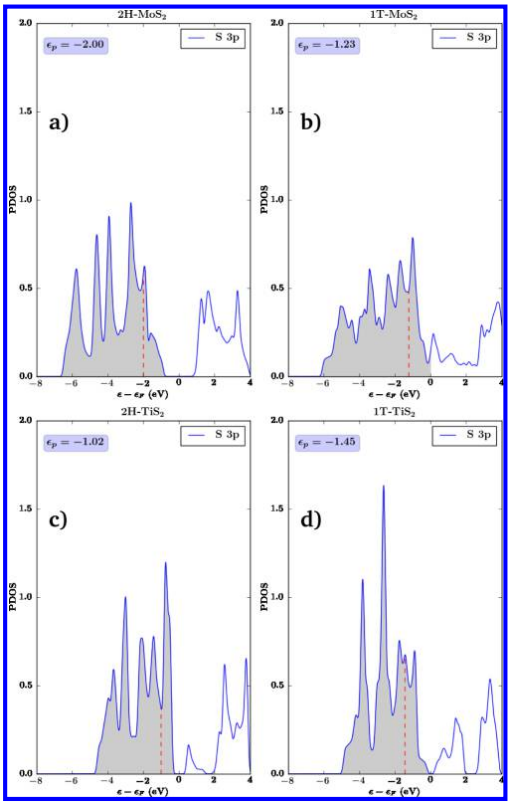

Figure 5. (a) Density of states (DOS) plot of MoS_2 and TiS_2 in the 2H and 1T structures. MoS_2 and TiS_2 belong to two different groups as shown in Figure 4). ϵ_p denotes the position of the center of the p band with respect to the Fermi level. The shaded region corresponds to occupied states.

monolayers. The calculated position of the p-band center (ϵ_p) (obtained as the first moment of the projected density of states) with respect to the Fermi level of the pristine monolayers explains the difference in reactivity of the two groups. A higher-lying p level indicates possible stronger effects of hybridization with the hydrogen s state.[16] The calculated ϵ_p for MoS_2 in the 1T structure lies closer to the Fermi level as compared with the 2H structure, whereas for TiS_2, the ϵ_p for the 2H structure lies closer to the Fermi level as compared with the 1T structure. Table 2 shows the adsorption energy (ΔH_{ads}^H) and center of p band for compounds selected from the groups to which MoS_2 and TiS_2 belong. As can be seen from the Table, other compounds also show the same correlation between ϵ_p and ΔH_{ads}^H. These results show that the nature of the metal atom[35] along with the symmetry of the structure has a significant effect on the reactivity.

We calculate for 0.25 ML coverage the heats of adsorption (ΔH_{ads}^H) including error bars (σ) with the BEEF-vdW functional to assess the confidence interval of heats of adsorption.[22] As mentioned earlier, we add zero point and entropic corrections of 0.32 eV in all the heats of adsorption to get the free energy of adsorption. Here we assume that the corrections will not vary

DOI: 10.1021/acs.jpclett.5b00353
J. Phys. Chem. Lett. 2015, 6, 1577–1585

Table 2. Heat of Adsorption of Hydrogen, ΔH^{H}_{ads}, and the Center of the p Band, ϵ_p, for Compounds Belonging to Different Groups in the 2H and 1T Structures[a]

2H	ϵ_p	ΔH^{H}_{ads}	1T	ϵ_p	ΔH^{H}_{ads}
MoS_2	−2.00	1.68 ± 0.07	MoS_2	−1.23	0.10 ± 0.13
$MoSe_2$	−1.74	1.82 ± 0.13	$MoSe_2$	−1.46	0.64 ± 0.11
WS_2	−2.32	1.95 ± 0.08	WS_2	−1.37	0.23 ± 0.14
WSe_2	−2.03	2.03 ± 0.14	WSe_2	−1.29	0.78 ± 0.15
TiS_2	−1.02	−0.05 ± 0.13	TiS_2	−1.45	0.40 ± 0.09
$TiSe_2$	−0.89	0.44 ± 0.12	$TiSe_2$	−1.38	0.90 ± 0.10
ZrS_2	−0.96	0.11 ± 0.10	ZrS_2	−1.42	0.94 ± 0.07
$ZrSe_2$	−0.80	0.51 ± 0.10	$ZrSe_2$	−1.34	1.19 ± 0.09

[a]Grouping of the compounds is performed based on the group of the periodic table to which the metal atom in MX_2 belongs.

much for different compounds, hence we choose the same correction as we have calculated for 1T-MoS_2 monolayer structure. Since the optimum value of free energy (ΔG^{opt}) for HER is ∼0.0 eV, we consider the range of free energy from −0.5 to 0.5 eV to take into account the effect of coverage, strain, and so on.[8,36] Having an allowable range of free energy, mean adsorption energies along with uncertainties allows us to calculate the probability ($P(|\Delta G| \leq 0.5)$) of a material having free energy for HER in the given interval. Assuming a Gaussian distribution of uncertainties around the mean value, $\overline{E}$, of the adsorption, probabilities can be calculated as

$$P(|\Delta G| \leq 0.5) = \frac{1}{\sqrt{2\pi\sigma^2}} \int_{-0.5-\overline{E}}^{0.5+\overline{E}} \exp\left(-\frac{E^2}{2\sigma^2}\right) \mathrm{d}E \quad (3)$$

The calculated probabilities will help in narrowing down the material space for potential experimental investigation by discarding the materials with very small probabilities. In Figure 6, we show the compounds in the 2H and 1T class of structures ranked according to the calculated probability measure. The Figure includes compounds with a probability as low as 0.15. This leads to 21 compounds in the 2H class of structures and 26 compounds in the 1T class of structures. For each compound, the calculated free energy is shown together with the error bar from the BEEF−vdW ensemble. We see that MoS_2 and WS_2 appear on the list of candidates for the 1T structure (although not with the highest probability) in support of the recent experiments indicating possible hydrogen evolution for these systems.[8,10] The only compounds that appear on both the 2H and 1T lists are NbS_2, RhS_2, RuS_2, IrS_2, CoS_2, $ScSe_2$, RuO_2, and $TaTe_2$, illustrating the fact that the chemical activity is very sensitive to the crystal structure.

Having identified possible 2D materials with promising binding properties for hydrogen, it is appropriate to investigate the stability of these materials further. There are two possibilities that may hamper the growth and stability of the 2H or 1T phases of the 2D materials found to be active for HER: (1) much higher stability of the competing bulk structures or the standard states, thus leading to the dissociation of the 2D phase into these compounds, and (2) relative stability of the 2H and 1T phases also matters. For example, if the 2H phase of a material is HER-active but is much higher in energy than the 1T structure, it is unlikely that the material can be synthesized and stabilized in the 2H structure. Therefore, the HER-active 2D materials must not lie above a certain degree of metastability with respect to the competing bulk structures or the standard states, and also it should not be energetically too high with respect to the other 2D phase of the material. In the present work, we do not explore the stability of compounds in water because a recent study has shown that with stabilizing agents compounds can be stabilized in water, making this criterion less important.[37] The presence of water might also have an effect on the adsorption energies, but in the current work having a fairly wide window of the free energy of adsorption for the candidate materials, we expect to have allowed for the effect of water.

Calculated data to address the previously described issues are collected in Table 3a,b. The second column of the Table shows the calculated standard heats of formation, ΔH, for the monolayers (as shown for all the compounds in Figure 2) in the 2H and 1T classes of structure, respectively. The third column ΔH_{hull} is calculated using structural information from the OQMD database.[38] The OQMD database contains standard DFT energy calculations for a large selection of known compounds from the ICSD database[39] plus a number of standard structures. In the case of binary systems, this results in

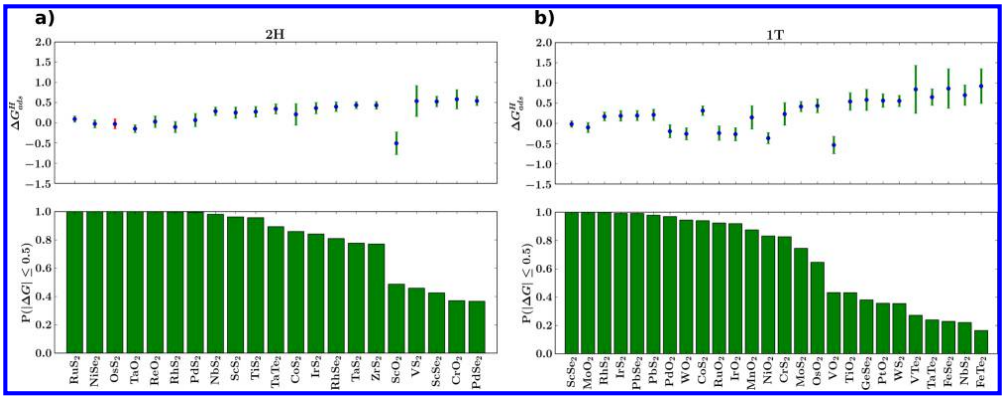

Figure 6. (a) 2H compounds having a free energy of hydrogen adsorption (ΔG^{H}_{ads}) in the range of (−0.5, 0.5) eV along with uncertainties for 0.25 ML coverage and probabilities ($P(|\Delta G| \leq 0.5)$) as calculated from eq 3. Red error bars indicate that the structure is unstable with respect to the standard states.

DOI: 10.1021/acs.jpclett.5b00353
J. Phys. Chem. Lett. 2015, 6, 1577−1585

Table 3. (a) Relevant Energies for Analysis of the Stabilities of the Obtained HER Candidates in the 2H-Derived Structures[a] and (b) Similar Table for the 1T Candidates[b]

(a)

2H-MX_2	ΔH	ΔH_{hull}	ΔH_{hull}	$\Delta H_{expt.}$	ref 40	$\Delta H_{2H/1T}$	$P(\lvert\Delta G\rvert \leq 0.5)$
RuS_2	−0.31	−0.70	0.39	−0.71	no	−0.01	1.00
$NiSe_2$	−0.21	−0.34	0.13	−0.38	no	0.17	1.00
OsS_2	0.34	−0.60	0.94	NA	no	−0.01	1.00
TaO_2	−2.58	−3.00	0.42	NA	no	−0.07	1.00
ReO_2	−0.91	−1.42	0.51	−1.52	no	0.05	1.00
RhS_2	−0.11	−0.48	0.37	NA	no	0.07	1.00
PdS_2	0.01	−0.31	0.32	−0.28	yes	0.17	1.00
NbS_2	−1.21	−1.20	−0.01	NA	yes	−0.04	0.98
ScS_2	−1.46	−1.46	0.00	NA	no	−0.06	0.96
TiS_2	−1.23	−1.37	0.14	−1.41	yes	0.15	0.96
$TaTe_2$	−0.32	−0.45	0.13	NA	yes	0.00	0.89
CoS_2	−0.33	−0.48	0.15	−0.51	no	0.01	0.86
IrS_2	−0.11	−0.48	0.37	−0.46	no	0.22	0.84
$RhSe_2$	−0.17	−0.45	0.28	NA	no	0.07	0.81
TaS_2	−1.24	−1.22	−0.02	−1.22	yes	−0.02	0.78
ZrS_2	−1.55	−1.73	0.18	−1.99	yes	0.19	0.77
ScO_2	−2.74	−3.17*	0.43	NA	no	0.05	0.49
VS_2	−1.16	−1.14	−0.02	NA	no	−0.02	0.46
$ScSe_2$	−1.30	−1.25*	−0.05	NA	no	−0.01	0.43
CrO_2	−1.99	−2.15	0.16	−2.01	no	0.03	0.37
$PdSe_2$	−0.02	−0.33	0.31	NA	yes	0.22	0.37

(b)

1T-MX_2	ΔH	ΔH_{hull}	ΔH_{hull}	$\Delta H_{expt.}$	ref 40	$\Delta H_{1T/2H}$	$P(\lvert\Delta G\rvert \leq 0.5)$
$ScSe_2$	−1.34	−1.25*	−0.09	NA	no	0.01	1.00
MoO_2	−1.79	−1.95	0.16	−2.04	no	0.31	1.00
RhS_2	−0.32	−0.48	0.16	NA	no	−0.07	1.00
IrS_2	−0.30	−0.48	0.18	−0.46	no	−0.22	0.99
$PbSe_2$	0.04	−0.31*	0.35	NA	no	−0.22	0.99
PbS_2	0.03	−0.32*	0.35	NA	no	−0.28	0.98
PdO_2	−0.48	−0.41	−0.07	NA	no	NA	0.97
WO_2	−1.61	−1.89	0.28	NA	no	0.24	0.94
CoS_2	−0.34	−0.48	0.14	−0.51	no	−0.01	0.94
RuO_2	−0.71	−0.94	0.23	−1.05	no	−0.20	0.92
IrO_2	−0.70	−0.94	0.24	−0.86	no	NA	0.92
MnO_2	−2.00	−1.98	−0.02	−1.80	no	−0.43	0.87
NiO_2	−1.01	−0.79*	−0.22	NA	no	NA	0.83
CrS_2	−0.77	−0.71	−0.06	NA	yes	0.12	0.83
MoS_2	−0.66	−0.93	0.27	−0.95	yes	0.28	0.74
OsO_2	−0.23	−1.10	0.87	−1.02	no	NA	0.65
VO_2	−2.47	−2.63	0.16	−2.48	no	−0.10	0.43
TiO_2	−3.10	−3.29	0.19	−3.26	no	−1.11	0.43
$GeSe_2$	−0.27	−0.34	0.07	−0.39	no	NA	0.38
PtO_2	−0.61	−0.62	0.01	NA	no	NA	0.36
WS_2	−0.59	−0.78	0.19	−0.90	yes	0.18	0.35
VTe_2	−0.40	−0.45	0.05	NA	yes	0.00	0.27
$TaTe_2$	−0.32	−0.45	0.13	NA	yes	0.00	0.24
$FeSe_2$	−0.48	−0.56	0.08	NA	no	−0.05	0.23
NbS_2	−1.18	−1.20	0.02	NA	yes	0.04	0.22
$FeTe_2$	−0.11	−0.20	0.09	−0.25	no	−0.02	0.16

[a]ΔH denotes the calculated standard heat of formation. ΔH_{hull} denotes the heat of formation of the most stable compound (i.e., at the convex hull) in the OQMD database.[38] The symbol * in superscript corresponds to the situation, where no bulk structure with the compound composition lies on the convex hull according to the database. In that case, ΔH_{hull} is calculated as a linear combination of several structures. ΔH_{hull} denotes the difference between the two previous columns; that is, it shows how much the 2D compound lies above or below the convex hull. $\Delta H_{expt.}$ indicates the experimental standard heats of formation as listed in the OQMD database. Lebègue al.[40] have analyzed the possibilities for forming 2D compounds based on the layered character of the bulk structures and their result is also listed in the Table. $\Delta H_{2H/1T}$ is the difference between the energies in the two (possibly distorted) 2H and 1T structures. Finally, $P(\lvert\Delta G\rvert \leq 0.5)$ is the probability that the free energy of hydrogen adsorption lies within 0.5 eV from zero, as described in Figure 6. All the energies are in eV/atom. [b]NA in the seventh column indicates that due to massive reconstructions the compound is discarded from the 2H class. All energies are in eV/atom.

DOI: 10.1021/acs.jpclett.5b00353
J. Phys. Chem. Lett. 2015, 6, 1577−1585

calculations of the most stable structures as a function of relative concentration of the two constituents identifying the so-called convex hull of lowest energy structures. For a given MX_2 compound, we extract the structure with the lowest energy at this 1:2 composition of the M-X phase diagram from the database. In most cases a compound with the 1:2 composition exists as the most stable one. If that is not the case we extract the two structures that linearly combine to give the lowest energy of the convex energy hull at the 1:2 composition. We note that all structures are reoptimized and energies are calculated with the approach we use here. The fourth column, ΔH_{hull}, shows our calculated heat of formation with respect to the convex hull. If two structures are used to obtain the energy of the hull, ΔH_{hull}, then it is indicated with an asterisk on the number. For comparison, the experimental heats of formation for the most stable compounds are shown in the third column when available in the OQMD database. As can be seen, the calculated heats of formation are in good agreement with the experimental data with a RMS deviation of only 0.09 eV. The fourth column shows the difference between columns 1 and 2, that is, how much the energy of the 2D material is above (or below) the energy at the convex hull. The seventh column in Table 3 shows the heat of formation of the 2H (1T) class of structure with respect to the 1T (2H) class of structures $\Delta H_{\text{2H/1T}}$ ($\Delta H_{\text{1T/2H}}$). We find that the energy difference between the catalytically active candidate and its analogue in the other structure is usually not very large. As previously mentioned HER-active materials like MoS_2 and WS_2 in the 1T phase have a degree of metastability as high as 0.3 eV/atom with respect to the 2H phase and lie above the hull by ∼0.3 eV/atom; nevertheless, they have been synthesized and stabilized under ambient conditions.[10] Surprisingly, none of the other HER-active materials differ from their corresponding 2D analogue in energy by >0.3 eV/atom. Therefore, in the list of proposed HER materials, if the material can be synthesized and stabilized in one of the two phases, then it is highly likely that it can be synthesized and stabilized in the other phase as well.

Some of the compounds like PdS_2 and $PdTe_2$, which have been found to be HER-active in the current work, have also been suggested to exist in monolayer form by Lebègue al.[40] As can be seen from Table 3a,b, PdS_2 and $PdTe_2$ lie above the hull by ∼0.35 eV. Therefore, we choose a threshold of 0.4 eV for ΔH_{hull} for stability of compounds. The given criteria narrows the list of the candidates, specifically OsS_2, ReO_2, $OsSe_2$, ScO_2, and RuO_2 in the 2H class of candidates and OsO_2 in the 1T class of candidates do not fulfill this criteria. The names of these compounds are italicized in Table 3a,b. A few monolayers in Table 3a,b have lower energy than the energy of the convex hull. One of the reasons for this behavior might be the existence of other more stable bulk structures than the ones considered in the OQMD database, for example, structures obtained by stacking the 2D layers.

Additionally, we also compare our findings of 2D materials for HER with the recent study by Lebègue et al.[40] that is based on predicting the existence of 2D materials from experimental bulk structures. The exiguous overlap between our results and the ones by Lebègue al. arises from the fact that our conclusions are based on thermodynamic arguments obtained with ab initio calculations, whereas the work of Lebègue al. relies more on heuristic arguments of the ability of cleaving a bulk along a direction of weak bonding. The compounds of the MX_2 class proposed in their work are all present in our work, thus supporting our approach. A few compounds in Table 3a,b are written in bold. We select them based on the work by Lebègue et al.[40] by looking for "yes" in the column VI in Table 3a,b because it is highly likely that they can be synthesized and stabilized with minimal effort.

In the current study, we suggest several 2D materials in the 2H and 1T structures as potential candidates for the hydrogen evolution reaction. The activity of the basal plane in all of the discovered candidates will provide a much larger number of active sites as compared with 2D materials like 2H MoS_2, where only edges are active. Our analysis is using the calculated adsorption free energy as a well-established descriptor for hydrogen evolution. We furthermore investigate the stability of the compounds in some detail by comparing heats of formation of both competing layered phases and bulk structures. Recent experimental stabilization of different layered phases seem to indicate that fairly large metastability of several tenths of an eV/atom can be overcome by appropriate synthesis routes, making it likely that many of the suggested compounds could be experimentally synthesized. It has recently been demonstrated that the MoS_2 and WS_2 in the 1T phase can evolve hydrogen, and these systems also appear in our screening, but other identified systems should according to the calculations provide higher activity. The calculations therefore invite further investigation of some of the best candidates suggested here.

■ ASSOCIATED CONTENT

Supporting Information

Lattice constants and adsorption energy of hydrogen are provided in the tables. This material is available free of charge via the Internet at http://pubs.acs.org.

■ AUTHOR INFORMATION

Corresponding Author

*E-mail: kwj@fysik.dtu.dk.

Notes

The authors declare no competing financial interest.

■ ACKNOWLEDGMENTS

We acknowledge CASE (Catalysis for Sustainable Energy) initiative of the Danish Ministry of Science for funding the project. The Center for Nanostructured Graphene is sponsored by the Danish National Research Foundation, Project DNRF58. We thank Jens K. Nørskov and Charlie Tsai from SUNCAT (Stanford University) for helpful discussions.

■ REFERENCES

(1) Dresselhaus, M. S.; Thomas, I. L. Alternative Energy Technologies. *Nature* **2001**, *414*, 332−337.

(2) Crabtree, G. W.; Dresselhaus, M. S.; Buchanan, M. V. The Hydrogen Economy. *Phys. Today* **2004**, *57*, 39−44.

(3) Greeley, J.; Jaramillo, T. F.; Bonde, J. L.; Chorkendorff, I.; Nørskov, J. K. Computational High-Throughput Screening of Electrocatalytic Materials for Hydrogen Evolution. *Nat. Mater.* **2006**, *5*, 909−913.

(4) Okamoto, Y.; Ida, S.; Hyodo, J.; Hagiwara, H.; Ishihara, T. J. Synthesis and Photocatalytic Activity of Rhodium-doped Calcium Niobate Nanosheets for Hydrogen Production from a Water/Methanol System without Cocatalyst Loading. *J. Am. Chem. Soc.* **2011**, *133*, 18034−18037.

(5) Cobo, S.; Heidkamp, J.; Jacques, P.-A.; Fize, J.; Fourmond, V.; Guetaz, L.; Jousselme, B.; Ivanova, V.; Dau, H.; Palacin, S.; et al. A Janus Cobalt-Based Catalytic Material for Electro-Splitting of Water. *Nat. Mater.* **2012**, *11*, 802−807.

DOI: 10.1021/acs.jpclett.5b00353
J. Phys. Chem. Lett. 2015, 6, 1577−1585

(6) Liu, P.; Rodriguez, J. A. Catalysts for Hydrogen Evolution from the [NiFe] Hydrogenase to the Ni_2P (001) Surface: The Importance of Ensemble Effect. *J. Am. Chem. Soc.* **2005**, *127*, 14871−14878.
(7) Popczun, E. J.; McKone, J. R.; Read, C. G.; Biacchi, A. J.; Wiltrout, A. M.; Lewis, N. S.; Schaak, R. E. Nanostructured Nickel Phosphide as an Electrocatalyst for the Hydrogen Evolution Reaction. *J. Am. Chem. Soc.* **2013**, *135*, 9267−9270.
(8) Voiry, D.; Yamaguchi, H.; Li, J.; Silva, R.; Alves, D. C. B.; Fujita, T.; Chen, M.; Asefa, T.; Shenoy, V. B.; Eda, G.; et al. Enhanced Catalytic Activity in Strained Chemically Exfoliated WS_2 Nanosheets for Hydrogen Evolution. *Nat. Mater.* **2013**, *12*, 850−855.
(9) Lukowski, M. A.; Daniel, A. S.; Meng, F.; Forticaux, A.; Li, L.; Jin, S. Enhanced Hydrogen Evolution Catalysis from Chemically Exfoliated Metallic MoS_2 Nanosheets. *J. Am. Chem. Soc.* **2013**, *135*, 10274−10277.
(10) Voiry, D.; Salehi, M.; Silva, R.; Fujita, T.; Chen, M.; Asefa, T.; Shenoy, V. B.; Eda, G.; Chhowalla, M. Conducting MoS_2 Nanosheets as Catalysts for Hydrogen Evolution Reaction. *Nano Lett.* **2013**, *13*, 6222−6227.
(11) Wang, H.; Lu, Z.; Kong, D.; Sun, J.; Hymel, T. M.; Cui, Y. Electrochemical Tuning of MoS_2 Nanoparticles on Three-dimensional Substrate for Efficient Hydrogen Evolution. *ACS Nano* **2014**, *8*, 4940−4947.
(12) Jaramillo, T. F.; Jørgensen, K. P.; Bonde, J.; Nielsen, J. H.; Horch, S.; Chorkendorff, I. Identification of Active Edge Sites for Electrochemical H_2 Evolution from MoS_2 Nanocatalysts. *Science* **2007**, *317*, 100−102.
(13) Enyashin, A. N.; Yadgarov, L.; Houben, L.; Popov, I.; Weidenbach, M.; Tenne, R.; Bar-Sadan, M.; Seifert, G. New Route for Stabilization of 1T-WS_2 and MoS_2 Phases. *J. Phys. Chem. C* **2011**, *115*, 24586−24591.
(14) Bollinger, M. V.; Jacobsen, K. W.; Nørskov, J. K. Atomic and Electronic Structure of MoS_2 Nanoparticles. *Phys. Rev. B* **2003**, *67*, 085410.
(15) Hinnemann, B.; Moses, P. G.; Bonde, J.; Jørgensen, K. P.; Nielsen, J. H.; Horsch, S.; Chorkendorff, I.; Nørskov, J. K. Biomemetic Hydrogen Evolution: MoS_2 Nanoparticles as Catalyst for Hydrogen Evolution. *J. Am. Chem. Soc.* **2005**, *127*, 5308−5309.
(16) Tsai, C.; A.-Pedersen, F.; Nørskov, J. K. Tuning the MoS_2 Edge-Site Activity for Hydrogen Evolution via Support Interactions. *Nano Lett.* **2014**, *14*, 1381−1387.
(17) Enkovaara, J.; Rostgaard, C.; Mortensen, J. J.; Chen, J.; Dulak, M.; Ferrighi, L.; Gavnholt, J.; Glinsvad, C.; Haikola, V.; Hansen, H. A.; et al. Electronic Structure Calculations with GPAW: A real-space Implementation of the Projector Augmented-wave Method. *J. Phys.: Condens. Matter* **2010**, *22*, 253202.
(18) Kresse, G.; Joubert, D. From Ultrasoft Pseudopotentials to the Projector Augmented-Wave Method. *Phys. Rev. B* **1999**, *59*, 1758−1775.
(19) Perdew, J. P.; Burke, K.; Ernzerhof, M. Generalized Gradient Approximation Made Simple. *Phys. Rev. Lett.* **1996**, *77*, 3865.
(20) Stevanovic, V.; Lany, S.; Zhang, X.; Zunger, A. Correcting Density Functional Ttheory for Accurate Predictions of Compound Enthalpies of Formation: Fitted Elemental-phase Reference Energies. *Phys. Rev. B* **2012**, *85*, 115104.
(21) Monkhorst, H. J.; Pack, J. D. Special Points for Brillouin-zone Integrations. *Phys. Rev. B* **1976**, *13*, 12.
(22) Wellendorff, J.; Lundgaard, K. T.; Møgelhøj, A.; Petzold, V.; Landis, D. D.; Nørskov, J. K.; Bligaard, T.; Jacobsen, K. W. Density Functionals for Surface Science: Exchange-correlation Model Development with Bayesian Error Estimation. *Phys. Rev. B* **2012**, *85*, 235149.
(23) Medford, A. J.; Wellendorff, J.; Vojvodic, A.; Studt, F.; A.-Pedersen, F.; Jacobsen, K. W.; Bligaard, T.; Nørkov, J. K. Assessing the Reliability of Calculated Catalytic Ammonia Synthesis Rates. *Science* **2014**, *345*, 197.
(24) Irikura, K. K. Experimental Vibrational Zero-Point Energies: Diatomic Molecules. *J. Phys. Chem. Ref. Data* **2007**, *36*, 389.
(25) Linstrom, P. J., Mallard, W. *NIST Chemistry WebBook*; NIST Standard Reference Database 69; National Institute of Standards and Technology: Gaithersburg, MD, 1998.
(26) Kan, M.; Wang, J. Y.; Li, X. W.; Zhang, S. H.; Li, Y. W.; Kawazoe, Y.; Sun, Q.; Jena, P. Structures and Phase Transition of a MoS_2 Monolayer. *J. Phys. Chem. C* **2014**, *118*, 1515−1522.
(27) Ataca, C.; ahin, H.; Ciraci, S. Stable, Single-Layer MX_2 Transition-Metal Oxides and Dichalcogenides in a Honeycomb-Like Structure. *J. Phys. Chem. C* **2012**, *116*, 8983−8999.
(28) Lin, Y.-C.; Dumcenco, D. O.; Huang, Y.-S.; Suenaga, K. Atomic Mechanism of the Semiconducting-to-Metallic Phase Transition in Single-Layered MoS_2. *Nat. Nanotechnol.* **2014**, *9*, 391−396.
(29) Stokes, H. T.; Hatch, D. M. FINDSYM: Program for Identifying the Space Group Symmetry of a Crystal. *J. Appl. Crystallogr.* **2005**, *38*, 237−238.
(30) Tongay, S.; Fan, W.; Kang, J.; Park, J.; Koldemir, U.; Suh, J.; Narang, D. S.; Liu, K.; Ji, J.; Li, J.; et al. Monolayer Behaviour in Bulk ReS_2 Due to Electronic and Vibrational Decoupling. *Nat. Commun.* **2014**, *5*, 3252.
(31) Rossnage, K. On the Origin of Charge-Density Waves in Select Layered Transition-Metal Dichalcogenides. *J. Phys.: Condens. Matter* **2011**, *23*, 213001.
(32) Dolui, K.; Sanvito, S. Dimensionality Driven Charge Density Wave Instability in TiS_2. *arXiv* **2013**, arXiv:1310.1866v1 [cond-mat.mes-hall].
(33) Trasatti, S. Work Function, Electronegativity, and Electrochemical Behaviour of Metals: III. Electrolytic Hydrogen Evolution in Acid Solutions. *J. Electroanal. Chem.* **1972**, *39*, 163.
(34) Bockris, J. O.; Reddy, A. K. N.; Gamboa-Aldeco, M. *Modern Electrochemistry 2A*, 2nd ed.; Kluwer Academic/Plenum Publishers: New York, 1998.
(35) (a) Tsai, C.; Chan, K.; Nørskov, J. K.; Abild-Pedersen, F. Understanding the Reactivity of Layered Transition-Metal Sulfides: A Single Electronic Descriptor for Structure and Adsorption. *J. Phys. Chem. Lett.* **2014**, *5*, 3884−3889. (b) Tsai, C.; Chan, K.; Nørskov, J. K.; Abild-Pedersen, F. Theoretical Insights into the Hydrogen Evolution Activity of Layered Transition Metal Dichalcogenides. *Surf. Sci.* **2015**, 10.1016/j.susc.2015.01.019.
(36) Seitz, L. C.; Chen, Z.; Forman, A. J.; Pinaud, B. A.; Benck, J. D.; Jaramillo, T. F. Modeling Practical Performance Limits of Photoelectrochemical Water Splitting Based on the Current State of Materials Research. *ChemSusChem* **2014**, *7*, 1372.
(37) Mubeen, S.; Lee, J.; Singh, N.; Moskovitsb, M.; McFarland, E. W. Stabilizing Inorganic Photoelectrodes for Efficient Solar-to-Chemical Energy Conversion. *Energy Environ. Sci.* **2013**, *6*, 1633.
(38) Saal, J. E.; Kirklin, S.; Aykol, M.; Meredig, B.; Wolverton, C. Materials Design and Discovery with High-Throughput Density Functional Theory: The Open Quantum Materials Database (OQMD). *JOM* **2013**, *65*, 1501−1509.
(39) Belsky, A.; Hellenbrandt, M.; Karen, V. L.; Luksch, P. New developments in the Inorganic Crystal Structure Database (ICSD): Accessibility in Support of Materials Research and Design. *Acta Crystallogr.* **2002**, *B58*, 364−369.
(40) Lebègue, S.; Björkman, T.; Klintenberg, M.; Nieminen, R. M.; Eriksson, O. Two-Dimensional Materials from Data Filtering and Ab Initio Calculations. *Phys. Rev. X* **2013**, *3*, 031002.

DOI: 10.1021/acs.jpclett.5b00353
J. Phys. Chem. Lett. 2015, 6, 1577−1585

THE JOURNAL OF PHYSICAL CHEMISTRY Letters

Addition/Correction

pubs.acs.org/JPCL

Correction to "Two-Dimensional Metal Dichalcogenides and Oxides for Hydrogen Evolution: A Computational Screening Approach"

Mohnish Pandey, Aleksandra Vojvodic, Kristian S. Thygesen, and Karsten W. Jacobsen*

J. Phys. Chem. Lett. **2015**, *6*(9), 1577−1585. DOI: 10.1021/acs.jpclett.5b00353

The estimation of the correction to the calculated hydrogen adsorption energy to obtain the free energy of adsorption is wrong. We state in the present version of the manuscript (pg 1578 column 2) that the zero-point correction for the adsorbed hydrogen is 0.39 eV and that for the H_2 molecule is 0.54 eV. The correct values should be 0.20 and 0.27 eV. This means that the correction to the energy becomes 0.26 eV instead of the quoted 0.32 eV. The conclusions of the Letter are essentially unchanged because the error is smaller than the calculated error bars on the individual calculated heats of formation and much smaller than the energy window of 0.5 eV used for identifying good HER candidates. Furthermore, the estimated correction is just an estimate based on a single system (MoS_2) and can be expected to have some variation from system to system that is not taken into account. However, because of the change in the correction term Figure 6 and the last column of Table 3 change in detail. The changes are fairly small, but because the probability factor P is used for ordering, some of the systems are swapped in Figure 6 and Table 3. We have included the figure and table the way they would look if a correction value of 0.26 eV is used instead.

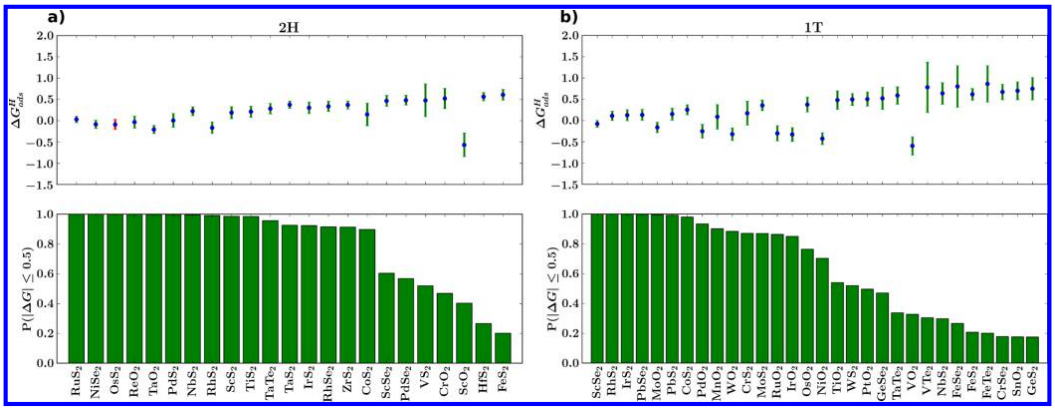

Figure 6.

Table 3

2 H-MX_2	ΔH	ΔH_{hull}[a]	δH_{hull}	$\Delta H_{expt.}$	ref 1	$\Delta H_{2H/1T}$	$P(\lvert\Delta G\rvert \leq 0.5)$
RuS_2	−0.31	−0.70	0.39	−0.71	no	−0.01	1.00
$NiSe_2$	−0.21	−0.34	0.13	−0.38	no	0.17	1.00
OsS_2	0.34	−0.60	0.94	NA	no	−0.01	1.00
ReO_2	−0.91	−1.42	0.51	−1.52	no	0.05	1.00
TaO_2	−2.58	−3.00	0.42	NA	no	−0.07	1.00
PdS_2	0.01	−0.31	0.32	−0.28	yes	0.17	1.00
NbS_2	−1.21	−1.20	−0.01	NA	yes	−0.04	1.00
RhS_2	−0.11	−0.48	0.37	NA	no	0.07	0.99
ScS_2	−1.46	−1.46	0.00	NA	no	−0.06	0.99
TiS_2	−1.23	−1.37	0.14	−1.41	yes	0.15	0.98
$TaTe_2$	−0.32	−0.45	0.13	NA	yes	0.00	0.96
TaS_2	−1.24	−1.22	−0.02	−1.22	yes	−0.02	0.93
IrS_2	−0.11	−0.48	0.37	−0.46	no	0.22	0.92
$RhSe_2$	−0.17	−0.45	0.28	NA	no	0.07	0.92
ZrS_2	−1.55	−1.73	0.18	−1.99	yes	0.19	0.91

DOI: 10.1021/acs.jpclett.5b01299
J. Phys. Chem. Lett. 2015, 6, 2669−2670

Table 3 Continued

2 H-MX_2	ΔH	ΔH_{hull}[a]	δH_{hull}	$\Delta H_{expt.}$	ref 1	$\Delta H_{2H/1T}$	$P(\lvert\Delta G\rvert \leq 0.5)$
CoS_2	−0.33	−0.48	0.15	−0.51	no	0.01	0.90
$ScSe_2$	−1.30	−1.25*	−0.05	NA	no	−0.01	0.60
$PdSe_2$	−0.02	−0.33	0.31	NA	yes	0.22	0.57
VS_2	−1.16	−1.14	−0.02	NA	no	−0.02	0.52
CrO_2	−1.99	−2.15	0.16	−2.01	no	0.03	0.47
ScO_2	−2.74	−3.17*	0.43	NA	no	0.05	0.40
HfS_2	−1.62	−1.80	0.18	NA	yes	0.22	0.26
FeS_2	−0.54	−0.73	0.19	−0.59	no	0.05	0.06
1 T-MX_2	ΔH	ΔH_{hull}[a]	δH_{hull}	$\Delta H_{expt.}$	ref 1	$\Delta H_{1T/2H}$	$P(\lvert\Delta G\rvert \leq 0.5)$
$ScSe_2$	−1.34	−1.25*	−0.09	NA	no	0.01	1.00
RhS_2	−0.32	−0.48	0.16	NA	no	−0.07	1.00
IrS_2	−0.30	−0.48	0.18	−0.46	no	−0.22	1.00
$PbSe_2$	0.04	−0.31*	0.35	NA	no	−0.22	1.00
MoO_2	−1.79	−1.95	0.16	−2.04	no	0.31	1.00
PbS_2	0.03	−0.32*	0.35	NA	no	−0.28	0.99
CoS_2	−0.34	−0.48	0.14	−0.51	no	−0.01	0.98
PdO_2	−0.48	−0.41	−0.07	NA	no	NA	0.93
MnO_2	−2.00	−1.98	−0.02	−1.80	no	−0.43	0.90
WO_2	−1.61	−1.89	0.28	NA	no	0.24	0.88
CrS_2	−0.77	−0.71	−0.06	NA	yes	0.12	0.87
MoS_2	−0.66	−0.93	0.27	−0.95	yes	0.28	0.87
RuO_2	−0.71	−0.94	0.23	−1.05	no	−0.20	0.86
IrO_2	−0.70	−0.94	0.24	−0.86	no	NA	0.85
OsO_2	−0.23	−1.10	0.87	−1.02	no	NA	0.76
NiO_2	−1.01	−0.79*	−0.22	NA	no	NA	0.70
TiO_2	−3.10	−3.29	0.19	−3.26	no	−1.11	0.54
WS_2	−0.59	−0.78	0.19	−0.90	yes	0.18	0.52
PtO_2	−0.61	−0.62	0.01	NA	no	NA	0.50
$GeSe_2$	−0.27	−0.34	0.07	−0.39	no	NA	0.47
$TaTe_2$	−0.32	−0.45	0.13	NA	yes	0.00	0.34
VO_2	−2.47	−2.63	0.16	−2.48	no	−0.10	0.32
VTe_2	−0.40	−0.45	0.05	NA	yes	0.00	0.30
NbS_2	−1.18	−1.20	0.02	NA	yes	0.04	0.30
$FeSe_2$	−0.48	−0.56	0.08	NA	no	−0.05	0.26
FeS_2	−0.61	−0.73	0.12	−0.59	no	−0.06	0.21
$FeTe_2$	−0.11	−0.20	0.09	−0.25	no	−0.02	0.20
$CrSe_2$	−0.63	−0.46	0.17	NA	yes	0.02	0.18
SnO_2	−1.33	−2.10	0.77	−1.99	no	NA	0.18
GeS_2	−0.42	−0.55	0.13	−0.42	no	NA	0.17

[a]The symbol * in superscript corresponds to the situation where no bulk structure with the compound composition lies on the convex hull according to the database. In that case, ΔH_{hull} is calculated as a linear combination of several structures.

REFERENCES

(1) Lebègue, S.; Björkman, T.; Klintenberg, M.; Nieminen, R. M.; Eriksson, O. Two-Dimensional Materials from Data Filtering and *Ab Initio* Calculations. *Phys. Rev. X* **2013**, 3, 031002.

DOI: 10.1021/acs.jpclett.5b01299
J. Phys. Chem. Lett. 2015, 6, 2669−2670

Supplementary Information: Two-dimensional Metal Dichalcogenides and Oxides for Hydrogen Evolution: A Computational Screening Approach

Mohnish Pandey,[†] Aleksandra Vojvodic,[‡] Kristian S. Thygesen,[†,¶] and Karsten W. Jacobsen[*,†]

Center for Atomic-scale Materials Design, Department of Physics, Technical University of Denmark, DK - 2800 Kongens Lyngby, Denmark, SUNCAT Center for Interface Science and Catalysis, SLAC National Accelerator Laboratory 2575 Sand Hill Road, California 94025, United States, and Center for Nanostructured Graphene (CNG), Department of Physics, Technical University of Denmark, DK - 2800 Kongens Lyngby, Denmark

E-mail: kwj@fysik.dtu.dk

[*]To whom correspondence should be addressed

[†]Center for Atomic-scale Materials Design, Department of Physics, Technical University of Denmark, DK - 2800 Kongens Lyngby, Denmark

[‡]SUNCAT Center for Interface Science and Catalysis, SLAC National Accelerator Laboratory 2575 Sand Hill Road, California 94025, United States

[¶]Center for Nanostructured Graphene (CNG), Department of Physics, Technical University of Denmark, DK - 2800 Kongens Lyngby, Denmark

Table 1: Adsorption energies ΔH^H_{ads} (in eV) and lattice constants a (in angstrom) of the compounds with 2H structure and 2×2 unitcell as shown in Figure 4.

2H-MX_2	ΔH^H_{ads}	a	2H-MX_2	ΔH^H_{ads}	a	2H-MX_2	ΔH^H_{ads}	a
ScS_2	-0.072	7.56	$ScSe_2$	0.205	7.88	CoS_2	-0.114	6.45
$CoSe_2$	0.425	6.72	RuO_2	-0.986	5.83	RuS_2	-0.231	6.71
$RuSe_2$	0.389	6.94	$RuTe_2$	0.406	7.4	RhS_2	-0.425	6.83
$RhSe_2$	0.075	7.12	$RhTe_2$	0.727	7.57	PdS_2	-0.255	7.81
$PdSe_2$	0.22	8.04	ReO_2	-0.295	5.6	ReS_2	0.897	6.31
$ReSe_2$	1.279	6.9	$ReTe_2$	1.653	7.42	OsS_2	-0.35	6.77
$OsSe_2$	0.409	7.03	$OsTe_2$	1.058	7.5	IrS_2	-0.384	6.85
$IrSe_2$	0.04	7.11	$PtTe_2$	0.573	7.84	PbO_2	-1.778	6.47
$ScTe_2$	0.934	7.26	TiS_2	-0.05	6.72	$TiSe_2$	0.436	6.98
$TiTe_2$	0.683	7.49	VO_2	-1.173	5.53	VS_2	0.216	6.35
VSe_2	0.806	6.71	VTe_2	1.043	7.2	CrO_2	0.259	5.19
CrS_2	1.228	6.09	$CrSe_2$	1.564	6.41	$CrTe_2$	1.447	6.95
$MnSe_2$	1.926	6.72	$MnTe_2$	3.009	7.35	FeO_2	-1.436	5.44
FeS_2	0.347	6.32	$FeTe_2$	1.684	7.15	CoO_2	-1.788	5.52
$CoTe_2$	0.77	7.25	$NiSe_2$	-0.348	7.03	$NiTe_2$	0.693	7.44
ZrS_2	0.108	7.14	$ZrSe_2$	0.511	7.4	$ZrTe_2$	0.698	7.84
NbS_2	-0.038	6.73	$NbSe_2$	0.361	6.94	$NbTe_2$	0.51	7.37
MoO_2	1.263	5.65	MoS_2	1.681	6.35	$MoSe_2$	1.824	6.66
$MoTe_2$	1.742	7.09	$PdTe_2$	0.421	8.05	HfS_2	0.302	7.08
$HfSe_2$	0.643	7.35	$HfTe_2$	0.755	7.82	TaO_2	-0.467	5.96
TaS_2	0.113	6.72	$TaSe_2$	0.498	6.94	$TaTe_2$	0.487	7.39
$IrTe_2$	0.022	7.6	WO_2	1.842	5.68	WS_2	1.95	6.36
WSe_2	2.033	6.66	WTe_2	1.874	7.1	ScO_2	-0.829	6.48

Table 2: Adsorption energies ΔH^H_{ads} (in eV) and lattice constants a (in angstrom) of the compounds with 1T structure and 2×2 unitcell as shown in Figure 4.

1T-MX_2	ΔH^H_{ads}	a	1T-MX_2	ΔH^H_{ads}	a	1T-MX_2	ΔH^H_{ads}	a
CoS_2	-0.008	6.41	$CoSe_2$	0.486	6.71	$CoTe_2$	0.647	7.26
CrO_2	-1.462	5.85	FeO_2	-1.196	5.65	FeS_2	0.354	6.39
$FeSe_2$	0.54	6.76	$FeTe_2$	0.601	7.28	GeO_2	1.561	5.82
GeS_2	0.487	6.87	$GeSe_2$	0.26	7.26	HfO_2	2.104	6.46
HfS_2	1.179	7.3	$HfSe_2$	1.41	7.53	$HfTe_2$	1.318	7.97
IrO_2	-0.59	6.33	IrS_2	-0.137	7.12	$IrSe_2$	0.714	7.43
$IrTe_2$	0.662	7.78	MnO_2	-0.173	5.81	$MnSe_2$	1.042	6.97
$MnTe_2$	2.882	7.48	MoO_2	-0.424	5.83	MoS_2	0.096	6.34
$MoSe_2$	0.643	6.58	$MoTe_2$	0.909	6.98	NbS_2	0.376	6.79
$NbSe_2$	0.714	6.96	$NbTe_2$	0.47	7.29	NiO_2	-0.686	5.71
NiS_2	0.447	6.74	$NiSe_2$	0.756	7.09	$NiTe_2$	0.994	7.56
OsO_2	0.115	6.23	OsS_2	0.999	6.97	$OsTe_2$	1.223	7.72
PbO_2	-1.017	6.84	$PbSe_2$	-0.127	8.02	PdO_2	-0.515	6.23
PdS_2	0.37	7.1	$PdSe_2$	0.813	7.46	$PdTe_2$	0.659	8.05
PtO_2	0.242	6.35	PtS_2	0.839	7.14	$PtSe_2$	1.009	7.49
$PtTe_2$	0.966	8.03	ReO_2	0.997	5.63	ReS_2	1.485	6.16
$ReSe_2$	1.593	6.33	$ReTe_2$	1.531	6.81	RhO_2	-1.285	6.23
RhS_2	-0.151	7.01	$RhSe_2$	0.406	7.18	$RhTe_2$	0.607	7.59
RuO_2	-0.563	6.17	RuS_2	0.509	6.78	$RuSe_2$	0.862	6.92
$RuTe_2$	0.731	7.54	ScO_2	-2.259	6.49	ScS_2	-0.926	7.48
$ScSe_2$	-0.338	7.71	$ScTe_2$	0.57	7.64	SnO_2	0.437	6.51
SnS_2	0.877	7.39	$SnSe_2$	0.778	7.72	$SnTe_2$	0.44	8.24
TaO_2	0.893	6.14	TaS_2	1.041	6.8	$TaSe_2$	0.794	6.99
$TaTe_2$	0.327	7.36	TiO_2	0.218	6.02	TiS_2	0.402	6.89
$TiSe_2$	0.901	7.08	$TiTe_2$	1.083	7.51	VO_2	-0.857	5.82
VS_2	0.522	6.35	VSe_2	0.69	6.74	VTe_2	0.52	7.21
WO_2	-0.58	5.83	WS_2	0.233	6.39	WSe_2	0.789	6.62
WTe_2	0.79	7.0	ZrO_2	1.706	6.49	ZrS_2	0.941	7.35
$ZrSe_2$	1.19	7.58	$ZrTe_2$	1.187	7.96	CoO_2	-1.55	5.68
PbS_2	-0.111	7.68	$CrTe_2$	0.639	7.36	MnS_2	0.469	6.75
CrS_2	-0.089	6.67	$CrSe_2$	0.41	6.87	$OsSe_2$	1.149	7.19

Paper III

New Light-Harvesting Materials Using Accurate and Efficient Bandgap Calculations

I. E. Castelli, F. Hüser, M. Pandey, H. Li, K. S. Thygesen, B. Seger, A. Jain, K. A. Persson, G. Ceder and K. W. Jacobsen Advanced Energy Materials 5 (2) (2015)

ADVANCED ENERGY MATERIALS
www.advenergymat.de

New Light-Harvesting Materials Using Accurate and Efficient Bandgap Calculations

Ivano E. Castelli, Falco Hüser, Mohnish Pandey, Hong Li, Kristian S. Thygesen, Brian Seger, Anubhav Jain, Kristin A. Persson, Gerbrand Ceder, and Karsten W. Jacobsen*

Electronic bandgap calculations are presented for 2400 experimentally known materials from the Materials Project database and the bandgaps, obtained with different types of functionals within density functional theory and (partial) self-consistent GW approximation, are compared for 20 randomly chosen compounds forming an unconventional set of ternary and quaternary materials. It is shown that the computationally cheap GLLB-SC potential gives results in good agreement (around 15%) with the more advanced and demanding eigenvalue-self-consistent GW. This allows for a high-throughput screening of materials for different applications where the bandgaps are used as descriptors for the efficiency of a photoelectrochemical device. Here, new light harvesting materials are proposed to be used in a one-photon photoelectrochemical device for water splitting by combining the estimation of the bandgaps with the stability analysis using Pourbaix diagrams and with the evaluation of the position of the band edges. Using this methodology, 25 candidate materials are obtained and 5 of them appear to have a realistic possibility of being used as photocatalyst in a one-photon water splitting device.

1. Introduction

High-throughput materials design is becoming more and more important in materials science thanks to theory developments that make computer simulations more reliable, and to an increase in computational resources. During the last decade, the search for stable binary and ternary alloys,[1] batteries,[2] carbon capture and storage,[3] photovoltaics,[4,5] dye sensitized solar cells,[6] and water splitting materials[7,8] has been guided by computational studies. The huge amount of data produced during these studies has been collected in several databases, for example, the Materials Project database,[9] the AFLOWLIB consortium[1] and the Computational Materials Repository.[10,11]

Experimental data are also collected into databases such as the Inorganic Crystal Structure Database (ICSD)[12] and the Landolt-Börnstein database[13]: the former contains around 160 000 crystal structures, the latter collects the electronic, magnetic, thermodynamic properties of 250 000 compounds. The ICSD database is one of the most complete repositories for crystal information. Despite this, the electronic properties are not always available and so they are not included.

One of the tasks for computational condensed matter scientists is to fill in the missing information in experimental databases. In this paper, we present the calculations of around 2400 bandgaps of known materials using the GLLB-SC potential by Gritsenko, van Leeuwen, van Lenthe, and Baerends,[14] (GLLB) adapted by Kuisma et al.[15] to include the correlation for solids (-SC). The GLLB-SC potential is implemented in the framework of density functional theory (DFT) in the electronic structure code GPAW.[16,17] The structures under investigation are obtained from the Materials Project database.[9] As of March 2014, it contains around 50 000 structures optimized with DFT from the ICSD entries. We then compare the bandgaps of 20 compounds calculated with different methods, namely local density approximation (LDA), GLLB-SC, GW approximations (G_0W_0, GW_0, and GW) and the range-separated hybrid functional by Heyd, Scuseria, and Ernzerhof (HSE06). At the end, we apply a screening procedure, discussed in detail and used in previous works,[7,8] to find new light harvesting materials suitable for water splitting devices.

2. The Calculation of Bandgaps

Experimental databases mostly contain information about the crystal structure of materials. It is more complicated to

Dr. I. E. Castelli, Dr. F. Hüser, M. Pandey, Dr. H. Li, Prof. K. S. Thygesen, Prof. K. W. Jacobsen
Center for Atomic-scale Materials Design
Department of Physics
Technical University of Denmark
Kongens Lyngby, DK 2800, Denmark
E-mail: ivca@fysik.dtu.dk
Dr. B. Seger
Center for Individual Nanoparticle Functionality
Department of Physics
Technical University of Denmark
Kongens Lyngby, DK 2800, Denmark
Dr. A. Jain, Dr. K. A. Persson
Computational Research Division
Lawrence Berkeley National Laboratory
Berkeley, CA 94720, USA
Prof. G. Ceder
Massachusetts Institute of Technology
Cambridge, MA 02139, USA

DOI: 10.1002/aenm.201400915

obtain access to information about the electronic structure of compounds. The bandgap is a key discriminating property for a large number of applications, including solar absorbers, thermoelectrics, transparent conductors, contact and buffer layers, etc. In recent works,[7,8] the bandgap has been used as a descriptor for the efficiency of a light absorber. In this part, we calculate the electronic bandgaps of experimentally known compounds. All the structures investigated here are available in the Materials Project database[9] and have been previously optimized using the generalized gradient approximation (GGA) functional by Perdew, Burke, and Ernzerhof (PBE), and GGA PBE+U for some of the structures.[18] While standard DFT usually gives good result for the optimization of the crystal structure, it fails in the calculation of bandgaps.[19] The Kohn-Sham bandgaps of semiconductors, given by the minimum energy difference between the bottom of the conduction band and the top of the valence band, are seriously underestimated because of the approximate description of the exchange-correlation functionals, the self-interaction error,[20] and the missing derivative discontinuity.[21] Many-body methods, such as the GW approximation, give more reliable results with an increase (at least one order of magnitude) of the computational cost. Hybrid functionals, e.g., PBE0 or HSE06, that incorporate a portion of Hartree-Fock exact exchange, usually give reasonable results for semiconductors,[22] but fail for metals and wide bandgap insulators.[23,24] All these methods are expensive to be used in a screening project of several thousands of materials and, in particular the GW approximation, can only be efficiently used to refine the results obtained with computationally cheaper approximations.[25]

Here, the bandgaps are calculated using the GLLB-SC functional,[16] that is an improved description of the original GLLB functional[14] adapted for solids. The GLLB functional contains by construction the evaluation of the derivative discontinuity. It is a further approximation to the KLI approximation to the exact exchange optimized effective potential (EXX-OEP).[26] The fundamental, or quasi-particle (QP), bandgap is given as the difference in the ionization potential (IP) and the electron affinity (EA) and thus directly linked to photo-emission and inverse photo-emission measurements. The Kohn-Sham (KS) bandgap differs from the QP gap by the derivative discontinuity, Δ_{xc}:

$$E_{\text{gap}}^{\text{QP}} = \text{IP} - \text{EA} = E_{\text{gap}}^{\text{KS}} + \Delta_{xc}. \quad (1)$$

GW, on the other hand, gives directly QP energies. It is important to keep in mind that the bandgaps obtained from optical measurements can be significantly lower than the QP gaps due to excitonic effects, and one thus speaks of an optical bandgap instead.[27]

The GLLB-SC functional has been recently tested against other computational methods (mainly non-self-consistent G_0W_0) and experiments for single metal oxides,[8] for semiconductors,[28] and for perovskite materials for light harvesting.[25] The GLLB-SC results are expected to be within an error of 0.5 eV. We thus expect that this accuracy is good enough for projects involving thousands of calculations required in a screening study. In addition, with the GLLB-SC is possible to calculate larger crystal structures. For example, recently, the GLLB-SC has been widely used to calculate the bandgaps of 240 organometal halide perovskites[29] which show very interesting optical properties for light harvesting and energy conversion.[30] We note that the GLLB-SC has also given good results for the position of the *d*-states in noble metals such as silver.[31]

The Materials Project database is constantly updated and so far we have calculated the bandgaps of around 2400 materials. Those materials have been selected because of their relative simple structure, their stability and because they show a bandgap at the GGA level. Despite its low computational cost, the GLLB-SC functional is at least twice as expensive as a standard GGA calculation[32] and it is demanding to calculate the bandgaps of large crystal structures of more than 40/50 atoms. Around 6 months has been the computational time required for the bandgap calculations for the 2400 materials using Niflheim, the supercomputer facility installed at DTU Physics. On a single core machine, the time required would have been around 16.5 years. All the calculated quasi-particle gaps, together with the corresponding ids from the Materials Project and ICSD databases and the chemical formula, are listed in the Supporting Information. In addition, this information is included and freely available in both the Materials Project database and the Computational Materials Repository.

The distribution of the bandgaps, calculated with GLLB-SC, of the 2400 materials is shown in **Figure 1** (in blue). Even though very large bandgap insulators have been found, the region with a large number of materials correspond to the visible light range, between 1.5 and 3.0 eV. When the stability in water at pH = 7 and at potential 0 V versus normal hydrogen electrode (NHE) is considered by means of Pourbaix diagrams,[33] the number of materials that might be stable is significantly reduced. The Pourbaix diagrams give information about the thermodynamics of the reactions, while other factors, such as kinetics and surfaces passivation, are not included. For these and other reasons, here we have considered two energy thresholds to define if a material is stable (ΔE = 1 and 0 eV/atom, shown in red and green bars in the figure, where ΔE is the total energy difference between the material and the most stable phases in which it can separate). Within the energy threshold of 1 eV/atom, more than 50% of the small bandgap semiconductors are unstable in water, while it seems that all the materials

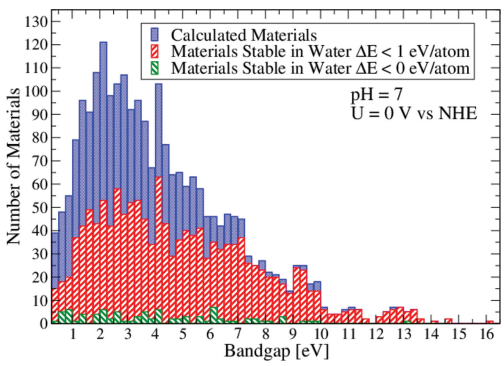

Figure 1. Histogram of the GLLB-SC bandgaps for all the 2400 calculated materials (in blue). We consider the two energy thresholds 1 eV/atom (in red) and 0 eV/atom (in green) for the stability in water, which is calculated at zero potential (U = 0 V vs NHE) and neutral pH.

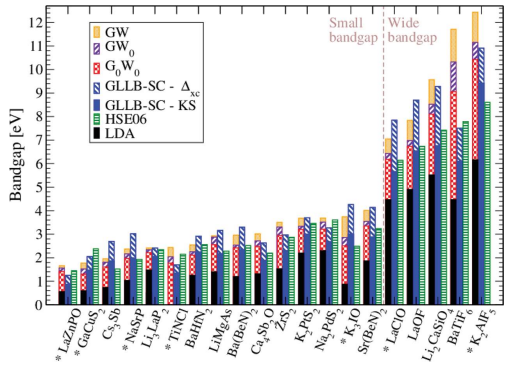

Figure 2. Bandgaps at Γ-point of 20 structure calculated with LDA (in black), GW approximations with PPA (G_0W_0 in red, GW_0 in purple and GW in orange), GLLB-SC (in blue), and HSE06 (in green). Both the KS bandgap and the derivative discontinuity are indicated for the GLLB-SC gaps. The materials for which the Γ-point gap corresponds to the bandgap, are indicated with *.

with a gap larger that 10 eV are stable in water. Only around 4% of the materials are stable, when the more strict threshold of 0 eV/atom is used. This may indicate that considering a ΔE larger than zero can help to identify the materials that are experimentally observed to be stable in water.

The electronic structures of 20 materials, randomly picked from the calculated set to cover the full bandgap range and with a reasonable unit cell size, were also calculated using the non-self-consistent G_0W_0 and the eigenvalue-self-consistent GW_0 and GW as well as the HSE06 hybrid scheme (**Figure 2**). This unconventional set of structures contains ternary and quaternary materials including oxides, nitrides, sulfides, phosphates and chlorides and thus it is a broader set compared to the ones used elsewhere in the literature.[34]

QP gaps were obtained in the G_0W_0 approximation in a plane wave representation using LDA wavefunctions and eigenvalues as starting point. A detailed description of the implementation of this method in GPAW can be found in ref. [28]. The initial Kohn-Sham states and energies were calculated in a plane wave basis with kinetic energies up to 600 eV. The same value is used for determining the exact exchange contributions. The G_0W_0 self-energy was carefully converged with respect to k points, number of bands and plane wave cutoff energy for each material individually. Typically, a $(7 \times 7 \times 7)$ k-point sampling, 100–200 eV energy cutoff and unoccupied bands up to the same energy (a few hundred bands in total) were found to be sufficient in order to converge band gaps within less than 0.1 eV. Both, the plasmon pole approximation (PPA) by Godby and Needs[35] and the explicit frequency dependence of the dielectric function, $\varepsilon(\omega)$, have been used, yielding almost identical results.

It is well known that G_0W_0 underestimates bandgaps compared to experiments and better results can be obtained using (partial) self-consistent GW[34] where the LDA wavefunctions are kept fixed while the eigenvalues are updated self-consistently. Recently,[28] it was shown for a set of well known semiconductors and insulators, that the MAEs for GLLB-SC and G_0W_0 with respect to experiments are 0.4 and 0.3 eV, respectively, with a tendency of the former to overestimate the gaps, while the latter underestimates them.

Two levels of (partial) self-consistency have been investigated: i) in the case of GW_0, the self-consistency in the eigenvalues is performed for the Green's functions (G) only, whereas ii) in the case of GW, the eigenvalues are updated both in G and in the dielectric matrix of the screened potential (W). In general, for the 20 materials described in this section, three or four iterations are necessary to converge band gaps within less than 30 meV and 50 meV for GW_0 and GW, respectively. Due to the high computational costs, the k-point mesh and energy cutoff used for GW_0 and GW are coarser than the ones used for G_0W_0. Typically the low convergence criteria of $(3 \times 3 \times 3)$ k-point sampling and 100 eV energy cutoff are used for GW_0 and GW. The band gaps are then extrapolated to the dense k-point grids and high plane wave cut off, using the difference between the low and high convergence parameters in the G_0W_0 calculations. For more details about GW_0 and GW, see ref. [34] and references therein.

Hybrid functional based calculations were performed with the range-separated screened-exchange HSE06 functional.[36,37] The wavefunctions were expanded in a plane-wave basis with a 700 eV cutoff. We use a Monkhorst-Pack[38] grid of $33 \times (a_x^{-1}, a_y^{-1}, a_z^{-1})$ k-points, where a_x, a_y and a_z are the lattice constants in x, y and z direction, respectively, and the Γ-point is always included. In the current work, all HSE06 calculations were performed non-self-consistently from the PBE ground state density and wavefunctions. Generally, there is good agreement between the non-self-consistent calculations and the self-consistently obtained results[24] which indicates that self-consistency will not be important in the current work.

For all materials in this study, comparison between the different methods is shown by means of the direct Γ point gap, in order to avoid the need for interpolation of the band structure in the case that the minimum of the conduction band is not located at a high symmetry point in the Brillouin zone.

Figure 2 shows the bandgaps for the 20 selected materials calculated with LDA, different levels of the GW approximation, HSE06, and GLLB-SC. Only a few experimental data points are available, and mainly optical measurements which are therefore not directly comparable with our values. Ideally photoemission and inverse photoemission measurements could be used to compare to our calculated bandgaps, but these are not available for this set of structures.

It is natural to divide the 20 materials into small and wide bandgap semiconductors to give a better evaluation of the signed and mean absolute and relative errors[39] for the different methods studied here (**Table 1** for the small gap set). Similar data for the wide gaps is reported in the Supporting Information together with the comparison of band structures calculated with different methods for two compounds.

As expected, for both the groups, LDA seriously underestimates the bandgaps. The mean absolute error (MAE) of GLLB-SC with respect to G_0W_0 and to HSE06 is larger than 0.5 eV for the small bandgaps with a clear tendency for GLLB-SC to overestimate the bandgaps with respect to HSE06 and to G_0W_0 as shown by the signed error and **Figure 3**a,b. G_0W_0 and HSE06 are very close, with a MAE of approximately 0.25 eV (G_0W_0

Table 1. Mean absolute (signed) error, in eV, for the small bandgaps of the materials in Figure 2 calculated using LDA, GLLB-SC, HSE06, G_0W_0, GW_0 and GW.

xc_{ref}	LDA	GLLB-SC	HSE06	G_0W_0	GW_0	GW
xc						
LDA	–	1.64 (−1.64)	1.21 (−1.21)	1.08 (−1.08)	1.30 (−1.30)	1.59 (−1.59)
GLLB-SC	1.64 (1.64)	–	0.61 (0.43)	0.59 (0.56)	0.52 (0.34)	0.38 (0.05)
HSE06	1.21 (1.21)	0.61 (−0.43)	–	0.25 (0.13)	0.29 (−0.09)	0.46 (−0.38)
G_0W_0	1.08 (1.08)	0.59 (−0.56)	0.25 (−0.13)	–	0.22 (−0.22)	0.51 (−0.51)
GW_0	1.30 (1.30)	0.52 (−0.34)	0.29 (0.09)	0.22 (0.22)	–	0.29 (−0.29)
GW	1.59 (1.59)	0.38 (−0.05)	0.46 (0.38)	0.51 (0.51)	0.29 (0.29)	–

underestimates with respect to HSE06). The GW_0 approximation gives a MAE of around 0.5 eV for the GLLB-SC and slightly less than 0.3 eV for HSE06 and the other two GW levels. The GLLB-SC is the closest to the self-consistent GW with a MAE of 0.38 eV when compared with HSE06 and G_0W_0 which have a MAE close to 0.5 eV.

GLLB-SC has a mean relative errors (MRE) with respect to GW equal to 15% better that the MRE for HSE06 and G_0W_0 (16 and 18%, respectively), while GW_0 performs better with an error of 10%. The HSE06 error increases to 23% for the wide bandgap set, as shown in the Supporting Information.

The computational costs required for the methods are very different. G_0W_0 is one or two orders of magnitude more expensive that GLLB-SC which is slightly more expensive than a standard GGA calculation. HSE06 is slightly more expensive than GLLB-SC but still cheaper than G_0W_0. The computational cost increases even further for the (partial) self-consistent GW where more iterations are needed.

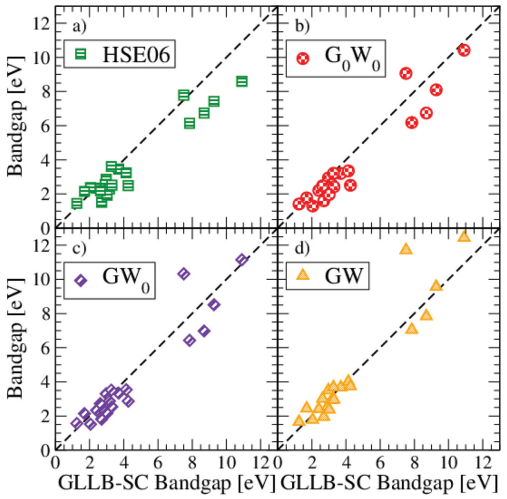

Figure 3. a) HSE06, b) G_0W_0, c) GW_0, and d) GW bandgaps as a function of the GLLB-SC gaps. All the methods except GW underestimate the gaps with respect to the GLLB-SC. The signed error of GLLB-SC and GW is 0.05 eV.

The bandgaps calculated with GLLB-SC can now be used as a descriptor in a screening study. In the following section, we propose a handful of materials that can be used in a water splitting device using a high-throughput screening approach.

3. Screening for Water Splitting Materials

The starting point of a screening study is to define the descriptors that correlate the microscopic quantities calculated using ab-initio quantum mechanics simulations with the macroscopic properties of a material.[40] For example, the formation enthalpy of a compound can describe its stability, the bandgap its absorption properties, and so on.

The set of data calculated here can provide the search space for the computational screening of materials for different applications, such as light absorbers (photovoltaics and photocatalysis), transparent conductors, and thermoelectrics. Here, we illustrate this approach by proposing a handful of materials that can be used to produce energy through photoelectrochemical splitting of water into oxygen and hydrogen using solar light. In a water splitting device, solar energy is used to divide water into hydrogen and oxygen: the solar light is harvested by a semiconductor and electron-hole pairs are created. The electrons and holes then reach the surface of the semiconductor where, if they are at the right potentials with respect to the redox levels of water, the electrons reduce the protons and the holes oxidize the water. The properties required by a semiconductor to be used in this device are: i) stability, ii) high light absorption, iii) photogenerated charges with appropriate energies. In addition iv) good electron-hole mobility, v) high catalytic activity, vi) non-toxicity, and vii) cost-effectiveness are desirable properties. The screening is based on three criteria: stability, bandgap in the visible light range, and band edges of the semiconductor well positioned versus the redox levels of water. These represent the descriptors for the properties (i–iii), i.e., a stable material with a well positioned bandgap in the visible light range. A more detailed explanation of the water splitting device can be found in previous works.[7,8]

Previous studies have described the search for new compounds to be used in a water splitting cell both in the perovskite crystal symmetry (cubic,[7,8] double,[41] and layered in the Ruddlesden Popper phase[25]) and in the oxynitride and nitride class of materials using a data mining approach.[42] Here, instead of searching for completely new materials, we consider structures

already optimized by nature, i.e., known to exist. While no new compounds will be proposed, this scheme has the advantage of the known synthesis procedure so that testing and validation can be prioritized.

Although all the materials studied here are experimentally known, i.e., they are stable, or at least metastable, little is known about their stability in contact with water. The corrosion problem can be investigated using the so-called Pourbaix diagrams, where solid and dissolved substances are combined in a single phase diagram so that the stable species (solid and/or aqueous ion) can be determined, as a function of pH and potential. The total energies of the solid phases, taken from the ICSD and the Materials Project databases,[9,12] are obtained with DFT (using the RPBE xc-functional[43]). Data for the dissolved ions, instead, come from experiments.[44,45] This method for evaluating stability in water has been already investigated and validated elsewhere.[33,46]

It is difficult to define a single energy threshold under which a material is considered stable because of metastability, reaction kinetics, effect and passivation of the surfaces as well as inaccuracy in the calculations and experiments. Here, we consider a generous energy threshold of 1 eV/atom. We propose 25 compounds (**Figure 4**), that also fulfill the criteria relating to the bandgap and band edges positions, stable in a potential window corresponding to the working potential of the device (bare redox levels of water plus reaction overpotentials and quasi-Fermi levels, i.e., between –0.4 and 2.2 V) and in neutral pH (pH = 7). Neutral pH is desirable because it is not harmful to environment and not corrosive however the efficiency of the device can be improved by operating at very acid or alkaline conditions.

The bandgaps have been calculated with the GLLB-SC functional. The bare energy required to split water is 1.23 eV. This energy is not enough to run the water splitting reactions and some overpotentials are needed (0.1 eV for hydrogen evolution and 0.4 eV for oxygen production[47]). When the semiconductor is under illumination and electron-hole pairs are created, the electron and hole densities are above their equilibrium values and a single Fermi level cannot describe their populations. The quasi-Fermi levels describe these non-equilibrium populations, located ≈0.25 eV below (above) the conduction (valence) bands for an undoped semiconductor and they correspond to the effective energy of the photogenerated electrons and holes. The minimum bandgap to run the water splitting reaction is at least 2 eV. The maximum realistic efficiency of a water splitting device is around 7%.[48] This efficiency is quite low, especially when compared with the standard technologies for photovoltaics. A higher efficiency can be obtained using a multiphoton device[7,49] albeit increasing the technological difficulties and thus the price of the device. In this work, we focus on the one-photon device emphasizing the simplicity of the device rather than efficiency.[50]

There are several methods to obtain the positions of the band edges,[51,52] all computationally rather demanding and not suited to be used in a screening study. Here, the positions of the band edges have been calculated using an empirical equation based on the geometrical average of the electronegativities in the Mulliken scale of the individual atoms that form the

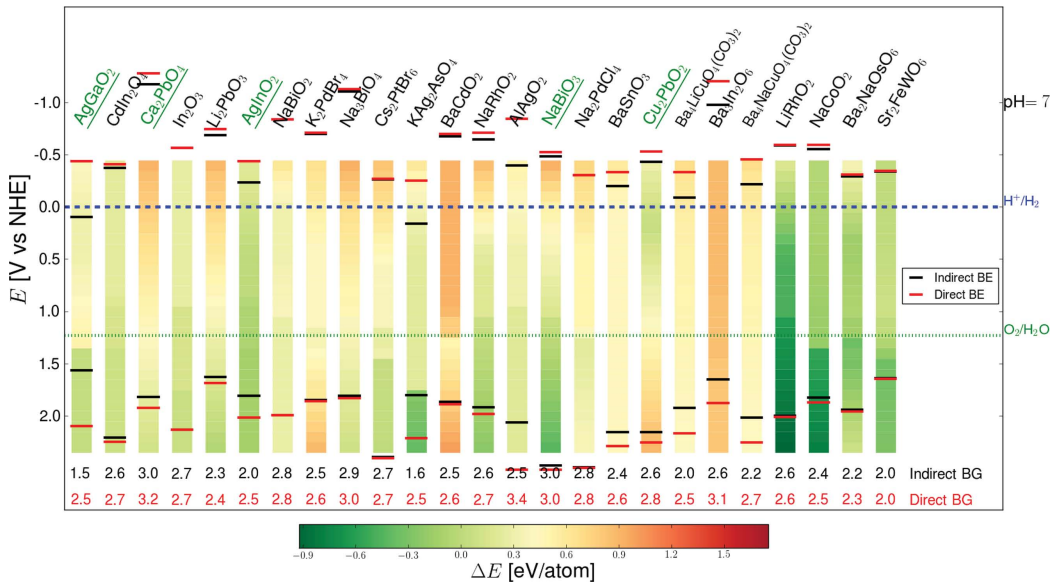

Figure 4. The most stable materials with potential for one-photon water splitting. The stability in water of each material is calculated as the energy difference between the material and the most stable phases (solid and aqueous) in which it can separate in a potential range between –0.4 and 2.2 V and at pH = 7. The color scale runs from green (i.e., stable) to red (unstable compounds). In the plot, the indirect and direct positions of the valence and conduction band edges (BE) are indicated in black and red as well as the indirect and direct bandgap (BG).

structure.[53] For example, the valence (conduction) band edges of ZrS_2 is:

$$E_{VB,CB} = (\chi_{Zr}\chi_S^2) \pm E_{gap}/2 + E_0, \quad (2)$$

where χ_{Zr} and χ_S are the electronegativities of Zr and S, E_{gap} the calculated bandgap, and $E_0 = -4.5$ V the difference between the normal hydrogen electrode (NHE) and vacuum level.

The screening criteria can be summarized as: stability in water: $\Delta E \leq 1.0$ eV/atom; bandgap: $1.7 \leq E_{gap} \leq 3.0$ eV; and band edges position: $CB_{edge} < -0.1$ V vs NHE and $VB_{edge} > 1.6$ V vs NHE.

Figure 4 shows the 25 stable semiconductors fulfilling the screening requirements out of the 2400 calculated materials. The figure combines the evaluation of the stability using Pourbaix diagrams, calculated at pH = 7 and in a potential range between −0.4 and 2.2 eV, where stable and unstable compounds are indicated in green and red, and the indirect and direct positions of the valence and conduction band edges are drawn with black and red lines, respectively. In particular, oxides tend to be more stable at the oxidative potential, as the O_{2p} orbitals, that usually form the valence band of oxides, are low in energy and thermodynamically favorable. In general, the problem of stability in water is important but not crucial to the design a new light harvester material. Necessarily, the photoharvester can be protected by transparent protective shields that remove the problem of corrosion due to water and oxygen and hydrogen ions in solution.[54] On the other hand, the use of a transparent shield increases the manufacturing difficulties and the total cost of the photodevice.

We performed a literature search for available information of the candidate materials of Figure 4. In particular, we are interested in data regarding stability in water, light absorption, and industrial applications. Five materials of Figure 4 (green underlined formula) have a realistic possibility of success as a one-photon photocatalytic water splitting material. Ca_2PbO_4 has an optical bandgap of approximately 1.8 eV[55] and it is used as a primer for stainless steel due to its lower toxicity compared to lead oxide.[56] Cu_2PbO_2 was originally synthesized by Szillat et al. and they showed the material was insoluble in basic solutions.[57] This compound has an optical bandgap of 1.7 eV and is naturally p-type semiconductor.[58] α-$AgGaO_2$ has been shown to have a bandgap of 2.4 eV whereas a bandgap of 2.1–2.2 eV has been found for β-$AgGaO_2$.[59,60] $AgInO_2$ has a bandgap of 1.9 eV.[60] $AgGaO_2$ and $AgInO_2$ have been successfully tested for photocatalytic degradation of alcohols.[59,60] $NaBiO_3$ has a bandgap of 2.6 eV, and has already been used for photocatalytic degradation of pollutants.[61] Using computational modeling, Liu et al. found a bandgap of 2.2 eV and a valence and conduction band that straddles the water splitting redox reactions.[62]

Some materials show an experimental bandgap above 3.0 eV and thus are unsuited for an effective water splitting catalyst. For example, $BaSnO_3$, which has already been proposed as a light harvester material in previous work[7,8] in which the cubic perovskites have been investigated, has a bandgap of 3.1–3.3 eV and luminesces at 1.4 eV.[63] It has been tested for photochemical H_2 and O_2 evolution using sacrificial donors, however its water splitting activity is inhibited due to defect-assisted recombination.[64] In_2O_3 has a bandgap near 3.4 eV (however some papers report a bandgap of 2.8 eV[65]) and a conduction band near 0.00 V vs RHE.[66] It has been used as a photocatalyst[67] or to enhance the catalytic performances of photocatalysts, such as $LaTiO_2N$.[68] A detailed analysis of all the candidate materials is reported in the Supporting Information.

4. Conclusions

In this work, we have calculated the bandgaps of approximately 2400 known materials, available in the Materials Project database, using a recently implemented functional that includes the evaluation of the derivative discontinuity.

As a first step, we compared the bandgaps calculated with the GLLB-SC potential with several levels of the GW approximation and hybrid HSE06 scheme for 20 materials. We showed that the agreement between GLLB-SC and GW is rather good, with a MRE of around 15% better than the agreement between G_0W_0 (or HSE06) and GW and with a significant savings in the computational cost.

Secondly, we have applied a screening procedure to the set of calculated materials with the goal of finding new materials to be used in a one-photon water splitting device. We combined the calculation of the bandgaps with the evaluation of Pourbaix diagrams to estimate the materials' stability in water with the evaluation of the band edge positions to determine whether the photogenerated charges carry the energy necessary to initiate a water splitting reaction. An a posteriori literature search shows that at least five of them (Ca_2PbO_4, Cu_2PbO_2, $AgGaO_2$, $AgInO_2$, and $NaBiO_3$) might be suitable to be used in a water splitting device and require further experimental investigation.

The calculated data may be of relevance for other applications within sustainable energy materials and all the data are made available to the public in the Materials Project database and in the Computational Materials Repository.

Supporting Information

Supporting Information is available from the Wiley Online Library or from the author.

Acknowledgments

The authors acknowledge support from the Catalysis for Sustainable Energy (CASE) initiative funded by the Danish Ministry of Science, Technology and Innovation, from the Danish National Research Foundation for funding The Center for Individual Nanoparticle Functionality (CINF) (DNRF54) and from the Center on Nanostructuring for the Efficient Energy Conversion (CNEEC) at Stanford University, an Energy Frontier Research Center founded by the US Department of Energy, Office of Science, Office of Basic Energy Sciences under award number DE-SC0001060. Work at the Lawrence Berkeley National Laboratory was supported by the Assistant Secretary for Energy Efficiency and Renewable Energy, under Contract No. DE-AC02-05CH11231. The Materials Project work is supported by Department of Energy's Basic Energy Sciences program under Grant No. EDCBEE.

Received: June 3, 2014
Revised: July 29, 2014
Published online: August 21, 2014

[1] S. Curtarolo, W. Setyawan, G. L. Hart, M. Jahnatek, R. V. Chepulskii, R. H. Taylor, S. Wang, J. Xue, K. Yang, O. Levy, M. J. Mehl, H. T. Stokes, D. O. Demchenko, D. Morgan, *Comput. Mater. Sci.* **2012**, *58*, 218.
[2] G. Ceder, Y.-M. Chiang, D. R. Sadoway, M. K. Aydinol, Y.-I. Jang, B. Huang, *Nature* **1998**, *392*, 694.
[3] L.-C. Lin, A. H. Berger, R. L. Martin, J. Kim, J. A. Swisher, K. Jariwala, C. H. Rycroft, A. S. Bhown, M. W. Deem, M. Haranczyk, B. Smit, *Nat. Mater.* **2012**, *11*, 633.
[4] J. Hachmann, R. Olivares-Amaya, S. Atahan-Evrenk, C. Amador-Bedolla, R. S. Sanchez-Carrera, A. Gold-Parker, L. Vogt, A. M. Brockway, A. Aspuru-Guzik, *J. Phys. Chem. Lett.* **2011**, *2*, 2241.
[5] M. d'Avezac, J.-W. Luo, T. Chanier, A. Zunger, *Phys. Rev. Lett.* **2012**, *108*, 027401.
[6] K. B. Ørnsø, J. M. Garcia-Lastra, K. S. Thygesen, *Phys. Chem. Chem. Phys.* **2013**, *15*, 19478.
[7] I. E. Castelli, D. D. Landis, K. S. Thygesen, S. Dahl, I. Chorkendorff, T. F. Jaramillo, K. W. Jacobsen, *Energy Environ. Sci.* **2012**, *5*, 9034.
[8] I. E. Castelli, T. Olsen, S. Datta, D. D. Landis, S. Dahl, K. S. Thygesen, K. W. Jacobsen, *Energy Environ. Sci.* **2012**, *5*, 5814.
[9] Materials Project - A Materials Genome Approach, http://materialsproject.org/ (accessed August 2014) .
[10] D. D. Landis, J. S. Hummelshoj, S. Nestorov, J. Greeley, M. Dulak, T. Bligaard, J. K. Norskov, K. W. Jacobsen, *J. Comput. Sci. Eng.* **2012**, *14*, 51.
[11] Computational Materials Repository, https://cmr.fysik.dtu.dk/ (accessed August 2014).
[12] ICSDWeb, http://www.fiz-karlsruhe.de/icsd_web.html (accessed July 2014).
[13] The Landolt-Börnstein Database, http://www.springermaterials.com/docs/index.html (accessed May 2014).
[14] O. Gritsenko, R. van Leeuwen, E. van Lenthe, E. J. Baerends, *Phys. Rev. A* **1995**, *51*, 1944.
[15] M. Kuisma, J. Ojanen, J. Enkovaara, T. T. Rantala, *Phys. Rev. B* **2010**, *82*, 115106.
[16] J. J. Mortensen, L. B. Hansen, K. W. Jacobsen, *Phys. Rev. B* **2005**, *71*, 35109.
[17] J. Enkovaara, C. Rostgaard, J. J. Mortensen, J. Chen, M. Dulak, L. Ferrighi, J. Gavnholt, C. Glinsvad, V. Haikola, H. A. Hansen, H. H. Kristoffersen, M. Kuisma, A. H. Larsen, L. Lehtovaara, M. Ljungberg, O. Lopez-Acevedo, P. G. Moses, J. Ojanen, T. Olsen, V. Petzold, N. A. Romero, J. Stausholm-Møller, M. Strange, G. A. Tritsaris, M. Vanin, M. Walter, B. Hammer, H. Häkkinen, G. K. H. Madsen, R. M. Nieminen, J. K. Nørskov, M. Puska, T. T. Rantala, J. Schiøtz, K. S. Thygesen, K. W. Jacobsen, *J. Phys. Condens. Matter* **2010**, *22*, 253202.
[18] A. Jain, S. P. Ong, G. Hautier, W. Chen, W. D. Richards, S. Dacek, S. Cholia, D. Gunter, D. Skinner, G. Ceder, K. A. Persson, *APL Mater.* **2013**, *1*, 011002.
[19] J. P. Perdew, *Int. J. Quantum Chem.* **1985**, *28*, 497.
[20] J. P. Perdew, A. Zunger, *Phys. Rev. B* **1981**, *23*, 5048.
[21] R. W. Godby, M. Schlüter, L. J. Sham, *Phys. Rev. Lett.* **1986**, *56*, 2415.
[22] J. Heyd, J. E. Peralta, G. E. Scuseria, R. L. Martin, *J. Chem. Phys.* **2005**, *123*, 174101.
[23] J. E. Moussa, P. A. Schultz, J. R. Chelikowsky, *J. Chem. Phys.* **2012**, *136*, 204117.
[24] J. Paier, M. Marsman, K. Hummer, G. Kresse, I. C. Gerber, J. G. Ángyán, *J. Chem. Phys.* **2006**, *124*, 154709.
[25] I. E. Castelli, J. M. García-Lastra, F. Hüser, K. S. Thygesen, K. W. Jacobsen, *New J. Phys.* **2013**, *15*, 105026.
[26] J. D. Talman, W. F. Shadwick, *Phys. Rev. A* **1976**, *14*, 36.
[27] G. Onida, L. Reining, A. Rubio, *Rev. Mod. Phys.* **2002**, *74*, 601.
[28] F. Hüser, T. Olsen, K. S. Thygesen, *Phys. Rev. B* **2013**, *87*, 235132.
[29] I. E. Castelli, J. M. García-Lastra, K. S. Thygesen, K. W. Jacobsen, *APL Mater.* DOI: 10.1063/1.4893495.
[30] I. Borriello, G. Cantele, D. Ninno, *Phys. Rev. B* **2008**, *77*, 235214.
[31] J. Yan, K. W. Jacobsen, K. S. Thygesen, *Phys. Rev. B* **2011**, *84*, 235430.
[32] Typically a k-point mesh finer than a GGA calculation is required. For the calculations presented here, we have used a k-point sampling equal to $35 \times a_i^{-1}$ in each direction, where a_i is the lattice constant, with Γ-point are included.
[33] I. E. Castelli, K. S. Thygesen, K. W. Jacobsen, *Top. Catal.* **2013**, *57*, 1.
[34] M. Shishkin, G. Kresse, *Phys. Rev. B* **2007**, *75*, 235102.
[35] R. W. Godby, R. J. Needs, *Phys. Rev. Lett.* **1989**, *62*, 1169.
[36] J. Heyd, G. E. Scuseria, M. Ernzerhof, *J. Chem. Phys.* **2003**, *118*, 8207.
[37] A. V. Krukau, O. A. Vydrov, A. F. Izmaylov, G. E. Scuseria, *J. Chem. Phys.* **2006**, *125*, 224106.
[38] H. J. Monkhorst, J. D. Pack, *Phys. Rev. B* **1976**, *13*, 5188.
[39] The signed error (SE), is calculated as $\mathrm{SE} = \frac{1}{n}\sum_n E_{\mathrm{gap}}^{\mathrm{xc}} - E_{\mathrm{gap}}^{\mathrm{xc}_{\mathrm{ref}}}$, and the mean absolute error (MAE) as $\mathrm{MAE} = \frac{1}{n}\sum_n \left| E_{\mathrm{gap}}^{\mathrm{xc}} - E_{\mathrm{gap}}^{\mathrm{xc}_{\mathrm{ref}}} \right|$, where $E_{\mathrm{gap}}^{\mathrm{xc}}$ indicates the bandgaps calculated with the test exchange-correlation (xc) functional, $E_{\mathrm{gap}}^{\mathrm{xc}_{\mathrm{ref}}}$ and the bandgaps obtained with the reference functional. The mean relative error (MRE) is given by $\mathrm{MRE} = \frac{1}{n}\sum_n \left| \frac{E_{\mathrm{gap}}^{\mathrm{xc}} - E_{\mathrm{gap}}^{\mathrm{xc}_{\mathrm{ref}}}}{E_{\mathrm{gap}}^{\mathrm{xc}_{\mathrm{ref}}}} \right|$.
[40] S. Curtarolo, G. L. W. Hart, M. B. Nardelli, N. Mingo, S. Sanvito, O. Levy, *Nat. Mater.* **2013**, *12*, 191.
[41] I. E. Castelli, K. S. Thygesen, K. W. Jacobsen, *MRS Online Proc. Lib.* **2013**, *1523*.
[42] Y. Wu, P. Lazic, G. Hautier, K. Persson, G. Ceder, *Energy Environ. Sci.* **2013**, *6*, 157.
[43] B. Hammer, L. B. Hansen, J. K. Nørskov, *Phys. Rev. B* **1999**, *59*, 7413.
[44] J. W. Johnson, E. H. Oelkers, H. C. Helgeson, *Computers Geosci.* **1992**, *18*, 899.
[45] M. Pourbaix, *Atlas of Electrochemical Equilibria in Aqueous Solutions*, *v. 1*, *Pergamon Press, London* **1966**.
[46] K. A. Persson, B. Waldwick, P. Lazic, G. Ceder, *Phys. Rev. B* **2012**, *85*, 235438.
[47] S. Trasatti, *Croat. Chem. Acta*, **1990**, *63*, 313.
[48] M. R. Weber, M. J. Dignam, *Int. J. Hydrogen Energy* **1986**, *11*, 225.
[49] M. Gratzel, *Nature* **2001**, *414*, 338.
[50] B. A. Pinaud, J. D. Benck, L. C. Seitz, A. J. Forman, Z. Chen, T. G. Deutsch, B. D. James, K. N. Baum, G. N. Baum, S. Ardo, H. Wang, E. Millere, T. F. Jaramillo, *Energy Environ. Sci.* **2013**, *6*, 1983.
[51] Y. Wu, M. K. Y. Chan, G. Ceder, *Phys. Rev. B* **2011**, *83*, 235301.
[52] P. G. Moses, C. G. V. de Walle, *Appl. Phys. Lett.* **2010**, *96*, 021908.
[53] M. A. Butler, D. S. Ginley, *J. Electrochem. Soc.* **1978**, *125*, 228.
[54] B. Seger, A. B. Laursen, P. C. K. Vesborg, T. Pedersen, O. Hansen, S. Dahl, I. Chorkendorff, *Angew. Chem. Int. Ed.* **2012**, *51*, 9128.
[55] R. P. Diez, E. J. Baran, A. E. Lavat, M. C. Grasselli, *J. Phys. Chem. Solids* **1995**, *56*, 135.
[56] K. Rubesova, D. Sykorova, *J. Sol-Gel Sci. Technol.* **2009**, *49*, 228.
[57] H. Szillat, C. L. Teske, *Z. Anorg. Allge. Chem.* **1994**, *620*, 1307.
[58] H. Yanagi, J. Tate, R. Nagarajan, A. W. Sleight, *Solid State Commun.* **2002**, *122*, 295.
[59] Y. Maruyama, H. Irie, K. Hashimoto, *J. Phys. Chem. B* **2006**, *110*, 23274.
[60] S. X. Ouyang, N. Kikugawa, D. Chen, Z. G. Zou, J. H. Ye, *J. Phys. Chem. C* **2009**, *113*, 1560.
[61] T. Kako, Z. G. Zou, M. Katagiri, J. H. Ye, *Chem. Mater.* **2007**, *19*, 198.
[62] J. J. Liu, S. F. Chen, Q. Z. Liu, Y. F. Zhu, J. F. Zhang, *Chem. Phys. Lett.* **2013**, *572*, 101.
[63] H. Mizoguchi, P. M. Woodward, C. H. Park, D. A. Keszler, *J. Am. Chem. Soc.* **2004**, *126*, 9796.
[64] W. Zhang, J. Tang, J. Ye, *J. Mater. Res.* **2007**, *22*, 1859.
[65] J. Lv, T. Kako, Z. Li, Z. Zou, J. Ye, *J. Phys. Chem.C* **2010**, *114*, 6157.
[66] E. Y. Wang, L. Hsu, *J. Electrochem. Soc.* **1978**, *125*, 1328.
[67] A. Kudo, I. Mikami, *J. Chem. Soc., Faraday Trans.* **1998**, *94*, 2929.
[68] C. M. Leroy, A. E. Maegli, K. Sivula, T. Hisatomi, N. Xanthopoulos, E. H. Otal, S. Yoon, A. Weidenkaff, R. Sanjines, M. Gratzel, *Chem. Commun.* **2012**, *48*, 820.

ADVANCED ENERGY MATERIALS

Supporting Information

for *Adv. Energy Mater.,* DOI: 10.1002/aenm.201400915

New Light-Harvesting Materials Using Accurate and Efficient Bandgap Calculations

Ivano E. Castelli, Falco Hüser, Mohnish Pandey, Hong Li, Kristian S. Thygesen, Brian Seger, Anubhav Jain, Kristin A. Persson, Gerbrand Ceder, and Karsten W. Jacobsen*

New Light Harvesting Materials Using Accurate and Efficient Bandgap Calculations - Supplementary Materials Information

Ivano E. Castelli,[a] Falco Hüser,[a] Mohnish Pandey,[a] Hong Li,[a] Kristian S. Thygesen,[a] Brian Seger,[b] Anubhav Jain,[c] Kristin Persson,[c] Gerbrand Ceder,[d] and Karsten W. Jacobsen[a]

This Supplementary Information is divided in three sections. (i) First, we expand the comparison between the different methods to calculate the bandgaps, looking at the signed, mean absolute and relative errors for the investigated set of 20 materials. In addition, the band structures calculated with GLLB-SC are compared with the eigenvalues obtained from HSE06 and from the different levels of GW, for the two materials ZrS_2 and $BaHfN_2$. (ii) Second, a feasibility study of all the candidate materials for one-photon water splitting shown in Figure 4, is reported by looking at the literature available about these materials. In the manuscript, only the five more realistic materials and the materials known to the community are described. (iii) Third, the complete list of calculated bandgaps with their id are reported. These data are also freely available on the Materials Project database [1] and on the Computational Materials Repository. [2]

Comparison of Different Methods to Calculate the Bandgaps

Figure 2 in the manuscript, shows the bandgaps for a set of materials calculated with LDA, different levels of the GW approximation, HSE06, and GLLB-SC. The set of materials has been divided into small and wide bandgap semiconductors and only the analysis of the errors of the small bandgap set has been reported. Here, we expand the analysis also to the wide bandgap materials.

Table 1 shows the mean absolute (signed) errors for the wide bandgaps. GLLB-SC is the exchange-correlation functional that approximates better the eigenvalue-self-consistent GW with an MAE of 1.54 eV, slightly better than G_0W_0 (MAE of 1.62 eV). The performance of HSE06 versus GW is considerably worst for the wide bandgap set compared with the small gap ensemble. In fact, for the small bandgaps, the MAE is 0.46 eV, worse than GLLB-SC and better than G_0W_0, while for the wide gaps, the MAE is 2.38 eV. This is even more clear from the MRE (Table 2), where the mean relative error

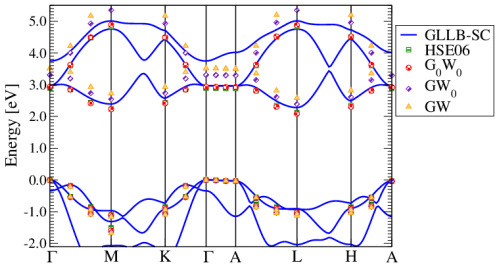

Fig. 1 Band structure, aligned to the valence band, of ZrS_2 (id 1186) calculated with GLLB-SC (blue lines), HSE06 (green squares), G_0W_0 (red dots), GW_0 (purple diamonds), and GW (orange triangles).

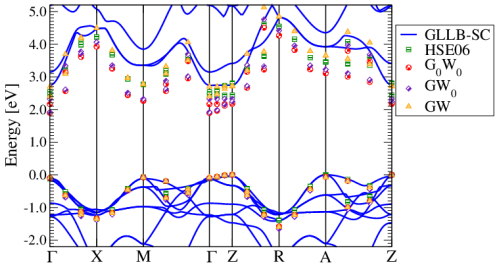

Fig. 2 Band structure, aligned to the valence band, of $BaHfN_2$ (id 10322) calculated with GLLB-SC, HSE06, and different GW levels.

for GLLB-SC and G_0W_0 with respect to GW is slightly better for wide gap sets compared to the small set (14.7% and 15.1% for the GLLB-SC and 16.1% and 18.0% for the G_0W_0, respectively), while it is much worst for the wide gaps set with respect to the small gaps set for HSE06 (22.7% and 16.4%, respectively). As expected for construction, GW_0 gives an improvement of the results of G_0W_0, and gives the best approximation to the GW gaps. Despite this, the computational cost required by any level of GW is at this stage to high to be used in a high-throughput screening and cheaper methods should be preferred. The materials thus identified can be then studied with more accurate methods.

For both HSE06 and GW levels, the computational costs

[a] *Center for Atomic-scale Materials Design, Department of Physics, Technical University of Denmark, DK 2800 Kongens Lyngby, Denmark.*
[b] *Center for Individual Nanoparticle Functionality, Department of Physics, Technical University of Denmark, DK 2800 Kongens Lyngby, Denmark.*
[c] *Computational Research Division, Lawrence Berkeley National Laboratory, 1 Cyclotron Rd, Berkeley, CA 94720, USA.*
[d] *Massachusetts Institute of Technology, Cambridge, MA 02139, USA.*

xc \ xc_{ref}	LDA	GLLB-SC	HSE06	G_0W_0	GW_0	GW
LDA	—	3.75 (−3.75)	2.23 (−2.23)	3.30 (−3.00)	3.57 (−3.57)	4.62 (−4.62)
GLLB-SC	3.75 (3.75)	—	1.62 (1.51)	1.37 (0.75)	1.39 (0.17)	1.54 (−0.87)
HSE06	2.23 (2.23)	1.62 (−1.51)	—	0.76 (−0.76)	1.34 (−1.34)	2.38 (−2.38)
G_0W_0	3.00 (3.00)	1.37 (−0.75)	0.76 (0.76)	—	0.58 (−0.58)	1.62 (−1.62)
GW_0	3.57 (3.57)	1.39 (−0.17)	1.34 (1.34)	0.58 (0.58)	—	1.04 (−1.04)
GW	4.62 (4.62)	1.54 (0.87)	2.38 (2.38)	1.62 (1.62)	1.04 (1.04)	—

Table 1 Mean absolute (signed) error, in eV, for the wide bandgaps of the materials in Figure 2 calculated using LDA, GLLB-SC, HSE06, G_0W_0, GW_0 and GW as exchange-correlation functionals.

xc \ xc_{ref}	LDA	GLLB-SC	HSE06	G_0W_0	GW_0	GW
LDA	—	56.8 (42.3)	50.3 (30.2)	47.9 (35.7)	52.4 (39.4)	56.7(45.7)
GLLB-SC	156.9 (73.3)	—	27.2 (22.5)	28.0 (18.5)	22.0 (17.0)	15.1 (14.7)
HSE06	121.4 (44.6)	20.3 (17.9)	—	13.0 (8.1)	12.8 (13.6)	16.4 (22.7)
G_0W_0	103.1 (58.9)	19.5 (16.3)	10.0 (9.5)	—	9.0 (6.2)	18.0 (16.1)
GW_0	124.9 (70.5)	17.9 (17.1)	12.6 (17.0)	10.1 (6.7)	—	9.9 (10.6)
GW	153.3 (91.0)	15.4 (18.6)	19.7 (31.0)	22.7 (19.4)	11.4 (11.9)	—

Table 2 Mean relative error, in %, for the small (wide) bandgaps of the materials in Figure 2 calculated using LDA, GLLB-SC, HSE06, G_0W_0, GW_0 and GW as exchange-correlation functionals.

only allow for calculations on rather coarse *k*-point grids. An accurate interpolation of the band structure from these points is not possible, since both methods are non-selfconsistent. Nevertheless, we can compare the band structures obtained with GLLB-SC with the two last occupied and two first unoccupied eigenvalues of some *k*-points (mainly high-symmetry points). For ZrS_2 (Figure 1), the band structure and the bandgap calculated with GLLB-SC is very similar to the ones obtained from HSE06 and GW levels. Different levels of GW differ from each other only by a constant shift corresponding to the difference in the bandgaps. The situation is different for $BaHfN_2$ (Figure 2). Whereas the valence bands are almost identical, there are significant changes in the conduction bands. Around the Γ-point, the order of the two lowest conduction bands changes from GLLB-SC through HSE06 to G_0W_0. For both the cases, an increase of the level of self-consistency, from G_0W_0 to GW, has only the effect of a constant shift of the unoccupied bands equal to the bandgap difference. These two examples shows two cases of excellent matching and differences between the methods, respectively.

Literature Review of the Candidate Materials

In this section, we list the information found in the literature for the candidate materials of Figure 4. In the manuscript, the materials with a realistic possibility of success have been described together with $BaSnO_3$ and In_2O_3 that are the candidates of the list already known to the water splitting community. We describe now the remaining materials.

- $AlAgO_2$: Sheets *et al.* have shown that $AlAgO_2$ has an optical bandgap of 3.6 eV.[3] In an unrelated study published at almost the same time, Ouyang *et al.* found a bandgap of 2.95 eV.[4] While there is a significant difference in bandgaps, both are too large for optimal absorption from the solar spectrum.
- $BaCdO_2$: this was originally synthesized by von Schnering.[5] Very little is known about this material.*
- $Ba_3In_2O_6$: initially synthesized by Mader *et al.*[6], is toxic and harmful[7]. Very little is known about this material.
- $Ba_4LiCuO_4(CO_3)_2$: originally synthesized by Tams *et al.*.[8] Very little is known about this material.
- $Ba_4NaCuO_4(CO_3)_2$: this material was initially synthesized by Vernooy *et al.*[9] Very little is known about this material.
- Ba_2NaOsO_6: this is a Mott-insulator and a ferromagnetic material,[10] which was originally synthesized by Stitzer *et al.*[11] The material is black, thus indicating its bandgap is probably below 1.7 eV, and it is toxic.[7]
- $CdIn_2O_4$: originally synthesized by Shannon *et al.*[12] This material is typically n-type and can be highly doped. Can be found in either a spinel, inverted spinel, or an orthorhombic structure. This material has been shown to have a bandgap of $2.67 - 3.24$ eV.[13]
- Cs_2PtBr_6: this material was produced only one time, thus there is little information on it.[14]
- Li_2PbO_3: there are two forms of this material,[15,16] neither have been investigated thoroughly. It is toxic and harmful.[7]
- $LiRhO_2$: Scheer *et al.* synthesized a α-$LiRhO_2$.[17] Hobbie *et al.* synthesized a black β-$LiRhO_2$.[18] Little information is known on the photochemical properties of either of these phases.
- $NaBiO_2$: it was originally synthesized by Schwedes *et al.*[19] Very little information is known on this material.
- Na_2PdCl_4: this material is reddish brown, but slightly soluble in water.[20]
- Na_3BiO_4: it was originally synthesized by Schwedes *et al.*[21] Little is known about this material.
- $NaCoO_2$: Takahashi *et al.* showed that theoretically the bandgap should be 1.3 eV.[22] $NaCoO_2$ can be oxidized by iodine (redox potential 0.54 V vs NHE), thus it is highly unlikely that this material will be stable enough to do water oxidation.[23]
- $NaRhO_2$: originally synthesized by Hobbie *et al.*[24] It can be oxidized by $Na_2S_2O_8$, thus it is unlikely that it will be stable during O_2 evolution conditions.[25]
- KAg_2AsO_4: this material has only been synthesized by Curda *et al.*[26] There is very little information on this material.
- K_2PdBr_4: this material has a bandgap of around 2 eV, but it is water soluble.[27]
- Sr_2FeWO_6: this material is black, with a bandgap of 0.1 eV.[28]

Calculated Bandgaps

In this section, we report the chemical formulas, the ids, and the bandgaps of the calculated 2400 materials. The information reported here are also available electronically in the Materials Project database[1] and in the Computational Materials Repository.[2]

* Very little is known normally means it has only been synthesized once.

Formula	MP Id	ICSD Id	Gap	Formula	MP Id	ICSD Id	Gap	Formula	MP Id	ICSD Id	Gap
$CoAs_2$	2715	42613	0.1 (0.3)	Sr_2Pb	30828	105624	0.1 (0.1)	CaAgP	12277	10016	0.1 (0.3)
SrMgSi	15642	42457	0.1 (0.1)	Rh_2S_3	17173	15344	0.1 (0.1)	SrMgGe	15643	42458	0.1 (0.1)
$TaAgS_3$	5821	84910	0.1 (0.4)	K_2MnSe_2	8716	65456	0.1 (0.2)	NaCuSe	7433	12155	0.1 (0.1)
$V_4As_2O_{13}$	32447	60781	0.1 (0.1)	Li_2MnO_3	18988	202639	0.1 (0.2)	$Cr_4InCuSe_8$	20809	250246	0.1 (0.1)
YNiSb	11520	105331	0.2 (1.3)	Tl_4Te_3Pb	20740	648621	0.2 (0.2)	$InAgTe_2$	22386	104476	0.2 (0.2)
$CsMnBr_3$	23048	9703	0.2 (0.3)	ScNiSb	3432	76695	0.2 (1.3)	Na_4CoO_4	31593	4196	0.2 (0.2)
YSbPt	4964	649578	0.2 (0.2)	$RbMnBr_3$	505596	9704	0.2 (0.3)	$CsMnI_3$	540609	10042	0.2 (0.3)
$Cs_2K_4Fe_2O_5$	541234	65942	0.2 (0.2)	CaAgAs	5615	604730	0.2 (0.3)	Li_3LaSb_2	8405	49625	0.2 (1.0)
Li_2AgSb	16238	52589	0.2 (0.2)	Cu_2GeS_3	15252	85138	0.2 (0.2)	Sr_2Sn	978	652722	0.2 (0.2)
CdSb	1321	52831	0.2 (0.5)	$CuAgO_2$	7237	93880	0.2 (0.2)	CaAsAu	3927	107915	0.2 (0.3)
Sb	104	55402	0.2 (0.5)	ZrSnTe	9289	80190	0.2 (0.3)	$PbAu_2$	19871	56261	0.2 (0.4)
Li_2ZnGe	12411	171498	0.2 (0.4)	CaSbAu	16245	52662	0.2 (0.3)	VPO_4	18835	82286	0.2 (0.2)
$CsIn_3$	542339	102867	0.2 (0.4)	Nb_3I_8	27772	25767	0.2 (0.3)	$MoBr_3$	23312	9422	0.2 (0.2)
$CuSe_2O_5$	3199	245059	0.2 (0.3)	$MoCl_3$	22853	83878	0.3 (0.3)	YIr	30746	104600	0.3 (1.1)
As_2Rh	15954	42616	0.3 (0.4)	$Cs_6Fe_2O_5$	541385	73134	0.3 (0.3)	Ba_3CrN_3	12905	154802	0.3 (0.5)
$Sr(As_3Pt_2)_2$	14500	62518	0.3 (0.4)	$Ba(ZnP)_2$	7426	12145	0.3 (0.8)	SiRu	189	85209	0.3 (0.5)
HfSnPd	11869	106773	0.3 (1.3)	Sb_2Ru	20928	42608	0.3 (0.6)	BaSnHg	11819	106311	0.3 (0.5)
CaPAu	10677	52661	0.3 (0.3)	Cs_2CoSe_2	8770	67392	0.3 (0.3)	$Ca(CdSb)_2$	7430	12151	0.3 (0.4)
LaP_5	1864	96545	0.3 (1.0)	Na_2In	510678	106857	0.3 (0.4)	CaAgSb	11214	56982	0.4 (0.6)
C	48	617290	0.4 (0.4)	K_3FeO_3	504570	16534	0.4 (0.4)	LiAlGe	5920	152087	0.4 (1.7)
ReTeS	5222	82721	0.4 (0.8)	$TlTe_3Pt_2$	9251	78787	0.4 (0.6)	$HfCu_2Te_3$	3650	655974	0.4 (0.6)
FeSi	871	633541	0.4 (0.4)	$FeTe_2$	20653	42727	0.4 (0.8)	LiSi	795	160538	0.4 (0.9)
GePtSe	20817	822	0.5 (1.1)	Te_2Ru	267	106001	0.5 (1.3)	LiAlSi	3161	152086	0.5 (2.2)
P_2Rh	15953	42615	0.5 (0.9)	$CdAs_2$	471	20518	0.5 (1.0)	$Sr(ZnAs)_2$	7770	23248	0.5 (0.5)
La_3MnGaS_7	504891	38413	0.5 (0.6)	MgB_4	365	653968	0.5 (1.0)	Sb_2Ir	1247	42620	0.5 (0.8)
TiS_2	2156	651217	0.5 (1.0)	SrCuSb	10749	53339	0.5 (0.9)	$AlVFe_2$	5778	107814	0.5 (0.8)
$LiScI_3$	28835	73339	0.5 (0.7)	$BaBiO_3$	22942	151894	0.5 (1.1)	$Al_2(FeSi)_3$	29110	83664	0.5 (0.6)
OsS_2	20905	647750	0.6 (1.0)	GaAs	2534	107946	0.6 (0.6)	Sb_2Os	2695	647757	0.6 (1.0)
AuSe	2793	73700	0.6 (1.5)	$RbGa_3$	31493	103943	0.6 (0.8)	P	157	150873	0.6 (0.6)
CoP_2	14285	38316	0.6 (0.7)	Mg_2Ge	408	151389	0.6 (1.6)	$Cd(PtO_2)_3$	8212	35407	0.6 (0.6)
YB_4Mo	7691	20081	0.6 (0.7)	LaTeAs	10383	280231	0.6 (0.6)	$Sr(PIr)_2$	15074	73531	0.6 (0.6)
$Si_3Ag_3(SnP_3)_2$	18310	52595	0.6 (0.8)	Si_3Ru_2	22192	95586	0.6 (0.6)	BaP_3Pt_2	28373	62520	0.6 (0.8)
$Zr_3Ni_3Sb_4$	17926	87995	0.6 (0.9)	$CsCuBr_3$	27336	10184	0.6 (0.7)	$Ba(CdAs)_2$	8281	30917	0.6 (0.7)
Mg_2Sn	2343	158181	0.6 (1.9)	$GaAgTe_2$	4899	156128	0.6 (0.6)	K_2CdPb	504498	10041	0.6 (0.7)
$InAuO_2$	19723	95672	0.6 (1.5)	$Ba(GeAs)_2$	27810	26417	0.7 (0.9)	Mg_2Si	1367	163708	0.7 (2.5)
As_2Ru	766	42578	0.7 (1.2)	$Ca(ZnAs)_2$	9571	100064	0.7 (0.7)	Al_2Os	7188	58108	0.7 (1.5)
ScSbPt	7173	77948	0.7 (0.7)	$GaCuTe_2$	3839	600219	0.7 (0.7)	LiZnSb	9919	42064	0.7 (0.7)
YP_5	9854	409188	0.7 (1.2)	$FeAs_2$	2008	41805	0.7 (1.0)	KAg_3Se_2	9782	402643	0.7 (0.8)
$Sr(CdAs)_2$	7771	23249	0.7 (0.7)	SrCuP	16321	53323	0.7 (1.2)	CaCuP	8432	49740	0.7 (1.6)
P_3Au_2	27258	8058	0.7 (1.2)	$Ca(PIr)_2$	11168	95756	0.7 (0.7)	$CaCrP_2O_7$	19134	411743	0.7 (0.7)
SiSbPt	11152	413194	0.7 (0.8)	$Ba(As_3Pt_2)_2$	14501	62519	0.7 (0.7)	P_2Ir	10155	44661	0.8 (1.8)
$TlBiSe_2$	29662	43314	0.8 (0.8)	Si_3NiP_4	8311	39452	0.8 (0.9)	TiS_3	9920	42072	0.8 (0.8)
KSnSb	3486	40816	0.8 (0.8)	KSb_2	29055	80945	0.8 (1.1)	$Ca(CdAs)_2$	7067	100065	0.8 (0.8)
KGa_3	181	103649	0.8 (0.9)	$K_2Ag_4S_3$	7494	863	0.8 (0.8)	SrCaPb	21166	172008	0.8 (0.8)
$TaTe_4I$	28691	67533	0.8 (0.9)	Te	19	161690	0.8 (0.8)	CaCuAs	4120	659435	0.8 (0.9)
$CsScCl_3$	27359	10474	0.8 (1.1)	$TlPd_2Se_3$	7038	78786	0.8 (0.9)	$Sc(AlC)_3$	4798	660402	0.8 (2.2)
$Tl(TeMo)_3$	16096	90811	0.8 (1.0)	SnTe	1883	652763	0.8 (0.8)	AgF_3	18536	80477	0.8 (1.0)
Ag_3Te_2Au	5710	604788	0.8 (0.9)	$PtSe_2$	1115	649594	0.9 (1.2)	SrCaSn	20726	172007	0.9 (0.9)
$FeSe_2$	760	633489	0.9 (1.5)	$Na_2Pd_3O_4$	27562	6157	0.9 (0.9)	P_2Pd	28266	48163	0.9 (1.1)
Si_3P_2Pt	29157	84944	0.9 (1.5)	Rb_2Te_5	31002	30734	0.9 (1.1)	$Tl(MoSe)_3$	3411	53119	0.9 (1.0)
BaCaGe	16252	52681	0.9 (0.9)	BaCaSi	16253	52682	0.9 (0.9)	$GaAgSe_2$	5518	52570	0.9 (0.9)

AuSeBr	27199	2897	0.9 (1.3)	CoPSe	10368	53060	0.9 (1.1)	$Y_3Sb_4Au_3$	13654	957	0.9 (1.0)
KZnSb	7438	12161	0.9 (0.9)	Ba_2CuClO_2	551456	1038	0.9 (1.1)	KZnAs	7421	10459	0.9 (0.9)
BaCaSn	11265	58641	0.9 (0.9)	Na_4FeO_3	19026	23635	0.9 (0.9)	Ta_2CrO_6	31629	51175	0.9 (0.9)
Ca_2Sb	9925	42135	0.9 (1.0)	ZrI_3	23282	32704	0.9 (1.0)	La_2CoIrO_6	18862	79496	0.9 (0.9)
$RbAg_3Te_2$	10481	90872	1.0 (1.0)	Ag_2BiO_3	23558	415958	1.0 (1.0)	$PdSe_2$	2418	170327	1.0 (1.5)
Ca_2Si	2517	158275	1.0 (1.0)	$TlBiTe_2$	27438	15412	1.0 (1.0)	$CdSiAs_2$	3078	609980	1.0 (1.0)
Hg_2GeSe_4	3167	59911	1.0 (1.0)	$CsAg_3Se_2$	16234	52558	1.0 (1.0)	$TlPt_2Se_3$	541487	78785	1.0 (1.1)
Bi_4RuI_2	541771	406949	1.0 (1.0)	Ca_3GeO	17193	413383	1.0 (1.0)	$Ag_3Ge_5P_6$	17862	70055	1.0 (1.2)
$Ta_2Pd_3Se_8$	18010	73318	1.0 (1.2)	Cs_2SnI_6	27636	22105	1.0 (1.0)	PtI_3	28268	47120	1.0 (1.0)
$BaAs_2$	31243	414139	1.0 (1.0)	MnP_4	487	100786	1.0 (1.1)	Cu_2O	361	172174	1.0 (1.0)
$HfSe_3$	15622	42075	1.0 (1.3)	KSnAs	3481	40815	1.0 (1.0)	Te_3As_2	484	54097	1.0 (1.0)
Ca_2Ge	304	44854	1.0 (1.0)	$Sr(GaTe_2)_2$	6987	41166	1.0 (1.2)	FeP_2	20027	633072	1.0 (1.3)
$TaCuS_3$	3102	660123	1.0 (1.0)	$NbTeI_3$	540924	35377	1.0 (1.1)	$SrHfN_2$	9383	82538	1.0 (1.8)
$Tl_2(CdSb)_3$	29741	76500	1.0 (1.0)	$ZrSe_2$	2076	109291	1.1 (1.9)	Mg_3Sb_2	2646	245692	1.1 (1.9)
PtS	288	654379	1.1 (1.2)	TlSe	1836	652068	1.1 (1.4)	Ca_3SiO	11649	413382	1.1 (1.1)
PtO_2	1285	647320	1.1 (1.4)	$RbSc_5Te_8$	13336	245998	1.1 (1.3)	Si	149	150530	1.1 (3.1)
As_2Ir	15649	42573	1.1 (1.2)	$LiAuI_4$	505462	406967	1.1 (1.2)	Bi_4RuBr_2	541772	406951	1.1 (1.1)
CdP_4	7904	25605	1.1 (1.3)	LiAs	7943	26472	1.1 (1.3)	Ba_2GeAs_2	8195	35151	1.1 (1.3)
Li_3LaP_2	8407	49627	1.1 (1.5)	GeTe	938	159907	1.1 (1.2)	GeAs	9548	86361	1.1 (1.2)
Sc_4C_3	15661	42760	1.1 (1.1)	Si_3Os_2	16608	95590	1.1 (1.1)	$LaAs_2$	505640	280294	1.1 (1.4)
Na_3InAs_2	21622	300139	1.1 (1.1)	$NaNbSe_2$	7939	26287	1.1 (1.5)	In_2HgTe_4	19765	25652	1.1 (1.1)
LaZnAsO	549589	163779	1.1 (1.1)	NbSbRu	505297	83929	1.1 (2.0)	$KZrCuSe_3$	9318	80625	1.1 (1.1)
Sb_2WO_6	541435	75595	1.1 (1.1)	$SiCu_2Se_3$	15896	88236	1.1 (1.1)	$ZrTlCuSe_3$	7050	82561	1.1 (1.1)
$TiNb_3O_6$	29699	280002	1.1 (1.3)	$TaTlS_3$	10795	412385	1.1 (1.1)	FeSbS	27904	24161	1.1 (1.2)
$NaTiCuS_3$	505171	73886	1.1 (1.1)	SiTePt	29397	400487	1.1 (1.2)	Li_3Bi	23222	58797	1.2 (1.8)
As_2Os	2455	42610	1.2 (1.4)	Sr_2Ge	2576	53923	1.2 (1.2)	$Ca(MgBi)_2$	29208	100048	1.2 (1.2)
$BaLaI_4$	30111	412276	1.2 (1.2)	$ZrSe_3$	1683	652241	1.2 (1.4)	Ba_3P_4	14289	38322	1.2 (1.2)
CdTe	406	161693	1.2 (1.2)	CoAsS	4627	43221	1.2 (1.4)	AgF	7592	18008	1.2 (2.6)
$LiNbS_2$	7936	26284	1.2 (1.9)	Ba_2GeP_2	8194	35150	1.2 (1.4)	$LaRhO_3$	5163	172353	1.2 (1.2)
PdS_2	13682	16694	1.2 (1.9)	$Rb_2Ni_3Se_4$	18691	78976	1.2 (1.4)	$LiBiO_3$	29077	82277	1.2 (1.3)
Sr_3GeO	30950	413385	1.2 (1.2)	TiSnPt	30847	105799	1.2 (1.9)	LaZnPO	7060	85777	1.2 (1.2)
Ga_2HgTe_4	16337	53575	1.2 (1.2)	LaCuTeS	10288	88012	1.2 (1.2)	$CsZrCuSe_3$	7152	280701	1.2 (1.2)
Tl_5Se_2Br	28921	75960	1.2 (1.2)	Na_4FeO_4	19022	59585	1.2 (1.2)	$RuSe_2$	1922	650611	1.2 (1.4)
InP	20351	640192	1.2 (1.2)	SrAs	1049	83353	1.2 (1.8)	$SrLaI_4$	505793	412275	1.2 (1.2)
K_2SnBi	31486	107616	1.2 (1.3)	CdSe	2691	620439	1.3 (1.3)	ScN	2857	157501	1.3 (2.2)
K_2SnTe_5	28080	36215	1.3 (1.4)	$Ba(MgBi)_2$	29209	100049	1.3 (1.3)	Tl_2Te_3	29711	410895	1.3 (1.5)
SrCaGe	12418	172006	1.3 (1.3)	$GeAs_2$	17524	23872	1.3 (1.4)	Rb_2As_3	15556	409381	1.3 (1.4)
$CdGeP_2$	3668	42895	1.3 (1.3)	MgP_4	384	42030	1.3 (1.4)	NaZnP	4824	160955	1.3 (1.3)
$NbSeI_3$	541817	410743	1.3 (1.3)	$KNbS_2$	7938	26286	1.3 (1.6)	NaSb	7944	26473	1.3 (1.4)
$Ba(CdP)_2$	8279	30915	1.3 (1.4)	$Tl_2Pt_2O_7$	13801	22215	1.3 (1.3)	Tl_3GeTe_3	17217	49658	1.3 (1.5)
$Ba_2Tl_2O_5$	18327	6322	1.3 (1.3)	Te_2I	27655	107	1.3 (1.3)	$NbTeBr_3$	28038	35376	1.3 (1.4)
$P_{10}Au_7I$	27370	12162	1.3 (1.4)	$Ba(ScTe_2)_2$	17501	416326	1.3 (1.3)	Ta_3I_7	23238	14211	1.3 (1.4)
$NaNbS_2$	7937	26285	1.3 (1.9)	SnSe	691	108293	1.3 (1.4)	$CsAuI_3$	28453	59269	1.3 (1.3)
$LiCuO_2$	9158	74978	1.3 (1.6)	NbFeSb	9437	83928	1.3 (2.0)	HfBrN	30302	51773	1.3 (1.3)
Ag_2CO_3	4691	281040	1.3 (2.1)	In_2HgS_4	22356	56081	1.3 (1.5)	$Sb(IF_3)_2$	504965	63301	1.3 (1.3)
SrCaSi	7084	172005	1.3 (1.3)	VS_4	541155	64770	1.3 (1.4)	$CuTe_2Cl$	30971	641	1.3 (1.7)
Sr_2Si	1106	160102	1.3 (1.3)	$HfTlCuSe_3$	9397	82563	1.3 (1.3)	KCuSe	7435	12157	1.3 (1.3)
$ZrBr_3$	23247	32703	1.3 (1.4)	$Ca_3(CoO_3)_2$	18792	246282	1.3 (1.3)	PbSe	20667	657561	1.4 (1.4)
$TlInTe_2$	22791	640633	1.4 (1.5)	P_2Os	2319	42609	1.4 (1.7)	$Bi_2Pt_2O_7$	23341	161104	1.4 (1.4)
BeP_2	27148	2262	1.4 (1.5)	Li_4NCl	29149	84649	1.4 (2.0)	TlAgSe	29238	100710	1.4 (1.4)
BaNaBi	31235	413810	1.4 (1.4)	ZrCoBi	31451	107120	1.4 (2.1)	$Cs_2Ni_3Se_4$	14336	33891	1.4 (1.6)
Sr_3As_4	15339	100110	1.4 (1.6)	Cs_2PdI_6	505635	280189	1.4 (1.5)	Te_2Mo	602	24155	1.4 (1.4)
P_2Pt	730	647971	1.4 (1.9)	LiZnN	7575	16790	1.4 (1.4)	Na_2SbAu	7774	23255	1.4 (1.5)

$Sr(ZnP)_2$	8276	30911	1.4 (1.4)	$K(MoS)_3$	8116	30752	1.4 (1.5)	$Rb(MoS)_3$	8117	30753	1.4 (1.5)
$Ca_3(GeAs_2)_2$	18504	16455	1.4 (1.5)	$Ba(AgTe)_2$	18501	246048	1.4 (1.4)	Cs_2PtI_6	23060	37193	1.4 (1.4)
RbPb	21525	409436	1.4 (1.4)	KPb	21526	401436	1.4 (1.4)	Cd_2As_3I	27577	8216	1.4 (1.7)
Te_2Br	27648	106	1.4 (1.5)	$ZnCu_2GeS_4$	6408	152752	1.4 (1.4)	In_2HgSe_4	20731	25649	1.4 (1.4)
TiCoSb	5967	624920	1.4 (2.2)	$SnSe_2$	665	43857	1.4 (1.8)	NbI_3O	546285	418088	1.4 (1.4)
$K_2Pd_3Se_4$	14339	33894	1.4 (1.5)	$CoAgO_2$	19178	246157	1.4 (1.7)	$InAgS_2$	19833	156129	1.4 (1.4)
Ag_2GeS_3	9900	41711	1.4 (1.5)	RbSb	7444	14030	1.4 (1.4)	$ZrCl_3$	22871	32702	1.4 (1.6)
$ReCl_3$	23174	62222	1.4 (1.4)	$Ca(BC)_2$	10289	88019	1.5 (1.9)	$GaAgO_2$	11020	95665	1.5 (2.5)
$Zn(InTe_2)_2$	20832	25650	1.5 (1.5)	PbS	21276	657560	1.5 (1.5)	$Rb_2(NbCl_3)_3$	22976	404165	1.5 (1.6)
$ZrCl_2$	23162	30052	1.5 (1.6)	ClO_2	23207	67663	1.5 (1.5)	Rb_3Bi	23304	58849	1.5 (1.6)
$LiAg_3O_2$	27227	4204	1.5 (1.5)	$RbAuBr_3$	27300	9577	1.5 (1.6)	$NaAg_3O_2$	27303	9627	1.5 (1.5)
$Sr_3(InP_2)_2$	28324	61335	1.5 (1.5)	Te_4MoBr	29190	82245	1.5 (1.5)	SrLiBi	510112	58800	1.5 (1.5)
SrP	7931	26262	1.5 (2.1)	K_2Te_2Pt	8623	40432	1.5 (2.1)	K_2Se_3	7670	1264	1.5 (1.7)
$CdHgO_2$	9146	74848	1.5 (1.5)	$Ba_3(Si_2P_3)_2$	27887	29261	1.5 (1.5)	$Na_{10}CaSn_{12}$	30252	240006	1.5 (1.5)
Nb_2Se9	541106	62538	1.5 (1.5)	LaS_2	1508	418405	1.5 (2.0)	CuBiSeO	23116	74475	1.5 (1.6)
Bi_2SeO_2	552098	411143	1.5 (2.3)	NaSnP	29529	409010	1.5 (2.0)	K_2NiAs_2	9673	300120	1.5 (1.5)
TaSbRu	31454	107123	1.5 (2.5)	VCu_3Se_4	21855	629148	1.5 (1.8)	$CdCu_2GeS_4$	13982	26150	1.5 (1.5)
Y_4OsBr_4	28744	71513	1.5 (1.5)	Hg_2As_3Br	28899	75169	1.5 (1.7)	$TlInS_2$	20042	42419	1.5 (2.0)
CuP_2	927	653601	1.5 (1.6)	$CuSbSe_2$	20331	30358	1.5 (1.6)	$CuBiS_2$	22982	34936	1.5 (1.7)
$BaCu_2SnSe_4$	12364	170857	1.5 (1.5)	Ba_2FeMoO_6	510675	246544	1.5 (1.6)	$Mg(BiO_3)_2$	28447	50005	1.5 (1.5)
$NaZrCuSe_3$	505172	73888	1.5 (1.5)	$FeSi_2$	1714	23408	1.5 (1.5)	NbI_5	31487	25503	1.5 (1.6)
TeRhCl	22945	56853	1.6 (1.7)	$CsAuCl_3$	23484	417363	1.6 (1.6)	Y_2Cl_3	27678	23337	1.6 (1.7)
$NaAuSe_2$	29139	84004	1.6 (1.7)	Ca_3BiN	31149	106320	1.6 (1.6)	$ZnSiAs_2$	3595	611411	1.6 (1.6)
KAg_2AsO_4	12015	409793	1.6 (2.5)	NaSe	15668	43408	1.6 (1.6)	TeAuI	504668	1661	1.6 (1.7)
$NaTaN_2$	5475	76382	1.6 (2.0)	$MgAs_4$	7623	1079	1.6 (1.6)	Sr_3SbN	7752	152052	1.6 (1.6)
BaP_3	7808	23618	1.6 (1.6)	Rb_2Te_3	2095	77994	1.6 (1.7)	$Sr(CdP)_2$	8277	30912	1.6 (1.6)
$Ca(ZnP)_2$	9569	100062	1.6 (1.6)	RbAs	10802	412594	1.6 (1.6)	$K_2Ni_3S_4$	17228	81731	1.6 (1.8)
Rb_3Sn_4Au	17401	107445	1.6 (1.7)	PdI_2	27747	25120	1.6 (1.6)	$Na_{10}SrSn_{12}$	30253	240007	1.6 (1.6)
KCuTe	7436	12158	1.6 (1.6)	$BaAg_2GeS_4$	7394	10040	1.6 (2.4)	SnS	2231	156130	1.6 (1.8)
$Rb_2Pd_3Se_4$	14340	33895	1.6 (1.7)	$CuTe_2Br$	31036	67252	1.6 (1.9)	Sb_2Se_3	2160	171569	1.6 (1.6)
BaCuN	505338	86064	1.6 (1.6)	KTe	2072	96741	1.7 (1.7)	Li_3Sb	2074	642341	1.7 (3.3)
YN	2114	161075	1.7 (2.0)	$NaInTe_2$	22483	25346	1.7 (2.0)	Ga_2Te_5	2371	32034	1.7 (1.7)
GeSe	700	637866	1.7 (1.7)	AuClO	27265	8190	1.7 (1.9)	TiBrN	27849	27395	1.7 (1.7)
TiNCl	27850	27396	1.7 (1.7)	$YAgTe_2$	12903	154792	1.7 (1.7)	$RbPt_2Se_3$	14797	69439	1.7 (1.7)
FeS_2	1522	109374	1.7 (2.1)	$Zn(GaTe_2)_2$	15777	44888	1.7 (1.7)	Ga_2HgSe_4	4730	83712	1.7 (1.7)
$Ba(PdS_2)_2$	505230	79930	1.7 (1.9)	$TeAuBr_8$	541134	63129	1.7 (1.8)	$Cs_2Pd(IBr_2)_2$	543024	240480	1.7 (1.8)
SrLiSb	7756	172216	1.7 (1.7)	Na_2AsAu	7773	23254	1.7 (1.8)	$Ca(CdP)_2$	9570	100063	1.7 (1.7)
Na_5GeAs_3	16861	300187	1.7 (1.8)	KNa_4GeAs_3	16921	300204	1.7 (1.8)	Si_2Os	17123	42730	1.7 (1.8)
$Sr_3(GeAs_2)_2$	17504	16454	1.7 (1.7)	$Ca(RhO_2)_2$	17998	170597	1.7 (1.7)	TaI_2O	29027	80109	1.7 (1.8)
Bi_4O_7	30303	51778	1.7 (1.9)	$CdAg_4Ge_2S_7$	542200	95121	1.7 (1.7)	$PtBr_3$	23165	23127	1.7 (1.7)
Tl_2O	551470	77699	1.7 (1.7)	$NaCuO_2$	4541	203080	1.7 (2.0)	$RbCu_3S_2$	10985	409646	1.7 (1.8)
LiCaSb	16264	52775	1.7 (1.7)	$ReSe_2$	541582	81813	1.7 (1.7)	$K_2Sn_2Se_5$	8966	72379	1.7 (2.0)
TePb	19717	153711	1.7 (1.7)	RuS_2	2030	56019	1.7 (2.1)	$KZrCuS_3$	9317	80624	1.7 (1.7)
K_2VCuSe_4	15220	84303	1.7 (1.9)	$NaHfCuSe_3$	505448	402578	1.7 (1.7)	BaLiSb	10485	280574	1.8 (1.9)
BaLiAs	10616	56445	1.8 (1.8)	$Ba(InTe_2)_2$	21183	41168	1.8 (2.0)	ZnTe	2176	162756	1.8 (1.8)
$Tl_2Sn_2S_3$	28011	33531	1.8 (1.9)	$KAuSe_2$	29138	84003	1.8 (2.0)	Zr_2SN_2	11583	96971	1.8 (2.8)
$Cd(GaTe_2)_2$	13949	25646	1.8 (1.8)	KAgSe	16236	52586	1.8 (1.8)	$Cs_2Pd_3Se_4$	504855	33892	1.8 (1.9)
WBr_6	504993	62048	1.8 (1.8)	$NaSbS_2$	5414	43909	1.8 (1.9)	$AuCl_2$	541656	201436	1.8 (1.9)
KYO_2	8409	49650	1.8 (1.8)	RbTe	9064	73179	1.8 (2.2)	Ca_3AlAs_3	17186	32727	1.8 (1.8)
Ga_7Te_{10}	18388	400668	1.8 (1.8)	NaGe	29657	43275	1.8 (1.8)	$K_2LiInAs_2$	505431	402147	1.8 (1.9)
Ba_3GaP_3	541715	402177	1.8 (1.8)	BaCuTeF	13287	245624	1.8 (1.8)	VCu_3S_4	3762	628957	1.8 (2.1)
Cd_2SnO_4	5966	69297	1.8 (1.8)	$TlPt_2S_3$	9272	78784	1.8 (1.8)	$KV(CuS_2)_2$	6376	402924	1.8 (1.9)
LiP	9588	100465	1.8 (2.0)	$RbCuPdSe_5$	11115	281424	1.8 (1.8)	Rb_2VAgSe_4	14635	50462	1.8 (2.0)

$Sr(InTe_2)_2$	20397	41167	1.8 (2.0)	$LaCuSe_2$	11790	99675	1.8 (1.8)	$CuTe_2I$	31037	67253	1.8 (1.9)
Rb_3Sb	16319	77991	1.8 (1.9)	$CuRhO_2$	14116	29214	1.8 (1.9)	KSb	1536	56529	1.8 (1.8)
$NaPt_2Se_3$	28987	78788	1.8 (1.8)	$BaYAgTe_3$	10337	88717	1.9 (2.1)	BP	1479	615154	1.9 (4.1)
$Cd(InSe_2)_2$	22304	151954	1.9 (1.9)	$Zn(InSe_2)_2$	22607	25647	1.9 (1.9)	InSe	22691	41477	1.9 (1.9)
AgBr	23231	65061	1.9 (3.2)	Au_2O_3	27253	8014	1.9 (2.1)	$Bi(TeBr_2)_2$	29127	83806	1.9 (2.0)
Ca_3BN_3	30315	95814	1.9 (1.9)	$NbCl_4$	31040	1010	1.9 (1.9)	Sr_3P_4	14288	38321	1.9 (2.0)
Na_2PtSe_2	14588	40429	1.9 (2.3)	$MoSe_2$	1634	644334	1.9 (1.9)	$ScAgSe_2$	12908	155115	1.9 (2.4)
$ScTlSe_2$	13313	418475	1.9 (2.1)	PdF_4	13868	1555	1.9 (1.9)	B	160	108026	1.9 (2.4)
Rb_3Ge_4Au	17830	413724	1.9 (2.1)	P_4Ru	504443	2492	1.9 (2.1)	TiI_4	541013	39820	1.9 (2.0)
Li_3As	757	43987	1.9 (2.9)	$BaSe_2$	7547	16358	1.9 (2.0)	Al_2HgTe_4	7910	25641	1.9 (1.9)
Na_3Sb	7956	26882	1.9 (1.9)	K_2As_2Pd	8147	32009	1.9 (2.0)	K_2P_3	8262	33259	1.9 (1.9)
K_5As_2Au	8683	40698	1.9 (2.0)	Cs_2As_2Pd	8857	69647	1.9 (2.1)	$TlPd_3O_4$	5478	2276	1.9 (2.1)
$Ca(MgSb)_2$	9565	100045	1.9 (2.5)	Ba_4Sb_2O	9774	402284	1.9 (1.9)	$Ba(MgSb)_2$	9567	100047	1.9 (2.6)
$ZrSnS_3$	17324	73711	1.9 (1.9)	K_2Se_5	18609	72380	1.9 (1.9)	I	23153	67704	1.9 (2.0)
TeI	23273	66641	1.9 (1.9)	Rb_5SiAs_3	17490	300191	1.9 (2.0)	$Nb_2Hg_2O_7$	13803	22226	1.9 (2.3)
$AlTlSe_2$	9579	100130	1.9 (2.1)	YZnAsO	546011	163780	1.9 (1.9)	$LaTaN_2O$	550514	411138	1.9 (1.9)
Cs_2Se_3	7449	14095	1.9 (1.9)	Na_2AgSb	7392	10010	1.9 (2.1)	$CuSe_2Br$	29567	410004	1.9 (1.9)
Hg_2P_3Cl	28875	74771	1.9 (2.4)	$CuSe_2Cl$	31038	68292	1.9 (2.0)	VAg_3O_4	18889	417469	1.9 (2.3)
$HfTlCuS_3$	9396	82562	1.9 (1.9)	$CuSbS_2$	4468	418753	1.9 (2.1)	$NaNbN_2$	7017	72557	1.9 (2.1)
K_3As	14018	26887	1.9 (2.0)	$FeMoO_4$	541843	43013	1.9 (1.9)	$Cs_2Ni_3S_4$	28486	63010	1.9 (2.1)
PPdSe	3123	77772	1.9 (1.9)	Na_2PdS_2	10223	76533	2.0 (2.4)	Rb_2P_3	2079	654296	2.0 (2.1)
$PdPbF_4$	20805	108992	2.0 (2.2)	$TlInSe_2$	22232	640526	2.0 (2.1)	$InAgO_2$	22660	202429	2.0 (2.5)
K_2AgBi	27549	1156	2.0 (2.2)	Tl_2PdCl_4	29889	89601	2.0 (2.5)	$ScTlS_2$	13312	418474	2.0 (3.0)
Rb_2As_2Pt	13445	107529	2.0 (2.0)	Cs_2P_3	14652	65185	2.0 (2.2)	$Cd(RhO_2)_2$	14100	28954	2.0 (2.0)
$ZnGeP_2$	4524	637511	2.0 (2.1)	GaTe	542812	153456	2.0 (2.1)	Li_3P	736	240861	2.0 (3.3)
$KTlO_2$	8175	33553	2.0 (2.2)	K_2PtSe_2	8621	40430	2.0 (2.5)	$Ca_2Pt_3O_8$	8710	65412	2.0 (2.0)
Ba_2ZnN_2	9307	80377	2.0 (2.0)	$Fe(SiP)_4$	9198	79005	2.0 (2.1)	$K_3Na_2SnAs_3$	18447	40560	2.0 (2.0)
$Ge_19(PI)_4$	23420	63194	2.0 (2.0)	K_2Te_2As	29380	300184	2.0 (2.1)	K_2SnTe_3	29835	409483	2.0 (2.0)
Cs_3Ge_4Au	510341	413725	2.0 (2.1)	K_2WSe_4	18138	59242	2.0 (2.0)	$Ba(YTe_2)_2$	17872	90335	2.0 (2.0)
$Ta(ICl)_2$	28683	69688	2.0 (2.0)	Sc_2CCl_2	28479	59124	2.0 (2.3)	$GaCuS_2$	5238	156786	2.0 (2.0)
$BaGe_2$	2139	157612	2.0 (2.0)	Ca_3VN_3	9029	72118	2.0 (2.0)	$Ba_4LiCu(CO_5)_2$	15472	401122	2.0 (2.5)
WSe_2	1821	40752	2.0 (2.0)	$Rb(SbSe_2)_2$	9798	402887	2.0 (2.3)	$Co(ReO_4)_2$	31516	51015	2.0 (2.0)
SbIrS	8630	41400	2.0 (2.3)	$Zn(RhO_2)_2$	5146	109298	2.0 (2.0)	Sr_2FeWO_6	19266	153430	2.0 (2.0)
$KAuBr_4$	29694	280033	2.0 (2.0)	ZnSe	1190	162755	2.1 (2.1)	$Sr_3(SiAs_2)_2$	11677	16453	2.1 (2.1)
$K_2NaInAs_2$	21510	300137	2.1 (2.1)	GeS	2242	653896	2.1 (2.1)	AlSb	2624	151218	2.1 (2.4)
Bi_2SO_2	27891	29451	2.1 (2.4)	$Co(ClO_4)_2$	31621	33288	2.1 (2.1)	$Cs(SbSe_2)_2$	3312	415580	2.1 (2.4)
O_2	12957	156481	2.1 (2.2)	$AlAgTe_2$	14092	28746	2.1 (2.1)	Tl_2GeSe_3	14242	35043	2.1 (2.3)
Be_2C	1569	616185	2.1 (5.5)	$NaNbO_2$	3744	300244	2.1 (2.1)	Ag_3SbS_3	4515	64986	2.1 (2.6)
K_2GeAs_2	8930	71222	2.1 (2.1)	Al_2Te_5	9254	78941	2.1 (2.4)	LiBeAs	9562	100004	2.1 (2.3)
$Ti(SnO_2)_2$	18288	163230	2.1 (2.1)	$Sr_3(GeP_2)_2$	18351	41182	2.1 (2.1)	$Na_4Ge_2Te_5$	28107	37183	2.1 (2.1)
PtI_2	28319	60760	2.1 (2.2)	$Ba(TeP_2)_2$	31275	412643	2.1 (2.2)	$Be_2Te_7Cl_6$	505788	391156	2.1 (2.2)
$BiAuBr_6$	541774	407220	2.1 (2.1)	Pb_3O_4	542494	36253	2.1 (2.1)	LiBC	9244	78731	2.1 (2.5)
$SrTiN_2$	9517	85770	2.1 (2.1)	In_2S_3	22216	151645	2.1 (2.1)	Ca_4Bi_2O	551873	416137	2.1 (2.3)
Cs_2CuF_6	28692	65259	2.1 (2.2)	$PdSeO_3$	545482	249504	2.1 (2.4)	$TaCu_3Te_4$	9295	80282	2.1 (2.4)
Na_2CuAs	15685	43937	2.1 (2.3)	CuBr	22913	30090	2.1 (2.1)	$RbCuO_2$	7467	15096	2.1 (2.4)
KZnP	7437	12160	2.1 (2.1)	Na_2CuP	7639	1153	2.1 (2.4)	K_2VCuS_4	15147	81414	2.1 (2.4)
Rb_2VCuS_4	15219	84302	2.1 (2.4)	$HfSnS_3$	8725	65667	2.1 (2.1)	Ag_2PdCl_4	28557	65239	2.1 (2.2)
$Tl_2Sn(AsS_3)_2$	6023	300252	2.1 (2.2)	$K_2Pd_3S_4$	9910	41885	2.1 (2.2)	$KInTe_2$	19851	73410	2.1 (2.3)
$AgHgAsS_3$	6215	653762	2.1 (2.3)	NaP	7440	14009	2.1 (2.1)	$FeBr_2$	22880	409571	2.1 (2.1)
$BaCu_2SnS_4$	17954	52685	2.1 (2.1)	$Cr_2Ag_2O_7$	504441	2433	2.1 (2.1)	$BaPt_2S_3$	29289	201146	2.1 (2.3)
$FeSO_4$	19254	240947	2.1 (2.1)	Sc_2CdS_4	10953	94994	2.2 (2.2)	In_6Ge_2PtO9	22186	170897	2.2 (2.4)
$RbInTe_2$	22255	75346	2.2 (2.5)	Ca_2NCl	22936	153101	2.2 (2.3)	Te_3Cl_2	27628	105	2.2 (2.3)
K_2PtBr_6	27691	23771	2.2 (2.2)	K_4CdAs_2	29585	300190	2.2 (2.3)	$NaTlO_2$	3056	644919	2.2 (2.3)

Ca_4Sb_2O	13660	16353	2.2 (2.5)	Ba_2SiTe_4	14448	49751	2.2 (2.2)	$NaSe_2$	15514	402584	2.2 (2.3)
$AgAuF_4$	16060	90071	2.2 (2.2)	Hg_2GeO_4	13995	26340	2.2 (2.2)	Na_3P	1598	171012	2.2 (2.2)
$RhBr_3$	504719	28245	2.2 (2.3)	KPt_2S_3	510130	40062	2.2 (2.2)	PtS_2	762	659963	2.2 (2.3)
CsTe	8361	83351	2.2 (2.2)	Na_2AgAs	8411	49007	2.2 (2.2)	$Ba(AgS)_2$	8579	50183	2.2 (2.2)
Na_3SbSe_4	8703	65141	2.2 (2.2)	Ca_2ZnN_2	8818	69049	2.2 (2.3)	Sr_2ZnN_2	9306	80376	2.2 (2.2)
Ba_2HfS_4	9321	80652	2.2 (2.2)	ZrS_3	9921	42073	2.2 (2.3)	HfS_3	9922	42074	2.2 (2.2)
$NaLi_2Sb$	5077	54244	2.2 (3.0)	$GaAgS_2$	5343	156785	2.2 (2.2)	$Sr_5Mo_2N_7$	31231	413932	2.2 (2.2)
BaP_{10}	504809	35295	2.2 (2.4)	Rb_5GeP_3	17978	300186	2.2 (2.2)	Ag_3PS_4	12459	416585	2.2 (2.2)
KLi_2As	28994	78938	2.2 (2.2)	$HgAsO_3$	30284	411230	2.2 (2.6)	WS_2	224	56014	2.2 (2.3)
$VNCl_4$	27868	28128	2.2 (2.2)	$BaHgS_2$	28007	32648	2.2 (2.2)	Sr_3GaN_3	7191	281259	2.2 (2.3)
GaSe	1943	43540	2.2 (2.2)	$Hf(Te_2Cl_3)_2$	29419	401589	2.2 (2.2)	$HgPSe_3$	7293	2565	2.2 (2.2)
$Ba_4NaCu(CO_5)_2$	6841	80606	2.2 (2.7)	K_2VAgS_4	8900	66840	2.2 (2.3)	$K(SnSe_2)_2$	28769	72386	2.2 (2.4)
La_2S_3	7475	15151	2.2 (2.2)	$SrTaNO_2$	552454	411137	2.2 (2.2)	$RbCuSe_4$	18365	404225	2.2 (2.2)
Hg_2P_3Br	28874	74770	2.2 (2.2)	$AgHg_3SbO_6$	12362	170764	2.2 (2.3)	ZrS_2	1186	56012	2.3 (3.0)
Li_2PbO_3	22450	35182	2.3 (2.4)	$NaInSe_2$	22473	25558	2.3 (2.5)	K_2PdCl_6	23067	33709	2.3 (2.3)
$CsSnBr_3$	27214	4071	2.3 (2.3)	$CsGeI_3$	28377	62559	2.3 (2.3)	$PAuS_4$	30938	413009	2.3 (2.5)
Hf_3N_4	11660	97997	2.3 (2.3)	Ag_3AsS_3	4431	61806	2.3 (2.7)	$ZnSiP_2$	4763	648145	2.3 (2.3)
AsSeI	505373	200799	2.3 (2.3)	$K_2Cd_2O_3$	7534	16223	2.3 (2.3)	$CaPdF_4$	8161	32674	2.3 (2.3)
$K_3Sb_2Au_3$	9273	78977	2.3 (2.5)	K_5P_2Au	14624	40700	2.3 (2.4)	$NaAg_3S_2$	16992	73198	2.3 (2.3)
Tl_2TeS_3	17172	391285	2.3 (2.5)	BiTeI	22965	74501	2.3 (2.4)	Ba_5P_4	17566	413273	2.3 (2.5)
$KGaTe_2$	17965	411170	2.3 (2.3)	Cs_2VAgS_4	8684	50460	2.3 (2.4)	KSe	9268	73172	2.3 (2.7)
LiBeP	9915	42037	2.3 (2.6)	Ag_2HgI_4	23485	150343	2.3 (2.3)	$NbCu_3Se_4$	4043	628479	2.3 (2.7)
Rb_2SnAs_2	8931	71223	2.3 (2.4)	K_2PAu	9687	300201	2.3 (2.3)	$AlCuTe_2$	8017	28735	2.3 (2.3)
Cs_2SnAs_2	8934	71226	2.3 (2.5)	SbI_3Cl_8	23536	32662	2.3 (2.3)	K_2TiS_3	28766	72377	2.3 (2.3)
KP	7441	14010	2.3 (2.3)	$PdSO_4$	28952	79559	2.3 (2.3)	Rb_2VAgS_4	8901	66841	2.3 (2.4)
Cd_2GaAgS_4	6356	170108	2.3 (2.3)	$BaZrS_3$	540771	23288	2.3 (2.3)	Na_2PtS_2	10246	87219	2.4 (2.8)
Cs_3Sb	10378	53243	2.4 (2.7)	$LiInTe_2$	20782	162674	2.4 (2.4)	ZnO	2133	163380	2.4 (2.4)
InBr	22870	55189	2.4 (2.6)	AgCl	22922	64734	2.4 (4.1)	Ga_2PdI_8	30946	413230	2.4 (2.5)
Cs_2TiS_3	3247	660177	2.4 (2.5)	BaLiP	13277	416890	2.4 (2.4)	$AlAgSe_2$	14091	28745	2.4 (2.4)
$Cd(GaSe_2)_2$	3772	163949	2.4 (2.4)	$Cs_2Pd_3S_4$	510268	26250	2.4 (2.5)	CdS	672	154188	2.4 (2.4)
Li_2PdO_2	7608	61199	2.4 (2.7)	Cs_2O	7988	27919	2.4 (3.1)	$Ba(MgAs)_2$	8280	30916	2.4 (2.8)
SiP_2	9996	43098	2.4 (2.4)	$K_2NaGaAs_2$	9676	300129	2.4 (2.4)	$Cs_2Pt_3Se_4$	14338	33893	2.4 (2.5)
$Tl_2B_2Se_7$	16183	411468	2.4 (2.4)	Na_5SiAs_3	18139	300188	2.4 (2.4)	$CsGaTe_2$	17688	402613	2.4 (2.4)
$K_2In_3AgSe_6$	21705	54859	2.4 (2.4)	$Tl_2Au_4S_3$	29898	51235	2.4 (2.4)	MoS_2Cl_3	504716	28062	2.4 (2.4)
$InGaSe_3$	504952	62930	2.4 (2.4)	$AlCuSe_2$	8016	28734	2.4 (2.4)	$BaSnO_3$	3163	43138	2.4 (2.6)
K_4HgAs_2	29484	402573	2.4 (2.4)	Li_2PdO_2	545750	19007	2.4 (2.8)	HgO	1224	40316	2.4 (2.8)
HgI_2	23192	150345	2.4 (2.4)	Nb_2SnO_6	3324	163815	2.4 (2.5)	$NaAsS_2$	5942	655219	2.4 (2.4)
$KNb(CuSe_2)_2$	6599	655976	2.4 (2.4)	$LaCuS_2$	4841	415078	2.4 (2.4)	Tl_3BSe_3	28490	40375	2.4 (2.6)
$CrHgO_4$	19380	416147	2.4 (2.4)	Cu_3PS_4	3934	412240	2.4 (2.4)	$CsLa_2CuSe_4$	505815	93680	2.4 (2.5)
Sb_2S_3	2809	171853	2.4 (2.5)	$NaCoO_2$	18921	96428	2.4 (2.5)	Na_6P_4W	9007	71647	2.4 (2.4)
$BaLaCuTe_3$	17063	88715	2.4 (2.4)	Ta_2FeO_6	31755	401264	2.4 (2.4)	Ca_3PN	11824	106350	2.5 (2.5)
GaP	2490	635041	2.5 (2.7)	K_2PdBr_4	27138	1982	2.5 (2.6)	Ta_3N_5	27488	16253	2.5 (2.6)
$MgSiP_2$	2961	642734	2.5 (2.5)	Al_2HgSe_4	3038	33827	2.5 (2.5)	$BaZrN_2$	3104	74905	2.5 (2.5)
KAg_2PS_4	12532	420033	2.5 (3.3)	Si_4P_4Ru	14983	79006	2.5 (2.6)	$SrLi_4N_2$	15845	87413	2.5 (2.7)
CdP_2	913	62336	2.5 (2.6)	$CdSiP_2$	4666	44260	2.5 (2.5)	$RbAuBr_4$	510267	26022	2.5 (2.6)
K_2PdO_2	540584	6158	2.5 (2.6)	$BaCdO_2$	7899	25555	2.5 (2.6)	K_2PtS_2	7928	26258	2.5 (3.0)
Rb_2PtS_2	7929	26259	2.5 (2.9)	$Ba(MgP)_2$	8278	30914	2.5 (3.1)	PtF_4	8943	71579	2.5 (2.5)
RbTeAu	9008	71652	2.5 (2.5)	$Rb_3Sb_2Au_3$	9274	78978	2.5 (2.7)	$AlAgO_2$	9631	95662	2.5 (3.4)
$Ti(PS_3)_2$	13666	16403	2.5 (2.5)	Ca_6GaN_5	17875	33795	2.5 (2.6)	Sr_3TaAs_3O	18199	409567	2.5 (2.5)
AgI	22925	161579	2.5 (2.5)	P_2PtO_7	29282	200871	2.5 (2.5)	$Na_2W_4O_{13}$	32533	6141	2.5 (3.0)
$RbIn_3S_5$	542654	59667	2.5 (2.5)	$LiAlB_{14}$	8204	35336	2.5 (2.9)	Rb_2SiAs_2	6960	60617	2.5 (2.8)
CuCl	22914	23988	2.5 (2.5)	K_2SiAs_2	6984	40426	2.5 (2.8)	Na_4HgP_2	28591	67260	2.5 (2.6)
$Ba(AuO_2)_2$	9297	80327	2.5 (2.5)	As_2Se_3	909	44058	2.5 (2.7)	Ba_2GeSe_4	11902	414166	2.5 (2.5)

$Si_2Hg_6O_7$	28712	69123	2.5 (2.8)	SiAs	1863	153457	2.5 (2.6)	InS	20094	660105	2.5 (2.7)
Ba_2PbO_4	20098	66544	2.5 (3.0)	SbSeI	22996	31292	2.5 (2.6)	Sc_2S_3	401	654308	2.5 (2.5)
Cs_6GaSb_3	9697	300216	2.5 (2.5)	TlV_3O_8	18996	65773	2.5 (2.5)	TlP_5	27411	15021	2.5 (2.6)
WO_3	510417	653651	2.5 (2.5)	$CsYHgSe_3$	11123	281440	2.6 (2.6)	$CdIn_2O_4$	21047	159740	2.6 (2.7)
$CsIn_5S_8$	22007	40878	2.6 (2.7)	Li_3N	2251	156902	2.6 (2.7)	$Nb(SCl)_2$	27362	10484	2.6 (2.6)
$IrBr_3$	27397	14212	2.6 (2.7)	Ag_2S	31053	98454	2.6 (2.8)	$SrPdF_4$	12622	108990	2.6 (2.6)
$Rb_2Pt_3S_4$	4030	649518	2.6 (2.7)	Cs_2TeI_6	540957	38105	2.6 (2.9)	ZrBrN	541912	87797	2.6 (2.6)
$NaRhO_2$	8830	66280	2.6 (2.7)	Tl_3AsS_3	9791	100292	2.6 (2.8)	RbSe	9063	73177	2.6 (2.8)
Rb_3AsSe_4	18305	404080	2.6 (2.6)	Na_5SnP_3	18317	300189	2.6 (2.6)	Sc_2PbSe_4	542826	154528	2.6 (2.7)
SnO_2	856	157449	2.6 (2.6)	Cu_2PbO_2	29396	400657	2.6 (2.8)	$Rb_2Sn_2O_3$	7863	24816	2.6 (2.6)
$Sr_5(AuO_4)_2$	28796	71965	2.6 (2.6)	$CdSi(CuS_2)_2$	6449	16924	2.6 (2.6)	$Sr(AuO_2)_2$	9298	80328	2.6 (2.7)
$NaAgF_4$	7386	9903	2.6 (2.7)	$AgSbS_2$	3922	94647	2.6 (2.7)	$AuCl_3$	27647	22146	2.6 (2.7)
Ca_3AsN	4192	657356	2.6 (2.6)	$NaAuO_2$	20343	409547	2.6 (2.9)	$Ba_3In_2O_6$	20352	65258	2.6 (3.1)
$KHgF_3$	7483	15170	2.6 (2.6)	$SnGeS_3$	5045	637796	2.6 (2.7)	$LiRhO_2$	14115	29213	2.6 (2.6)
$RbHgSbSe_3$	6300	90067	2.6 (2.8)	$RbIn_5S_8$	20938	40877	2.7 (2.8)	AlAs	2172	659140	2.7 (3.2)
In_2O_3	22323	24325	2.7 (2.7)	Bi_2S_3	22856	201066	2.7 (2.7)	Br	23154	201692	2.7 (2.7)
NaSi	2402	409953	2.7 (2.9)	$RhCl_3$	27770	25764	2.7 (2.8)	$Pd(SeCl_3)_2$	28175	39435	2.7 (2.8)
$PdCl_2$	29487	404624	2.7 (2.8)	Cs_2PtBr_6	30062	77381	2.7 (2.7)	$P_2Pd_3S_8$	3006	35361	2.7 (2.8)
LiMgAs	12558	107954	2.7 (3.2)	$KYTe_2$	16763	419995	2.7 (3.6)	K_2AgSb	7643	1155	2.7 (2.8)
Al_2ZnTe_4	7908	25639	2.7 (2.7)	Al_2CdTe_4	7909	25640	2.7 (2.7)	NaBeAs	9573	100091	2.7 (2.9)
$Na_2B_2Se_7$	5004	658692	2.7 (2.8)	$Ca(MgAs)_2$	9564	100041	2.7 (3.0)	$KBaPSe_4$	18156	414637	2.7 (2.7)
IBr	27639	22120	2.7 (2.8)	$KAuCl_4$	27181	2607	2.7 (2.7)	$Rb_4Zr_3Se_{14}$	542013	280636	2.7 (2.8)
Na_3MoN_3	541291	67565	2.7 (2.7)	NaMgAs	5962	41798	2.7 (2.7)	BiTeCl	28944	79362	2.7 (2.8)
$VHgO_3$	541588	82242	2.7 (2.8)	$InSbS_3$	21365	300207	2.7 (2.8)	$CsCuF_4$	540921	35264	2.7 (2.8)
$Rb_2NbCuSe_4$	15222	84305	2.7 (3.0)	Na_2ZrSe_3	7219	412158	2.7 (2.9)	$K_2NbCuSe_4$	9003	73324	2.7 (2.8)
$Ca(AuO_2)_2$	2898	83386	2.7 (2.7)	Cs_2ZrSe_3	9856	409294	2.7 (2.7)	$HfPbS_3$	22147	65668	2.7 (2.7)
AgHgSI	23140	54796	2.7 (2.7)	Hg_2WO_4	32542	90085	2.7 (3.0)	$SrCu_2GeS_4$	18685	10005	2.7 (2.8)
$K_2LiGaAs_2$	9703	401208	2.7 (2.7)	$ZrFeCl_6$	28208	39666	2.7 (2.7)	$BaHfN_2$	10322	50994	2.8 (2.8)
$NaBiO_2$	22984	173624	2.8 (2.8)	$Ca_3C_3Cl_2$	28160	33818	2.8 (2.9)	K_4CdP_2	28302	61084	2.8 (2.9)
$TlAuCl_4$	28368	62107	2.8 (2.8)	Ga_2TeSe_2	28423	64617	2.8 (2.8)	$Cs_2Au_2Se_3$	29194	85708	2.8 (2.8)
$K_3Ag_3As_2$	14206	32016	2.8 (2.8)	$ZnPdF_6$	13983	26165	2.8 (2.8)	$RbYTe_2$	16764	419996	2.8 (3.6)
$La_4Se_3O_4$	4412	419128	2.8 (2.8)	Tl_3BO_3	4584	10196	2.8 (2.8)	Ga_2HgS_4	4809	67220	2.8 (2.8)
Tl_3BS_3	505399	202528	2.8 (3.0)	Cl_2O	505466	407768	2.8 (2.8)	$RbBiS_2$	505761	52735	2.8 (3.2)
$CsNbN_2$	8978	72546	2.8 (2.8)	$Sr_3(AlP_2)_2$	9843	409134	2.8 (2.8)	$AgAsS_2$	13740	18101	2.8 (2.9)
$CsLaCdTe_3$	12491	173316	2.8 (2.8)	K_7TaAs_4	18073	380110	2.8 (2.9)	InI	23202	55179	2.8 (2.9)
Na_2PdCl_4	29359	202971	2.8 (2.8)	Rb_2TeI_6	28070	36009	2.8 (3.0)	$Cs_3Na_2SnP_3$	17707	50533	2.8 (2.8)
$Sr(InSe_2)_2$	21733	41555	2.8 (2.8)	$NbCu_3S_4$	5621	108392	2.8 (3.2)	HgI	22859	157981	2.8 (2.9)
SnS_2	1170	650992	2.8 (3.1)	$LaBi_2IO_4$	546672	92424	2.8 (3.2)	$Cs(SbS_2)_2$	8890	67976	2.8 (3.0)
$TlSbS_2$	28230	35498	2.8 (2.8)	Tl_2PAuS_4	9510	85680	2.8 (2.9)	$K_2Sn_2O_3$	8624	40463	2.8 (2.8)
NaAgO	6983	49752	2.8 (2.9)	LaSO	28626	68498	2.8 (3.4)	LiCuO	5127	49755	2.8 (3.1)
K_3InP_2	20256	300141	2.8 (2.8)	$KTa(CuSe_2)_2$	6013	659203	2.8 (2.8)	$RbTa(CuSe_2)_2$	11925	414274	2.8 (2.9)
$Cs_2Ti(CuSe_2)_2$	10489	280646	2.8 (3.0)	$Cs_2NbCuSe_4$	15223	84306	2.8 (3.1)	Ba_2VN_3	17696	80177	2.8 (2.8)
Sr_2VN_3	17012	80176	2.8 (2.8)	Ca_2VN_3	17892	409644	2.8 (2.9)	$NaAlTe_2$	10163	44701	2.9 (3.0)
Rb_2PtC_2	10919	94395	2.9 (2.9)	Sr_2PbO_4	20944	16806	2.9 (3.1)	K_2NaInP_2	21511	300132	2.9 (2.9)
Na_2PtO_2	22313	25018	2.9 (3.2)	CdO_2	2310	109339	2.9 (3.0)	Na_3BiO_4	27345	10319	2.9 (3.0)
K_2TeI_6	27688	23649	2.9 (3.1)	K_4BeAs_2	29584	300111	2.9 (2.9)	$ZnGeN_2$	2979	155463	2.9 (2.9)
MgB9N	30091	280938	2.9 (2.9)	RbAu	30373	58428	2.9 (4.0)	Ga_2PdBr_8	30945	413229	2.9 (2.9)
$BaPdF_4$	12623	108991	2.9 (2.9)	SrLiP	13276	416889	2.9 (3.0)	B_6O	1346	656231	2.9 (2.9)
AlP	1550	609021	2.9 (4.6)	BaAgTeF	16742	419382	2.9 (2.9)	InTeI	505356	100703	2.9 (2.9)
Ag_2SO_4	5625	52356	2.9 (3.1)	HgF	706	72354	2.9 (3.7)	AuF_3	942	80478	2.9 (3.0)
K_2SiP_2	8235	36367	2.9 (3.3)	Sr_4As_2O	8299	33904	2.9 (2.9)	K_4HgP_2	8753	67263	2.9 (3.0)
Ca_4As_2O	8789	68203	2.9 (3.1)	Cs_2SiP_2	8932	71224	2.9 (3.4)	NbNO	7596	1031	2.9 (3.0)
Hg_2NO_4	5824	61437	2.9 (2.9)	$K_2NaAlAs_2$	9069	73280	2.9 (3.0)	$Cs_2Pt_3S_4$	13992	26266	2.9 (2.9)

$K_4Ta_2S_{11}$	18664	410672	2.9 (2.9)	TlI_3	28329	61349	2.9 (3.0)	K_3SnSe_3	541875	410863	2.9 (3.0)
Rb_2S_3	7446	14092	2.9 (3.0)	K_2CuP	8446	61082	2.9 (2.9)	K_2CuAs	15684	43936	2.9 (2.9)
K_2AgP	9778	402572	2.9 (2.9)	SrCuSeF	21228	172798	2.9 (2.9)	$BaSnS_2$	12181	2587	2.9 (3.0)
SbSI	23041	28305	2.9 (3.0)	$ReNClF_5$	23098	33542	2.9 (2.9)	$BaYAgSe_3$	6647	104237	2.9 (3.1)
$LiInSe_2$	20187	56532	2.9 (2.9)	$Ba(AlTe_2)_2$	28505	41165	2.9 (2.9)	GeAsSe	505360	100828	2.9 (2.9)
Sr_4PdO_6	505606	88135	2.9 (2.9)	$Na_2LiGaAs_2$	9722	402111	2.9 (2.9)	YSF	10086	87130	3.0 (3.0)
$KSbS_2$	11703	60138	3.0 (3.1)	Ca_2PbO_4	21137	36629	3.0 (3.2)	$As(BrF_2)_3$	28159	33811	3.0 (3.1)
$Pd(SCl_3)_2$	28174	39434	3.0 (3.1)	Sn_2OF_5	29590	409393	3.0 (3.6)	Na_3AgO_2	3527	24817	3.0 (3.1)
NaSrP	13275	416887	3.0 (3.0)	Tl_3VS_4	5513	655086	3.0 (3.0)	Tl_2PtCl_6	504695	26710	3.0 (3.0)
AuBr	505366	200287	3.0 (3.0)	Ca_4P_2O	5380	402952	3.0 (3.2)	LaSF	5394	93350	3.0 (3.0)
$CsBiS_2$	541378	72975	3.0 (3.1)	$K_2B_2Se_7$	542637	658693	3.0 (3.1)	SiP	2798	87149	3.0 (3.0)
GaN	805	153890	3.0 (3.0)	$Zr(PS_3)_2$	8203	35298	3.0 (3.2)	Sr_4P_2O	8298	33903	3.0 (3.1)
$Cs_2NbAgSe_4$	14637	50464	3.0 (3.1)	$BaLa_2ZnS_5$	16452	93711	3.0 (3.1)	$NaBiO_3$	23054	91776	3.0 (3.0)
BiIO	22987	24610	3.0 (3.3)	Al_2PdCl_8	504547	15595	3.0 (3.0)	$K_3Cu_3As_2$	14205	32015	3.0 (3.1)
$CsCu_3O_2$	553303	413342	3.0 (3.1)	$Hg_3(TeBr)_2$	27853	27402	3.0 (3.0)	$PPbSe_3$	20316	655565	3.0 (3.1)
$NaNb(CuS_2)_2$	6181	84301	3.0 (3.0)	K_4ZnP_2	11719	67261	3.1 (3.1)	PBr_5	22874	15559	3.1 (3.2)
K_2PdCl_4	22956	27522	3.1 (3.1)	$PtCl_2$	23290	98668	3.1 (3.1)	$IrCl_3$	27666	23171	3.1 (3.2)
KTlO	27716	1570	3.1 (3.5)	$K_3Al_2As_3$	28347	60950	3.1 (3.1)	$CdPdF_6$	13984	26166	3.1 (3.1)
Tl_2SiSe_3	14241	35042	3.1 (3.3)	Y_2MgSe_4	15803	76052	3.1 (3.1)	Mg_3P_2	2514	642725	3.1 (3.1)
Rb_2GeSe_3	9794	402719	3.1 (3.1)	SnI_2	27194	2831	3.1 (3.2)	ZrP_2S_7	31014	50701	3.1 (3.2)
$K_3Cu_3P_2$	7439	12163	3.1 (3.2)	YBi_2BrO_4	553243	92418	3.1 (3.4)	YBi_2IO_4	551816	92432	3.1 (3.5)
$HgPS_3$	27178	2564	3.1 (3.2)	V_2O_5	510583	157988	3.1 (3.3)	SbSBr	22971	61802	3.1 (3.2)
Sr_2GeSe_4	30293	413023	3.1 (3.1)	K_2NaGaP_2	9666	300112	3.1 (3.2)	$Rb_2Ti(CuS_2)_2$	7129	280644	3.1 (3.3)
SeBr	540943	37017	3.1 (3.2)	$KAgF_4$	7387	72715	3.1 (3.2)	$NbAgO_3$	12725	55649	3.1 (3.6)
$HgSO_4$	3228	100316	3.1 (3.4)	Tl_3SbS_4	15360	100849	3.1 (3.1)	$Hg(AuF_4)_2$	29170	85414	3.2 (3.2)
$PtPbF_6$	20458	4057	3.2 (3.5)	PbF_3	20652	23467	3.2 (3.2)	Rb_2PbO_3	21489	1413	3.2 (3.2)
$InGaO_3$	22606	30339	3.2 (3.4)	K_2SeBr_6	23036	36228	3.2 (3.5)	BeTe	252	616439	3.2 (4.9)
InOF	27175	2521	3.2 (3.2)	$Ca(AuF_6)_2$	28153	39315	3.2 (3.2)	$Cd(AuF_4)_2$	29169	85413	3.2 (3.2)
P_2PdO_6	29274	200677	3.2 (3.3)	$AsCl_5$	30106	412103	3.2 (3.2)	K_3GeSe_3	14435	47112	3.2 (3.2)
$Ba(BeN)_2$	12927	415304	3.2 (3.2)	CaTe	1519	619618	3.2 (4.2)	Ba_2PdF_6	505621	88802	3.2 (3.2)
Cs_2PtC_2	505825	94397	3.2 (3.2)	AsS	542810	153281	3.2 (3.2)	BaS_2	684	42134	3.2 (3.2)
$MgPdF_6$	7921	26163	3.2 (3.2)	HgF_2	8177	33614	3.2 (3.2)	$Rb_2B_2Se_7$	16184	411469	3.2 (3.3)
$Zn(AuF_4)_2$	17512	65286	3.2 (3.3)	$Ba_2SnSe_3F_2$	17805	171344	3.2 (3.2)	$RbPSe_6$	17945	170334	3.2 (3.2)
Na_3GeSe_3	18411	61400	3.2 (3.2)	RbI_3	28328	61348	3.2 (3.3)	$Cs_7Au_5O_2$	510075	95821	3.2 (3.3)
$KBi(WO_4)_2$	510667	419114	3.2 (3.3)	Rb_2WS_4	17048	281586	3.2 (3.2)	$AsSe_3(ClF_2)_3$	23575	75450	3.2 (3.3)
$CuBS_2$	12954	156413	3.2 (3.2)	$NaV(OF)_2$	18953	75418	3.2 (3.6)	LaCuSeO	552488	96758	3.2 (3.2)
YBi_2ClO_4	552604	92405	3.2 (3.4)	Ba_2BiSbO_6	23127	1429	3.2 (4.0)	V_2CdO_6	550436	15926	3.2 (3.2)
$Rb_2TaCuSe_4$	11924	414272	3.2 (3.4)	NaCuO	14580	49756	3.2 (3.3)	$Hg_2P_2S_7$	27171	2490	3.2 (3.5)
$Hg_3(TeCl)_2$	504706	27401	3.2 (3.2)	$K_2TaCuSe_4$	8972	72427	3.2 (3.3)	$KSb(PSe_3)_2$	7123	90152	3.2 (3.3)
$KPSe_6$	18625	170333	3.2 (3.2)	Na_4SnSe_4	28768	72384	3.2 (3.2)	Cs_2AgSbS_4	510710	55367	3.2 (3.2)
$TaTl(CuS_2)_2$	9815	402636	3.2 (3.2)	$SbBr_5F_6$	541259	69056	3.2 (3.2)	Ca_4PdO_6	10299	88134	3.2 (3.2)
$Mg(InS_2)_2$	20493	53096	3.3 (3.3)	Li_4PbO_4	22170	38350	3.3 (3.3)	KLi_6BiO_6	23582	72840	3.3 (3.3)
ICl_3	27729	24714	3.3 (3.3)	LiCaN	31468	107304	3.3 (3.3)	Li_2ZrN_2	3216	78790	3.3 (4.0)
Sr_2LiReO_6	12525	418991	3.3 (3.3)	Cd_2SiO_4	4530	50531	3.3 (3.4)	GeI_2	504756	23176	3.3 (3.6)
Ga_2S_3	539	34647	3.3 (3.3)	$Rb_2Cd(PSe_3)_2$	541897	50959	3.3 (3.4)	Au_2S	947	612282	3.3 (3.3)
$CdPS_3$	5328	79556	3.3 (3.7)	Ag_2SeO_3	16913	78388	3.3 (3.4)	CsI_3	22876	27252	3.3 (3.3)
Ca_2PI	23040	6068	3.3 (3.6)	TaTeBr9	29716	410949	3.3 (3.4)	Cs_2PdCl_4	30314	95812	3.3 (3.3)
K_2GeSe_3	9692	300233	3.3 (3.4)	$Sr(CuO)_2$	13900	25002	3.3 (3.3)	$GaCuI_4$	29403	400817	3.3 (3.3)
CsCuO	541037	37079	3.3 (3.3)	$TaCu_3S_4$	10748	53335	3.3 (3.7)	$Ba(GaSe_2)_2$	7841	24386	3.3 (3.4)
$Hg_3(SeCl)_2$	27851	27400	3.3 (3.3)	K_2SnSe_3	9693	300234	3.3 (3.3)	$MgCrO_4$	19120	18117	3.3 (3.4)
PbO	20442	647260	3.3 (3.7)	K_2PAuS_4	9509	85679	3.3 (3.3)	$YCuS_2$	10533	92458	3.3 (3.3)
$YCuPbS_3$	542802	152555	3.3 (3.5)	InI_2	505387	201607	3.3 (3.3)	$TlBr_2$	504527	14216	3.3 (3.3)
$Pt(SCl_4)_2$	28721	66012	3.3 (3.3)	$Zn(SbO_3)_2$	3188	30409	3.3 (3.3)	$K_3V_5O_{14}$	540787	24068	3.3 (3.4)

BaTe	1000	616165	3.4 (3.7)	CsAuO	10548	409553	3.4 (3.4)	$K_2Mg(PSe_3)_2$	11643	413168	3.4 (3.4)
Rb_2PtCl_6	23350	29028	3.4 (3.4)	Rb_2TeBr_6	23383	49521	3.4 (3.6)	GaTeCl	27449	15582	3.4 (3.4)
Be_4TeO_7	27608	1322	3.4 (3.4)	PI_2	29443	203216	3.4 (3.5)	RuS_3Cl_8	29568	410112	3.4 (3.4)
$Cd(GaO_2)_2$	3443	159739	3.4 (3.4)	GaS	2507	654685	3.4 (3.5)	KS	1287	43406	3.4 (3.7)
SiC	7631	156190	3.4 (4.5)	K_3SiTe_3	7657	1238	3.4 (3.6)	KPS_3	8267	33278	3.4 (3.4)
RbCaAs	9845	409177	3.4 (3.5)	Na_3AlP_2	5122	402081	3.4 (3.5)	$Mg(ScS_2)_2$	14307	37423	3.4 (3.4)
Li_2PdF_6	13985	26167	3.4 (3.4)	Sr_2LiReN_4	10556	411454	3.4 (3.4)	Cs_2WS_4	17361	249347	3.4 (3.4)
$RbSnI_3$	29405	400934	3.4 (3.4)	$CsSnI_3$	27381	14070	3.4 (3.5)	$Tl_6Si_2O_7$	27228	4230	3.4 (3.4)
Ca_4GeN_4	29808	280251	3.4 (3.4)	CsI_2Br	504641	23120	3.4 (3.4)	Ge_3N_4	13852	23672	3.4 (3.4)
$SbPbClO_2$	23138	36159	3.4 (3.4)	Rb_2SnSe_3	9145	74844	3.4 (3.4)	Ba_3BPO_3	9712	402017	3.4 (3.6)
Cs_2HgI_4	28421	63110	3.4 (3.4)	RbCuO	8665	40159	3.4 (3.4)	$HgMoO_4$	19363	2533	3.4 (3.6)
$K_2W_2O_7$	19037	67284	3.4 (3.9)	$CaCrO_4$	19215	83387	3.4 (3.4)	Ba_3BAsO_3	9793	402682	3.4 (3.5)
$Li_{10}BrN_3$	28989	78819	3.4 (3.7)	$Hg_2P_2O_7$	504981	59280	3.4 (3.8)	K_2TeSe_3	504959	63012	3.4 (3.5)
Al_2Se_3	11674	14373	3.5 (3.5)	$K_2Pb_2O_3$	20694	1412	3.5 (3.5)	BiSCl	23318	100173	3.5 (3.5)
Cs_2TeBr_6	23405	27695	3.5 (3.7)	AuI	27725	24619	3.5 (3.6)	Tl_2TeBr_6	31076	99127	3.5 (3.6)
Al_2CdSe_4	3159	51422	3.5 (3.5)	$LiAuF_4$	12263	9908	3.5 (3.5)	$NaTl_2RhF_6$	14037	27340	3.5 (3.5)
CsAgO	14579	49754	3.5 (3.5)	$Sr_2Sb_2O_7$	4103	77062	3.5 (3.8)	$ZnPtF_6$	8256	37444	3.5 (3.5)
RbAgO	8603	49753	3.5 (3.5)	Na_3AsSe_3	8686	50491	3.5 (3.5)	Rb_3BAs_2	9718	402082	3.5 (3.6)
RbCaSb	9846	409178	3.5 (3.6)	K_4BeP_2	9872	300110	3.5 (3.5)	$Hg_3(SF)_2$	7580	16927	3.5 (3.6)
RbAuSe	9731	402190	3.5 (3.6)	$TlBS_2$	8946	71593	3.5 (3.6)	RbAuO	10547	409552	3.5 (3.5)
K_2NbAgS_4	15214	84292	3.5 (3.6)	$RbSbS_2$	15366	200263	3.5 (3.5)	$Sr_3(GaN_2)_2$	16945	170441	3.5 (3.5)
K_2S_5	17146	44675	3.5 (3.5)	$Tl_3B_3S_{10}$	17823	73086	3.5 (3.5)	AsI_3	23218	56567	3.5 (3.6)
$KTlBr_4$	28048	35418	3.5 (3.5)	La_3AgSnS_7	542888	417316	3.5 (3.5)	SrCuSF	12444	157433	3.5 (3.5)
$Ba(CuO)_2$	7374	9456	3.5 (3.5)	SbI_3	23281	56569	3.5 (3.5)	$NaAuF_4$	7388	9905	3.5 (3.5)
KCuO	14296	37325	3.5 (3.6)	SrTe	1958	652879	3.5 (4.2)	$PbCN_2$	19727	410915	3.5 (3.8)
$NaInS_2$	20289	640036	3.5 (3.7)	$ScPS_4$	6999	67559	3.5 (3.6)	$BiVO_4$	613172	653651	3.5 (3.5)
$CaPSe_3$	11007	412765	3.6 (3.7)	ZnS	10695	162754	3.6 (3.6)	$ScAgO_2$	11022	95668	3.6 (4.0)
$CsBr_2F$	28650	69124	3.6 (3.7)	K_2PtCl_4	22934	37014	3.6 (3.6)	BiSBr	23324	31389	3.6 (3.6)
CsAu	2667	150971	3.6 (4.1)	TlF_3	2632	18029	3.6 (3.6)	Ga_2TeS_2	27255	8028	3.6 (3.6)
$MgPSe_3$	30943	413165	3.6 (3.6)	$KAuF_6$	12442	415874	3.6 (3.6)	K_2ZnTe_2	12535	420088	3.6 (3.7)
La_2TeO_2	4547	89557	3.6 (3.9)	K_2PdF_4	504853	33888	3.6 (3.7)	$Rb_2Zn_3O_4$	505501	40754	3.6 (3.6)
$LiInO_2$	5488	639886	3.6 (4.2)	Al_2HgS_4	7906	25635	3.6 (3.6)	Tl_4SiS_4	8479	59170	3.6 (3.8)
KAgO	8660	40154	3.6 (3.6)	LaSeF	7738	21010	3.6 (3.6)	$RbAu_3Se_2$	9385	82541	3.6 (3.8)
KAuSe	9881	40759	3.6 (3.7)	NaS_2	12180	2586	3.6 (3.6)	Ba_2LiReN_4	10555	411453	3.6 (3.6)
Rb_2S_5	16911	100321	3.6 (3.6)	$Ba_3(AlN_2)_2$	17133	410578	3.6 (3.7)	Na_3SiTe_3	17291	15579	3.6 (3.6)
$Mg(AuF_4)_2$	17555	65287	3.6 (3.6)	K_4SnSe_4	18132	72385	3.6 (3.6)	$LiGaI_3$	29345	202642	3.6 (3.6)
ZrI_4	541112	62243	3.6 (3.6)	HgBr	23177	157980	3.6 (3.9)	NClO	505727	411511	3.6 (3.7)
$SrSnO_3$	2879	161783	3.6 (3.7)	Ba_2CaMoO_6	19403	45317	3.6 (3.7)	As_2PbO_6	20015	81063	3.6 (4.0)
$V_2Cd_2O_7$	18740	62081	3.6 (3.8)	$NbAgO_3$	5537	55646	3.6 (3.6)	Na_3SbS_4	10167	44707	3.7 (3.7)
$BaPSe_3$	11008	412768	3.7 (3.8)	$CsYCdSe_3$	11116	281433	3.7 (3.7)	$SrMg_2N_2$	10550	410826	3.7 (3.7)
$KInP_2S_7$	22583	91755	3.7 (3.7)	PCl_5	23228	26661	3.7 (3.7)	$NClO_6$	27774	25817	3.7 (3.7)
Rb_2NaRhF_6	14038	27341	3.7 (3.7)	K_2NaRhF_6	14039	27342	3.7 (3.7)	$Cd(GaS_2)_2$	4452	619872	3.7 (3.7)
InBrO	504656	24059	3.7 (3.8)	$CsPS_3$	504838	33277	3.7 (3.7)	$AlAgS_2$	5782	604698	3.7 (3.7)
Al_2ZnSe_4	7907	25636	3.7 (3.7)	$Ba_4Li(SbO_4)_3$	7971	202200	3.7 (3.8)	$CdPtF_6$	5858	78906	3.7 (3.7)
Sr_3ScRhO_6	18247	51137	3.7 (3.7)	KAlTe	18347	411171	3.7 (3.7)	LaI_3	27979	31596	3.7 (3.8)
$NbAlCl_8$	28358	62029	3.7 (3.7)	Rb_2CdO_2	28364	62054	3.7 (3.7)	Na_4SeO_5	29871	411401	3.7 (3.8)
$K_2Zn_3O_4$	504936	62146	3.7 (3.7)	Ba_2SnS_4	541832	42036	3.7 (3.7)	$AgNO_3$	552185	374	3.7 (4.0)
Cs_2HfI_6	29398	201308	3.7 (3.8)	$SrPSe_3$	7198	412766	3.7 (3.7)	Hg_2SO_4	7461	15005	3.7 (4.3)
$V_2Zn_2O_7$	19707	2886	3.7 (3.8)	$PbWO_4$	540719	811	3.7 (3.7)	OsO_3F_2	28845	73732	3.7 (3.7)
K_2TeBr_6	22963	65115	3.8 (3.9)	BiPbClO$_2$	23084	31860	3.8 (3.8)	Ba_2YBiO_6	23137	65555	3.8 (3.8)
$TlCl_2$	27205	4031	3.8 (3.8)	SBr	28099	37020	3.8 (3.9)	$BiClF_8$	28194	39555	3.8 (3.8)
B_6P	28395	62748	3.8 (4.0)	$KBiO_2$	30988	16239	3.8 (3.8)	$Ba_2ZnGe_2S_6O$	17244	14174	3.8 (3.8)
$CsBr_3$	504635	22130	3.8 (3.8)	$KAgCO_3$	541966	409484	3.8 (3.8)	$SrCrO_4$	542885	160793	3.8 (3.8)

B_6As	624	107916	3.8 (3.8)	$CsRb_2PdF_5$	8202	35286	3.8 (3.8)	RbS	9062	73176	3.8 (3.9)
K_3BP_2	9664	300104	3.8 (3.9)	$K_3Nb_3(BO_6)_2$	15248	85091	3.8 (3.8)	K_3AsSe_3	18594	50492	3.8 (3.8)
TlI	22858	55193	3.8 (3.9)	$PICl_6$	27824	26594	3.8 (3.8)	K_2CdO_2	27742	25004	3.8 (3.8)
CdI_2	28248	38116	3.8 (3.9)	$LiInI_4$	541001	36599	3.8 (3.8)	$AlCuS_2$	4979	42124	3.8 (3.8)
K_2NaAlP_2	9068	73279	3.8 (3.9)	Sb_2O_3	2136	647390	3.8 (3.8)	$CdMoO_4$	19039	84455	3.8 (3.9)
Rb_2TaCuS_4	11923	414271	3.8 (4.0)	$Ba_2Bi_2O_5$	28670	69864	3.8 (3.8)	$AlCuO_2$	3748	60844	3.8 (4.5)
Sr_3CdPtO_6	10392	280518	3.8 (3.9)	$KSbO_2$	10417	411214	3.9 (3.9)	$CsGeCl_3$	22988	62557	3.9 (3.9)
$MoPbO_4$	25054	56111	3.9 (4.0)	$AlICl_6$	27935	26510	3.9 (3.9)	Cs_2PtCl_4	29216	100155	3.9 (3.9)
$BrNO_3$	29526	407765	3.9 (3.9)	$SrTiO_3$	4651	170091	3.9 (3.9)	$LiBiO_2$	504893	46022	3.9 (3.9)
$KAuF_4$	5309	10327	3.9 (3.9)	$TaTl_3Se_4$	10644	52431	3.9 (3.9)	$Sr_2SnS_3F_2$	17676	171346	3.9 (3.9)
Ba_2CdS_3	18309	66654	3.9 (3.9)	PI_3	27529	311	3.9 (3.9)	Na_3TlO_2	29454	202028	3.9 (4.1)
$Sr(InS_2)_2$	21781	300176	3.9 (3.9)	$HgPb_2(ClO)_2$	546862	74973	3.9 (4.3)	$Cd(AsO_3)_2$	7128	280576	3.9 (4.2)
MgV_2O_6	504510	10391	3.9 (3.9)	Rb_2TiCl_6	27827	26689	3.9 (3.9)	$SbCl_5$	23176	250363	3.9 (3.9)
$Rb_2Cr_2O_7$	19658	15034	3.9 (3.9)	$Hf(PS_3)_2$	14444	47228	3.9 (4.0)	$Mg_2V_2O_7$	32500	2321	3.9 (3.9)
$Sr(BeN)_2$	11919	413356	4.0 (4.1)	$CsAgBr_2$	23454	150301	4.0 (4.3)	CsS	29266	200474	4.0 (4.2)
GaI_3	30954	413457	4.0 (4.0)	$RbAuF_4$	3419	33952	4.0 (4.0)	Al_2ZnS_4	4842	76278	4.0 (4.0)
Rb_2PbO_2	504598	2267	4.0 (4.0)	GeS_2	542613	654304	4.0 (4.1)	$CaMg_2N_2$	5795	411175	4.0 (4.0)
Ba_2ZnS_3	5587	653999	4.0 (4.0)	Rb_3BP_2	9720	402084	4.0 (4.1)	Li_2PtF_6	13986	26168	4.0 (4.0)
SrTlPS$_4$	17090	249346	4.0 (4.0)	Mg_2GeS_4	17441	23525	4.0 (4.1)	Sr_2NbN_3	17701	51028	4.0 (4.1)
$RbLiZn_2O_3$	18422	67145	4.0 (4.0)	$CsICl_2$	22990	14260	4.0 (4.1)	SCl_2	28128	38351	4.0 (4.0)
$K_3Nb_3Si_2O_{13}$	17059	15938	4.0 (4.0)	RbAuS	9010	71654	4.0 (4.2)	$AsPO_5$	14367	36649	4.0 (4.1)
$Ba(InS_2)_2$	21943	46020	4.0 (4.0)	$RbLaSe_2$	7176	281067	4.0 (4.4)	Sc_2SO_2	7288	2450	4.0 (4.4)
$CsCu_3S_2$	7786	23326	4.0 (4.1)	CaV_2O_6	32526	21064	4.0 (4.1)	Tl_3VO_4	32479	80667	4.0 (4.0)
K_2LiAlP_2	6450	77275	4.0 (4.2)	$ScVO_4$	19247	78073	4.0 (4.0)	$RbLiCrO_4$	18741	72548	4.0 (4.1)
$BaCrO_4$	19662	62560	4.0 (4.0)	Li_2GePbS_4	19896	281011	4.0 (4.1)	$CsCu_2Br_3$	23017	49613	4.0 (4.0)
Sr_2GeS_4	4578	25381	4.0 (4.1)	VCl_3O	504820	36214	4.0 (4.0)	$Ba(AuF_4)_2$	28719	65289	4.0 (4.0)
$InPS_4$	20790	1699	4.1 (4.2)	$SiSe_2$	22142	651863	4.1 (4.1)	TlBr	22875	61532	4.1 (4.1)
BrF_3	23297	31689	4.1 (4.3)	KSn_2Br_5	23541	151983	4.1 (4.3)	Tl_2TeCl_6	27833	26705	4.1 (4.3)
Bi_3ClO_4	29558	409330	4.1 (4.3)	$KTaO_3$	3614	56440	4.1 (4.6)	$NaGe_2N_3$	14433	47100	4.1 (4.2)
Nb_2O_5	1595	653737	4.1 (4.6)	K_3GeS_3	14434	636776	4.1 (4.1)	Ba_2SiSe_4	14447	49750	4.1 (4.1)
K_2PtF_6	3821	87360	4.1 (4.1)	$LiAlTe_2$	4586	162672	4.1 (4.1)	Tl_2SiS_3	8190	35041	4.1 (4.2)
Na_5ReO_6	8253	38382	4.1 (4.1)	$Ca_2Ta_2O_7$	14026	27121	4.1 (4.1)	Rb_2TaAgS_4	15217	84295	4.1 (4.1)
$Sr_3(AlN_2)_2$	17129	74824	4.1 (4.1)	$Ba_2Nb_6Te_2O_{21}$	16998	405107	4.1 (4.1)	Ba_2TaN_3	17400	74503	4.1 (4.1)
$TiTl_2O_3$	17986	6105	4.1 (4.1)	Bi_3BrO_4	29447	201691	4.1 (4.2)	$GaPS_4$	30979	2613	4.1 (4.1)
Li_6MoN_4	8804	66095	4.1 (4.2)	BaZnSO	548469	171239	4.1 (4.1)	KAuS	7077	202178	4.1 (4.2)
Li_4MoO_5	19117	40270	4.1 (4.1)	Ba_2InO_3F	19956	81876	4.1 (4.6)	$Sr_4Ti_3O_{10}$	31213	34630	4.1 (4.3)
$Nb_2Cd_2O_7$	5472	161921	4.1 (4.3)	$RbSbO_2$	10418	411216	4.2 (4.3)	$CaIn_2O_4$	22766	52390	4.2 (4.2)
Rb_2TeCl_6	22975	29027	4.2 (4.3)	BiBrO	23072	29144	4.2 (4.5)	KAs_4IO_6	23126	65207	4.2 (4.6)
BPS_4	27724	24618	4.2 (4.6)	Rb_2SeCl_6	27829	26692	4.2 (4.4)	Ga_4GeO_8	29455	202044	4.2 (4.2)
$RbBiO_2$	29521	407208	4.2 (4.2)	$SnBr_2$	29862	411177	4.2 (4.3)	$Sr_3(BS_3)_2$	30239	412879	4.2 (4.3)
SbS_2NF_6	12368	170871	4.2 (4.2)	$ZnPbF_6$	13610	15107	4.2 (4.2)	BaSe	1253	616124	4.2 (4.4)
TiO_2	390	161908	4.2 (4.5)	$YAgO_2$	510034	95674	4.2 (4.4)	TaTeCl9	541877	410947	4.2 (4.3)
Rb_2PtF_6	8192	35108	4.2 (4.2)	$CaPtF_6$	8255	37443	4.2 (4.2)	Li_2O_2	841	152183	4.2 (4.2)
ZnO_2	8484	60763	4.2 (4.3)	$BaLa_2PtO_5$	8809	68794	4.2 (4.2)	Ga_2O_3	886	83645	4.2 (4.2)
$CsAu_3Se_2$	9386	82542	4.2 (4.4)	$NbBO_4$	8615	63202	4.2 (4.2)	K_3SbS_4	9781	402642	4.2 (4.2)
Cs_2TaAgS_4	15218	84296	4.2 (4.2)	$Ba_2SnS_3F_2$	17918	171343	4.2 (4.2)	K_3AlTe_3	18378	300168	4.2 (4.4)
PbI_2	22883	77325	4.2 (4.3)	$RbPbI_3$	23517	6067	4.2 (4.2)	$KBiP_2S_7$	23572	74019	4.2 (4.2)
BiI_3	22849	36182	4.2 (4.2)	$Te_6Br_2O_{11}$	29251	200007	4.2 (4.2)	Ca_3PI_3	27272	9026	4.2 (4.2)
Cd_4OF_6	505174	74031	4.2 (4.2)	K_2TeS_3	505556	280023	4.2 (4.2)	$LaBN_2$	505493	410598	4.2 (4.3)
Li_4GeS_4	510033	95649	4.2 (4.3)	$CdCN_2$	10969	95264	4.2 (4.2)	Sr_3BPO_3	9702	401207	4.2 (4.4)
Y_2NCl_3	28580	65829	4.2 (4.7)	Na_3PS_4	28782	72860	4.2 (4.2)	$K_2SrTa_2O_7$	7148	93492	4.2 (4.5)
CaSe	1415	619572	4.2 (5.1)	$ReAgO_4$	7094	280086	4.2 (4.2)	$LiVO_3$	19440	23477	4.2 (4.2)
TeO_2	2125	159326	4.2 (4.2)	WOF_4	540636	10393	4.2 (4.2)	$NaYS_2$	10226	76543	4.3 (5.1)

Na_4ReN_3	10419	411243	4.3 (4.4)	$NaSr_4(BN_2)_3$	10811	92577	4.3 (5.0)	TlCl	23167	29107	4.3 (4.3)
ClF	29504	406442	4.3 (4.3)	Ca_3AsBr_3	504488	426	4.3 (4.4)	K_3BrO	504857	33920	4.3 (4.3)
$SrZnO_2$	5637	25556	4.3 (4.3)	K_3IO	28171	36512	4.3 (4.3)	K_4I_2O9	27764	25694	4.3 (4.3)
Na_3AuO_2	28365	62066	4.3 (4.3)	$KGaI_4$	29402	400816	4.3 (4.3)	$CsPbI_3$	540839	27979	4.3 (4.3)
$BaHgO_2$	3915	83411	4.3 (4.9)	$ScCuO_2$	3642	151929	4.3 (4.7)	$ZnWO_4$	18918	162683	4.3 (4.3)
$CdWO_4$	19387	87937	4.3 (4.4)	$NaGeSbO_5$	6526	39689	4.3 (4.3)	K_3AuSe_2	15571	402000	4.3 (4.3)
MgTe	1039	642883	4.4 (4.4)	CsBrF	22935	84020	4.4 (4.4)	$CsPbCl_3$	23037	29072	4.4 (4.4)
Li_2Te	2530	642399	4.4 (5.2)	$KTlCl_4$	27385	14105	4.4 (4.4)	BiF_5	27743	25023	4.4 (4.6)
Cs_2SeCl_6	27830	26693	4.4 (4.5)	Na_4SnS_4	29628	42035	4.4 (4.4)	$CsNO_2$	3288	50328	4.4 (4.5)
ZrSO	3519	31721	4.4 (5.0)	Li_3AuS_2	15999	280535	4.4 (4.4)	BeSe	1541	616419	4.4 (5.9)
$K_2B_2S_7$	4351	657809	4.4 (4.5)	Na_5InS_4	505414	300175	4.4 (4.4)	$NaInO_2$	5175	34600	4.4 (4.6)
ZrNCl	542791	151468	4.4 (4.4)	$Zn(GaO_2)_2$	5794	81113	4.4 (4.5)	Na_3AsS_3	5830	1036	4.4 (4.4)
Cs_2PtF_6	9262	78955	4.4 (4.4)	Na_3GaSe_3	17148	300164	4.4 (4.4)	Sr_2TaN_3	17518	96126	4.4 (4.5)
Na_5AsO_5	17816	411721	4.4 (4.5)	K_3TaS_4	18148	59355	4.4 (4.4)	$RbInI_4$	28198	36601	4.4 (4.4)
$TlCdBr_3$	28219	39808	4.4 (4.4)	$Ge_2S_3Br_2$	540792	24370	4.4 (4.5)	$InGaBr_4$	541283	69652	4.4 (4.5)
$CaHgO_2$	7041	80717	4.4 (5.0)	K_4Br_2O	28627	68505	4.4 (4.4)	HgCl	22897	157979	4.4 (4.6)
$Sr_4Li(BN_2)_3$	9723	402173	4.4 (5.1)	$VInO_4$	25113	155162	4.4 (4.4)	$LiSbO_3$	4995	203032	4.4 (4.4)
KVO_3	18815	44528	4.4 (4.4)	Y_6WO_{12}	19005	92037	4.4 (4.5)	KCuS	28270	49008	4.4 (4.4)
Li_5ReN_4	3838	92468	4.4 (4.4)	Rb_2SnO_2	27931	24805	4.5 (4.5)	Sn_2OF_2	27480	948	4.5 (4.6)
InClO	27702	24058	4.5 (4.7)	NO_2	2789	201142	4.5 (4.5)	Ca_3AsCl_3	28069	36002	4.5 (4.7)
$Ti(SeO_3)_2$	29260	200203	4.5 (4.5)	$CsBiO_2$	29506	406564	4.5 (4.5)	Sr_2SnS_4	30294	413024	4.5 (4.5)
PbF_4	341	78895	4.5 (4.7)	SrSe	2758	53949	4.5 (5.0)	Ge_2N_2O	4187	200849	4.5 (4.6)
Rb_2HgO_2	5072	66276	4.5 (4.5)	P_2S_5	541788	409061	4.5 (4.6)	Tl_6SeI_4	28517	40520	4.5 (4.5)
$MgGeN_2$	7798	23502	4.5 (4.5)	KNaTe	8755	67276	4.5 (4.5)	$KBaPS_4$	17088	414639	4.5 (4.5)
I_2O_5	23261	27516	4.5 (4.5)	$Rb_4In_2S_5$	27670	23253	4.5 (4.5)	$BaNb_2O_6$	28150	39272	4.5 (4.8)
Li_4TaN_3	505795	412585	4.5 (4.7)	La_2SeO_2	7233	25804	4.5 (4.9)	SnF_3	8289	33786	4.5 (4.8)
$CsSbO_2$	510273	59329	4.5 (4.5)	$HgBr_2$	23292	30290	4.5 (4.5)	Rb_2HgF_4	8962	72352	4.5 (5.6)
$TiBr_4$	27634	22103	4.5 (4.5)	$LiCa_4(BN_2)_3$	6799	400339	4.5 (5.1)	$NaVCdO_4$	19449	151411	4.5 (4.5)
$GaCuCl_4$	505410	300103	4.5 (4.5)	$LaVO_4$	19162	411083	4.5 (4.5)	K_2HgS_2	28859	74500	4.5 (4.5)
$Hg_3(BO_3)_2$	4710	409688	4.5 (4.6)	$BaTi(BO_3)_2$	11659	97972	4.6 (4.6)	BiClO	22939	29143	4.6 (5.2)
Na_2O_2	2340	109276	4.6 (4.9)	K_2SnCl_6	23499	6058	4.6 (4.6)	Tl_2SnCl_6	27832	26700	4.6 (4.7)
Na_2Te	2784	656377	4.6 (4.6)	$LiGaBr_3$	28327	61338	4.6 (4.6)	$KLaSiS_4$	12924	414544	4.6 (4.6)
BaS	1500	616059	4.6 (4.7)	CsNaTe	5339	107569	4.6 (4.6)	$CsAgCl_2$	542772	150299	4.6 (4.9)
K_2HgO_2	5860	66275	4.6 (4.6)	$CaGeN_2$	7801	23523	4.6 (4.6)	NaLiTe	8754	67274	4.6 (4.6)
$BaTeO_3$	5431	10106	4.6 (4.6)	$NaAlSe_2$	17060	300173	4.6 (4.6)	Rb_3TaS_4	17220	51115	4.6 (4.6)
$TlSnF_7$	17649	78899	4.6 (4.6)	$LiInGeO_4$	17854	62229	4.6 (4.6)	$Na_2Si_2Se_5$	18562	49001	4.6 (4.7)
KIO_3	23487	20198	4.6 (4.6)	SBr_2O	28407	62972	4.6 (4.7)	Cs_2AgI_3	540881	30658	4.6 (4.6)
Cs_2HgF_4	8963	72353	4.6 (5.6)	$TaTl_3S_4$	7562	16571	4.6 (4.6)	$KNaV_2O_6$	19432	153450	4.6 (4.6)
$CsCu_2Cl_3$	23065	49612	4.6 (4.6)	$NaVO_3$	19083	2103	4.6 (4.6)	Sr_2ZnWO_6	19282	72811	4.6 (4.7)
Na_3AgS_2	9634	201800	4.6 (4.8)	Tl_6SI_4	27938	29265	4.6 (4.6)	$LiZnPS_4$	11175	95785	4.7 (5.0)
Cl_2	22848	201696	4.7 (4.8)	$GaBr_2$	28384	62665	4.7 (4.7)	$KLaS_2$	15781	44942	4.7 (4.9)
$BaZnO_2$	4236	25812	4.7 (4.7)	$NaNbO_3$	4514	28152	4.7 (4.7)	CsO	7896	25529	4.7 (4.8)
$BaTiO_3$	5020	100464	4.7 (5.0)	$Sr(BS_2)_2$	8947	71594	4.7 (4.7)	$RbLaS_2$	9361	81394	4.7 (5.0)
BI_3	23189	28328	4.7 (4.9)	$TlIO_3$	22981	62106	4.7 (4.7)	$Ba_3(GaS_3)_2$	29302	201421	4.7 (4.7)
$KAg(NO_3)_2$	18429	100711	4.7 (4.7)	$RbGeIO_6$	549697	73613	4.7 (4.8)	HfNCl	541911	87795	4.7 (4.7)
Sr_2CaWO_6	18742	36460	4.7 (4.7)	Ba_2CaWO_6	19182	246117	4.7 (4.8)	Sr_2MgWO_6	19420	155310	4.7 (4.7)
Ba_3Nb_2ZnO9	7249	157044	4.7 (4.9)	$TaPCl_{10}$	504684	26097	4.7 (4.7)	Rb_2SnCl_6	23059	29026	4.8 (4.8)
SO_2	27726	24645	4.8 (5.2)	Li_5Br_2N	29025	78836	4.8 (4.9)	$Sr(BiO_2)_2$	29048	80668	4.8 (4.8)
$TeSeO_4$	29299	201413	4.8 (4.9)	$Ba(BS_2)_2$	30126	412516	4.8 (4.9)	Tl_2ZnI_4	30532	37099	4.8 (4.9)
$AlBiBr_6$	31268	414262	4.8 (4.8)	KBS_2	15012	79614	4.8 (4.8)	CaS	1672	619540	4.8 (5.5)
KLiTe	4495	67887	4.8 (4.8)	SCl	504824	37016	4.8 (4.9)	Al_2CdS_4	5928	25634	4.8 (4.8)
$InPO_4$	7566	16618	4.8 (5.0)	HfSO	7787	23327	4.8 (5.5)	$CsAu_3S_2$	9384	82540	4.8 (5.0)
$Sr_2Ta_2O_7$	12286	601	4.8 (4.8)	$MgSe_2O_5$	16771	402917	4.8 (4.8)	Ba_3Te_2O9	17009	100797	4.8 (4.8)

$NbBiO_4$	23413	74338	4.8 (4.9)	$TaCl_4F$	27854	27413	4.8 (4.8)	$KTlF_4$	27209	4046	4.8 (4.8)
$TiSO_5$	505270	80627	4.8 (4.8)	$RbCdBr_3$	504529	808	4.8 (4.9)	$K_3Ta_3(BO_6)_2$	9870	201143	4.8 (4.9)
Ba_2SnO_4	3359	81850	4.8 (5.1)	$Cd_2B_2O_5$	7210	281357	4.8 (4.8)	$MgWO_4$	18875	67905	4.8 (4.9)
Tl_2MoO_4	18938	280608	4.8 (4.8)	Sr_2CdWO_6	19014	245683	4.8 (4.9)	$Ca_3V_2O_8$	542076	412273	4.8 (4.9)
$SrTeO_4$	4274	60507	4.8 (4.8)	$Ca(BeN)_2$	11918	413357	4.9 (5.0)	PbBrF	23008	155011	4.9 (4.9)
KAs_4BrO_6	23083	65206	4.9 (5.1)	Na_3BS_3	29976	411608	4.9 (5.0)	Na_2Se	1266	54281	4.9 (4.9)
Tl_3AsO_4	15573	407561	4.9 (5.1)	MgSe	13031	159398	4.9 (4.9)	BaO	1342	616005	4.9 (4.9)
Rb_2O	1394	77906	4.9 (5.3)	$LiGaS_2$	3647	96914	4.9 (4.9)	$CdCO_3$	4385	156755	4.9 (5.7)
OsO_4	540783	23803	4.9 (4.9)	K_2ZnO_2	8187	34603	4.9 (4.9)	CsNaSe	8658	41322	4.9 (5.0)
$ZnSe_2O_5$	18373	2355	4.9 (4.9)	$MgTi_2O_5$	28232	37232	4.9 (4.9)	$RbIO_3$	27193	2825	4.9 (4.9)
$BaSbClO_2$	545500	200962	4.9 (4.9)	$InBO_3$	7027	75254	4.9 (5.3)	$LaCuO_2$	20072	18102	4.9 (5.0)
KGeNO	6955	60002	4.9 (4.9)	KNaSe	28595	67278	4.9 (4.9)	$CaMoO_4$	19330	409785	4.9 (4.9)
P_3N_5	1954	95782	4.9 (5.6)	SrS	1087	249177	5.0 (5.4)	Rb_2Se	11327	36584	5.0 (5.2)
KSn_2Cl_5	23539	151982	5.0 (5.0)	$RbBS_2$	15013	79615	5.0 (5.0)	Tl_3PO_4	5709	60780	5.0 (5.2)
$SrGa_4O_7$	18253	10316	5.0 (5.0)	$Ba_2Ga_2S_5$	18421	38256	5.0 (5.0)	Sr_2InI_5	23504	152021	5.0 (5.0)
$CsIO_3$	28295	61009	5.0 (5.0)	$CsSnCl_3$	27394	14199	5.0 (5.0)	$Cs_2Zn_3S_4$	505633	53242	5.0 (5.0)
RbLiSe	9250	78878	5.0 (5.0)	Na_3SbO_4	7404	10320	5.0 (5.0)	NaLiSe	28603	67359	5.0 (5.0)
Li_2WO_4	19260	1044	5.0 (5.1)	$CdSe_2O_5$	9178	75230	5.0 (5.2)	Li_6WN_4	3503	153620	5.0 (5.0)
$La_2Sn_2O_7$	4086	153813	5.0 (5.0)	$Al_6Cd_4TeO_{12}$	9535	86155	5.0 (5.0)	Ta_2O_5	10390	280396	5.1 (5.3)
$PbSeO_3$	20716	98376	5.1 (5.1)	Rb_3InS_3	22303	23252	5.1 (5.1)	$AsBr_3$	23317	24579	5.1 (5.3)
$CdBr_2$	27934	25782	5.1 (5.1)	$BiBO_3$	31250	413621	5.1 (5.1)	$TiCdO_3$	13641	15989	5.1 (5.1)
BeS	422	616413	5.1 (7.5)	$MgGeO_3$	4819	201664	5.1 (5.2)	Rb_2ZnI_4	505748	56425	5.1 (5.1)
$Cs_2Sn(GeO_3)_3$	540707	19031	5.1 (5.2)	$CsCdBr_3$	541899	87261	5.1 (5.1)	$TlNO_3$	5915	75253	5.1 (5.2)
$Cd_4P_6SN_{12}$	8921	71019	5.1 (5.1)	Sr_2BN_2F	10234	50843	5.1 (5.1)	$K_3Ta_3Si_2O_{13}$	16855	15937	5.1 (5.1)
K_3BS_3	29975	411607	5.1 (5.2)	Pb_2OF_2	27355	10416	5.1 (5.3)	$Ba_3Zn_6Si_4TeO_{20}$	543034	416231	5.1 (5.1)
Sn_3BrF_5	23452	200031	5.1 (5.1)	$BaBiIO_2$	551243	97511	5.1 (5.3)	$NbInO_4$	9595	100695	5.1 (5.3)
$Sr_3V_2O_8$	19386	73258	5.1 (5.2)	$Y_2Sn_2O_7$	3370	160115	5.1 (5.1)	$KInBr_4$	22932	47141	5.2 (5.2)
$RbPb_2Br_5$	23043	26663	5.2 (5.4)	Al_2S_3	2654	300213	5.2 (5.2)	K_2Te	1747	641376	5.2 (5.2)
$CaInBr_3$	505024	54138	5.2 (5.4)	RbO	7895	25528	5.2 (5.3)	KLiSe	8756	67277	5.2 (5.3)
$CaTiGeO_5$	17784	171795	5.2 (5.2)	K_3PS_4	17989	24599	5.2 (5.2)	$Cd_2P_2O_7$	27686	23542	5.2 (5.5)
$Sr_3Te_4O_{11}$	30026	56798	5.2 (5.3)	Ta_2ZnO_6	17765	36289	5.2 (5.2)	Ba_2YNbO_6	7251	172407	5.2 (5.2)
$NaCaVO_4$	19302	32573	5.2 (5.2)	$HgCl_2$	22855	76648	5.2 (5.2)	$LiAlSe_2$	7117	280225	5.2 (5.2)
$CaPS_3$	9789	405192	5.2 (5.2)	$MgMoO_4$	19047	20418	5.2 (5.3)	$LiAl(MoO_4)_2$	19209	16175	5.2 (5.2)
Na_4WO_5	19334	85063	5.2 (5.2)	$RbLa(WO_4)_2$	19680	27737	5.2 (5.2)	$Sr(AlSe_2)_2$	8422	49732	5.2 (5.2)
Li_4TeO_5	4804	202326	5.2 (5.3)	$RbTlF_4$	27210	4047	5.2 (5.3)	$CdSeO_3$	9186	75273	5.2 (5.2)
$BaPS_3$	11006	412764	5.3 (5.3)	$AgClO_4$	22993	9629	5.3 (6.1)	Na_3BiO_3	27914	23347	5.3 (5.3)
$PbBr_2$	28077	36170	5.3 (5.4)	LiBeN	29463	402341	5.3 (5.4)	$LiNO_3$	8180	67981	5.3 (5.6)
Na_3SbO_3	8076	23346	5.3 (5.3)	Rb_3PS_4	16863	409818	5.3 (5.3)	$Zn(IO_3)_2$	23360	54086	5.3 (5.3)
$TlCdCl_3$	28218	39807	5.3 (5.3)	$Ga_{10}GePb_3O_{20}$	504827	37178	5.3 (5.4)	La_3TaO_7	510513	55655	5.3 (5.3)
$Ca(SbO_3)_2$	9125	74539	5.3 (5.6)	Na_4Br_2O	28599	67283	5.3 (5.3)	$KSbO_3$	547792	33546	5.3 (5.4)
$Ba_3V_2O_8$	19365	418460	5.3 (5.4)	$SrPS_3$	9788	405191	5.3 (5.3)	$P_4N_3Cl_{11}$	28792	71913	5.3 (5.3)
$ScTl(MoO_4)_2$	19450	250340	5.3 (5.3)	SnF_2	7457	14195	5.3 (6.0)	$SnCl_2$	29179	81979	5.3 (5.3)
Sr_2BN_2Cl	23131	406392	5.4 (5.6)	Li_2Se	2286	642355	5.4 (5.8)	$LiBiF_6$	27419	15119	5.4 (5.4)
Na_3PS_3O	11738	98651	5.4 (5.4)	$LiNbO_3$	3731	415526	5.4 (5.4)	$NaNO_3$	4531	420041	5.4 (5.5)
$CsAl(MoO_4)_2$	542116	280947	5.4 (5.4)	SbOF	7609	19019	5.4 (5.6)	Li_3BS_3	5614	380104	5.4 (5.4)
K_2Se	8426	60440	5.4 (5.5)	$CdSO_4$	8459	60571	5.4 (5.7)	$Ba(SbO_3)_2$	9127	74541	5.4 (5.5)
Ba_2ZnO_3	17911	36659	5.4 (5.4)	$Cd(IO_3)_2$	27640	1397	5.4 (5.5)	$TlBO_2$	28244	36404	5.4 (5.4)
$SrTa_2O_6$	17715	39706	5.4 (5.4)	PBr_2N	23457	27271	5.4 (5.4)	K_3VO_4	19052	4138	5.4 (5.4)
Ca_2SnO_4	4747	173626	5.4 (5.4)	$AlTl(MoO_4)_2$	18733	250339	5.4 (5.4)	$SrMoO_4$	18834	245802	5.4 (5.4)
$KAl(MoO_4)_2$	19352	28018	5.4 (5.4)	Na_4SnO_4	9655	202818	5.4 (5.4)	$RbNbO_3$	3283	200854	5.4 (5.4)
$PbSeO_4$	22342	40921	5.5 (5.6)	$AsCl_2F_3$	23444	33884	5.5 (5.5)	SrO_2	2697	647474	5.5 (5.7)
PBr_3	27257	8052	5.5 (5.5)	$CsBiF_6$	27422	15122	5.5 (5.6)	$Te_2O_3F_2$	29185	82162	5.5 (5.5)
Cs_3As_5O9	30300	413151	5.5 (5.6)	MgS	1315	659124	5.5 (6.3)	SiS_2	1602	27205	5.5 (5.8)

$BaSiN_2$	3777	170269	5.5 (5.6)	La_2SO_2	4511	260145	5.5 (6.0)	$SrSiN_2$	4549	170270	5.5 (5.6)
$TaBO_4$	4624	402404	5.5 (5.5)	Rb_2CdCl_4	505668	51168	5.5 (5.9)	Tl_2CO_3	543045	241245	5.5 (5.6)
SeO_2	726	59712	5.5 (5.9)	Mg_3TeO_6	3118	23611	5.5 (5.7)	Rb_2S	8041	29208	5.5 (5.8)
K_2O	971	641282	5.5 (5.9)	KNO_3	5158	28077	5.5 (5.5)	$LiTa_3O_8$	7638	493	5.5 (5.6)
Na_4I_2O	22937	67112	5.5 (5.5)	K_3BiO_3	29524	407293	5.5 (5.5)	$TaBiO_4$	30900	97423	5.5 (5.6)
NOF	505726	411510	5.5 (5.6)	$BaSn(GeO_3)_3$	540635	10384	5.5 (5.6)	$BaBiClO_2$	552806	79532	5.5 (5.5)
$SrBiBrO_2$	552234	97509	5.5 (5.6)	Na_3ClO	28602	67319	5.5 (5.5)	Cs_2LiVO_4	541190	40219	5.5 (5.5)
Cs_2NaVO_4	19447	65963	5.5 (5.6)	Sr_2YNbO_6	6019	163664	5.5 (5.5)	Rb_2LiVO_4	19123	40218	5.5 (5.5)
$RbLa(MoO_4)_2$	19687	42700	5.5 (5.6)	$SbBr_3$	27399	14217	5.5 (5.7)	$NaInBr_4$	28569	65462	5.5 (5.5)
BaO_2	1105	80750	5.6 (5.6)	BiOF	23074	24096	5.6 (5.6)	Na_2O	2352	644917	5.6 (5.6)
BrF_5	27987	31690	5.6 (5.6)	$BaAl_2Sb_2O_7$	12885	154362	5.6 (5.8)	Y_2SO_2	12894	154582	5.6 (5.7)
$CsGaS_2$	5038	41888	5.6 (5.7)	$YNbO_4$	5387	20335	5.6 (5.8)	CaN_6	676	412259	5.6 (5.6)
RbNaS	8799	68489	5.6 (5.7)	Li_3SbO_4	5769	279592	5.6 (5.6)	$KSeO_2F$	9205	78398	5.6 (5.6)
$In_2P_2O_7$	17100	412855	5.6 (5.6)	$LiGaCl_3$	29344	202641	5.6 (5.7)	Sr_2CuBrO_2	552537	65470	5.6 (5.7)
Na_2ZnGeO_4	6402	76314	5.6 (5.7)	$NaSr_3NbO_6$	6361	418494	5.6 (5.7)	Ga_2PbO_4	20496	80129	5.7 (5.8)
$BiCl_3$	22908	41179	5.7 (5.9)	$Ge_3(BiO_3)_4$	23560	201356	5.7 (5.8)	$MgSeO_4$	12630	109070	5.7 (5.8)
SnClF	504519	647	5.7 (5.7)	$CaWO_4$	510563	155792	5.7 (5.7)	$NaReO_4$	5558	52337	5.7 (5.7)
$Mg_2As_2O_7$	5618	23548	5.7 (5.7)	$BaAl_4S_7$	8258	33237	5.7 (5.8)	$BaTiOF_4$	16915	72740	5.7 (5.7)
$LiZnAsO_4$	18048	86184	5.7 (5.7)	Be_3N_2	18337	412667	5.7 (5.7)	Rb_4CdBr_6	28315	60625	5.7 (5.7)
$LiGaBr_4$	28326	61337	5.7 (5.7)	$CaNb_2O_6$	17101	15208	5.7 (5.7)	$Bi_3B_5O_{12}$	23549	412831	5.7 (5.9)
CsNaS	6973	41323	5.7 (5.7)	SrBiClO$_2$	547244	84636	5.7 (5.7)	$CsTa(BO_3)_2$	9309	80423	5.7 (5.9)
$SbAsO_3$	28109	37187	5.7 (5.8)	$Na_3Mo(OF)_3$	18753	97453	5.7 (5.8)	$AlCuCl_4$	28020	35050	5.7 (5.8)
$SbClF_8$	27314	9899	5.7 (5.7)	$TiTl_2F_6$	10402	410802	5.8 (5.9)	PbBrCl	22997	45881	5.8 (5.9)
CaH_2	23713	155987	5.8 (6.6)	BaH_2	23715	155989	5.8 (6.3)	K_2NaAlH_6	24412	152891	5.8 (5.8)
LiN_3	2659	155166	5.8 (6.2)	$ZnCN_2$	29826	280523	5.8 (6.1)	AlI_3	30930	391247	5.8 (5.8)
$Ba(IO_3)_2$	30991	23276	5.8 (5.9)	$Ca(AsO_3)_2$	4555	77379	5.8 (6.1)	$RbIn(MoO_4)_2$	504506	10186	5.8 (5.8)
Na_2S	648	656376	5.8 (5.8)	TlF	720	90996	5.8 (5.9)	Li_2ZnGeO_4	8184	34362	5.8 (5.8)
SnB_4O_7	13252	249206	5.8 (6.3)	Pb_2CO_4	505702	91714	5.8 (5.9)	KNaS	504938	62658	5.8 (5.8)
$BaPbF_6$	19799	25521	5.8 (5.8)	ScBrO	546279	170774	5.8 (5.8)	$BaMoO_4$	19276	161851	5.8 (5.8)
$RbTaO_3$	3033	2301	5.8 (5.8)	$AsClF_8$	27926	23775	5.9 (5.9)	$NaGaO_2$	3338	36652	5.9 (5.9)
K_2TiO_3	13133	162216	5.9 (5.9)	Mg_2PN_3	3933	50224	5.9 (6.6)	$CsMgI_3$	505586	87262	5.9 (6.0)
$CaBiClO_2$	553025	84635	5.9 (6.0)	As_2O_3	1581	655563	5.9 (6.0)	RbLiS	8751	67254	5.9 (5.9)
$TaInO_4$	8979	72569	5.9 (6.0)	$LiGaO_2$	5854	93087	5.9 (5.9)	Li_3BN_2	5001	155129	5.9 (6.2)
Rb_3GaO_3	13744	2270	5.9 (5.9)	Na_3ScBr_6	29417	401335	5.9 (5.9)	$K_4Zr_5O_{12}$	27377	14024	5.9 (5.9)
Sr_3Ga_4O9	30158	51546	5.9 (5.9)	$NaGaBr_4$	505084	69650	5.9 (5.9)	$GaAsO_4$	3996	41949	5.9 (5.9)
K_2S	1022	641321	6.0 (6.1)	$KNaLaNbO_5$	10942	94743	6.0 (6.0)	SrN_6	2131	412255	6.0 (6.0)
$CdCl_2$	22881	30255	6.0 (6.0)	SCl_2O	28406	62971	6.0 (6.0)	Zn_3S_2O9	30986	15280	6.0 (6.0)
$SrSeO_3$	3395	240888	6.0 (6.0)	$Sr_2ZnGe_2O_7$	17392	39159	6.0 (6.0)	GeO_2	733	59639	6.0 (6.1)
K_2TeO_3	8724	65640	6.0 (6.2)	$Li_{16}Ta_2N_8O$	14871	71696	6.0 (6.0)	$NaIO_3$	22989	29098	6.0 (6.1)
Li_2TeO_3	27231	4317	6.0 (6.2)	$Na_3In_2(PO_4)_3$	17349	84776	6.0 (6.1)	$SbCl_3$	22872	8258	6.0 (6.1)
$CsPbF_3$	20282	93438	6.0 (6.0)	$KAlAs_2O_7$	9230	79711	6.0 (6.1)	$CsSbClF_3$	23576	200296	6.0 (6.0)
Li_2SnO_3	3540	21053	6.0 (6.1)	$Zn(ReO_4)_2$	10326	51017	6.1 (6.1)	Li_2S	1153	54396	6.1 (7.0)
$LaBr_3$	23263	31581	6.1 (6.1)	$KCdCl_3$	23442	31357	6.1 (6.2)	CdF_2	241	250165	6.1 (6.6)
Ba_2YTaO_6	12385	171176	6.1 (6.1)	Ba_2LaTaO_6	13055	160169	6.1 (6.3)	Li_2TiGeO_5	13182	250297	6.1 (6.2)
$BaZrO_3$	3834	97462	6.1 (6.2)	KSO_4	7622	54024	6.1 (6.2)	BaI_2	23260	15707	6.1 (6.1)
$Ta_2Zn_3O_8$	28251	46001	6.1 (6.1)	Na_3NbO_4	27247	6116	6.1 (6.1)	$LiAlGeO_4$	16947	67238	6.1 (6.1)
$HfTe_3O_8$	18352	9078	6.1 (6.1)	$RbMgH_3$	23738	159176	6.1 (6.3)	Sr_2I_2O	551203	409896	6.1 (6.1)
K_2MoO_4	18914	150842	6.1 (6.2)	$PbCO_3$	19893	56101	6.1 (6.2)	$BaCN_2$	28898	75041	6.1 (6.1)
$KBrO_3$	22958	33663	6.2 (6.2)	PbClF	22964	30287	6.2 (6.2)	SrH_2	23714	155988	6.2 (6.9)
$BeAlH_5$	23719	156311	6.2 (6.2)	Rb_2ZrCl_6	27831	26694	6.2 (6.2)	Sr_4I_6O	29910	280585	6.2 (6.2)
$KReO_4$	4757	72503	6.2 (6.2)	$LaNbO_4$	5295	81618	6.2 (6.3)	Na_2CN_2	541989	411341	6.2 (6.3)
NaLiS	8452	61091	6.2 (6.2)	Na_5TaO_5	8957	72297	6.2 (6.2)	$KMgH_3$	23737	159175	6.2 (7.9)
$SrWO_4$	19163	155793	6.2 (6.2)	$MgPbF_6$	19734	15106	6.2 (6.2)	$La_3Ga_5SnO_{14}$	6788	55416	6.2 (6.2)

$AsCl_3$	23280	35133	6.3 (6.6)	$PbCl_2$	23291	27736	6.3 (6.5)	CsSrN9	29228	100461	6.3 (6.4)
$KAsO_2$	30298	413149	6.3 (6.4)	$MgSeO_3$	12271	494	6.3 (6.5)	$CaTaAlO_5$	15733	50718	6.3 (6.3)
BaN_6	1707	653607	6.3 (6.3)	$RbReO_4$	4035	52339	6.3 (6.3)	KLiS	8430	47229	6.3 (6.3)
$TaAlO_4$	14333	33885	6.3 (6.5)	$Ca_4Al_6TeO_{12}$	15312	86156	6.3 (6.3)	MgI_2	23205	52279	6.3 (6.4)
$CsMgH_3$	23751	162260	6.3 (6.6)	$MgSn(BO_3)_2$	11715	28266	6.3 (6.4)	$ScAsO_4$	546125	155920	6.3 (6.3)
Rb_2MoO_4	19212	24904	6.3 (6.3)	$Zn_4B_6O_{13}$	4812	100290	6.3 (6.4)	$NaAlI_4$	29395	400521	6.3 (6.3)
Ca_2BN_2F	10233	50842	6.3 (6.3)	$Si_3(BiO_3)_4$	23331	26787	6.4 (6.5)	$SrCN_2$	12317	59860	6.4 (7.1)
Rb_3AlO_3	14951	74969	6.4 (6.4)	$NaGe_2(PO_4)_3$	542919	164019	6.4 (6.5)	AlN	661	163953	6.4 (6.4)
GeF_2	7595	18030	6.4 (6.8)	Na_2GeO_3	5784	1622	6.4 (6.6)	$CsCdF_3$	8399	49582	6.4 (7.3)
Ba_3NaTaO_6	8961	72331	6.4 (6.4)	$YTaO_4$	5377	38420	6.4 (6.7)	$Rb_6Ge_2O_7$	18224	73551	6.4 (6.4)
$BaSeO_3$	6989	54156	6.4 (6.5)	$SrSn(BO_3)_2$	8000	28267	6.4 (6.8)	K_2CN_2	10408	411094	6.5 (6.5)
PCl_3	23230	27798	6.5 (6.6)	K_2ZnBr_4	23535	72931	6.5 (6.5)	ZrO_2	2858	157403	6.5 (6.5)
Al_2ZnO_4	2908	163268	6.5 (6.5)	$RbAsO_2$	30299	413150	6.5 (6.5)	$SbPO_4$	3439	62977	6.5 (6.8)
$MgSiN_2$	3677	90731	6.5 (6.8)	$ZrGeO_4$	8042	29262	6.5 (6.6)	$NaSc(GeO_3)_2$	8054	22503	6.5 (6.5)
$Zn_4P_6SN_{12}$	15833	76440	6.5 (6.7)	$SrGeO_3$	17464	59303	6.5 (6.6)	$CaGeO_3$	17761	403086	6.5 (6.6)
$SrCdP_2O_7$	17693	72672	6.5 (6.5)	$Ca_3Sc_2(GeO_4)_3$	21989	20215	6.5 (6.5)	Na_3AlH_6	23705	154673	6.5 (6.5)
$RbBrO_3$	28872	74768	6.5 (6.5)	Na_2ZnSiO_4	6391	34565	6.5 (6.6)	GeP_2O_7	28883	74876	6.5 (6.5)
Rb_2TiO_3	5403	78842	6.5 (6.5)	NaN_3	22003	77323	6.6 (7.0)	BBr_3	23225	173374	6.6 (6.8)
MgO_2	2589	41732	6.6 (6.7)	$SeOF_2$	27367	12110	6.6 (6.6)	SeF_4	29172	85451	6.6 (6.6)
Sr_2YSbO_6	12878	154033	6.6 (6.7)	$CaCN_2$	4124	418451	6.6 (7.3)	$YAsO_4$	8058	24513	6.6 (6.6)
Na_2SeO_4	5141	150706	6.6 (6.7)	$TlZnPO_4$	18168	74811	6.6 (6.7)	$NaScCl_4$	29432	402273	6.6 (6.7)
$Zr_4Cd(PO_4)_6$	541299	66820	6.6 (6.6)	Na_4GeO_4	2970	62595	6.6 (6.6)	KSO_2F	6560	93060	6.6 (6.6)
SnF_4	2706	78894	6.6 (6.8)	$KCdF_3$	9628	201329	6.6 (6.6)	$BaWO_4$	19048	155512	6.6 (6.6)
$BaBAsO_5$	9784	404439	6.6 (6.6)	$Mg(BeN)_2$	11917	413358	6.7 (7.3)	$ScCl_3$	23309	38235	6.7 (6.7)
K_2NaTlF_6	13798	22114	6.7 (6.7)	$RbScO_2$	7650	1270	6.7 (7.1)	$TlSbF_6$	8348	36264	6.7 (6.9)
KNa_2BO_3	8263	33261	6.7 (6.9)	$RbNa_2BO_3$	8872	67525	6.7 (6.9)	$BaSeO_4$	12010	409810	6.7 (6.8)
$BaGeO_3$	13863	23925	6.7 (6.7)	Li_2ZnSiO_4	17288	8237	6.7 (6.7)	$NaMgH_3$	23730	158251	6.7 (6.7)
$Sc_2(SeO_3)_3$	31065	98624	6.7 (6.8)	$Na_2Li_3GaO_4$	540945	37071	6.7 (6.7)	$S(ClO)_2$	28405	62970	6.7 (6.7)
$HfCl_4$	29422	402054	6.7 (6.7)	$RbSO_2F$	6384	93068	6.7 (6.7)	KCSN	6511	67582	6.7 (6.7)
$SrZrO_3$	4387	159454	6.7 (6.8)	$HfGeO_4$	9755	202080	6.7 (6.7)	$CaPbF_6$	20463	25522	6.8 (6.8)
$KHSeO_3$	24433	20862	6.8 (6.9)	CaI_2	30031	52280	6.8 (7.2)	Mg_3NF_3	7604	18320	6.8 (6.8)
$RbLaO_2$	7972	27331	6.8 (6.8)	KN_3	827	155168	6.8 (6.8)	Na_2SeO_3	5416	280941	6.8 (6.8)
Mg_4Ta_2O9	17481	65301	6.8 (6.8)	$KAsOF_4$	17539	9027	6.8 (6.8)	$K_2Li_3GaO_4$	17774	35290	6.8 (6.8)
$CaZn_2(PO_4)_2$	18308	202571	6.8 (6.9)	NaI	23268	61502	6.8 (6.8)	K_2BeO_2	27915	23633	6.8 (6.9)
Ba_4I_6O	29909	280584	6.8 (6.8)	Na_3BO_3	510256	1351	6.8 (6.9)	$CsBrO_3$	28873	74769	6.8 (6.8)
NaCSN	6633	954	6.8 (6.8)	KLi_6TaO_6	9059	73159	6.8 (6.9)	$TlSbF_4$	29286	201084	6.8 (6.8)
$ZnCl_2$	22909	15916	6.9 (6.9)	K_4CdCl_6	23392	60753	6.9 (7.0)	SrO	2472	249178	6.9 (7.0)
As_2SO_6	27230	4297	6.9 (7.0)	$NaCdF_3$	4360	163867	6.9 (6.9)	$KLaO_2$	7958	27001	6.9 (6.9)
$Rb_2Li_2GeO_4$	8450	61087	6.9 (7.0)	$NaSi_2N_3$	8973	72466	6.9 (6.9)	K_2SeO_4	5226	201882	6.9 (6.9)
$Ba_{10}P_6SO_{24}$	16990	410785	6.9 (6.9)	Rb_2Si_3SnO9	17382	19028	6.9 (7.2)	$K_3Na(SeO_4)_2$	17839	73463	6.9 (6.9)
$BaSi_3SnO9$	18502	10385	6.9 (7.1)	ZnF_2	1873	53981	6.9 (7.0)	K_2WO_4	18780	150840	6.9 (7.0)
SbF_3	1880	30411	6.9 (7.2)	K_3AlO_3	9157	74968	6.9 (6.9)	Sr_3GaO_4F	6509	50735	6.9 (7.0)
$ZnSO_4$	5126	71018	6.9 (7.0)	$PbSO_4$	22298	154273	7.0 (7.2)	$Ba(BrO_3)_2$	505008	40287	7.0 (7.1)
RbN_3	743	155169	7.0 (7.0)	$NaScO_2$	7914	25729	7.0 (7.7)	$Cs_2Li_2GeO_4$	8313	36532	7.0 (7.0)
$NaYGeO_4$	17543	85497	7.0 (7.1)	$Cs_6Si_2O_7$	18315	411665	7.0 (7.0)	$Na_3Ca_2TaO_6$	18480	280284	7.0 (7.0)
$BaLa_2BeO_5$	18414	65292	7.0 (7.0)	Rb_4CdCl_6	22930	151893	7.0 (7.0)	LiI	22899	414244	7.0 (7.0)
$PNCl_2$	23375	109272	7.0 (7.0)	Tl_2SnF_6	10401	410801	7.0 (7.0)	$LaGeBO_5$	19957	39262	7.0 (7.0)
HfO_2	352	173158	7.0 (7.0)	$AlGaCl_4$	541111	62232	7.0 (7.0)	$LaAlO_3$	2920	153830	7.1 (7.1)
$K_2ZrGe_2O_7$	16871	88843	7.1 (7.1)	$RbAlO_2$	14070	28373	7.1 (7.1)	Rb_2LiAsO_4	14363	36644	7.1 (7.2)
$KScO_2$	8188	34958	7.1 (7.5)	$CsNa_2BO_3$	8871	67524	7.1 (7.1)	Li_2CN_2	9610	200369	7.1 (7.2)
$Na_4Hf_2(GeO_4)_3$	14526	65807	7.1 (7.1)	$Zr_3Tl_2OF_{12}$	17315	48003	7.1 (7.1)	$RbZnPO_4$	18463	71778	7.1 (7.1)
Rb_3PbCl_5	29883	89570	7.1 (7.1)	$LiInP_2O_7$	8491	60935	7.1 (7.1)	CdS_2O_7	17586	63067	7.1 (7.1)
$Y_2C(NO)_2$	546864	245332	7.1 (7.1)	$CsSO_2F$	6368	93078	7.1 (7.2)	$CaMgAsO_4F$	7035	56862	7.1 (7.1)

La_2MgGeO_6	11585	97016	7.2 (7.3)	$NaBrO_3$	23339	28831	7.2 (7.2)	$TaAgF_6$	29993	411796	7.2 (7.2)
Si_2CN_4	30161	93544	7.2 (7.2)	$BAsO_4$	3277	413438	7.2 (7.6)	$ZnSnF_6$	13903	25012	7.2 (7.2)
Li_4GeO_4	4558	65177	7.2 (7.2)	$LiScO_2$	5840	36124	7.2 (7.2)	Na_4SiO_4	7500	62594	7.2 (7.3)
Cs_2NaAsO_4	8314	36533	7.2 (7.2)	Cs_2ZrO_3	8759	67345	7.2 (7.2)	$Cs_2Li_2TiO_4$	8294	33810	7.2 (7.3)
Si_3N_4	988	170006	7.2 (7.4)	$Ba_3(AsO_4)_2$	9783	404438	7.2 (7.2)	$CsZnPO_4$	18673	85457	7.2 (7.2)
$Sr_{10}P_6SO_{24}$	17447	410783	7.2 (7.2)	IF_5	23257	6021	7.2 (7.2)	$TlTeF_5$	29903	90619	7.2 (7.4)
$Ca_2Hf_7O_{16}$	27221	4136	7.2 (7.2)	$CsNa_3Li_{12}(GeO_4)_4$	17125	79098	7.2 (7.3)	$NaSbF_4$	29269	200573	7.2 (7.2)
CaO	2605	163628	7.3 (7.6)	Li_2CaGeO_4	7611	19024	7.3 (7.3)	$SrZn_2(PO_4)_2$	8810	68881	7.3 (7.3)
$SrGa_2(SiO_4)_2$	14235	34414	7.3 (7.3)	KLi_3GeO_4	18002	38324	7.3 (7.3)	KI	22898	52244	7.3 (7.3)
RbI	22903	61536	7.3 (7.3)	BaIF	22951	1128	7.3 (7.3)	$K_4Be_3O_5$	28158	33808	7.3 (7.3)
$LiGaSiO_4$	18147	65125	7.3 (7.3)	Na_4TiO_4	14726	69621	7.3 (7.3)	$NaLi_2AsO_4$	9066	73200	7.3 (7.4)
$LaAsO_4$	4917	155917	7.3 (7.3)	LaBrO	23023	84336	7.4 (7.4)	PbF_2	315	53984	7.4 (7.5)
$CdSnF_6$	13907	25017	7.4 (7.4)	$AlTlF_4$	3751	202458	7.4 (7.5)	$Ba_3Nb_2O_8$	542201	95193	7.4 (7.4)
K_2ZrO_3	18449	16264	7.4 (7.4)	$KZnPO_4$	18591	88955	7.4 (7.4)	NbF_5	18687	26647	7.4 (7.4)
SrIF	23046	159280	7.4 (7.4)	Zr_2P_2O9	27132	1922	7.4 (7.5)	Li_3AsO_4	9197	75927	7.4 (7.5)
$SrHfO_3$	3378	162906	7.4 (7.4)	BiF_3	23237	9015	7.5 (7.6)	$AlBr_3$	23288	39768	7.5 (7.5)
$CsMgBr_3$	29750	87260	7.5 (7.5)	Li_2TiF_6	7603	18313	7.5 (7.5)	$BaTiF_6$	8291	33789	7.5 (7.5)
$InBF_4$	8586	50218	7.5 (7.5)	Rb_2LiGaF_6	14638	50468	7.5 (7.5)	$RbGaCl_4$	30231	409650	7.5 (7.5)
$NaZnF_3$	3795	72320	7.5 (7.5)	$K_2Pb(SO_4)_2$	21099	76891	7.6 (7.8)	$LaCl_3$	22896	31574	7.6 (7.6)
$CsLiBr_2$	23057	245979	7.6 (7.9)	$CsAsF_4$	5707	54852	7.6 (7.6)	$AsPO_4$	8140	31879	7.6 (7.6)
$CsK_2Sc(PO_4)_2$	8564	61787	7.6 (7.7)	$ScBO_3$	8697	65010	7.6 (7.6)	$LiGeBO_4$	8873	67535	7.6 (7.8)
BN	984	35538	7.6 (7.9)	$NaAlO_2$	9212	79404	7.6 (7.6)	$LiYO_2$	7020	45511	7.6 (7.6)
Na_3YBr_6	29080	82355	7.6 (7.7)	ScOF	4661	100564	7.7 (7.7)	$Ba_2Zn_7F_{18}$	541827	40925	7.7 (7.7)
$AlAsO_4$	7849	24512	7.7 (7.7)	$K_6Si_2O_7$	30990	17064	7.7 (7.7)	InF_3	6949	38306	7.7 (7.7)
Na_2MgSiO_4	6406	15619	7.7 (7.7)	$CaAl_4O_7$	4867	44519	7.7 (7.7)	$La_2Hf_2O_7$	12533	153815	7.7 (7.7)
$NaPN_2$	10572	411818	7.8 (7.8)	$BaZnCl_4$	23373	410193	7.8 (7.8)	$BaBr_2$	27456	15706	7.8 (7.8)
$Na_4B_2O_5$	27564	10061	7.8 (7.8)	$SrBe_3O_4$	27791	26179	7.8 (7.8)	$GaPO_4$	3518	155446	7.8 (7.8)
$LiBiF_4$	505032	65404	7.8 (8.1)	$Sc_2Si_2O_7$	5594	16214	7.8 (7.9)	$Zn(PO_3)_2$	8230	36040	7.8 (7.8)
$K_3Sc(PO_4)_2$	17035	61786	7.8 (7.8)	Na_3TaF_8	17245	26611	7.8 (7.8)	LaClO	23025	84330	7.9 (7.9)
$MgBr_2$	30034	52366	7.9 (7.9)	$CsAlO_2$	14069	28372	7.9 (7.9)	Si_2N_2O	4497	415575	7.9 (7.9)
Na_2SiO_3	4533	74640	7.9 (8.1)	$ZrSiO_4$	4820	158108	7.9 (8.1)	$LiInF_4$	8892	66693	7.9 (7.9)
$Sc_2(SO_4)_3$	16800	411221	7.9 (7.9)	$K_2Li_{14}Zr_3O_{14}$	17208	65445	7.9 (7.9)	$SrCO_3$	3822	56099	7.9 (7.9)
Li_2NbF_6	9752	201755	7.9 (7.9)	$Y_2Be_2GeO_7$	541040	39122	7.9 (7.9)	$CsNbF_6$	11980	412444	8.0 (8.1)
NaBr	22916	61672	8.0 (8.0)	BCl_3	23184	27869	8.0 (8.1)	Li_6MgBr_8	29008	73275	8.0 (8.0)
$ScPO_4$	4200	201132	8.0 (8.2)	$NaBO_2$	3889	15967	8.0 (8.0)	$KNbF_6$	7571	16729	8.0 (8.0)
Ba_2LaC_3O9F	18111	250059	8.0 (8.2)	$Ca_4LaB_3O_{10}$	6076	250012	8.0 (8.0)	$CaBr_2$	22888	14220	8.1 (8.1)
CsBr	22906	44290	8.1 (8.1)	$RbLiBr_2$	28237	30719	8.1 (8.1)	$CsCaBr_3$	30056	77242	8.1 (8.2)
$SrLiBO_3$	10814	92842	8.1 (8.3)	$Sr_3Sc(BO_3)_3$	17562	75339	8.1 (8.2)	$NaTeF_5$	29355	202879	8.1 (8.1)
$Na_2Mg(CO_3)_2$	6026	100482	8.1 (8.1)	MgO	1265	161607	8.1 (8.1)	Na_2CO_3	22381	81003	8.2 (8.2)
$LiAlO_2$	3427	30249	8.2 (8.2)	$Sr(ClO_3)_2$	504991	61157	8.2 (8.3)	$BeSiN_2$	7913	25704	8.2 (8.4)
ZnP_4O_{11}	15438	300229	8.2 (8.2)	Sr_2SiO_4	18510	36041	8.2 (8.2)	LaOF	7100	76427	8.2 (8.4)
$Ba_2Mg(BO_3)_2$	9259	75986	8.2 (8.2)	LiBr	23259	27982	8.3 (8.3)	NaCNO	546500	27138	8.3 (8.5)
Mg_2BO_3F	7995	28096	8.3 (8.3)	$Na_3Sc_2(PO_4)_3$	16956	65406	8.3 (8.3)	$Ge(SF_6)_2$	28291	60079	8.3 (8.3)
$ZrPbF_6$	7310	4051	8.3 (8.3)	RbBr	22867	18017	8.4 (8.4)	KBr	23251	18015	8.4 (8.4)
AsF_3	28027	35132	8.4 (8.5)	YClO	504786	31667	8.4 (8.4)	$MgCO_3$	5349	156763	8.4 (8.9)
AsF_5	8723	65477	8.4 (8.4)	Ba_2SiO_4	17612	28476	8.4 (8.4)	$BaHf(PO_4)_2$	545548	245690	8.4 (8.5)
$BaSiO_3$	7339	6245	8.4 (8.5)	$BaLiBO_3$	6499	92843	8.4 (8.5)	YOF	3637	30623	8.5 (8.5)
$BaZnF_4$	3881	402926	8.5 (8.5)	$CaCO_3$	3953	158472	8.5 (8.5)	Tl_2SiF_6	5033	52292	8.5 (8.5)
$KAsF_6$	7569	16663	8.5 (8.5)	K_2ZnF_4	9583	100298	8.5 (9.4)	$KAlSiO_4$	9480	83449	8.5 (8.5)
$CsMgPO_4$	18329	260423	8.5 (8.5)	$BaBeSiO_4$	550751	86792	8.5 (8.6)	K_2CO_3	3963	66943	8.5 (8.5)
SrBrF	23024	155008	8.6 (8.6)	YCl_3	27455	15684	8.6 (8.6)	Li_4SiO_4	11737	98615	8.6 (8.8)
GaF_3	588	409507	8.6 (8.6)	$RbNa_3Li_{12}(SiO_4)_4$	17240	74865	8.6 (8.6)	$CsKNa_2Li_{12}(SiO_4)_4$	17718	74864	8.6 (8.7)
$Ba_3In_2F_{12}$	28274	48182	8.6 (8.6)	$CaMg(CO_3)_2$	6459	171508	8.6 (8.8)	$Sr_2MgSi_2O_7$	6564	155300	8.6 (8.8)

$Ba_2MgSi_2O_7$	9338	81117	8.6 (8.7)	$TlClO_4$	30530	33564	8.7 (8.7)	$HfSiO_4$	4609	59111	8.7 (8.8)
$Y_2Si_2O_7$	5652	281313	8.7 (8.7)	$KCaCO_3F$	6867	154685	8.7 (8.7)	BaBrF	23070	35393	8.8 (8.8)
Cs_2NaYCl_6	23120	245353	8.8 (8.8)	Li_2O	553090	108886	8.8 (8.8)	Li_2SiO_3	5012	100402	8.8 (9.0)
$RbMgCl_3$	504459	4036	8.8 (8.8)	La_2SO_6	4078	66824	8.8 (9.0)	$BaAl_2B_2O_7$	9844	409171	8.8 (8.8)
Li_2CaSiO_4	7610	19023	8.9 (9.3)	$Mg_3(BO_3)_2$	5005	31385	8.9 (9.2)	$Rb_2SrP_2O_7$	14354	39506	8.9 (8.9)
MgP_4O_{11}	15437	300214	8.9 (8.9)	$LiAlSiO_4$	18220	92708	8.9 (9.0)	$BaCl_2$	23199	15705	9.0 (9.0)
$BeBr_2$	30139	92584	9.0 (9.2)	$Na_2BeB_2O_5$	16737	249341	9.0 (9.0)	P_2O_5	2452	77377	9.0 (9.0)
$RbSbF_6$	9821	408071	9.0 (9.0)	$Cs_2SrP_2O_7$	14355	39507	9.0 (9.0)	$Mg_2B_2O_5$	18256	81229	9.0 (9.1)
$BaSnF_6$	8290	33788	9.0 (9.0)	$CsLiCl_2$	23364	245972	9.1 (9.3)	$Na_2S_2O_7$	31269	413049	9.1 (9.2)
$SrAl_2B_2O_7$	15939	89423	9.1 (9.1)	$CsSbF_6$	9636	201886	9.1 (9.1)	$Rb_2Zr_3OF_{12}$	17085	95848	9.1 (9.2)
$KSrPO_4$	17975	83598	9.1 (9.1)	$RbBaPO_4$	17832	72001	9.1 (9.1)	$KHCO_3$	23724	157166	9.1 (9.1)
$SrCl_2$	23209	28964	9.2 (9.5)	K_2MgCl_4	27207	4035	9.2 (9.4)	$LiBO_2$	3635	200891	9.2 (9.2)
$Mg_3(PO_4)_2$	14396	31005	9.2 (9.2)	$Rb_2B_4O_7$	16980	85093	9.2 (9.2)	$AlH_{12}(ClO_2)_3$	23743	22071	9.2 (9.2)
$Na_2Ca(PO_3)_4$	541522	81393	9.2 (9.2)	$NaAlP_2O_7$	16777	400462	9.2 (9.2)	Ca_4Cl_6O	23326	418946	9.2 (9.2)
$K_2Be_2PbF_8$	7385	9902	9.2 (9.3)	Al_2O_3	1143	161060	9.3 (9.3)	CsCl	22865	44289	9.3 (9.3)
$CsMgCl_3$	23004	54167	9.3 (9.3)	AlClO	27863	27812	9.3 (9.3)	$Ba_3(PO_4)_2$	3857	150866	9.3 (9.4)
$NaAlPO_4F$	8678	40522	9.3 (9.3)	$CsBePO_4$	15395	202604	9.3 (9.3)	$KNa_2(PO_3)_3$	17889	2346	9.3 (9.3)
$K_2Zr_3OF_{12}$	17888	281350	9.3 (9.3)	$Na_2B_4O_7$	17941	2040	9.3 (9.3)	Al_2O_3	552558	43732	9.3 (9.3)
$LaSiBO_5$	7051	83398	9.3 (9.3)	$Sr_3(PO_4)_2$	4632	150869	9.4 (9.5)	$RbLiCl_2$	504888	36216	9.4 (9.4)
$SrZnF_4$	5078	31367	9.4 (9.4)	$BaBe_2Si_2O_7$	12797	151563	9.4 (9.6)	$Mg(PO_3)_2$	18620	4280	9.4 (9.5)
$BaMgP_2O_7$	18343	39398	9.4 (9.4)	$SrMgP_2O_7$	18469	280782	9.4 (9.4)	$YAl_3(BO_3)_4$	6062	91962	9.4 (9.5)
$RbPO_3$	4135	74736	9.4 (9.4)	$Na_6S_2ClO_8F$	23657	26914	9.5 (9.5)	$MgSO_4$	7572	16759	9.5 (9.5)
$NaAlCl_4$	23363	35278	9.5 (9.5)	$SiCl_4$	28391	62279	9.5 (9.5)	$Ba(AlCl_4)_2$	505755	56735	9.5 (9.5)
Na_2SnF_6	8811	68980	9.5 (9.5)	$SrBPO_5$	6486	77519	9.5 (9.5)	NaCl	22862	240598	9.6 (9.6)
RbCl	23295	162798	9.6 (9.6)	$BaGeF_6$	14006	26614	9.6 (9.6)	Na_2SO_4	4770	81506	9.6 (9.6)
$KAl(SO_4)_2$	7645	60170	9.6 (9.6)	$LiClO_4$	30301	413238	9.6 (9.7)	Cs_2SnF_6	7297	281	9.6 (9.6)
$CaCl_2$	22904	246417	9.7 (9.7)	$NaClO_4$	22968	200405	9.7 (9.9)	Li_2GeF_6	7791	23406	9.7 (9.7)
Li_2BeSiO_4	8070	28307	9.7 (9.9)	$LiAlCl_4$	22983	35275	9.7 (9.7)	$CsAlCl_4$	27260	8118	9.7 (9.7)
SiO_2	6945	162615	9.7 (9.7)	$K_3Na(SO_4)_2$	22457	27658	9.8 (9.9)	KCl	23193	22156	9.8 (9.8)
BaClF	23432	35487	9.8 (9.9)	$KClO_4$	23526	35111	9.8 (9.8)	$Al_4(B_2O_5)_3$	510509	54854	9.8 (10.0)
YPO_4	5132	56113	9.8 (9.8)	$RbClO_4$	28433	63363	9.8 (9.8)	HfF_4	31033	66008	9.8 (9.9)
$TlBF_4$	510136	300222	9.8 (9.8)	$MgCl_2$	23210	26157	9.9 (9.9)	Li_3PO_4	13725	10257	9.9 (9.9)
K_2ZrF_6	5450	250371	9.9 (9.9)	$CaSnF_6$	8224	35713	9.9 (9.9)	$NaZr_2ZnF_{11}$	15141	81223	10.0 (10.1)
GeF_4	9816	202558	10.0 (10.2)	$SrSO_4$	5285	92608	10.0 (10.1)	$Rb_2Hf_3OF_{12}$	17256	95847	10.0 (10.0)
$BaZr_2F_{10}$	505400	202530	10.0 (10.0)	$Li_3B_7O_{12}$	16828	68475	10.0 (10.0)	$KLiSO_4$	6800	88829	10.0 (10.0)
$LaPO_4$	3962	21066	10.0 (10.0)	$CaSO_4$	4406	56107	10.1 (10.5)	SF_6	8560	63362	10.1 (10.1)
SiO_2	547211	162246	10.1 (10.1)	$AlPO_4$	7848	24511	10.2 (10.2)	LiCl	22905	27981	10.3 (10.3)
K_2GeF_6	14168	30310	10.3 (10.3)	$LiSiBO_4$	8874	67536	10.4 (10.8)	CsF	1784	53832	10.5 (10.8)
Rb_2GeF_6	8812	68982	10.5 (10.5)	Cs_2GeF_6	8217	35547	10.6 (10.6)	RbH_2OF	23700	415010	10.7 (10.7)
$CsBe_2BO_3F_2$	553342	20000	10.7 (10.7)	K_2HfF_6	14128	29514	10.8 (10.9)	B_2O_3	306	36066	10.8 (10.9)
Cs_2NaAlF_6	6528	93459	10.8 (10.8)	$BeCl_2$	23267	31696	10.9 (11.0)	ScF_3	10694	77071	11.0 (11.4)
KRb_2GaF_6	13190	416605	11.0 (11.0)	Li_2ZrF_6	4002	16793	11.0 (11.1)	$KBe_2BO_3F_2$	6870	155156	11.0 (11.0)
BeO	2542	163819	11.1 (11.1)	$LiCaGaF_6$	12829	152300	11.1 (11.2)	SiH_4	23739	159307	11.1 (11.1)
KBe_3ZnF9	18509	18022	11.2 (11.2)	Cs_2ZrF_6	7903	25598	11.2 (11.2)	RbF	11718	53828	11.3 (11.4)
$BeSO_4$	505568	44801	11.4 (11.5)	SrB_4O_7	5540	95300	11.4 (11.7)	$CsCOF_3$	14734	69971	11.4 (11.4)
Li_2CaHfF_8	16577	95248	11.4 (11.4)	CO_2	20066	22398	11.5 (11.5)	BPO_4	3589	150380	11.6 (11.6)
Cs_2CaF_4	15157	82616	11.7 (11.8)	Rb_2MgF_4	8861	69681	12.1 (12.2)	Cs_2HfF_6	13948	25600	12.2 (12.2)
KF	463	53824	12.2 (12.2)	$RbCaF_3$	3654	201253	12.3 (12.4)	KPF_6	4608	56258	12.4 (12.4)
NaF	682	53840	12.4 (12.4)	BaF_2	1029	53980	12.5 (12.6)	K_2MgF_4	31212	33519	12.5 (12.6)
$CsCaF_3$	7104	45309	12.5 (12.5)	MgF_2	1810	159315	12.5 (12.5)	PF_5	8511	62554	12.6 (12.6)
$KMgF_3$	3448	94089	12.7 (12.9)	$Rb_3NaBe_2F_8$	13630	15764	12.7 (12.8)	SrF_2	981	41402	12.7 (12.7)
$Cs_2NaAl_3F_{12}$	12309	15784	12.7 (12.7)	CaF_2	2741	656448	12.8 (13.0)	$KAlF_4$	2910	201949	12.8 (12.8)
$LiPF_6$	9143	74830	12.8 (12.8)	K_2NaAlF_6	6586	6027	12.8 (12.8)	$NaPF_6$	10474	90615	12.9 (12.9)

$BaSiF_6$	5588	201510	12.9 (12.9)	K_2AlF_5	9486	81864	12.9 (12.9)	$CaAlF_5$	8836	69563	13.0 (13.0)
$SrAlF_5$	16557	411509	13.0 (13.0)	YF_3	2416	26595	13.1 (13.1)	LaF_3	905	23972	13.1 (13.1)
$NaCaAlF_6$	17944	80542	13.2 (13.2)	Rb_2SiF_6	10492	38547	13.3 (13.3)	AlF_3	468	38305	13.3 (13.3)
K_2SiF_6	3042	38546	13.4 (13.4)	$LiYF_4$	3700	96727	13.4 (13.4)	Cs_2SiF_6	4047	38548	13.4 (13.4)
$Na_2LiBe_2F_7$	12240	9430	13.5 (13.6)	$LiCaAlF_6$	6134	150333	13.6 (13.6)	$SrBeF_4$	9726	404396	13.7 (13.7)
SiF_4	1818	48147	14.0 (14.4)	LiF	1138	53839	14.6 (14.6)	BeF_2	15951	41492	14.6 (14.8)
CF_4	1167	65786	16.0 (16.1)								

Table 3 List of the indirect (direct) bandgaps sorted for increasing gap, in eV, of the calculated 2450 structures. The chemical formulas, the Materials Project and ICSD Ids are also included.

References

[1] *Materials Project - A Materials Genome Approach*, http://materialsproject.org/.

[2] *Computational Materials Repository*, https://wiki.fysik.dtu.dk/cmr/ (Documentation) , and https://cmr.fysik.dtu.dk/ (Database).

[3] W. C. Sheets, E. S. Stampler, M. I. Bertoni, M. Sasaki, T. J. Marks, T. O. Mason, K. R. Poeppelmeier, Inorganic Chemistry **47**, 2696 (2008).

[4] S. Ouyang, Z. Li, Z. Ouyang, T. Yu, J. Ye, Z. Zou, Journal of Physical Chemistry C **112**, 3134 (2008).

[5] H. G. Schnering, Zeitschrift Fur Anorganische Und Allgemeine Chemie **314**, 144 (1962).

[6] K. Mader, H. Mullerbuschbaum, Zeitschrift Fur Anorganische Und Allgemeine Chemie **559**, 89 (1988).

[7] *The Landolt-Börnstein Database*, http://www.springermaterials.com/docs/index.html.

[8] G. Tams, H. Mullerbuschbaum, Zeitschrift Fur Naturforschung Section B-a Journal of Chemical Sciences **50**, 56 (1995).

[9] P. D. Vernooy, A. M. Stacy, Journal of Solid State Chemistry **95**, 270 (1991).

[10] A. S. Erickson, S. Misra, G. J. Miller, R. R. Gupta, Z. Schlesinger, W. A. Harrison, J. M. Kim, I. R. Fisher, Physical Review Letters **99** (2007).

[11] K. E. Stitzer, M. D. Smith, H. C. zur Loye, Solid State Sciences **4**, 311 (2002).

[12] R. D. Shannon, J. L. Gillson, R. J. Bouchard, Journal of Physics and Chemistry of Solids **38**, 877 (1977).

[13] T. Pisarkiewicz, K. Zakrzewska, E. Leja, Thin Solid Films **153**, 479 (1987).

[14] G. Ferrari, L. Coghi, Gazzetta Chimica Italiana **71**, 440 (1941).

[15] B. Brazel, R. Hoppe, Zeitschrift Fur Naturforschung Section B-a Journal of Chemical Sciences **37**, 1369 (1982).

[16] B. Brazel, R. Hoppe, Zeitschrift Fur Naturforschung Section B-a Journal of Chemical Sciences **38**, 661 (1983).

[17] J. J. Scheer, A. E. Vanarkel, R. D. Heyding, Canadian Journal of Chemistry-Revue Canadienne De Chimie **33**, 683 (1955).

[18] K. Hobbie, R. Hoppe, Zeitschrift Fur Anorganische Und Allgemeine Chemie **535**, 20 (1986).

[19] B. Schwedes, R. Hoppe, Zeitschrift Fur Anorganische Und Allgemeine Chemie **391**, 313 (1972).

[20] D. Choueiry, E.-i. Negishi, *Handbook of Organopalladium Chemistry for Organic Synthesis* (2002), ISBN 0-471-31506-0.

[21] B. Schwedes, R. Hoppe, Zeitschrift Fur Anorganische Und Allgemeine Chemie **393**, 136 (1972).

[22] Y. Takahashi, Y. Gotoh, J. Akimoto, Journal of Solid State Chemistry **172**, 22 (2003).

[23] S. Miyazaki, S. Kikkawa, M. Koizumi, Synthetic Metals **6**, 211 (1983).

[24] K. Hobbie, R. Hoppe, Zeitschrift Fur Anorganische Und Allgemeine Chemie **565**, 106 (1988).

[25] S. Park, K. Kang, W. Si, W. S. Yoon, Y. Lee, A. R. Moodenbaugh, L. H. Lewis, T. Vogt, Solid State Communications **135**, 51 (2005).

[26] J. Curda, E. M. Peters, W. Klein, M. Jansen, Zeitschrift Fur Kristallographie-New Crystal Structures **219**, 345 (2004).

[27] Y. Pelletier, C. Reber, Inorganic Chemistry **36**, 721 (1997).

[28] N. E. Massa, J. A. Alonso, M. J. Martinez-Lope, M. T. Casais, Physical Review B **72** (2005).

Paper IV

Band-gap engineering of functional perovskites through quantum confinement and tunneling

I. E. Castelli, M. Pandey, K. S. Thygesen and K. W. Jacobsen Physical Review B 91 (16), 165309 (2015)

Band-gap engineering of functional perovskites through quantum confinement and tunneling

Ivano E. Castelli,* Mohnish Pandey, Kristian S. Thygesen, and Karsten W. Jacobsen
Center for Atomic-scale Materials Design, Department of Physics, Technical University of Denmark, DK-2800 Kongens Lyngby, Denmark
(Received 30 December 2014; revised manuscript received 25 March 2015; published 24 April 2015)

An optimal band gap that allows for a high solar-to-fuel energy conversion efficiency is one of the key factors to achieve sustainability. We investigate computationally the band gaps and optical spectra of functional perovskites composed of layers of the two cubic perovskite semiconductors $BaSnO_3$ and $BaTaO_2N$. Starting from an indirect gap of around 3.3 eV for $BaSnO_3$ and a direct gap of 1.8 eV for $BaTaO_2N$, different layerings can be used to design a direct gap of the functional perovskite between 2.3 and 1.2 eV. The variations of the band gap can be understood in terms of quantum confinement and tunneling. We also calculate the light absorption of the different heterostructures and demonstrate a large sensitivity to the detailed layering.

DOI: 10.1103/PhysRevB.91.165309 PACS number(s): 68.35.bg, 73.21.Ac, 73.20.−r, 78.20.−e

I. INTRODUCTION

Functional oxides form a fascinating class of materials exhibiting a large range of phenomena and with great potential for technological applications. Some of their properties include high-temperature superconductivity, multiferroic and half-metallic behavior, thermoelectric, magnetocaloric, and photoconductivity effects, transport phenomena, and catalytic properties [1]. The oxides in the perovskite structure constitute an interesting subclass with high stability and new underexplored possibilities for producing layered heterostructures with atomically well-defined interfaces. Effects of quantum confinement in atomically layered perovskites have been discussed in several different heterosystems [2]. Yoshimatsu *et al.* [3–5] have studied quantum wells of the metal $SrVO_3$ embedded in an insulator, $SrTiO_3$, with photoemission, demonstrating that modifications of the electronic structure develop below six layers of $SrVO_3$ and that for a single layer a substantial gap appears. Other studies include confinement effects on the magnetic structure of $LaMnO_3/SrMnO_3$ superlattices [6] and recent investigations of how non-Fermi-liquid behavior appears when a $SrTiO_3$ quantum well embedded in $SmTiO_3$ is sufficiently thin [7]. More recently, Grote *et al.* [8] have investigated how to tune the band gap of tin- and lead-halide perovskites through effects of atomic layering and quantum confinement.

In the present work, we investigate the band gaps and the light-absorption properties of functional perovskites obtained by stacking cubic perovskite planes, with general formula ABO_3, in one direction (say, the z axis) while the other two directions preserve the cubic symmetry, as shown in Fig. 1. The possibilities for producing such structures are numerous, but little is known about the potential for systematic, quantitative control of their properties. We show that a large variation of the band gap can be obtained and that the size of the band gap for a particular stacking sequence can be understood in terms of confinement and tunneling behavior. Using these ingredients, an engineering of the band gap can be pursued to tune the gap to a desired window. This approach could potentially be used to achieve high efficiencies in light-harvesting devices.

More specifically, we consider combinations of the two cubic perovskite semiconductors $BaSnO_3$ and $BaTaO_2N$, indicated with α and β in Fig. 1, respectively [9]. The choice of these two materials as building blocks is based on the fact that both $BaSnO_3$ and $BaTaO_2N$ have been previously selected as good materials for light harvesting and photocatalytic water splitting [10,11] and their crystal lattices are rather similar, with the consequence that the obtained layered structure [12] will not be subjected to high stress.

All of the calculations presented in this work are performed in the framework of density functional theory (DFT) using the electronic structure code GPAW [13,14]. Due to the well-known problem of standard DFT with the underestimation of the band gaps, the gaps have been calculated using the GLLB-SC potential by Gritsenko, van Leeuwen, van Lenthe, and Baerends (GLLB) [15], modified by Kuisma *et al.* [16] to include the correlation for solids (-SC). This potential has been shown to provide realistic estimates of band gaps when compared with other more advanced computational methods and experiments for a range of semiconductors and insulators including oxides without too strong correlation effects [10,17–19]. One reason for the favorable comparison is the addition to the DFT Kohn-Sham gap of the so-called derivative discontinuity, which is explicitly calculated in the GLLB-SC approach. We have furthermore performed hybrid calculations using the functional proposed by Heyd, Scuseria, and Ernzerhof (HSE06) [20,21] as a comparison for a subset of the layered materials investigated in this work.

II. BAND GAPS

The compounds that we study here are all obtained by stacking n_α layers of α with n_β layers of β, where $1 \leqslant n_{\alpha(\beta)} \leqslant 6$, and then repeating this unit periodically. The lattice parameter is taken equal to the average value of the lattices of α and β (4.1 Å [22]). $BaSnO_3$ and $BaTaO_2N$ have been frozen in their perfect cubic perovskite symmetry, i.e., without any distortion. Even though distortions usually have large effects on the band gaps, $BaSnO_3$ and $BaTaO_2N$ have a high cubicity so that the changes in the band gaps are expected to be small. Keeping the structures frozen in the cubic symmetry furthermore allows us to analyze the changes in the electronic

*ivca@fysik.dtu.dk. Present address: Theory and Simulation of Materials (THEOS) and National Center for Computational Design and Discovery of Novel Materials (MARVEL), École Polytechnique Fédérale de Lausanne, CH-1015 Lausanne, Switzerland.

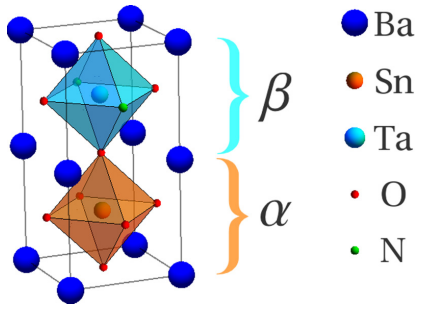

FIG. 1. (Color online) Unit cell of the $\alpha\beta$ structure. The cubic perovskite planes are stacked in the z direction, while the x and y directions maintain the usual periodicity of a cubic perovskite. α indicates the $BaSnO_3$ perovskite, and β the $BaTaO_2N$.

properties of the materials due only to the different stackings, regardless of any changes caused by structure relaxation.

Using GLLB-SC, $BaSnO_3$ shows an indirect band gap between the Γ and R points of 3.33 eV, while $BaTaO_2N$ is found to have a direct band gap at Γ of 1.84 eV. This compares favorably with experiments where the optical gaps have been measured, through diffuse reflectance spectra, to 3.1 and 1.9 eV for $BaSnO_3$ [23] and $BaTaO_2N$ [24], respectively. HSE calculations slightly underestimate the gaps (2.89 eV for $BaSnO_3$ and 1.71 eV for $BaTaO_2N$).

Figure 2 reports the band gaps for the 36 $\alpha_{n_\alpha}\beta_{n_\beta}$ structures as a function of the number of α and β planes. The gaps vary considerably spanning a region of 1 eV, illustrating the high degree of tunability of the band gap. The simplest combination with only one layer of α and β in the heterostructure gives the widest gap with a value of 2.26 eV, not too far from the average of the band gaps of the two constituent cubic perovskites. (For comparison, the HSE method gives again a slightly lower value of 2.04 eV.) More complex combinations exhibit reduced band

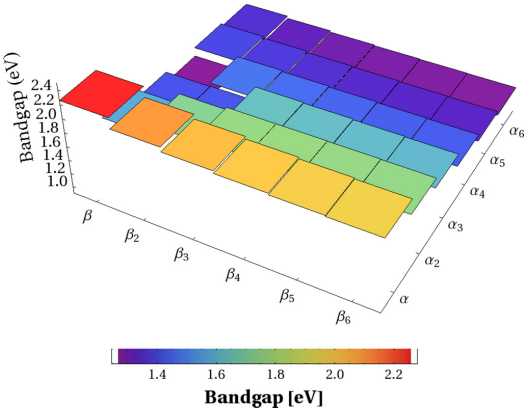

FIG. 2. (Color online) Calculated band gaps as a function of the number of α ($BaSnO_3$) and β ($BaTaO_2N$) layers. Each rectangle in the plot represents a layered periodic structure with sequence $\alpha_n\beta_m$.

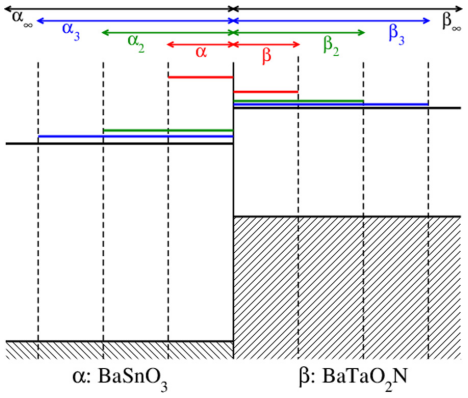

FIG. 3. (Color online) Sketch of the electronic level positions at an interface between layers of $BaSnO_3$ and $BaTaO_2N$. When the layer thickness is reduced, the local position of the conduction-band edge moves up due to confinement.

gaps depending on their composition. As we shall show in the following, the significant complicated variation of the band gap shown in Fig. 2 can essentially be understood in terms of electronic confinement and tunneling effects.

In Fig. 3, we sketch how the local band edges are positioned relative to each other for different layer thicknesses. For the thickest layer structure, $\alpha_6\beta_6$, we have the smallest band gap of 1.26 eV. The state at the valence-band maximum (VBM) is composed mainly of N_{2p} orbitals with a minor contribution from the O_{2p} orbitals and is located in the β part of the material. In fact, all of the mixed compositions have a direct band gap at the Γ point, with the VBM state of this character located in the β part of the material. The character of the VBM state can, for example, be seen in Figs. 4(a) and 4(c) for the $\alpha\beta$ and $\alpha_2\beta$ structures, respectively. Not only is the character of the VBM state the same for all structures, but the calculations also indicate that it does not move much relative to a low-lying atomic state in $BaTaO_2N$, and we shall therefore regard this level as fixed in the following and ascribe the variations to changes in the conduction band.

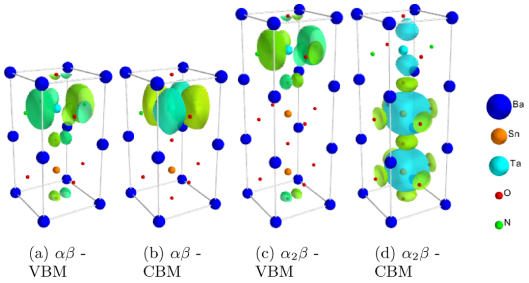

FIG. 4. (Color online) Wave functions of states at the valence-band maximum (VBM) and the conduction-band minimum (CBM) for some combinations of α and β layers.

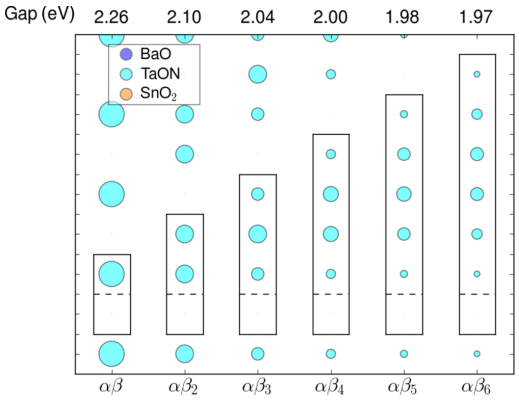

FIG. 5. (Color online) The figure illustrates the weights of the CBM state in real space. The vertical axes are along the stacking direction of the material and the areas of the circles indicate the weights of the CBM state for a particular atomic xy plane. The boxes show the extent of the supercell in the direction of the stacking (z), and the dashed lines mark the interfaces between the α and β layers. Above the figure, the calculated band gaps for the different stacking sequences are denoted. The CBM state is mainly composed of Ta d orbitals, as shown in Fig. 4(b).

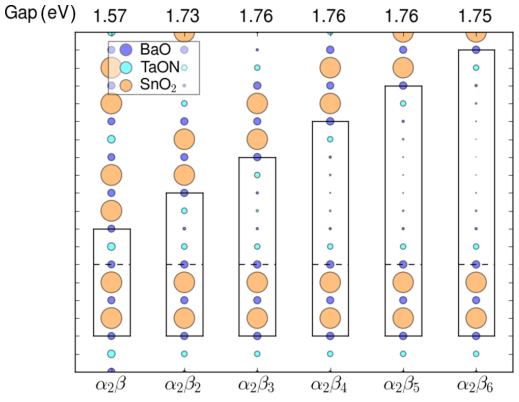

FIG. 6. (Color online) Weight of the CBM state in each xy plane of the $n_\alpha = 2$ structure. The CBM state is now composed of Sn s states, with some tunneling through the TaON plane [Fig. 4(d)]. The tunneling progressively reduces with the increase of β layers.

To understand the variation of the conduction-band minimum in Fig. 3, we first consider the compounds with the formula $\alpha\beta_{n_\beta}$, where the band gap decreases as a function of the number of β layers. The CBM states for these systems are located only on the TaON plane, as shown in Fig. 5, and generated by the Ta_{5d} orbitals, as plotted in Fig. 4(b) for the $\alpha\beta$ case. The variation of the band gap as a function of n_β is a result of quantum confinement. The empty states in the single α layer are shifted up out of reach, and the CBM state in β becomes less confined with the increase of the number of β layers in the $\alpha\beta_{n_\beta}$ structures, as can be seen in Fig. 5. The reduction of the confinement results in a down-shift of the CBM level and thus a reduced band gap, as also sketched in Fig. 3.

The situation is radically different for all the combinations $\alpha_{n_\alpha}\beta_{n_\beta}$, with $n_\alpha \geqslant 2$. Now the CBM state is not located in β, but in α. It is located mainly on the Sn_{5s} orbitals, as shown in Fig. 4(d). If, for example, we consider the compounds $\alpha_2\beta_n$, the CBM state is localized in the α_2 layers and essentially looks the same, as seen in Fig. 6. The band gap is therefore also largely unchanged for $n \geqslant 3$. For $n = 2$, a small reduction relative to the situation with $n \geqslant 3$ is seen and this reduction becomes even larger for $n = 1$ (see Fig. 2). We ascribe this reduction to quantum tunneling through the thin β layers. As can be seen in Fig. 6, the CBM states decay into the β layers and the tunneling coupling, for small thicknesses, will result in a lowering of the CBM level and thus a decrease of the band gap.

The interplay between quantum confinement and tunneling is seen most clearly for the $n_\beta = 1$ systems (Fig. 7). Ignoring the $\alpha\beta$ structure that has a different nature for the CBM level with respect to the other systems, the CBM state becomes less confined with the increase of the number of α layers, with the consequence of a decrease in the band gap. And as we have seen, the band gap is further reduced because of tunneling through the single β TaON layer. However, for larger thicknesses of the α layer, the tunneling effect is reduced because the now less-confined CBM state has lower amplitude at the interface. This interplay between confinement and tunneling leads to the increase of the band gap between $n_\alpha = 4$ and $n_\alpha = 5$.

As we have seen, the variation of the band gaps for the different periodic $\alpha_n\beta_m$ compounds can be understood from the confinement effects shown in the level diagram in Fig. 3 together with additional tunneling effects if β_1 or β_2 layers are present. Does this lesson apply to more complicated sequences

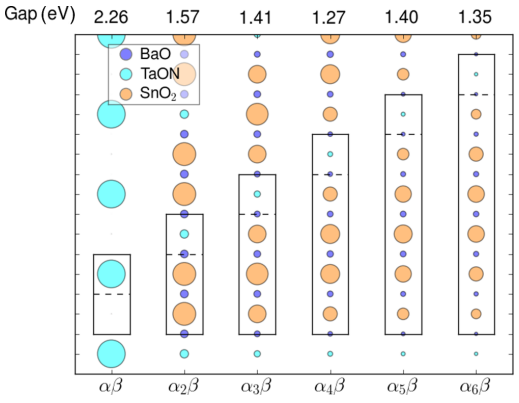

FIG. 7. (Color online) Weight of the CBM state in each xy plane of the $n_\beta = 1$ structure. The character of the CBM state changes drastically with n_α: TaON is responsible for the CBM state for the $n_\alpha = 1$ structure, while for $n_\alpha > 1$, it is SnO_2 [Figs. 4(b) and 4(d)]. The tunneling across the TaON plane has an effect until $n_\alpha = 4$.

of layers? Some test calculations seem to indicate so. A compound with the periodic repetition of $\alpha\beta\alpha\beta_{n_\beta}$ reproduces exactly the same gaps as the $\alpha\beta_{n_\beta}$. This is to be expected since from the level diagram in Fig. 3 we should expect the CBM state to be located in the β_{n_β} layer with little tunneling through the α layers. Another example is the systems with sequence $\alpha\beta\alpha_{n_\alpha}\beta$, which exhibit a small increase (up to about 0.2 eV) of the band gap for $n_\alpha \geqslant 2$ as compared to the $\alpha_{n_\alpha}\beta$ compounds. This can be understood in terms of reduced tunneling because the α_{n_α} layers are now separated by $\beta\alpha\beta$ instead of a single β layer reducing the tunneling effect.

III. OPTICAL PROPERTIES

A number of technological applications such as photovoltaics or photocatalysis depend on the availability of efficient absorbers of light in the visible spectrum. This requires an appropriate band gap of the material, and band-gap tuning is therefore a key issue. However, the band gap does not by itself provide any information about the magnitude of the matrix elements responsible for light absorption. For symmetry reasons, the light absorption can be dipole allowed or forbidden and—in particular for heterostructures—the transitions may take place between states with different degree of spatial overlap, giving rise to large variations of the absorption strengths.

To address this issue, we perform linear response calculations [25], using the adiabatic local density approximation (ALDA), and determine the optical absorption of the investigated systems focusing for simplicity on the systems with $n_\alpha = 1$ or $n_\beta = 1$ [26]. The optical absorption spectrum is calculated using time-dependent density functional theory (TDDFT) from the density response function χ. The response function evaluated at point $\mathbf{r}$ to first order in a time-dependent perturbation of frequency ω applied at point $\mathbf{r}'$ is $\chi(\mathbf{r},\mathbf{r}',\omega) = \delta n(\mathbf{r},\omega)/\delta V_{\text{ext}}(\mathbf{r}',\omega)$, where δn is the induced density under the perturbation caused by the external potential V_{ext}.

The microscopic dielectric matrix is defined as

$$\epsilon^{-1}_{\mathbf{G}\mathbf{G}'}(\mathbf{q},\omega) = \delta_{\mathbf{G}\mathbf{G}'} + \frac{4\pi}{|\mathbf{q}+\mathbf{G}|^2}\chi_{\mathbf{G}\mathbf{G}'}(\mathbf{q},\omega), \qquad (1)$$

where $\mathbf{G}$ and $\mathbf{G}'$ are reciprocal lattice vectors, and $\mathbf{q}$ is a wave vector of the first Brillouin zone. The optical absorption spectrum is given by $\text{Im}\epsilon(\mathbf{q}\to 0,\omega)$, where $\epsilon(\mathbf{q}\to 0,\omega) = \frac{1}{\epsilon^{-1}_{\mathbf{0}\mathbf{0}}(\mathbf{q}\to 0,\omega)}$.

Figure 8 shows the optical absorption for the $n_\alpha = 1$ systems. In the plot, we distinguish between the case where the light is polarized along the xy and the z directions. The xy plane, in fact, maintains the cubic symmetry, while the stacking of the layers takes place in the z direction. For these compounds, the CBM and VBM states are located in the same region of space, namely, in the TaON layers, and thus the absorption starts at the direct band gap and is quite intense, especially for polarizations in the xy direction. The situation is different for the $n_\beta = 1$ systems (Fig. 9), where the VBM state is located in the TaON layer, while the CBM state has most weight on the BaO_2 layers. The absorption here starts at much higher energies than the band gap (except for the $\alpha\beta$ compound, in black in the figure, which has the VBM and CBM states located in the same region). The first transition with appreciable weight is between two TaON states in the β layer, and the absorption curves are therefore fairly similar, independent of the band gap.

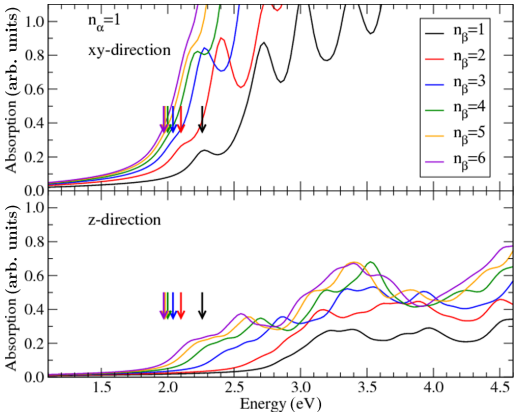

FIG. 8. (Color online) Calculated optical absorption for the $n_\alpha = 1$ systems. The direct band gaps are indicated with vertical arrows.

Table I reports the efficiencies of the two sequences. The efficiency is calculated as the percentage of the collected photons of the global solar spectrum at AM1.5 [27]. As also shown in Figs. 8 and 9, the efficiency is higher for light polarized in the xy direction than along z. $\alpha\beta_2$ and $\alpha_2\beta$ are almost comparable because the higher absorption properties of the former are balanced by the lower band gap of the latter, and the two systems collect almost the same amount of photons. The efficiency of the $\alpha\beta_{n_\beta}$ sequence always increases with the number of layers, while the one of $\alpha_{n_\alpha\beta}$ decreases even though the gap closes.

The calculations thus indicate that the absorption cross section at the $\alpha - \beta$ interface is quite limited and that the

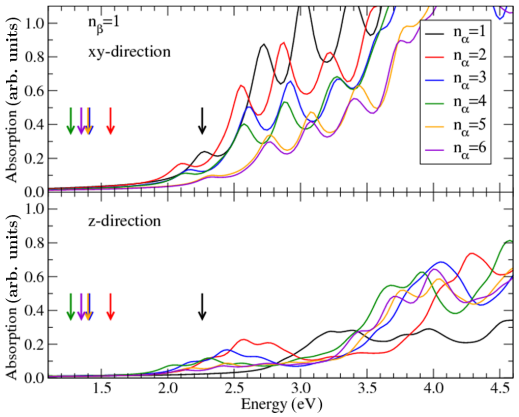

FIG. 9. (Color online) Calculated optical absorption for the $n_\beta = 1$ systems. The direct band gaps are indicated with vertical arrows.

TABLE I. Gap (in eV) and photon-absorption efficiency η (in %, for light polarized in the xy and z directions) of the sequences $\alpha\beta_{n_\beta}$ and $\alpha_{n_{\alpha\beta}}$, calculated for a thickness of 10^{-7} m. The efficiency calculated for the pure α and β cubic perovskites is included for comparison.

	Gap	η^{xy}	η^{z}		Gap	η^{xy}	η^{z}
α	3.33	0.1	0.1	β	1.84	14.9	6.4
$\alpha\beta$	2.26	4.3	0.9	$\alpha\beta$	2.26	4.3	0.9
$\alpha\beta_2$	2.10	7.0	1.5	$\alpha_2\beta$	1.57	5.3	2.1
$\alpha\beta_3$	2.04	8.9	2.4	$\alpha_3\beta$	1.41	4.3	2.0
$\alpha\beta_4$	2.00	10.0	3.0	$\alpha_4\beta$	1.27	4.1	2.0
$\alpha\beta_5$	1.98	10.7	3.5	$\alpha_5\beta$	1.40	2.8	1.5
$\alpha\beta_6$	1.97	11.3	3.8	$\alpha_6\beta$	1.35	2.6	1.5

band-edge states have to be localized in the same layers to obtain efficient absorption.

IV. CONCLUSIONS

In this work, we have investigated the electronic properties of perovskite heterostructures obtained by stacking $BaSnO_3$ and $BaTaO_2N$ layers. The band gap is seen to be tunable over the wide range of around 1 eV and the variation can be understood in terms of quantum confinement and tunneling. Confinement leads to up-shifts of the conduction-band minimum and thus to increase of the band gap, while tunneling effects reduce the confinement and lead to lower band gap. The tunneling effects are seen to decay over a few perovskite unit cells. The systems studied here are close to cubic and with similar lattice constants, but in general band-gap formation in layered perovskites can be expected to depend sensitively also on strain and lattice distortions/reconstructions [28].

The calculated optical absorption spectra for the heterostructures indicate that high absorption is only obtained if the VBM and CBM states are localized in the same spatial region. The design of heterostructures for efficient visible-light absorption therefore requires not only appropriate band gaps, but also tailored band-edge states with proper spatial overlap.

The stacking of $BaSnO_3$ and $BaTaO_2N$ layers that we have described here is a type-II heterojunction with the conduction band of $BaSnO_3$ above the valence band of $BaTaO_2N$. A type-I heterojunction can be designed using different perovskites. One example is $LaAlO_3$ (as α) and $LaTiO_2N$ (as β), with a calculated indirect band gap between Γ and R points of 6.11 and a direct gap at the Γ point of 1.49 eV, respectively, and where the band edges of $LaTiO_2N$ are placed in between the edges of $LaAlO_3$. Preliminary results show that due to the large band gap of α, there is no tunneling through the α layer and there is already a full confinement of the β layers with a single α [29]. In addition, the band gaps of the layered combinations are direct, with the VBM formed by N_{2p} orbitals and the CBM composed of Ti_{3d}. Also in this case, the stacking has the effect of placing the VBM and CBM closer together spatially. This fact might increase the absorption properties of the materials and, together with the possibility of tuning the band gap using quantum confinement and tunneling, can be used to design novel light-harvesting heterojunctions.

ACKNOWLEDGMENTS

The authors acknowledge support from the Catalysis for Sustainable Energy (CASE) initiative funded by the Danish Ministry of Science, Technology and Innovation, and from the Center on Nanostructuring for the Efficient Energy Conversion (CNEEC) at Stanford University, an Energy Frontier Research Center founded by the U.S. Department of Energy, Office of Science, Office of Basic Energy Sciences under Award No. DE-SC0001060. K.S.T. acknowledges support from the Danish Council for Independent Research Sapere Aude Program through Grant No. 11-1051390. The Center for Nanostructured Graphene is sponsored by the Danish National Research Foundation, Project No. DNRF58.

[1] F. M. Granozio, G. Koster, and G. Rijnders, Mater. Res. Bull. **38**, 1017 (2013).

[2] S. Stemmer and A. J. Millis, Mater. Res. Bull. **38**, 1032 (2013).

[3] K. Yoshimatsu, T. Okabe, H. Kumigashira, S. Okamoto, S. Aizaki, A. Fujimori, and M. Oshima, Phys. Rev. Lett. **104**, 147601 (2010).

[4] K. Yoshimatsu, E. Sakai, M. Kobayashi, K. Horiba, T. Yoshida, A. Fujimori, M. Oshima, and H. Kumigashira, Phys. Rev. B **88**, 115308 (2013).

[5] K. Yoshimatsu, K. Horiba, H. Kumigashira, T. Yoshida, A. Fujimori, and M. Oshima, Science **333**, 319 (2011).

[6] T. S. Santos, B. J. Kirby, S. Kumar, S. J. May, J. A. Borchers, B. B. Maranville, J. Zarestky, S. G. E. te Velthuis, J. van den Brink, and A. Bhattacharya, Phys. Rev. Lett. **107**, 167202 (2011).

[7] C. A. Jackson, J. Y. Zhang, C. R. Freeze, and S. Stemmer, Nat. Commun. **5**, 1 (2014).

[8] C. Grote, B. Ehrlich, and R. F. Berger, Phys. Rev. B **90**, 205202 (2014).

[9] We consider, for simplicity, only the simplest ordered structure of the nitrogen atoms. Some check calculations within the unit cells we use indicate that exchanging O and N atoms so that the number of O and N neighbors of the Ta atoms stays fixed only gives minor changes to both the stability and the band gap (changes less than 0.1 eV). If the O and N coordination of the Ta atoms is changed, the stability is significantly decreased.

[10] I. E. Castelli, T. Olsen, S. Datta, D. D. Landis, S. Dahl, K. S. Thygesen, and K. W. Jacobsen, Energy Environ. Sci. **5**, 5814 (2012).

[11] I. E. Castelli, D. D. Landis, K. S. Thygesen, S. Dahl, I. Chorkendorff, T. F. Jaramillo, and K. W. Jacobsen, Energy Environ. Sci. **5**, 9034 (2012).

[12] Layered perovskite usually is the name given to ABO_3 perovskites separated by some motifs. Some examples are the Ruddlesden-Popper and the Dion-Jacobson phases. In this work,

with layered perovskite, we indicate layers of cubic perovskites stacked in the z direction.

[13] J. J. Mortensen, L. B. Hansen, and K. W. Jacobsen, Phys. Rev. B **71**, 035109 (2005).

[14] J. Enkovaara, C. Rostgaard, J. J. Mortensen, J. Chen, M. Dulak, L. Ferrighi, J. Gavnholt, C. Glinsvad, V. Haikola, H. A. Hansen, H. H. Kristoffersen, M. Kuisma, A. H. Larsen, L. Lehtovaara, M. Ljungberg, O. Lopez-Acevedo, P. G. Moses, J. Ojanen, T. Olsen, V. Petzold, N. A. Romero, J. Stausholm-Møller, M. Strange, G. A. Tritsaris, M. Vanin, M. Walter, B. Hammer, H. Hakkinen, G. K. H. Madsen, R. M. Nieminen, J. K. Nørskov, M. Puska, T. T. Rantala, J. Schiøtz, K. S. Thygesen, and K. W. Jacobsen, J. Phys. Condens. Matter **22**, 253202 (2010).

[15] O. Gritsenko, R. van Leeuwen, E. van Lenthe, and E. J. Baerends, Phys. Rev. A **51**, 1944 (1995).

[16] M. Kuisma, J. Ojanen, J. Enkovaara, and T. T. Rantala, Phys. Rev. B **82**, 115106 (2010).

[17] F. Hüser, T. Olsen, and K. S. Thygesen, Phys. Rev. B **87**, 235132 (2013).

[18] I. E. Castelli, J. M. García-Lastra, F. Hüser, K. S. Thygesen, and K. W. Jacobsen, New J. Phys. **15**, 105026 (2013).

[19] I. E. Castelli, F. Hüser, M. Pandey, H. Li, K. S. Thygesen, B. Seger, A. Jain, K. A. Persson, G. Ceder, and K. W. Jacobsen, Adv. Energy Mater. **5**, 1400915 (2015).

[20] J. Heyd, G. E. Scuseria, and M. Ernzerhof, J. Chem. Phys. **118**, 8207 (2003).

[21] A. V. Krukau, O. A. Vydrov, A. F. Izmaylov, and G. E. Scuseria, J. Chem. Phys. **125**, 224106 (2006).

[22] The lattice parameters of α and β calculated with the PBEsol functional [30] are 4.12 and 4.08 Å, respectively, in very good agreement with the experimental values (4.11 Å for both α [31] and β [32]).

[23] H. Mizoguchi, H. W. Eng, and P. M. Woodward, Inorg. Chem. **43**, 1667 (2004).

[24] D. Yamasita, T. Takata, M. Hara, J. N. Kondo, and K. Domen, Solid State Ionics **172**, 591 (2004).

[25] J. Yan, J. J. Mortensen, K. W. Jacobsen, and K. S. Thygesen, Phys. Rev. B **83**, 245122 (2011).

[26] TDDFT-ALDA does not include excitonic effects. However, the exciton binding energy E_{exc} can be estimated using the Wannier-Mott model,

$$E_{\mathrm{exc}} = R\frac{\mu}{m}\frac{1}{\epsilon_{\mathrm{M}}^2},$$

where $R = 13.606$ eV, $\frac{1}{\mu} = \frac{1}{\mu_{\mathrm{c}}^*} + \frac{1}{\mu_{\mathrm{v}}^*}$, with μ_{c}^* and μ_{v}^* the hole and electron effective masses at the CBM and VBM, respectively, and ϵ_{M} is the macroscopic dielectric constant. Based on this, we estimate the exciton binding energies for $BaSnO_3$ and $BaTaO_2N$ to be of the order of 0.3 and 0.1 eV, respectively, and about 0.2 eV for the $\alpha\beta$ sequence.

[27] The efficiency η is given by

$$\eta = \frac{1}{n_{\mathrm{tot}}}\int_{\mathrm{gap}}^{\infty} ph_{\mathrm{abs}}(E)n_{\mathrm{ph}}(E)dE,$$

where n_{tot} is the total number of photons from the sun measured at AM1.5, $ph_{\mathrm{abs}}(E)$ is the photon absorptivity of the material, and $n_{\mathrm{ph}}(E)$ is the number of sun photons as a function of energy E, in eV. The photon absorptivity depends on the the absorption coefficient $\alpha(E)$ and on the depth of the material along the absorption direction L: $ph_{\mathrm{abs}}(E) = 1 - e^{-\alpha(E)L}$. The absorption coefficient is $\alpha(E) = \frac{2Ek(E)}{\hbar c}$, where $\hbar$ and c are the Planck constant and the speed of light, respectively, and k is obtained from the absorption spectrum as $k^2 = \frac{1}{2}(-\mathrm{Re}\epsilon + \sqrt{\mathrm{Re}^2\epsilon + \mathrm{Im}^2\epsilon})$.

[28] H. Li, I. E. Castelli, K. S. Thygesen, and K. W. Jacobsen, Phys. Rev. B **91**, 045204 (2015).

[29] The calculated gaps for this combination, as well as for the $BaSnO_3$-$BaTaO_2N$, are available in the Computational Materials Repository at https://cmr.fysik.dtu.dk/.

[30] J. P. Perdew, A. Ruzsinszky, G. I. Csonka, O. A. Vydrov, G. E. Scuseria, L. A. Constantin, X. Zhou, and K. Burke, Phys. Rev. Lett. **100**, 136406 (2008).

[31] H. Mizoguchi, P. M. Woodward, C.-H. Park, and D. A. Keszler, J. Am. Chem. Soc. **126**, 9796 (2004).

[32] F. Pors, R. Marchand, Y. Laurent, P. Bacher, and G. Roult, Mater. Res. Bull. **23**, 1447 (1988).